The mitochondrial ageing signature; seeing the light.

Tobias Weinrich Weinrich

UCL Institute of Ophthalmology

Supervised by:

Prof. Glen Jeffery

Prof. Kenneth Smith

A thesis submitted for the degree of Doctor of Philosophy (Ph.D)

‘I, Tobias Weinrich Weinrich confirm that the work presented in this thesis is my own. Where information has been derived from other sources, I confirm that this has been indicated in the thesis.'

Acknowledgments

There are so many people who have made the last 4 rollercoaster years possible. Without them, I would not be here. I need to thank you all. Of course, I also need to thank all the flies and mice and primates that have contributed involuntarily in this theses. Thank you.

Firstly, I would like to thank both Glen and Ken for giving me the opportunity (and trust me) in such interesting research projects. Without a doubt, there have been incredibly difficult moments over the past years. Without your help, mentoring and guidance I doubt this project would have got anywhere.

I would also like to thank all the colleagues in this period, especially Dr Jaimie Hoh Kam. Without her support, assistance and fun times, my time in this place would not have been the same. Also a special thanks to other colleagues who introduced me to new skills or ideas, Dr Kim Chisholm, Dr Marija Sajic, Dr Andrew Davies. Big thanks to Dr Asmaa, Dr Sivapathasuntharam, Harpreet, Joty, MSc students and all colleagues in Ken's lab. Hopefully I wasn't too annoying sometimes.

Everyone who has helped in this work, especially Prof Werner and Dr Ravi in California for their contribution in the S-cone paper, Prof Harvey (Greenwich) for introducing me to the carotenoids world, and Dr Thompson (Greenwich), for her help in the mitochondrial circadian function. All a big thanks. Thanks to Prof Mitrofanis, who regularly visits us from Australia, for showing interest in my research and to all your constructive feedback. Greatly appreciated.

Big thanks to my family, without who I wouldn't have made it to where I am. I cannot thank you for your unconditional support, love and care you have given me over the years. It is always appreciated, perhaps even if I don't always show it. And to you Eloi, even though you appear last on this list, I cannot put enough emphasis in how much your help and support has helped and kept me going in these rollercoaster years.

Danke. Thank you. Gracias. Gràcies.

Abstract

Mitochondrial dysfunction is a major feature of ageing, but also plays a role in pathological conditions, including inflammation. Mitochondria have been suggested as therapeutic targets, where improvements in mitochondrial function can lead to improvements in age-related physiological decline. The work described in this thesis involves the study of mitochondrial dysfunction in two models of ageing, *Drosophila* and primates. It reveals how mitochondrial dysfunction can be reverted with two different therapies and a putative method to assess mitochondrial function in vivo non-invasively. Also, the work revels some features of circadian mitochondrial function critical to such therapies.

Aged *Drosophila* flies treated with two 670 nm protocols show interesting phenotypes. A short treatment impacts positively mitochondrial function while changes in behaviours are limited and short term. A longer treatment windows triggers, in addition to changes in mitochondrial and metabolite profiles, robust improvements in memory, locomotor and visual function. However, stress responses seem to be unaltered except for chilled coma recovery time.

A trial supplementing 9-*cis*-β-carotene in *Drosohila* food expands median life span, and suggest a link with mitochondrial function. However, further research is required to understand this putative link between this carotene and mitochondrial function.

As with other biological functions, mitochondrial function oscillates during the day. We show data that supports the concept that mitochondria, especially electron transport chain complexes, anticipate the light phase reaching its zenith a few hours later, while their activity is minimal during the dark phase. However, we found no oscillation in the expression levels of our analysed electron transport chain complexes genes.

Cone photoreceptors in the retina are cells characterised by a high mitochondrial density. With ageing, however, photoreceptor physiological decline is not homogenous across the different types (S and M/L). We found no difference in cone photoreceptor numbers with ageing in our model (*M. fasciularis*) that could explain the observed differences in function. Additionally, stress related markers were investigated, but again, no differences could be observed between cone types.

Mitochondrial flavoprotein autofluorescence can be used to assess mitochondrial function *in vivo* in the retina. Our data shows that mitochondria are responsive to changes in inspired oxygen concentration. However, mitochondrial function was unaltered in our animal model with specific retinal inflammation.

Collectively, the findings in this thesis expand our understanding of how mitochondria contribute to the ageing process, and how we can modulate aged mitochondrial function to ameliorate the consequences of ageing. We also propose a method to study mitochondrial function *in vivo*¸ to further understand the role of this organelle in physiological and pathological conditions.

Impact statement

The increasing age of the human population is becoming a burden for national health systems, as the incidence of age related diseases increases. The research presented in this thesis has a potential impact both inside and outside academia, especially its application to human health. Within academia, it provides insight on how mitochondria are affected by ageing and the consequences of this for physiology and behaviour. Additionally, the thesis provides evidence that mitochondrial dysfunction can be improved with light therapy, encouraging the research of other therapies that focus on mitochondrial dysfunction. More interestingly, we have evidence that mitochondrial targeted therapy can be dependent on circadian factors, especially as we work with light. This needs to be taken into consideration when translating our research into the human condition. We also provide a method to investigate mitochondrial function *in vivo* non-invasively.

Our research has implications on human health and quality of life. The majority of human pathologies have mitochondrial implications, either directly or indirectly. If we are able to translate the applicability of the 670 nm into the clinic, the quality of life of affected patients could improve dramatically, especially in those diseases where mitochondrial dysfunction play a critical role, such as multiple sclerosis or age-related macular degeneration (AMD). Currently there are clinical trials with 670 nm in AMD whose preliminary data are promising. Furthermore, quality of life can be further improved in the wider population in terms of environmental lighting. The majority of artificial lighting used today contains none of the wavelengths known to impact positively on mitochondria. Changes in the way lights and screens are produced could boost red to near infra-red light delivery to humans, having a global impact on their quality of life, especially in ageing and environments where people spend more time indoors.

Similarly, carotenoids are commonly used in the food industry as natural colorants. The carotenoids used correspond to the all-*trans*-β-carotene, whose role as antioxidants in humans is controversial. In this research we show that another stereoisomer, 9-*cis*-β-carotene could have better antioxidant properties in *Drosophila*, data supported by other investigators in other animal and human studies. If correct, this form of carotenes could substitute the *all*-trans isomer in the food industry, and more importantly, be added as a supplement. The

interest of big food corporations, and perhaps pharmaceutical companies, in these compounds is extremely high, and if applied the impact on human health could be important.

Finally we put efforts into developing a method to investigate mitochondrial function *in vivo* non-invasively. Despite being in early phases, it should not be a big major problem to apply in the clinic. This could provide a tool to monitor mitochondrial function and, consequently, the efficacy of mitochondrial targeted therapy allowing personalised therapy.

Table of contents

List of Tables

List of figures

Abbreviations

DNA: Deoxyribonucleic acid

mtDNA: mitochondrial deoxyribonucleic acid

ROS: reactive oxygen species

ATP: Adenosine triphosphate

RNA: ribonucleic acid

NADH: reduced nicotinamide adenine dinucleotide

NAD+: oxidised nicotinamide adenine dinucleotide

ETC: electron transport chain

OXPHOS: oxidative phosphorylation

COX: cytochrome *c* oxidase

H_2O_2: hydrogen peroxide

O_2: oxygen

O_2^-: superoxide anion

SOD: superoxide dismutase

TNF: tumour necrosis factor

IL: interleukin

NO: nitric oxide

Hypotheses

1. Ageing biological systems are severely affected by mitochondrial dysfunction, especially in OXPHOS respiration.
2. Such mitochondrial dysfunction can be reverted with mitochondrial-targeted therapy, leading to an improvement in physiological function and behavioural responses.
3. Flavoprotein autofluorescence can be used to assess mitochondrial function *in vivo* in the retina, and consequences of the inflammatory process on aspects of mitochondrial function investigated.

Chapter 1. Introduction

1.1 Ageing

Ageing can be defined as the progressive decline in functional and physiological integrity. All biological systems are affected, including cellular structure and function, molecular interactions and physiological homeostasis. As a consequence, ageing is associated with a progressive increase in mortality and a wide spectrum of age related diseases.

Interestingly, studies in different model organisms have established that ageing is an evolutionary well-conserved process, both in genetic and biochemical pathways. Different studies have shown that by altering these genetic and biochemical pathways, we are able to influence the rate of ageing. This suggests that the ageing process is relatively plastic[1,2].

However, ageing is a very complex and multifactorial process, including genetic and environment factors. Typically the ageing process is characterised by mitochondrial dysfunction, stem cell exhaustion, altered intercellular communication, epigenetic alterations, genomic instability, deregulated nutrient sensing, altered proteostasis cellular senescence, and loss of physiological and regulatory processes[3]. At a more detailed level of physiological decline, different markers of age-related senescence can be observed in *Drosophila*. These include altered metabolism (decreased fat synthesis, reduced resting metabolic rate), reduced stress resistance, behaviour (reduced courtship, exploration and feeding, and increased sleep fragmentation), reduced reproductive capacity (reduced sperm and accessory fluid production and sperm competition success, decreased egg laying and hatching success), altered neuronal function (impaired learning and memory), modified physical activity (reduced voluntary walking and flying, impaired negative geotaxis), compromised cardiac function, reduced immune capacity, progressive dysplasia and reduced barrier function in the gut[4–7]. These physiological and metabolic changes are accompanied by a general up-regulation of genes related to immune and stress responses, a down-regulation of genes involved in mitochondrial function, protein turnover and reproduction[8]. However, the exact process of ageing is poorly understood.

These ageing features are key as they help to understand how any therapy that tries to target the ageing process may affect the progression of these metric

1.1.1 Theories of aging

As the exact process of ageing is poorly understood, different theories of ageing have been proposed in an attempt to explain ageing. These can be classified in two categories: ageing as a programmed process or ageing being caused by the accumulation of damage. The programmed theories emphasise that the ageing process is a regulated process arising as a consequence of a biological timetable. This regulation would alter gene expression that affects biological systems responsible for maintenance, repair and defence mechanisms.

The damage or error theories imply that different environmental or internal insults on living organisms cause damage inducing ageing. These theories can be further classified in five categories:

1. Wear and tear. Introduced by Weismann[9], which suggests that macromolecules and cells have vital elements that wear out over time resulting in ageing.
2. Rate of living. This theory suggests that lifespan depends on the organism's rate of oxygen basal metabolism. The higher the metabolic rate, the shorter their lifespan[10].
3. Cross-linking. In this theory, the accumulation of cross-linked proteins causes cellular damage and dysfunction, slowing down physiological processes resulting in ageing[11].
4. Free radicals and oxidative damage. First proposed by Gerschman[12], but developed by Harman[13], proposes that free radicals, in particular superoxide induce, damage to cellular macromolecular component, resulting in accumulated damage causing cell, tissues and organs to stop functioning. All cellular macromolecules, nucleic acids, proteins, sugars, lipids are susceptible to damage by free radicals.
5. Somatic deoxyribonucleic acid (DNA) damage. This theory postulates that DNA damages occur continuously. The majority of this damages is repaired by cellular mechanisms, however some accumulate and cannot be repaired by repair mechanisms or DNA polymerases. As the organism ages, these genetic mutations accumulate, and cells deteriorate and malfunction[14]. Of interest,

damage to mitochondrial DNA (mtDNA) might result in mitochondrial dysfunction. Consequently, ageing is the result of damage to the cells (and organisms) genetic integrity.

There are examples and evidence for each of the above categories. However, they are not mutually exclusive, as ageing can be a programmed process and accelerated by building up cellular damage.

Harman's free radical theory of ageing[12,13,15] is consistent with many studies, but many others clearly contradict this, as it has been shown that an increase in endogenous reactive oxygen species (ROS) does not lead to a decrease in lifespan[16]. However, it is accepted that the collective forms of damage are causal factors in the ageing process[17].

However, as dysregulation of the energy metabolism is a hallmark of ageing, mitochondria must play a crucial role in mediating and contributing with the ageing process, outside of their role as ROS producers[3].

1.2 Mitochondria

Mitochondria are double membrane-bound organelles found in the cytoplasm of eukaryotic cells. They are involved in the regulation of multiple metabolic, calcium and signalling pathways, and are key players in programmed cell death[18]. Mitochondrial respiration is the most important function, as it promotes energy production. Mitochondria are able to break down organic components into carbon dioxide and water in a process called oxidative phosphorylation. This process yields energy in the form of adenosine-triphosphate (ATP), the energy currency of cells.

With critical roles in energy production via OXPHOS, Krebs cycle and fatty acid oxidation, mitochondrial dysfunction has been associated with over 40 major health problems and diseases, including cancer, Alzheimer's disease, other neurodegenerative diseases and diabetes[19–21]. Mitochondria are also implicated in amino acid catabolism, ketone body synthesis, heme biosynthesis, urea cycle and calcium storage. With key roles in the energy metabolism and with major consequences of mitochondrial dysfunction, it is critically important to investigate different routes that help preserve optimal mitochondrial functions.

1.2.1 Structure

As semi-autonomous organelles, mitochondria are separated from the cytoplasm by the outer membrane Figure 1.1. This lipid bilayer is porous, allowing the transfer of small uncharged molecules and ions via porins such as the voltage-dependent anionic channels[22]. Larger molecules, such as proteins, need specific translocases. There is no membrane potential across the outer membrane due to its porosity. By contrast, the inner membrane behaves as a tight barrier for ions and molecules. Specific membrane transport proteins aid the transport of ions and molecules across the inner membrane. As a consequence, a natural electrochemical membrane potential is formed across the inner membrane. The inner membrane forms folds or invaginations, that extend deeply in the mitochondrial inner space, the matrix, forming structures called “cristae” increasing the membranes surface[23]. Embedded in the inner membrane are the protein complexes that promote the electrochemical gradient across the membrane, which is used to synthesise ATP in the process of oxidative phosphorylation (OXPHOS).

The mitochondrial membranes define two main different compartments: the matrix, surrounded by the inner membrane hosts the site of mtDNA replication, transcription and proteins synthesis. It also contains numerous enzymes and metabolic routes, such as the Krebs cycle or β-oxidation of fatty acids .The intermembrane space, a ~20 nm gap between the inner and outer membrane, necessary to establish the electrochemical gradient.

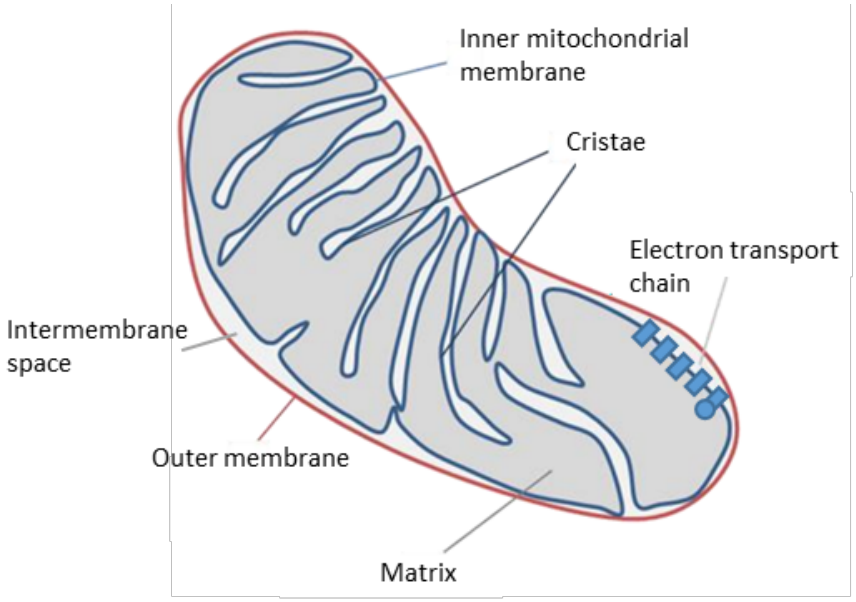

Figure 1.1. Mitochondrial structure. A diagram showing a schematic representation of an ovoid mitochondria with labelled compartments and structure.

1.2.2 Respiration

Mitochondria are the powerhouse of the cells. They are highly specialised in oxidising energy rich lipids and carbohydrates by OXPHOS, generating vast amounts of ATP. However, it is also the site of mitochondrial ROS production.

When carbohydrates enter the cell, these are broken down to pyruvate by glycolysis. The pyruvate is transported into the mitochondrial matrix, where it is converted into acetyl coenzyme A. This group joins the Krebs cycle for additional degradation, generating high energy-rich electrons in the form of reduced nicotinamide adenine dinucleotide (NADH) and carbon dioxide. Fatty acid oxidation also provides energy-rich electrons in the form of reduced flavin adenine dinucleotide ($FADH_2$). NADH and $FADH_2$ (reducing equivalents), transfer their energy-rich electrons to complex I and II of the electron transport chain, respectively. The electrons are then transferred to complex III and complex IV (cytochrome *c* oxidase, COX) through complex redox reactions.

Finally, the electrons are accepted by O_2 producing water. Simultaneously, the energy released from these redox reactions is used to pump H^+ ions out of the mitochondrial matrix into the intermembrane space, generating the proton gradient. Thus, the intermembrane space is charged positively while the matrix is charged negatively generating the mitochondrial membrane potential.

The stored energy in this proton gradient is dissipated by ATP synthase, synthesizing ATP, or by uncoupling proteins, dissipating energy in the form of heat. Hence, the ETC and Krebs cycle need to work coordinately as an optimal NAD^+/NADH ratio is required for efficient mitochondrial function.

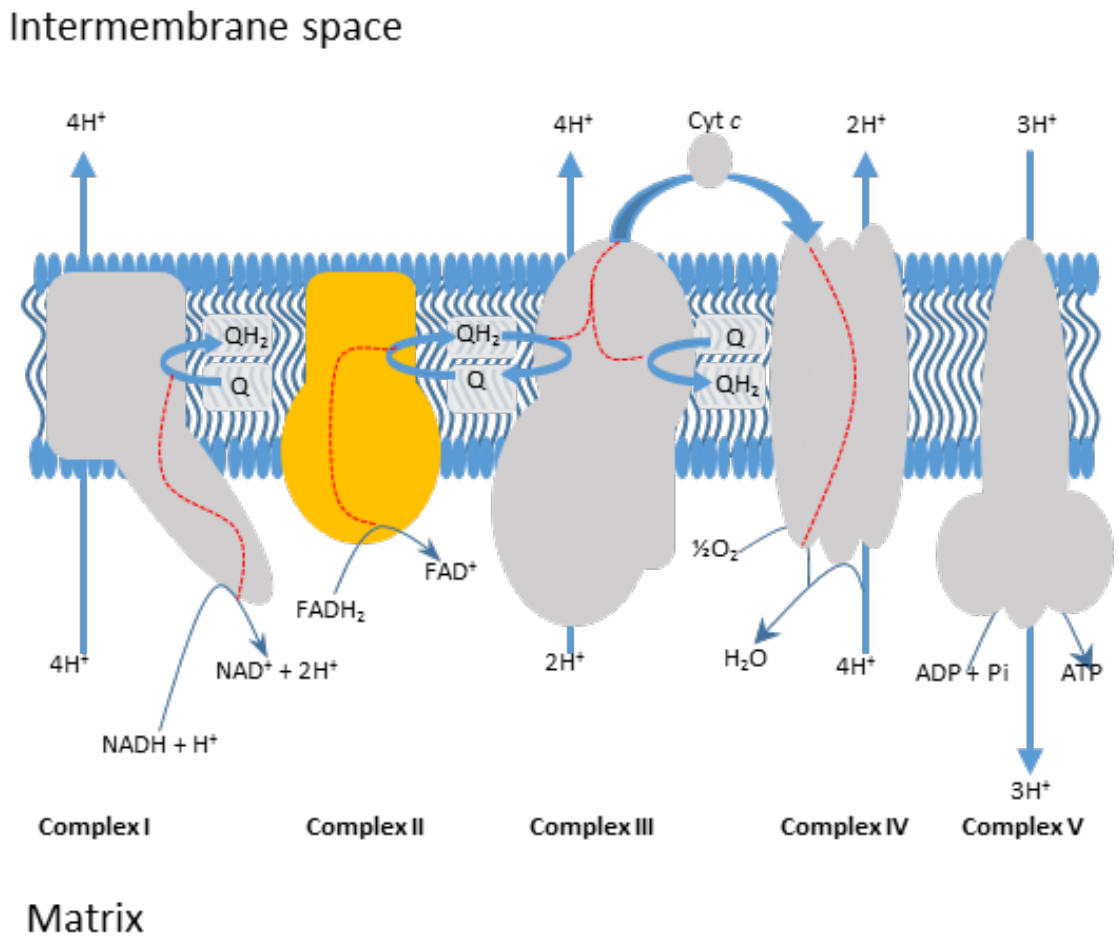

Figure 1.2. Oxidative phosphorylation. Electron transport chain complexes (I-IV) and ATP synthase (complex V) are embedded in the inner mitochondrial membrane. Electrons are accepted via complex I and II and transported to complex III and then to complex IV. Finally, oxygen is the final electron acceptor, reducing to water. The electron transfer (red dashed lines) provides the energy to pump proton across the membrane to the intermembrane space, generating the electrochemical gradient. Complex V uses the generated proton gradient to synthesise ATP. Figure adapted from Nijtmans et al.[24].

1.2.3 Generation of ROS

Mitochondria produce ROS, which play an important role in redox signalling from the mitochondria to the rest of the cell, but are also implicated in oxidative damage in the

organelle. In 1971, Loschen observed that the production of hydrogen peroxide (H_2O_2) was associated to OXPHOS metabolism[25]. Later work showed that H_2O_2 was formed due to superoxide anions (O_2^-) breakdown by superoxide dismutase (SOD) II in the mitochondrial matrix[26]. In the ETC, complex I produces the majority of O_2^-, produced in a reaction with flavin mononucleotide and molecular oxygen[27]. Complex III has been shown to also produce ROS especially during antimycin inhibition, and in complex IV, related to ageing[28]. Interestingly, the majority of ROS are produced in the mitochondrial matrix, and to act as signalling molecules they need to be transported across the inner mitochondrial membrane.

Hydroxyl radicals are produced by the Fenton reaction between H_2O_2 and iron, forming hydroxyl radicals and hydroxide ions. Among them, hydroxyl radicals are known to cause damage to many biological components. However, hydroxyl radicals are short lived, around the femtosecond, compared to H_2O_2 and O_2^-, which both have half lives in the microsecond range[29].

Additionally, nitric oxide (NO) is produced in mitochondria. Nitric oxide is generated by conversion of L-arginine to L-citrulline by nitric oxide synthase. Interestingly, NO, in a dose dependent manner, binds reversibly to the oxygen binding site of complex IV of the ETC, preventing the flow of electrons and decreasing the rate of OXPHOS respiration. When nitric oxide reacts with O_2^-, peroxynitrite is formed, oxidising lipid membranes. Peroxynitrite has also been implicated in the induction of apoptosis[30].

The role of ROS in redox signalling is essential to report mitochondrial homeostasis to other cellular components, including the nuclei. Hydrogen peroxide can modify proteins, acting as a posttranslational regulator. Related to mitochondrial biogenesis, it has been shown that H_2O_2 is able to oxidise and inhibit the catalytic centre of enzymes such as MAPK. Interestingly, the MAPK signalling cascades leads to the transcription of proliferator-activated receptor-gamma coactivator 1alpha (PGC1α), a transcription factor involved in the expression of antioxidants, but more importantly PGC1α is the master regulator of mitochondrial biogenesis. This enables an optimal balance between ROS and mitochondrial function[31].

Cells have defence mechanisms against aberrant ROS signalling and oxidative damage. Several mechanisms are in place to reduce ROS. The superoxide anion is reduced to H_2O_2 by SOD1 in the intermembrane space and cytosol; by SOD 2 and SOD3 in the

matrix and extracellular space respectively. Hydrogen peroxide can be catalysed by several mechanisms. Catalase is present in peroxisomes and converts it to water and oxygen. Peroxiredoxins also reduces H_2O_2 to water. And finally, glutathione peroxidases are also able to reduce H_2O_2, catalysing the oxidation of glutathione to glutathione sulphide by hydrogen peroxide[32].

1.2.3.1 Mitochondrial DNA

Mitochondria, like chloroplasts, are unique among all different cellular organelles. They contain the only nonnuclear source of DNA. Although mitochondrial DNA encodes essential proteins for mitochondrial function, the vast majority of mitochondrial proteins are nuclear encoded[33]. The mtDNA is a double-stranded circular molecule (approximately 16.5 kilobases). This unique DNA encodes for only 13 proteins, 2 ribosomal ribonucleic acids (RNAs) and 22 transfer RNAs. All 13 encoded proteins are components of the different respiratory complexes in the electron transport chain or the ATP synthase[34]. The majority of proteins essential for mitochondrial function are imported from the cytosol, as their genes are encoded in the nuclear genome.

In the absence of mtDNA, mitochondrial respiration and oxidative phosphorylation collapses. Unlike nuclear DNA, mtDNA is not protected by histones: this feature makes the mtDNA highly prone to mutations. Importantly, mutations on mtDNA can affect longevity[35,36].

The mtDNA replication occurs independently from the cellular cell cycle. In addition, a single mitochondrion can contain mtDNA of more than one genotype, termed heteroplasmy. In the presence of a pathogenic mutation, the levels of the pathogenic mtDNA copies will determine whether it will affect mitochondrial function. Typically, the threshold level for mutagenic copies to alter mitochondrial function is high. It is suggested that only mitochondrial mutations that lead to bioenergetic deficiency are the ones contributing to the ageing process[37].

The number of mtDNA copies depends on the tissue and cell type. There is evidence for decreases in mtDNA copy numbers with age, as well as mtDNA transcription activity in different species including mammals[38,39].

Even though mitochondria contain their own genome, their function is dependent on nuclear encoded products and environmental signals in order to accommodate to metabolic cellular requirements. Theses interactions require continuous communications

between the nuclei and mitochondria and *vice versa*. Although the primary mitochondrial function affects ageing, diverse metabolic and cellular alteration promote the ageing process, contributing to secondary modifications in mitochondrial energy homeostasis or mitochondrial biogenesis.

1.2.4 Mitochondria and ageing

The activities of the complexes in the electron transport chain are affected by ageing. Among them, cytochrome *c* oxidase (complex IV) is the most affected one[40]. Across different species, including mammals and *Drosophila*, the activity of this complex decreases by approximately 40%[41–43]. Cytochrome *c* oxidase is also the primary photo acceptor of light in the red to near-infrared region of the electromagnetic spectrum[44–46]. The cytochrome *c* oxidase complex contains four metal redox centres: CuA, CuB, Hem a and Hem a3. In the process of electron transfer, CuA accepts electrons from cytochrome, then they are transferred to Hem a and to CuB-Hem a3, where oxygen is reduced to water. These metal redox centres play a key role in accepting photons in the near to infra-red region of the electromagnetic spectrum.

As discussed earlier, mitochondria are main producers of ROS. During respiration, oxygen is reduced to water by complex IV (cytochrome *c* oxidase). However, this reduction is in several stages, producing a superoxide radical and hydrogen peroxide. These molecules are known as ROS, and commonly they remain bound to cytochrome *c* oxidase until the reduction to water is completed. Less frequently however, oxygen can also partially be reduced by interacting with other reduced components of the electron transport chain, complex I and III. This incomplete O_2 reduction generates ROS[47]. These short-lived ROS are potent inducers of oxidative damage to any biomolecule.

1.3 Inflammation

Inflammation is an adaptive process designed to limit the damage caused by infiltrated pathogens or other dangerous insults on the tissue by preventing the spread of pathogens, and promoting recovery. As such, the inflammatory process is a major first-line defence against infection and injury.

Despite the central nervous system (CNS) being ‘immune privileged’, it lacks a conventional lymphatic system (including the retina), and there is increasing evidence that the inflammatory process plays a major role in physiological, pathological and aging processes within the CNS[48]. Consequently, CNS inflammation has been

associated with severe neurological pathologies, including Parkinson's disease[49], multiple sclerosis[50] or Alzheimer's disease[51]. The eye, or specifically the retina, is not privileged either. Hence the retina is also affected in theses diseases. However, there are also retinal diseases characterised by an increased inflammatory process, such as age-related macular degeneration (AMD) or uveitis[52].

There is evidence that that the inflammatory process is associated with a failure of bioenergetics, not only affecting mitochondrial function directly (via cytokines and other cues), but also affecting the vascular system resulting in inadequate oxygen delivery (and uptake) leading to secondary mitochondrial dysfunction.

In the CNS, including retina, the inflammatory process is characterised by several aspects, including the activation of resident immune cells, such as microglia, and the recruitment of other immune cells, including mononuclear phagocytes and lymphocytes. Furthermore, inflammation is also linked with an excess production of ROS (to fight pathogens) and nitrogen oxide, inducing changes in the vasculature promoting permeability and disturbed blood-flow.

However, limited information exists on the effects of the inflammatory process on mitochondrial function.

1.3.1 Aging and inflammation

With age, the capacity of the body to function properly declines. The inflammatory process is an essential mechanism for normal body function, which is also affected by ageing. During inflammation, the process of repair and restoration following insult inadvertently disrupts cellular homeostasis. This injury-repair cycle, regulated by the inflammatory process is very efficient during youth, when optimal sensitivity and response to signalling molecules (cytokines, prostaglandins, etc.) ensure the general health of the circulating immune cells and tissue homeostasis. However, during ageing repeated and long-term injury-repair cycles change receptor expression and sensitivity to these signalling molecules. For the inflammatory process to work with the same efficiency, a greater concentration of these molecules is required. This is called immunosenescence, the ageing of the immune system as a whole, leading to a natural chronic low-grade inflammation in the elderly[53].

Additionally, increased circulating pro-inflammatory molecules recruit larger cell number to enter circulation from the hematopoietic tissues. Surprisingly, the main

receptor to detect pathogens (Toll-like receptors), and phagocytic activity decreases with age[54]. Consequently, the immune system has not only a lower capacity to fight infections, but also requires a more acute insult to generate an appropriate and effective response. Furthermore, in aged individuals there is a significant increase in the convalescence period required for recovery and clearance from pathogens, concomitant with a decline in tissue repair quality favouring disease progression and morbidity. The elevated levels of inflammatory mediators (cytokines, prostaglandins,…) inadvertly imply a systemic, low-grade, chronic, inflammatory status without an infection, known as inflammaging[55].

Mitochondria play an important role during inflammaging[56]. For instance, the complex Nlpr3 inflammasome acts as a sensor of damaged cellular and organelle components, and initiates the immune reaction necessary for physiological repair. Many signals that activate the inflammasome induce the synthesis and release of ROS. Conversely, mitochondrial dysfunction and cellular damage may also activate the Nlpr3 inflammasome, as many mitochondrial structural components are evolutionary conserved and resemble pathogen-associated molecular patterns, such as damaged un-methylated DNA, due to the phylogenic origin of mitochondria.

It is clear that ageing is a process mediated by the inflammatory process, but mitochondrial function cannot be excluded in this context. In fact, low-grade inflammation and the ageing process share some molecular pathways, such as DNA damage and oxidative stress.

1.3.2 Inflammation and mitochondria

Mitochondria have a role in pro-inflammatory signalling. However, inflammatory mediators can also alter mitochondrial function[57]. In both cases, mitochondrial ROS production increases.

It has been shown that in many inflammatory diseases, such as rheumatoid arthritis, cardiovascular diseases, neurodegenerative disease (including multiple sclerosis and Parkinson's disease), mitochondrial function is impaired. Many inflammatory mediators, including pro-inflammatory cytokines like tumour necrosis factor (TNF)-α, interleukin (IL) 1β or NO, may induce mitochondrial dysfunction. TNF-α and IL1β are able to inhibit complex I of the electron transport chain, decrease ATP production and

mitochondrial membrane potential[58]. Consequently, these inflammatory mediators promote the production of ROS, leading to subsequent oxidative stress.

NO also plays an important role too. NO reacts with the superoxide anion, generating peroxynitrite, which is an irreversible inhibitor of mitochondrial enzymes, affecting mitochondrial integrity[59]. Furthermore, NO is capable of reversibly inhibiting complex IV of the electron transport chain, associated with a decrease in ATP production and reduced mitochondrial membrane potential[59].

Taken together, mitochondrial respiratory complexes can be permanently altered by the inflammatory process (mainly via ROS production an oxidative stress and by peroxynitrite). Other mediators, such as NO and cytokines, induce reversible modifications to mitochondrial respiratory complexes. The combination of both effects, during low-grade chronic inflammation, leads to a sub-lethal mitochondrial damage, generating a vicious cycle of increased inflammation.

Preserving mitochondrial function and structure could reduce excessive oxidative stress, preserving tissue physiological function, and consequently delaying aging.

Chapter 2. The effect of 670 nm light on aged *Drosophila melanogaster*: exploring biochemical mechanisms and physiological, functional and behavioural responses.

The majority of the data shown in this section has been published in Neurobiology of Aging.

Weinrich, T. W., Coyne, A., Salt, T. E., Hogg, C., & Jeffery, G. (2017). Improving mitochondrial function significantly reduces metabolic, visual, motor and cognitive decline in aged *Drosophila melanogaster*. *Neurobiology of aging*, 60, 34-43.

and

Weinrich, T. W., Hogg, C., & Jeffery, G. (2018). The temporal sequence of improved mitochondrial function on the dynamics of respiration, mobility and cognition in aged *Drosophila*. *Neurobiology of aging,* 70, 140-147.

Publications can be found in the Appendix.

2.1 Introduction

2.1.1 *Drosophila* as a model

Drosophila has emerged as an excellent tool to study the complexity of the aging process. It has a relative short life-span (approximately 12 weeks), it is mainly composed of post-mitotic cells and the fly genome has been fully sequenced. Moreover, more than 50% of its genes have homologues in humans[5].

Like in other species, with age changes in behaviour, physiology and mitochondrial function are observed in *Drosophila*. Specifically in behaviour, there are clear differences in young *versus* old flies: young flies are very energetic and possess high fitness. As they age, they become progressively less active with reduced fitness[5].

Other features of ageing are related to increased oxidative stress and reduced mitochondrial function[37]. In *Drosophila*, ATP levels decline by 50% at 5-6 weeks, consistent with a decrease in the activity of cytochrome *c* oxidase[60]. The structure and number of mitochondria are altered during ageing, with mitochondrial numbers

declining and their size increasing[61], suggesting a dysregulation of mitochondrial dynamics due to mitochondrial dysfunction.

With age, there is a progressive deterioration of physiological function, known as functional senescence. Hence, there are clear parallelisms between *Drosophila* and mammals. A number of functions can be assessed in flies, and the majority of them decline with age[5]. Strikingly, much of the age-related functional decline occur rather quickly in the fly[5]. Furthermore, since adult *Drosophila* consist mostly of post-mitotic cells (except gut, where stem cells are found), any changes in function are associated with a failure to maintain homeostasis in existing cell population, as opposed to the inability to support continued cellular replication.

A number of different physiological, biochemical and behavioural assays have been developed for *Drosophila*, enabling the assessment of functional senescence and biochemical changes due to ageing. These assays allow us to monitor the consequences of ageing and test whether any intervention modulating mitochondrial function lead to functional improvements. These attributes make the aged fly a perfect tool in ageing and mitochondrial research.

2.1.1.1 Lifespan intervention: genetic and environmental effects

The rate of ageing is determined by both genetic and environmental factors[62]. By modifying these genetic and environmental factors we are able to modulate the aging process. Among the best known genetic methods to extend lifespan is the downregulation of the nutrient-sensor insulin/IGF signalling pathways and the mammalian target of rapamycin[63,64]. Other genetic interventions with an effect on lifespan include over-expression of the NAD^+ dependent histone deacetylase Sir2, loss of the G-protein coupled receptor methuselah, loss of the mitochondrial co-transporter I'm Not Dead Yet (INDY), as well as downregulation of the mitochondrial electron transport chain[65]. Different environmental factors also contribute to lifespan, including diet, oxidative stress and increased inflammation.

2.1.2 Light and Photobiomodulation

2.1.2.1 Light and matter interaction

Light is a type of electromagnetic radiation characterised by having both wave-like and particle-like properties. All living organisms on earth are immersed in electromagnetic

radiation, composed of oscillating electric and magnetic fields. The electromagnetic radiation travels space and transfers energy. Thus, light is energy.

An electromagnetic radiation wave has a unidirectional vector with three components: wavelength (λ, the distance between successive peaks or troughs), frequency (number of oscillations per second) and amplitude (distance between peak and troughs). Moreover, in quantum physics, electromagnetic radiation is composed of energy particles (photons) that travel the space at a speed of 3×10^8 m/s. The amount of photons establishes the brightness of the light, while the wavelength determines the colour.

A mixture of waves with different frequencies, amplitudes, and wavelengths are absorbed, scattered, and reflected by objects, including biological material. Therefore, when light is absorbed by biological systems, the energy in photons is transferred. This transfer of energy between photon and biological material may have effects on biological systems.

2.1.2.2 Photobiomodulation

Photobiomodulation can be defined as the use of light to modulate biological function or induce therapeutical effect in a non-destructive and non-thermal manner. Consequently, the effects of photobiomodulation implicate the conversion of luminous energy to metabolic energy with an effect on the biological function of cells.

The red to near-infra red wavelengths (λ = 600-1100 nm) have been shown to be the most effective light in inducing a beneficial effect *in vivo* on cells that do not have a specialised photopigment[66]. This is in part attributed to the narrow window where water does not absorb light (Figure 2.1) in the spectrum. Also, wavelengths in this range have higher penetration power compared to lower wavelength in the spectrum (violet and ultra violet). Furthermore, below 600 nm light is scattered in biological systems as melanin pigments and haemoglobin absorb lower wavelengths, as depicted in Figure 2.1. ***The optical window of photobiomodulation***. *Photobiomodulation in the red to near-infrared is dependent on the decreased absorption by water and other chromophores (haemoglobin and melanin) in these wavelengths. Image adapted from Chung et al.*[67]

In summary, photobiomodulation is based on the principle that molecules in biological systems are able to absorb photons and trigger downstream signalling pathways in response to light absorption.

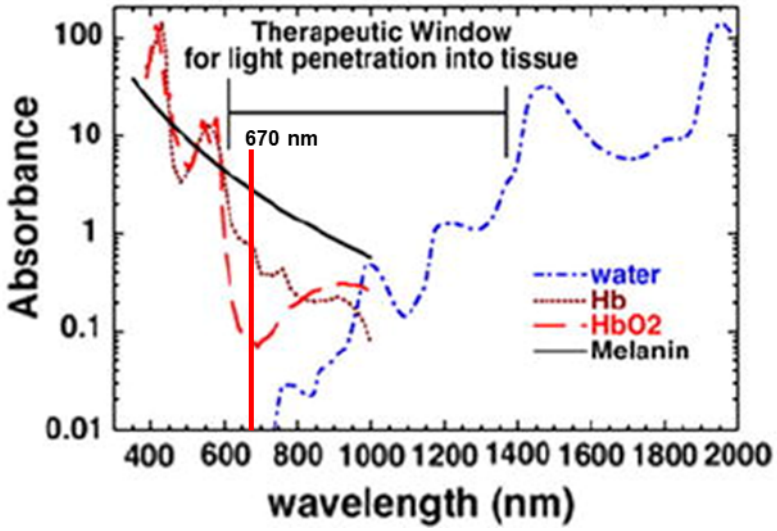

Figure 2.1. The optical window of photobiomodulation. Photobiomodulation in the red to near-infrared is dependent on the decreased absorption by water and other chromophores (haemoglobin and melanin) in these wavelengths. Image adapted from Chung et al.[67]

2.1.2.3 Mechanism of action: 670 nm

It is widely accepted that cytochrome *c* oxidase is the main biological photoacceptor of light in the red to near-infrared region of the electromagnetic spectrum[44–46]. Cytochrome *c* oxidase is a key enzyme in eukaryotic cells, particularly in the mitochondrial electron transport chain system.

Cytochrome *c* oxidase is complex IV of the mitochondrial electron transport chain, which catalyses the transfer of electrons from cytochrome *c* to oxygen reducing it to water. The expression of this enzymatic complex is tightly regulated and coupled to energy demand, free radical metabolism and cell death pathways.

The photochemistry of cytochrome *c* oxidase has been extensively characterised by Karu[44–46]. Specifically, cytochrome *c* oxidase contains four redox metal centres: CuA, CuB, Hem a, and Hem a3 as shown in Figure 2.2.a. These Cu elements are able to absorb light in the red to near-infra red spectrum (Figure 2.2.b). In particular, 670 nm increases the oxidation of cytochrome *c*, boosting the transfer of electrons, increasing oxygen consumption and mitochondrial membrane potential, highly correlated with peaks in COX catalytic activity and ATP content *in vivo*[68].

The secondary effects occur as a consequence of the primary effect described above. These include a cascade of downstream biochemical reactions that change cellular

homeostasis. Secondary effects are pleiotropic and can occur hours or days after light exposure.

After light exposure, the initial phase of secondary mechanisms is characterised by an increase in the NAD^+/NADH ratio and mitochondrial membrane potential, dissociation of nitric oxide from cytochrome *c* oxidase complex and an increase in the ATP pool[44]. This change in the ATP pool significantly alters cellular metabolism. Finally, all these secondary effects activate the retrograde signalling between the mitochondria and nuclei[69]. One consequence of retrograde signalling is potential changes in gene expression (Figure 2.3).

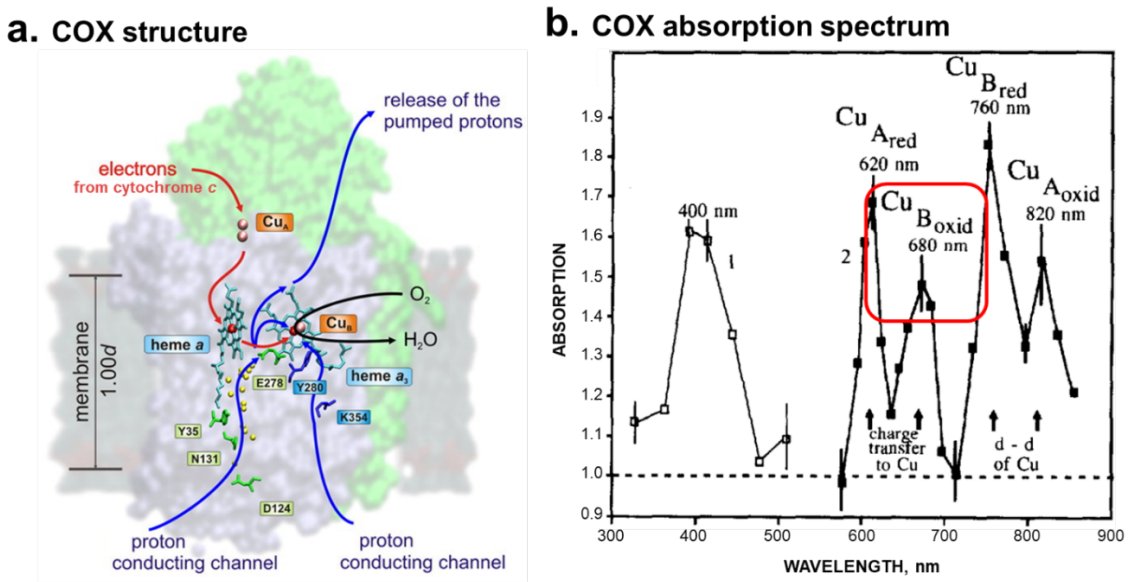

Figure 2.2. Structure and absorption spectrum of cytochrome *c* oxidase (COX). (**A**) Cytochrome *c* oxidase is an integral protein in the inner mitochondrial membrane containing redox active metal centres, copper (CuA and CuB) and heme groups (a and a3). The red arrows show the transfer of electron from cytochrome *c* to O_2, while the blue arrows show the proton transfer routes in the enzyme. (**B**) Cytochrome *c* oxidase absorption spectrum in the range λ=300-900 nm, with peaks assigned to oxidised and reduced CuA and B molecules. Of interest, the oxidised CuB absorption peak at 680 nm. Images modified from (**A**) Belevich et al[70] and (**B**) Karu[44].

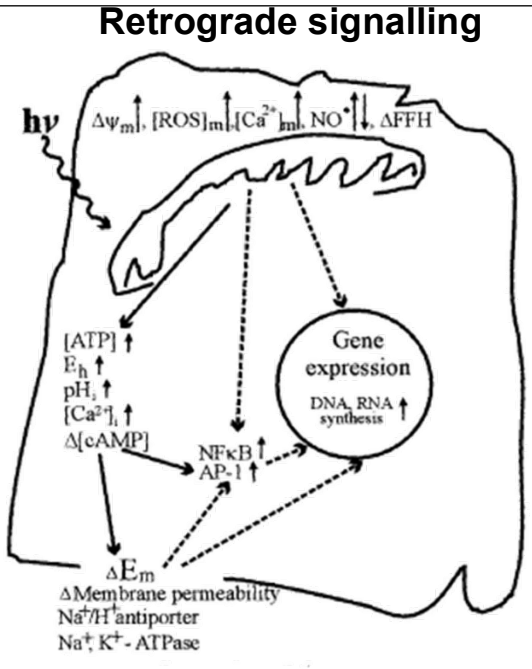

Figure 2.3. A schematic diagram representing the putative mitochondrial retrograde signalling. After light absorption by cytochrome *c* oxidase, changes in the energy homeostasis inside the mitochondria and cell occur. One consequence is the retrograde signalling between the mitochondria and cellular nuclei. Thus the retrograde signalling monitors the cellular energy homeostasis by a constant communication from the mitochondria to the nuclei reporting the mitochondrial energy status. Image adapted from Karu 2008[69].

2.1.2.4 670 nm on Drosophila

In *Drosophila*, daily 20 min life-long exposure to 670 nm increases mean life-span, global ATP levels and cytochrome *c* oxidase protein levels[71,72]. However, very little is known about 670 nm intervention therapy in aged flies.

2.1.3 Hypothesis

Here we investigate whether short-term 670 nm exposure ameliorates or improves functional senescence in aged flies. To date, no work has examined the consequences of short term 670 nm exposure in a model of aged fly known to have mitochondrial functional and structural dysfunction. Therefore I would like to test the hypothesis:

- Short-term 670 nm exposure on aged flies induces changes in the mitochondrial function,
- This improvement in mitochondrial efficiency leads to an overall improvement in healthspan, consequently improving or ameliorating functional senescence.

We will test different biochemical, physiological and behavioural assays in young (2 weeks), old (6 weeks) and old flies that have been treated for 1 week with 670 nm (5 weeks + 1 week 670 nm).

2.1.4 Aims

The specific aims of this study are to:

- Investigate the consequences of ageing in global ATP levels, metabolic rate, cytochrome *c* oxidase catalytic activity, relative mtDNA content, glycogen, glucose and triglyceride levels, increased stress load and resistance to food starvation and sensory, cognitive and locomotor function, by comparing young (2 weeks) and old (6 weeks) flies.
- Assess the effect of daily 20 min 670 exposure for seven days on aged flies (5 weeks + 1 week 670 nm exposure) on the parameters cited in 1.
- Explore the consequences of one dose 670 nm exposure in aged flies in regards to metabolic rate, global ATP levels and locomotor function.

From the results obtained above, infer putative downstream mechanisms of 670 nm that are affected to explain observed changes in function.

2.2 Materials and methods

2.2.1 Fly stocks and husbandry

The wild-type, outbred *Drosophila melanogaster* Dahomey laboratory stock was used throughout. Fly stocks were housed in population cages (20 cm W x 30 cm D x 20 cm H) with overlapping generations. For all experiments, newly hatched adults were collected and sorted selecting only male flies and kept at standard density of 30 male flies in food vials (25 x 95 mm) containing 10 mL food medium. Flies were aged in these vials and food was changed 3 times a week. All stocks and experimental vials were maintained and conducted under a 12 h:12 h / light:dark cycle at 25˚C and 70% humidity on normal cornmeal/sugar/yeast/agar medium (7% cornmeal, 6% sucrose, 1.2% yeast, 0.8% agar (w/v in water), and supplemented with 2% (v/v) of 10% Nipagin and 0.04% Carbendazim (w/v) in absolute ethanol).

2.2.2 670 nm exposure

Two different treating regimes were used. For single dose experiments, a 90 min exposure on 6 week old flies was given. In the case of 7 days treatment, five weeks old

flies were exposed to 670 nm for 20 min per day at 40 mW cm^2 for 7 days, illuminating flies from either side. An additional control group was used where the vials were blacked out with aluminium foil and placed in the 670 nm chamber. Light devices were built by C. H. Electronics UK and contained 50 670 nm LEDS over 20 cm^2.

2.2.3 Glucose and glycogen measurements.

Glucose and glycogen levels were determined as described previously[73]. Briefly, in each sample 5 flies were homogenised in 100 µL cold phosphate-buffered saline (PBS) with a motorised pellet pestle followed by 10 min at 70 ˚C treatment. The homogenate was diluted 1:3 in PBS and centrifuged at maximum speed for 3 min at 4 ˚C. The supernatant was collected, and glucose levels determined with the Glucose (hexokinase) Assay Kit (Sigma). The hexokinase reaction was performed for 15 min at room temperature and absorbance at 340 nm was measured using a plate reader. To determine glycogen levels, untreated samples were compared to samples supplemented with 1 µg/mL amyloglucosidase (Sigma). Amyloglucosidase was used to hydrolyse glycogen into glucose molecules. The absolute glycogen and glucose levels were determined by the standard glucose curve. A standard curve of glucose was used to determine the glycogen and free glucose content of *Drosophila*. To determine the glycogen levels, free glucose levels were subtracted to each corresponding glycogen sample. Samples and standard were analysed in duplicate. Free glucose and glycogen levels were normalised to protein levels in the corresponding homogenate. Protein concentration was determined in duplicate using the Pierce BCA Protein Assay Reagent Kit (ThermoFisher Scientific, UK). Samples were assayed in replicates of 5.

2.2.4 Triglyceride measurement

Glucose and glycogen levels were determined as described previously[73]. Briefly, 5 flies in each sample were homogenised in 100 µl PBS 0.05% Tween 20 (PBST) and heat treated for 10 min at 70 ˚C. Two aliquots of 20 µl for each sample were treated with PBST (free glycerol) and triglyceride reagent (Sigma) and incubated for 45 min at 37 ˚C. The triglyceride reagent was used to breakdown the triglycerides into fatty acids and glycerol. To measure the glycerol in the samples, free glycerol reagent (Sigma) was added and incubated for 5 min at 37 ˚C and absorbance determined at 540 nm with a plate reader. A glycerol standard curve was used to determine triglycerides content in each sample. To determine the triglycerides levels in *Drosophila*, the free glycerol levels (aliquot treated with PBST) were subtracted to the corresponding triglyceride

sample content (aliquot treated with triglyceride reagent). Samples and standard were analysed in duplicate. Free absolute glycerol and triglycerides levels were normalised to protein levels in the corresponding homogenate. Protein concentration was determined in duplicate using the Pierce BCA Protein Assay Reagent Kit. Samples were assayed in replicates of 5.

2.2.5 *Drosophila* starvation resistance/survival

Starvation resistance was assessed. 20 flies were placed in a vial containing 10 mL of 1% agar (Sigma) in distilled water. Mortality rate was determined by regularly counting the number of dead flies in each tube, diagnosed by the lack of a proper standing posture (every 8 hours for the first 2 days, then every 12 hours). Vials were changed every 24 hours. A total of 80 flies per group were used.

2.2.6 Heat stress

Heat stress was determined as previously published[74]. 15 flies were placed in empty vials, with no food or water. The flies were left to acclimatise at 25 °C for 30 min. A 1 h heat stress was applied by placing the vials in a water bath at 37 °C. Flies were left to recover for 30 min at 25 ° and transferred into fresh vials containing food. Living flies were recorded after 2, 4 and 24 h later. A total of 105 flies per group were tested for heat sensitivity.

2.2.7 Chilled Coma Recovery Time

Chilled Coma recovery time was determined as previously published[75]. Flies were placed in 5 mL vials (10-15 flies) and submerged in a -2 to 0 ˚C water bath, without causing immediate mortality. After the treatment, flies where left at RT and the spontaneous chill coma recovery time recorded, the time when the flies acquired a standing position. A total of 60 flies were used per group.

2.2.8 BCA Protein Assay Reagent Kit

Protein measurement was performed using a commercially available kit, BCA Protein Assay by ThermoFisher Scientific (catalogue number 23225, Dartford, UK). Bovine serum albumin (BSA) was used as a standard and the amount of protein was measured following the manufacturer's protocol. 25 µL from each sample was required as well as a standard (BSA, from 0 to 20 mg/mL) and the concentration was measured in a 96 well plate, clear bottom (Costar). 200 µL of working reagent was added and incubated for 60-70 min at room temperature. After the incubation period, the absorbance at 562 nm

was measured using Biotek ELX 800 microplate reader (Bio-Tek Instruments, UK). The corrected absorbance at 562 nm for each BSA standard was plotted vs. its concentration in mg/mL, and the standard curve was used to determine the protein concentration for each unknown sample.

2.2.9 Measurement of metabolic rate

The metabolic rate, as a way of measuring respiration, was measured following a protocol previously described with lab-made respirometers[76]. The respirometer is depicted in Figure 2.4. It consists of a 1 mL sealed pipette tip attached to a glass capillary, inserted in a container with coloured water. Each respirometer contained 5 flies. It contains soda lime, which absorbs expelled CO_2 decreasing the pressure in the capillary. The change in gas volume (in the form of decreased gas pressure) is measured by the displacement of fluid in the glass capillary. The measurement of expellec CO_2 is a mean of metabolic rate. The metabolic rate is measured over a period of 2 h.

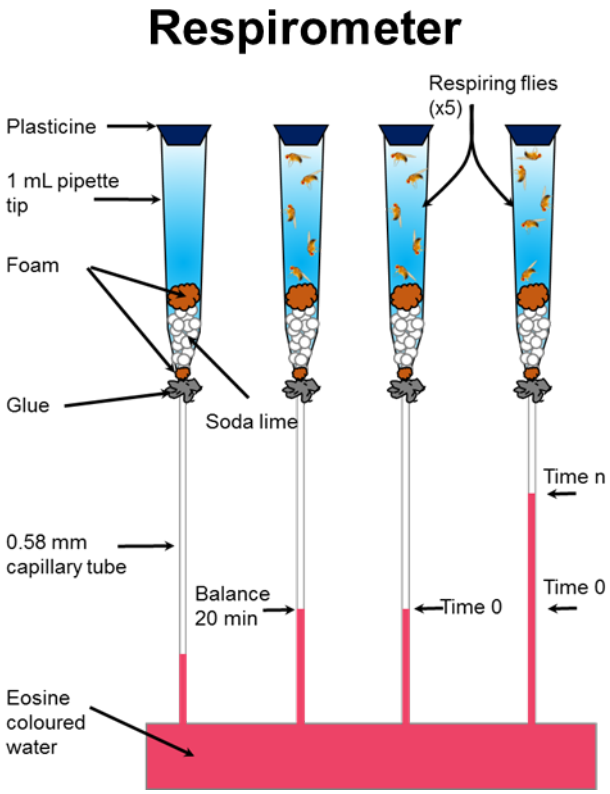

Figure 2.4. Schematic diagram of laboratory-made respirometers to measure whole body metabolic rate in *Drosophila*. CO_2 production was measured in simple respirometers where flies were sealed in glass pipette tubes that contained soda lime at their base. The end of the tube was placed in water containing eosin to colour it. This

method was developed by Yatsenko et al[76]. As the flies breath they produce CO_2 that is absorbed by the soda lime which reduces the air pressure in the pipette, which in turn results in coloured water moving up the tube. Hence, greater respiration results in greater movement of liquid up the capillary tube. Prior to measurement the animals are left for 20 mins for acclimatization and stabilisation.

2.2.10 Cytochrome *c* oxidase (complex IV) enzymatic assay

The specific activity of complex IV was measured following a protocol previously published[77]. Complex IV activity was measured by determining the rate of oxidation of reduced cytochrome *c* at 550 nm. The reaction mixture contained 5 mM MgCl2, 2 µg/ml rotenone, 2 µg/ml antimycin A, 1 mM DDM, 45 µM cytochrome c. Each test contained 15 µg of mitochondrial fraction. The reaction was inhibited with 4 mM KCN. Sodium dithionite was used to reduce cytochrome *c*[78]. Each group consisted of 5 replicates containing 15 flies each. Measurements were in duplicate.

2.2.11 ATP levels

ATP measurements were performed using a commercially available ATP determination kit, based on the luciferase assay (A22066 ThermoFisher Scientific, UK). Flies were prepared as previously described[74]. Briefly, 5 flies per sample were homogenised in 100 µL of 6M guanidine-HCl in extraction buffer (100 mM Tris and 4 mM EDTA, pH 7.8) followed by a 5 min at 95˚C treatment in order to inhibit ATPases. The samples were centrifuged at maximum speed for 3 min at 4 ˚C, and supernatant collected. The supernatant was diluted in 1/50 in extraction buffer and mixed with the reaction mix. Luminescence was measured in a plate reader luminometer. Whole fly ATP levels were obtained by interpolation from a standard curve of known ATP concentration. Relative ATP levels were calculated by dividing the whole fly ATP levels by their protein concentration, measured with a BCA assay.

2.2.12 Reactive oxygen species levels

ROS levels were measured using dichloro-dihydrofluorescein diacetate DCFH-DA as previously described[79]. The sample was prepared by homogenizing the heads of 10 flies in 200 µL ice-cold Tris-HCl buffer (0.4M; pH 7.4) followed by a 10 min centrifugation at 2000 x g at 4˚C. From each sample, 100 µL was added to each well of a microplate containing 15 µL of 5 µM DCFH-DA, and total volume adjusted to 200 µL with

homogenizing buffer. After 1 h incubation at room temperature, the plate was read in a sprectrofluorometer. ROS interact with DCFH-DA converting it into dichlorofluorescein (DCF). The conversion of DCFH-DA to DCF was measured at 489 nm excitation and 525 nm emission wavelength. 60 heads were used for 2 weeks old flies, 70 for 6 week old flies and 90 heads for the 670 nm treated group.

2.2.13 Immunofluorescence: Cytochrome *c* oxidase and β–actin.

To probe the flies for cytochrome *c* oxidase and β–actin staining, a standard protocol was used[80]. 10-15 flies per group were killed and decapitated in sterile PBS. The heads were fixed for 2 h in 4% paraformaldehyde in PBS at room temperature (RT). After fixation, the heads were incubated overnight (ON) at 4˚C in a 40% sucrose in PBS solution for cryoprotection. The following day, the fly heads were embedded in optimal cutting temperature compound and stored at -80˚C. 10 μm thick section were cut, and left to dry at RT for 6 hours, prior to storing them at -80C. The day the slides were stained for cytochrome *c* oxidase subunit III and β–actin, the sections were briefly rinsed in PBS, following a 4 h blocking step with 5% normal donkey serum in 0.5% Triton X-100 un PBS to block unspecific antibody binding. After blocking, the diluted primary antibody (1/800, goat anti cytochrome *c* oxidase subunit III, Santa Cruz Biotechnology, CA, USA, and 1/500 rabbit anti beta-actin, Abcam ab8227, Cambridge, UK) was applied and incubated for 24 h at 4˚C followed by a 1 h incubation at RT (diluted in PBS containing 2% NDS, Triton X-100 0.5%). The slides were washed 3 times with PBS + Triton-X 100 0.5% for 5 min each time. The fluorochrome conjugated secondary antibody was added and incubated for 3 hours at room temperature (Alexa donkey anti goat 568 nm, 1/1000, and Alexa donkey anti rabbit 488 nm, 1/1000, diluted in PBS containing 2% NDS, Triton X-100 0.5%). The slides were washed 3 times in PBS containing Triton X-100 0.5%, followed by a single wash in PBS only. The coverslips were added and mounted in Vectashield Hardset (Vector Laboratories, Burlingame, CA, USA). Slides were left to dry at room temperature for 2 h and sealed with nail varnish. Slides were stored at 4˚C.

2.2.14 Mitochondrial and cytosolic isolation, and DNA quantification

Mitochondrial and cytosolic isolation was performed as previously published[81]. 10 male flies were gently homogenised in 500 μl chilled isolation buffer (225 mM mannitol, 75 mM sucrose, 10 mM MOPS, 1 mM EGTA and 0.5% fatty acid free BSA, pH 7.2). The homogenised flies were centrifuged at 300 × g for 5 min at 4°C. To enrich for

mitochondria, the supernatant was centrifuged at 6000 × g for 10 min at 4°C. The pellet was resuspended in 100 µl respiration buffer (225 mM mannitol, 75 mM sucrose, 10 mM KCl, 10 mM Tris-HCl, 5 mM KH2PO4, pH 7.2). The supernatant is the cytosolic fraction. The freshly obtained fractions were processed for DNA quantification. For that purpose, RNA was removed by RNAse A treatment (Thermo Scientific), and the DNA was determined spectrophotometrically (NanoDrop ND-1000).

2.2.15 Climbing – negative geotaxis (locomotor)

The negative geotaxis assay was used to determine the motor function of the flies as previously described[82]. Briefly, the day before the assay was performed, 80 to 100 flies (for each group, control and 670 nm treated) were housed in 10 individuals per vial with CO_2 anaesthesia to minimise any side effects of the anaesthesia on the day of assay. The climbing apparatus consists of 2 empty polystyrene vials vertically joined with tape. The lower vial contains an 8 cm mark above the bottom. On the day of the assay, 10 flies were transferred to the empty bottom vial and flies were allowed to acclimatise to the new environment for 1 min. Then, the flies were gently tapped down to the bottom of the vial and number of flies that pass the 8 cm mark were counted in the first 10 seconds after the tap. The climbing index was determined as a percentage of flies that climbed above the 8 cm line relative to the total flies. Flies were allowed a resting time of 1 min prior to repeating the test. The trials were performed 10 times for each group of 10 flies.

2.2.16 Short term memory (cognitive)

An aversive phototaxis suppression assay (APS) was used was used to assess short term memory in flies, modified from Yousof et al[82]. Briefly, this test exploits the positive phototactic behaviour in flies in training them to associate light with an aversive stimuli (quinine, 1 µM). The day before the test was performed, flies were starved ON in empty food vials with wet filter paper. On the day of the assay, flies were transferred into empty food vials and assessed. The APS apparatus consists of two independent chambers joined by a trap door: the dark chamber and the lighted chamber (attached to a gooseneck light source), which also contains the quinine solution. Flies were trained in a dark environment by introducing them into the dark chamber of the APS apparatus and were allowed to acclimatise for 30 sec. After that, filter paper containing the aversive quinine solution was introduced into the light chamber, the light source was turned on and the trap door was opened. The flies with positive phototactic behaviour

were allowed to explore the light chamber for 1 min, when they were tapped back to the dark chamber. The trap door was closed and the light turned off. The flies were allowed 30 seconds of acclimatising. For each fly, 10 training tests were performed. Immediately after the training, 5 trials were conducted. In the same setting, if after 10 sec of light being turned on the fly did not cross into the light chamber containing the aversive quinine, it was considered as task learnt. This was repeated 5 times. After this, only flies that successfully passed at least once the task were used to assess short term memory.

After training and initial trial, the successfully trained flies were individually transferred into food vials and kept aside for 6 hours. After that time, flies were tested in the same way as before, as an indicator of short term memory.

2.2.17 Flicker electroretinogram (ERG)

Drosophila were immobilised with full eye accessibility on a microscope slide with Blue Tack® and nylon mesh avoiding movement interference. The mounted fly was placed in an electrically shielded dark recording chamber. A stainless steel indifferent (earth) electrode was inserted into the thorax. Visual stimulation consisted of trains of light flashes (50% duty cycle) at 0.5, 2, 5, 10, 20, 30, 50, 100 Hz (white light flashes at 0.3 W/m^2 (background 0.2mW/m2). Electrical responses to the flashes were recorded via an Axoprobe 1A amplifier, digitized (5 kHz) by a CED1401 interface and stored on a PC. Two weeks (N=8), 6 weeks (N=7) and 6 weeks exposed to 670 nm for one week (N=11) flies. The flicker ERG were obtained with the assistance of Professor Thomas E. Salt.

2.2.18 Experimental setup for Buridan paradigm

The Buridan paradigm refers to a situation where an animal is placed between 2 equally appealing stimuli, which in this case are visual targets in the form of vertical stripes inside a drum. The design for this experiment (Figure 2.5) was adapted from a previous publication[83]. The setup consists of a round white platform (90 mm in diameter), surrounded by a water moat at the bottom of a translucid paper cylinder (150 mm in diameter, 290 mm in height). The setup was uniformly illuminated with LED lights. Visual stimuli were achieved with 2 black cardboard stripes (11 mm in width, 290 cm in height), which were taped on the inside of the cylinder. The retinal size of the stripes

depended on the position of the fly on the platform, but was 11° wjem the fly was in the centre of the platform.

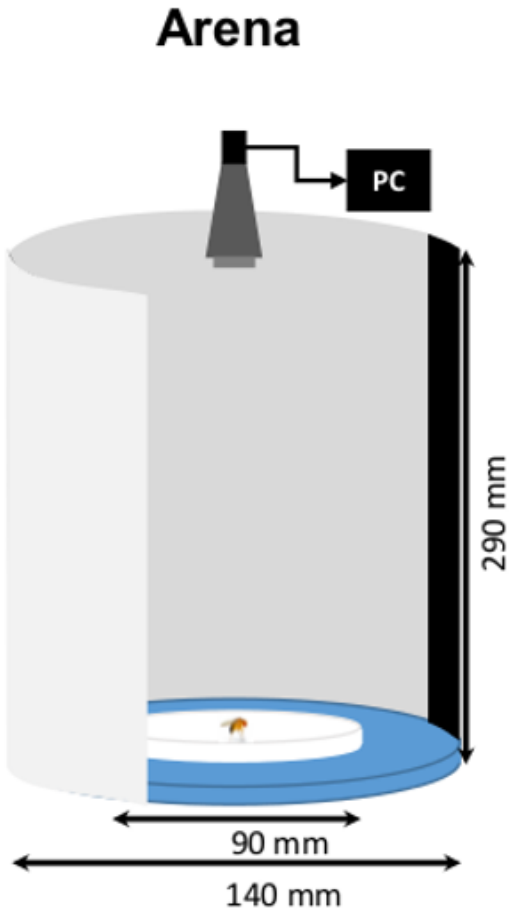

Figure 2.5. Schematic diagram of the open-field arena. Flies were placed on a circular island surrounded by water. A tall translucent screen homogenously illuminated surrounded the setting. Fly movement was filmed over a 15-minute period, and data were fed into a PC. Young flies explore the perimeter of the island circling its edge. Old flies tend to spend more of their time centrally and move less. This technique and the free software for analysis of movement were developed by Colomb et al [83].

2.2.19 Fly handling

One day before the experiment, the wings of the flies were clipped under CO_2 anaesthesia. Flies were left to recover overnight, in normal housing conditions. On the day of experiment, after the 670 nm exposure, flies were transferred to the experimental setup. Flies were not left to acclimatize to the environment. The duration of the experiment was set at 15 minutes. If flies jumped into the water moat, tracking was

automatically suspended and fly was returned to the platform using a brush. The experiment was then resumed.

2.2.20 Software analysis

The software for fly tracking (BuriTrack) and raw data processing (CeTrAn) is freely available from the internet. Fly movement was recorded with a standard commercial webcam (Logitech C270). The position coordinates of the fly and their trajectory data are obtained with the BuriTrack software. The software, CeTrAn, imports the position, coordinates, and trajectory data from the BuriTrack software. CeTrAn then extracts different metrics, including median speed, distance travelled, turning angle, total activity time, and trajectories[83].

2.2.21 Statistical analysis

Data were analysed with GraphPad Prism v.6 (San Diego CA, USA) and statistical analysis was undertaken using two-tailed Mann Whitney U test unless otherwise stated. Data presented are mean + SEM. The significance was asserted as * $p<0.05$, ** $p<0.01$, *** $p<0.001$.

2.2.22 Reagents

Reagents were purchased as indicated. All general chemicals were acquired from Sigma-Aldrich (UK).

2.3 Results

2.3.1 Effect of a single 90 min exposure on 6 weeks old *Drosophila*

2.3.1.1 Metabolic rate, cytochrome *c* oxidase catalytic activity, ATP levels and ROS.

To assess the initial effects of 670 nm exposure on aged flies, 6 week old flies were exposed to 670 nm light for 90 min. Various parameters were investigated to demonstrate that previous work done on the immediate effects of 670 nm exposure could be replicated in our *Drosophila* model.

It is known that the immediate consequences of 670 nm light exposure are an increase in respiration, an increase in the catalytic activity of cytochrome *c* oxidase (COX) and an augmented ATP pool as discussed in the previous section. Previous work in our laboratory showed that a lifelong 670 nm exposure increases ATP levels in *Drosophila*[71]. To assess whether a 90 min 670 nm light exposure had an effect on

respiration, COX activity and ATP pools, we measured metabolic rate before, during and after the exposure, and ATP levels at specific time periods after light treatment. We also assessed for COX activity and ROS levels after light exposure.

Figure 2.6 shows cumulative respiration and ATP levels after a 90 min 670 nm exposure. In the treated group of flies, there was a significant increase in the respiration rate 20 min after the start of 670 nm light compared to non-exposed flies. This increase in respiration rate was present for the remaining treatment period and after the light was switched off (Figure 2.6a).

An increase in respiration is associated with an increase in proton pumping into the intermembrane space, which will boost ATP production. Therefore we assessed ATP levels, shown in Figure 2.6b. However, we found that the increase in ATP levels followed a different pattern that of respiration. ATP levels increased significantly 3 hours after light exposure compared to the non-treated group, although a gradual non-significant increase was seen from 1h onward.

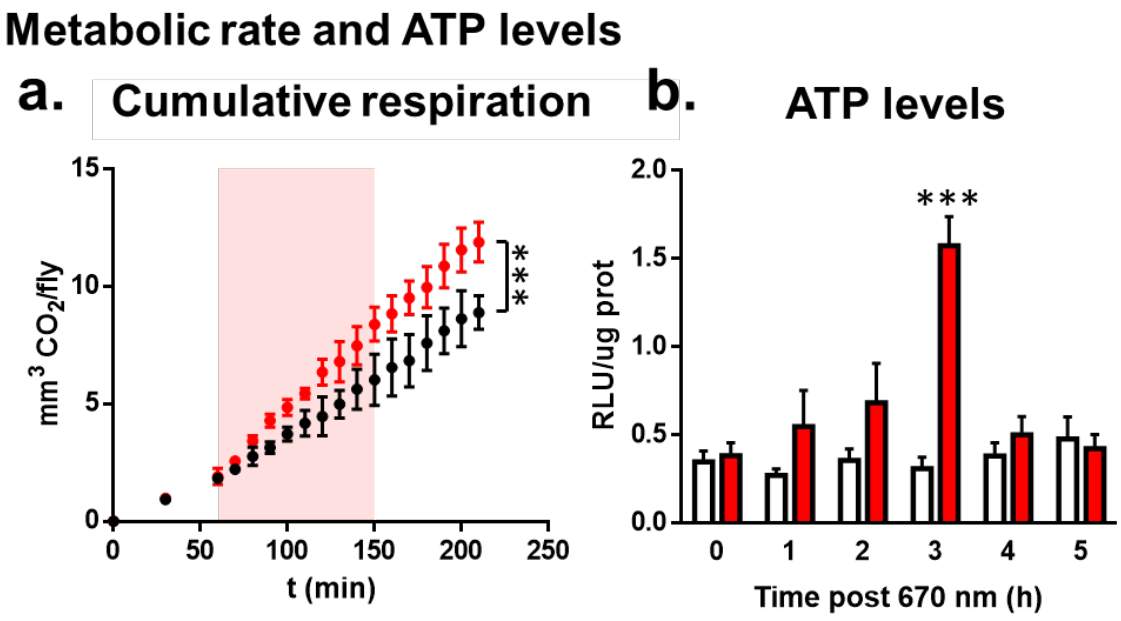

Figure 2.6. Cumulative CO_2 measurements and ATP levels with one 90 min exposure to 670 nm. (**A**) Cumulative CO_2 measurements in aged flies exposed to 670 nm (red) and unexposed controls (black). Measurements for both groups overlapped during the first 60 min. Light exposure started at 60 mins and remained on for 90 min represented by the pink shading. The profiles for the two groups of flies are significantly different (*** = ANOVA P<0.001). Differences between individual time

points become significant at 80 min and remained so (*** = Mann Whitney P<0.001). Differences between the groups continue to expand after the end of the 670 nm light exposure. (**B**) Whole body ATP levels in aged flies exposed to 670 nm (red) and their controls (non-exposed, white) at progressive time points after light exposure. ATP levels in 670 nm exposed animals started to increase within the first hour and peak sharply at 3 h. However, they declined returning to the normal range by 4 h. The peak found at 3 h is statistically significant (*** = Mann Whitney P<0.001). Six replicates containing 5 flies were used for each group. Data shown as mean + SEM.

The increase in metabolic rate was correlated with increased catalytic activity of COX in the 670 nm treated flies as shown in Figure 2.7a after 90 min 670 nm exposure.

We also investigated whether changes in ROS levels were associated with a single 90 min light exposure. The results are shown in Figure 2.7b. No changes were found in the ROS levels in the 670 nm treated compared to the non-treated fly group, when light exposure was for only 90 min.

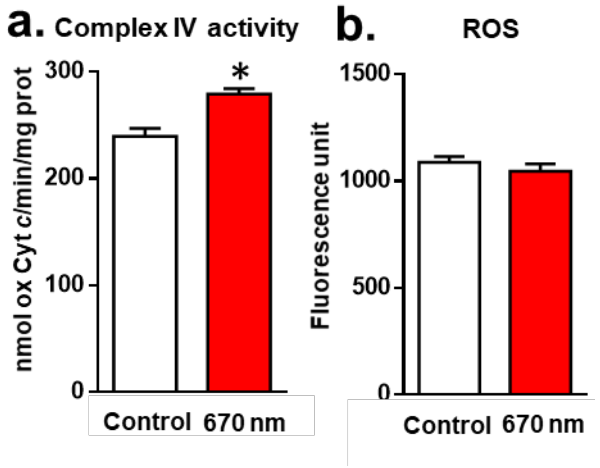

Figure 2.7. Effect of single 670 nm exposure on cytochrome c oxidase activity and ROS levels. (**A**) Enzymatic activity of cytochrome *c* oxidase (complex IV) was measured in 6 week old flies and in 6 week old flies treated with 670 nm for 90 min. After 90 min 670 exposure, the activity of cytochrome *c* oxidase increased significantly. (**B**) ROS levels were measured (absolute fluorescence). No changes in ROS levels were found between the groups (p=0.6894).

2.3.1.2 Respiration (metabolic rate) remains high for 4 days after a 90 min 670 nm exposure.

After establishing the onset of changes in respiration (approximately 20 min after light exposure), we asked how long such changes last following a single 90 min exposure. The results are shown in Figure 2.8, indicating an increased respiration over 4 days after a single exposure. On day 5, the metabolic rate declined sharply back to levels found in controls.

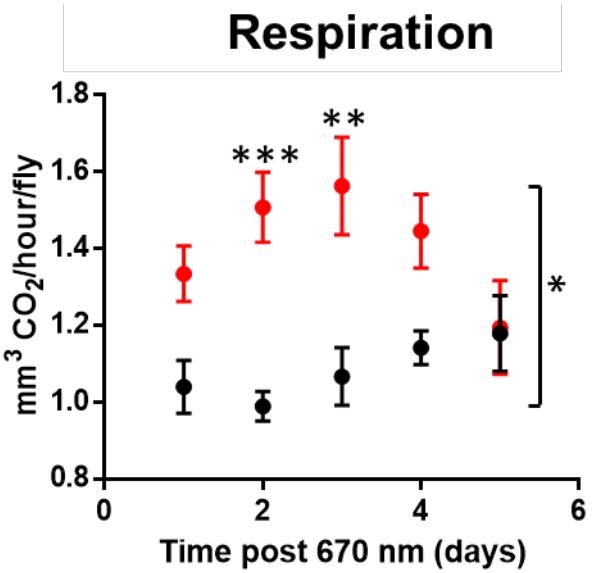

Figure 2.8. Respiration (metabolic rate) remains high for 4 days. Elevated respiration following a single exposure to 670 nm in aged flies (red) was measured over 5 days and compared to untreated controls (black). Differences between the two groups were statistically significant over the period measured (* = ANOVA $p<0.05$). Post hoc testing showed significance at 2 days (*** = Mann Whitney $p<0.001$) and 3 days (** = Mann Whitney $p<0.01$). Hence, single exposures retain their impact over 4 days. For each group and time-point, 6 replicates containing 5 flies each.

2.3.1.3 Changes in energy reserves

As 90 min 670 nm exposure affects the respiration rate and ATP levels, we asked whether this change in energy homeostasis has a fast direct effect on the energy reserves in the flies, glycogen, glucose and triglycerides. No changes were observed with one single 90 min exposure to 670 nm light in triglycerides, glycogen or glucose Figure 2.9. This may indicate that one dose is not enough to trigger changes in the energy reserves.

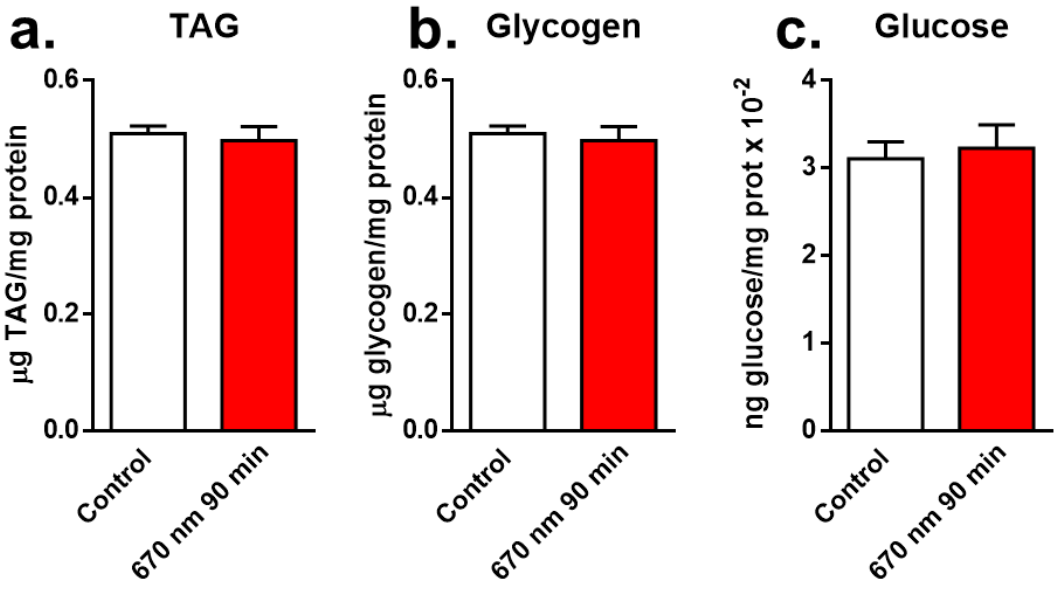

Figure 2.9. Changes in energy reserves after 90 min 670 nm exposure.
Triacylglycerides, TAG (**A**), glycogen (**B**) and glucose (**C**) were measured after90 min 670 nm exposure. No significant differences were found between 670 nm treated flies for 90 min and untreated flies. Results are shown as mean + SEM.

2.3.1.4 Climbing does not improve after 90 min 670 nm

Climbing was studied to see whether 90 min of exposure could improve locomotor function (Figure 2.10). A negative geotaxis assay was performed. No difference in the mean climbing index were seen between the control group and the 670 nm treated group. This may indicate that the mechanisms to achieve functional improvements (via secondary signalling routes) are slower and require more time to appear.

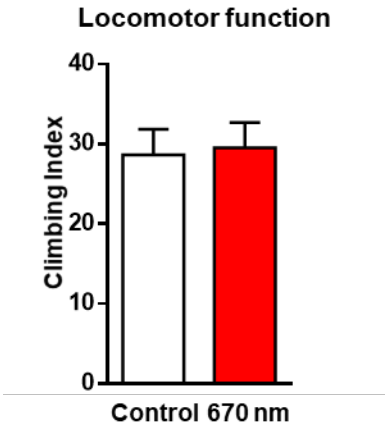

Figure 2.10. Locomotor function after single 90 min 670 nm exposure. After 90 min 670 nm exposure no differences were found in locomotor function between groups.

Although flies treated with 670 nm had a higher energy metabolism profile, this did not translate into a better climbing index. Data are shown as mean + SEM.

Taken together, the results are consistent with the primary mechanisms of action of 670 nm light, shown by increased respiratory rate (metabolic rate) correlated with increased COX catalytic activity, both associated with increased global ATP levels. However, no changes in ROS, whole body glycogen, glucose and triglycerides or improvement of locomotor function could be seen after a single 90 min exposure. The delay in increased ATP levels compared to respiration rate and COX activity, suggests that the immediate surplus of ATP produced is immediately consumed. Interestingly, the higher metabolic rate after light treatment remained high for 4 days. However, a single 90 min exposure was not enough to alter global ROS levels and energy reserves in the fly or to achieve functional improvement.

2.3.2 Walking activity and behaviour after 90 min 670 nm

Our data shows no changes in the locomotor activity in the geotaxis assay, an innate reactive escape response in which flies climb the wall of the cylinder after being tapped to the bottom. However, flies have a higher metabolic rate associated with an improvement in their energy metabolism with 670 nm. Although we could not find significant differences in the negative geotaxis assay, perhaps a more sensitive metric is needed to assess whether an acute improvement in energy homeostasis is translated into functional improvements. Therefore we chose to investigate changes in fly walking behaviour after an acute 670 nm light exposure.

We examined walking activity in an open-field arena where flies movements were tracked following acute exposure to 670 nm light, to associate small changes in the energy metabolism with small changes in behaviour. We tested two different situations. First, an environment devoid of any visual stimuli, indicative of endogenous locomotion, and second, an environment with visual stimulation in the form of two vertical black stripes, one on either side of the area, linking activity with behaviour.

Different parameters were used to study the walking behaviour:

1. Centrophobia: as an index for the likelihood of the fly staying in the centre of the platform. A low index indicates that the fly prefers to explore the platforms periphery.
2. Median speed: the midpoint of the fly's speed frequency distribution (mm/sec).

3. Distance travelled: total distance travelled by the fly during the whole experiment (15 min, in mm).
4. Activity time: sum of time periods where the fly is active. If there is absence of movement longer than 1 s, it is considered pause and not activity.
5. Turning angle: the angle between two consecutive vector movements.

2.3.2.1 Buridan paradigm: no stripes

When flies are placed in an open arena, they have a propensity to walk along the platform edge, exploring the limits of their environment, demonstrating signs of centrophobia[84]. This is true for young flies, as shown in our transition plots for young flies in Figure 2.11 (Young, Y). With age however, this pattern of behaviour is degraded, with older flies having a propensity to spend more time in the centre of the platform and with relatively random movements (Figure 2.11, Control (Old)). Thus, the centrophobic behaviour shown in the young flies, disappeared with age.

After an acute single 90 min of 670 nm light the behaviour of aged flies in the open arena changed significantly (Figure 2.11). We analysed their walking behaviour for several hours after light exposure (up to 7 h).

Directly after 670 nm treatment, the walking behaviour pattern in aged flies changed markedly as shown in the transition plot (0 h), mirroring young animals. This was repeated at different time points after the exposure, 1, 3, 5 and 7 hours. At these time points, the youthful pattern induced right after the 90 min light exposure in old flies, was gradually reduced, with animals showing progressively greater centrophobia. Although, in the case of centrophobia, an extra measurement after 24 h was taken, where the index was reduced to levels found prior to light exposure.

Together with transition plots and centrophobism, other parameters were analysed: speed of movement, the distance that they travelled in the time period, the amount of time they were active, and the angular size of their turns (Figure 2.12). All four metrics showed significant improvements after 90 min 670 nm treatment that declined progressively with time. The old flies exposed to the 670-nm light had increased speed of movement, travelled a greater distance, spent more time active, and were more directed in their movement with a reduction in the angles at which they made their turns, consistent with smaller turns as they circled the perimeter. However, improvements in all of these features were only statistically significant at time 0 hours,

although trends in improvement that were not significant could be seen at subsequent time points.

Taken together, the treated aged flies spent the majority of their time exploring the perimeter of their environment. This was associated with significant increased median speed, total distance travelled, activity time and a reduction in their turning angle, indicative of a youthful walking behaviour. This behaviour however, degraded to an aged behaviour over time.

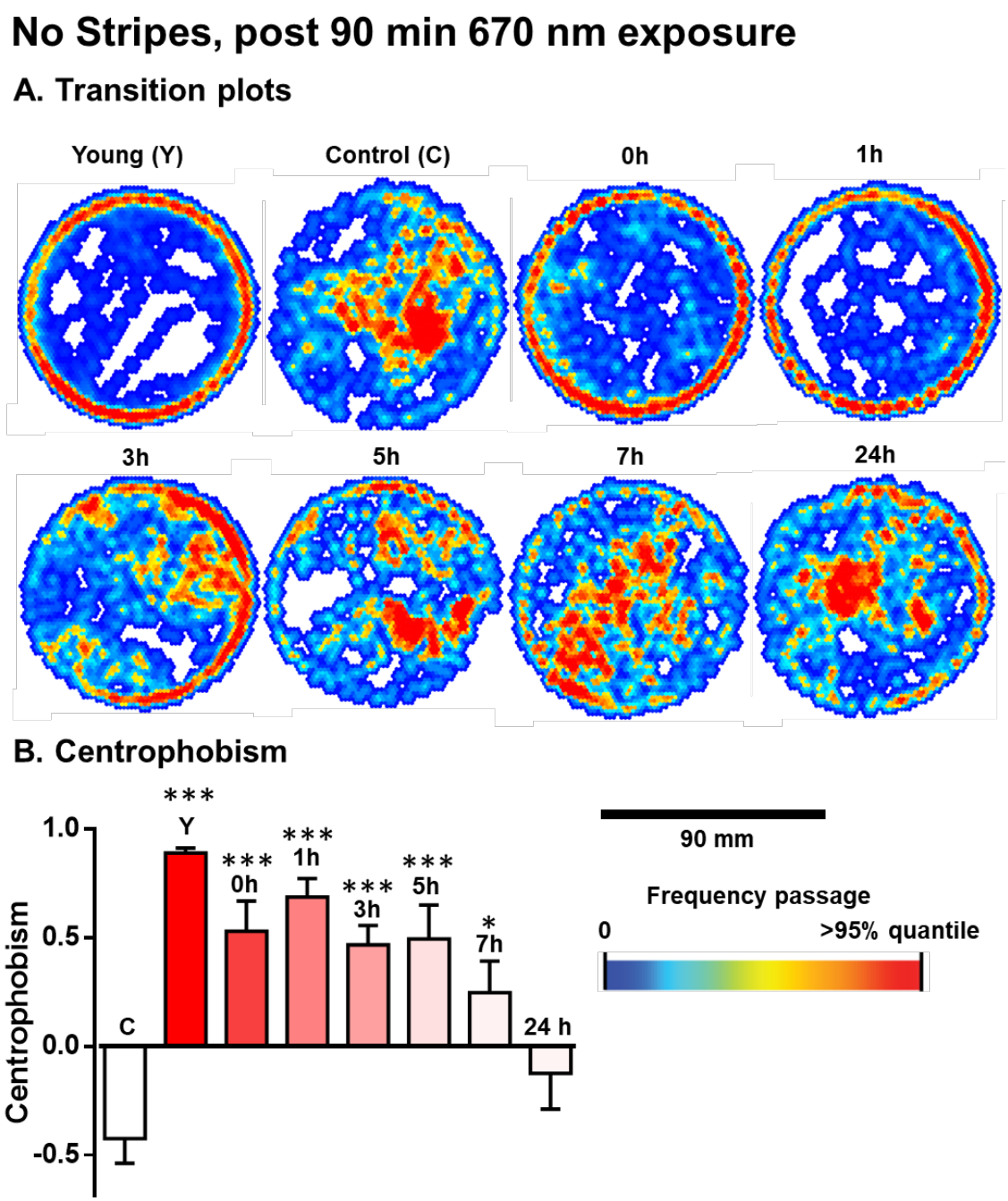

Figure 2.11 Transition plots and centrophobism index for endogenous locomotion. **A** and **B**. Relative frequency of fly passage at each position was plotted (dark blue indicated flies were rarely present, red means a frequency above the 95% quantile value, white indicates that no fly ever transitioned through this position). Young flies explored their environment and traced out its limits. The majority of their activity was around the edge displaying centrophobism, which is shown in the young control. Old flies spent a greater proportion of their time centrally and were generally less mobile as shown in the old control. Bars represent means and error bars standard errors, n=9 in each group. ***

p<0.001, ** p<0.01, * p<0.05. P values are shown when not significant, Mann Whitney-U test.

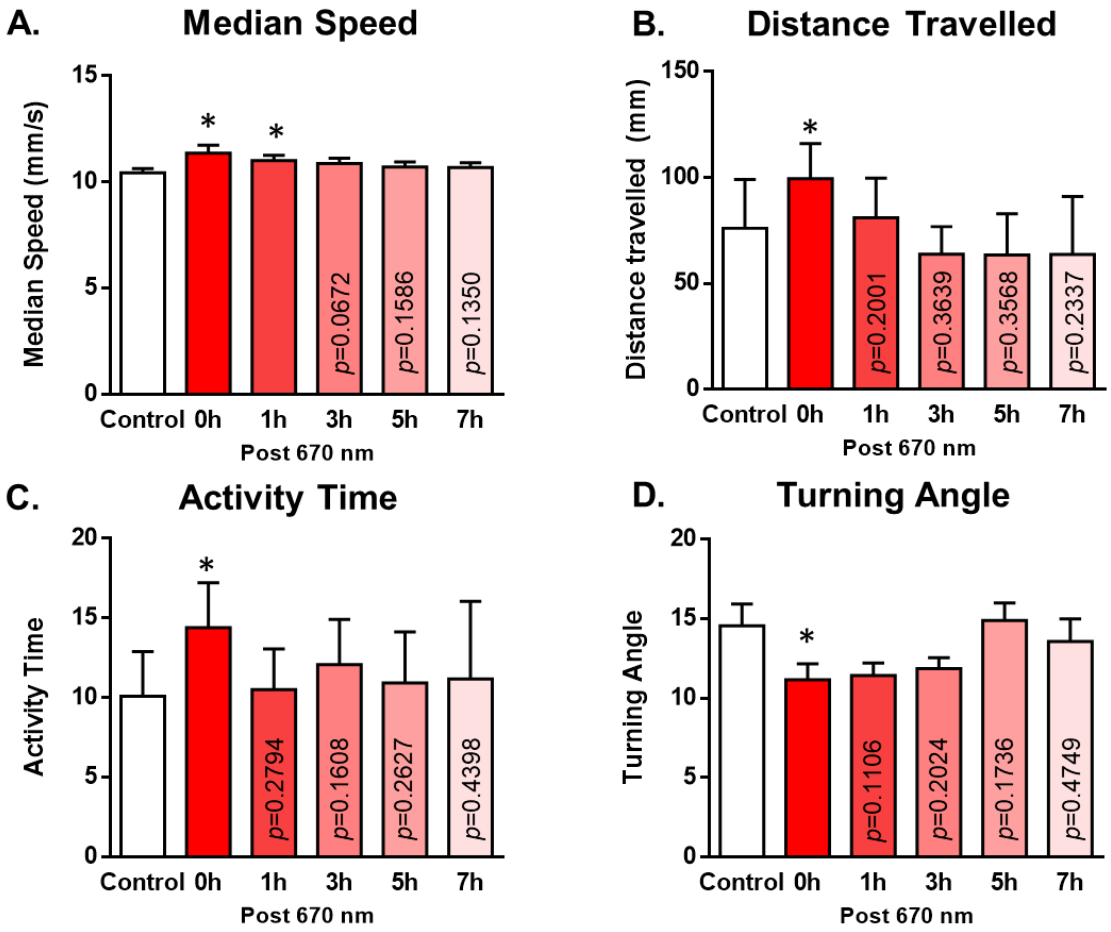

Figure 2.12 Fly trajectory metrics for endogenous locomotion. In the absence of visual targets, median speed (**A**), distance travelled (**B**), activity time (**C**) and turning angle (**D**) were only significantly improved immediately after 90 min 670 nm exposure (all metrics at 0 h, * p<0.05 Mann Whitney-U test). Bars represent SEM. N=9 in each group.

2.3.3 Buridan paradigm: 11˚ stripes

When we repeated the experiment with two vertical black stripes, one at each side of the arena, acting as visual stimuli, similar patterns were found as in endogenous locomotion. However, baseline differences between young and old flies were less marked with a greater proportion of old flies spending more time exploring the peripheries of their arena (

Figure ***2.13***).

In spite of this, exposure to 670 nm light reduced centrophobia, but this was not significant at the assessed times. However, significant differences were found in median speed, total distance travelled, activity times and the angular size of their turns, with values closer to young fly behaviour. All improved significantly at 0 hours. Median speed was also significantly improved at 1 hour, and the turning angle also improved significantly at 1 hour and 3 hours. Although centrophobia did not change significantly after 670 nm exposure, other metrics improved. This suggests that the addition of visual stimulators motivate the fly to explore its environment, both in un-treated and treated flies.

Despite visual stimuli affecting the flies' endogenous behaviour, treatment with 670 nm light improved measured parameters, translating improvements in energy homeostasis into functional improvements.

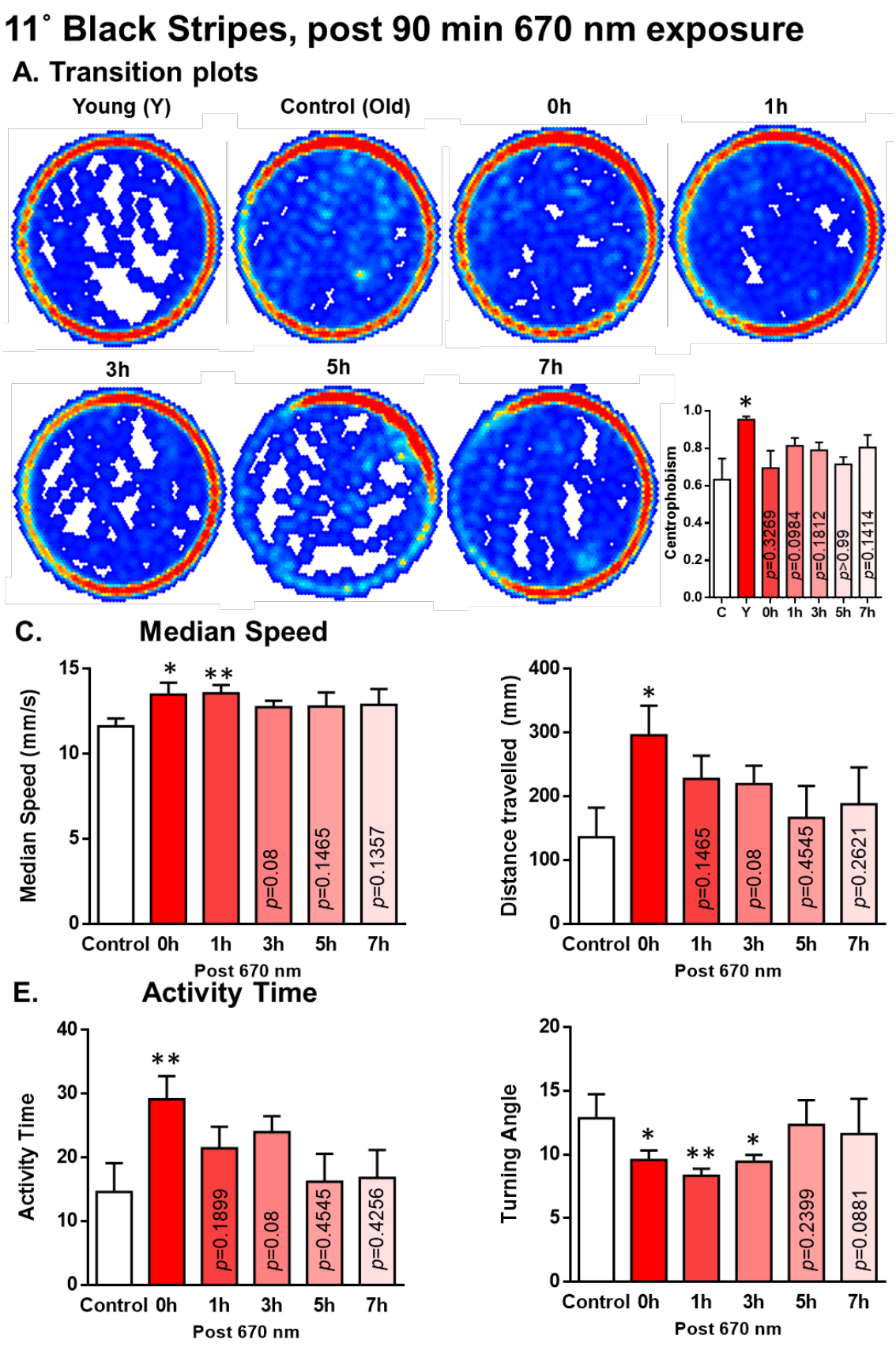
11˚ Black Stripes, post 90 min 670 nm exposure
A. Transition plots
Young (Y)
Control (Old)
0h
1h
3h
5h
7h
Centrophobism
C Y 0h 1h 3h 5h 7h
p=0.3269
p=0.0984
p=0.1812
p>0.99
p=0.1414
C. Median Speed
Median Speed (mm/s)
Control 0h 1h 3h 5h 7h
Post 670 nm
p=0.08
p=0.1465
p=0.1357
Distance travelled (mm)
p=0.1465
p=0.08
p=0.4545
p=0.2621
E. Activity Time
Activity Time
p=0.1899
p=0.08
p=0.4545
p=0.4256
Turning Angle
p=0.2399
p=0.0881

Figure 2.13 Transition plots and fly trajectory metrics for Buridan's paradigm with 11° stripes, at different time points after a 90 min 670 nm exposure. A and **B**. In the presence of visual targets (black stripes), aged flies show a reduced centrophobic index than compared to endogenous locomotion (Figure 2.11). However, their centrophobism index was lower in aged flies compared to young ones ($p<0.05$). Median speed (**C**), distance travelled (**D**), activity time (**E**) and turning angle (**F**) improved during the first three hours after 90 min 670 nm exposure. Error bars are SEM. N=9 in each group. Abbreviations: *$p<0.05$, **$p<0.01$ Mann Whitney-U test. P values are shown when not significant.

2.3.4 Consequences of a 7 day 670 nm light exposure in aged *Drosophila*

2.3.4.1 Increased metabolic rate, COX catalytic activity and ATP levels

To assess the effect of long term (7 days) 670 nm on mitochondrial respiratory rate, the metabolic rate and COX activity was assayed (Figure 2.14). After one week treatment, flies were assessed for their metabolic rate immediately after the last exposure in laboratory-made respirometers. As it is known that 670 nm interacts with complex IV of the electron transport chain we asked whether the increased respiration rate seen after a single light exposure is maintained in the 7 day treated flies. Flies exposed with 670 nm had significant increased CO_2 production correlated with increased COX catalytic activity (Figure 2.14 a and b). The relationship between moles of CO_2 produced and moles of O_2 consumed is linear in *Drosophila*[85], i.e. the amount of CO_2 produced is equivalent to the amount of O_2 consumed. Consequently the data indicates that 670 nm exposed flies consume more O_2 in relation to their age matched flies, achieving similar levels to those found in young flies (2 weeks). This is consistent with the idea of improved mitochondrial function as a result of 670 nm treatment.

Interestingly, 6 week old flies had reduced metabolic rate compared to young flies, which recovered with 670 nm exposure for 7 days, suggesting that old flies have reduced respiratory rate compared to young flies.

Similar results were found for complex IV activity (Figure 2.14b) and ATP levels (Figure 2.14c). The data for the additional control fly group (aluminium foil covered fly vials but *exposed* to 670 nm, gray bars) were similar to age matched 6 week old untreated flies. This suggests that the effects seen in the treated group are a consequence of 670 nm light exposure.

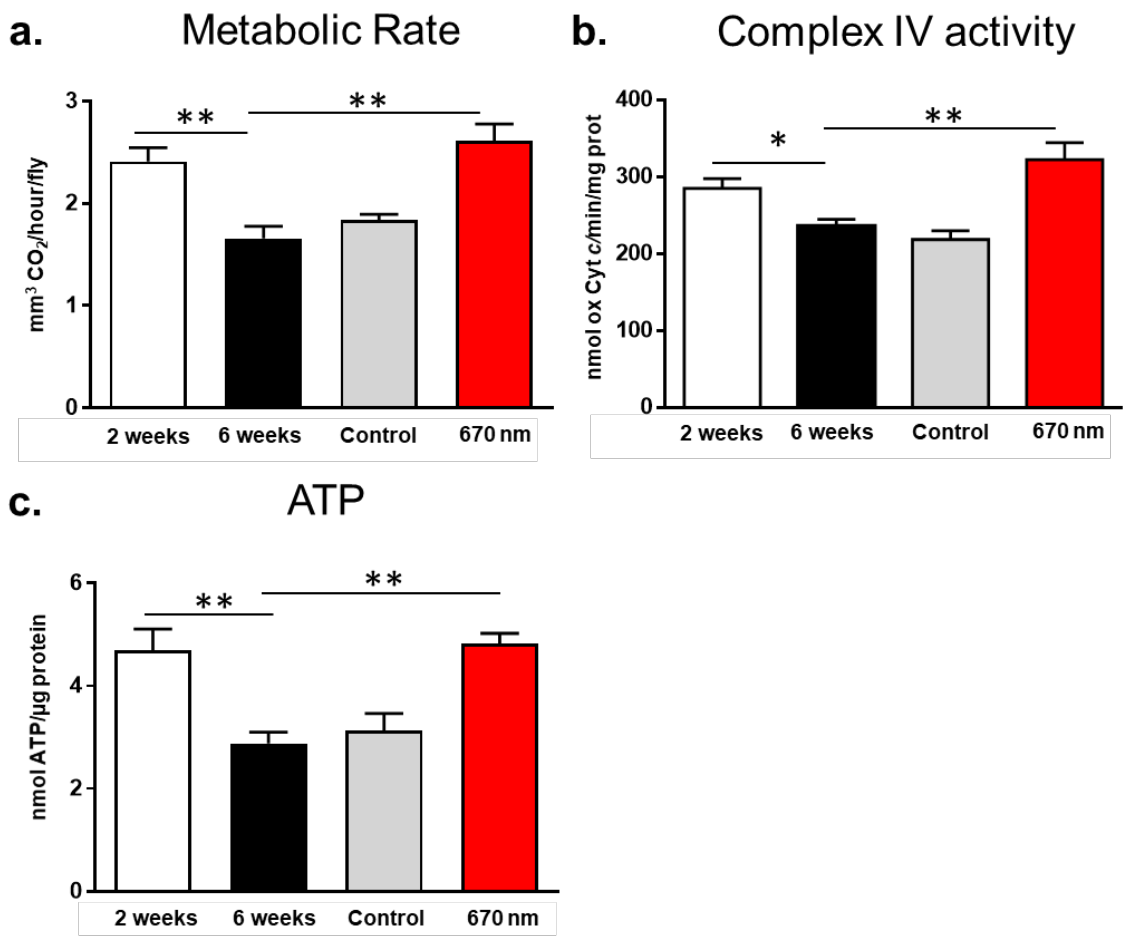

Figure 2.14. Effects of 7 days 670 nm exposure on metabolic rate, complex IV activity and ATP levels. (**A**) Metabolic rate was assessed in lab-made respirometers. Results are shown as the rate of CO_2 production per hour per fly. At 6 weeks there was a significant reduction in metabolic rate compared to 2 week old flies. 670 nm exposure improved metabolic rate back to the level found at 2 weeks. (**B**) 670 nm daily exposure for 7 days improved the activity of complex IV to levels found in 2 week old flies. (**C**) Whole fly ATP levels were measured. At 6 weeks there was a significant reduction in ATP content compared to 2 week old flies. 670 nm exposure significantly improved ATP levels. There were no statistically significant differences in the assessed parameters between the 6 week old flies and flies treated with 670 nm but in blacked out vials (grey bars, control). Results are shown as mean +SEM.

2.3.4.2 Increased cytochrome *c* oxidase expression levels

Levels of cytochrome *c* oxidase subunit III (COX III) were assessed by retinal immunohistochemistry to study whether increased respiration and COX catalytic activity was also reflected in the expression levels of COX in the mitochondrial electron

transport chain. The COXIII signal intensity was normalised to a protein that is not expected to change with 670 nm light exposure, β-actin. Immunostaining for COXIII shows wide distribution across the fly retina, as seen in Figure 2.15. At 6 weeks a decline in the levels of COXIII expression compared to the 2 week old flies was observed. 670 nm treatment for 1 week increased the COXIII expression compared to age matched controls and against the 2 week old flies.

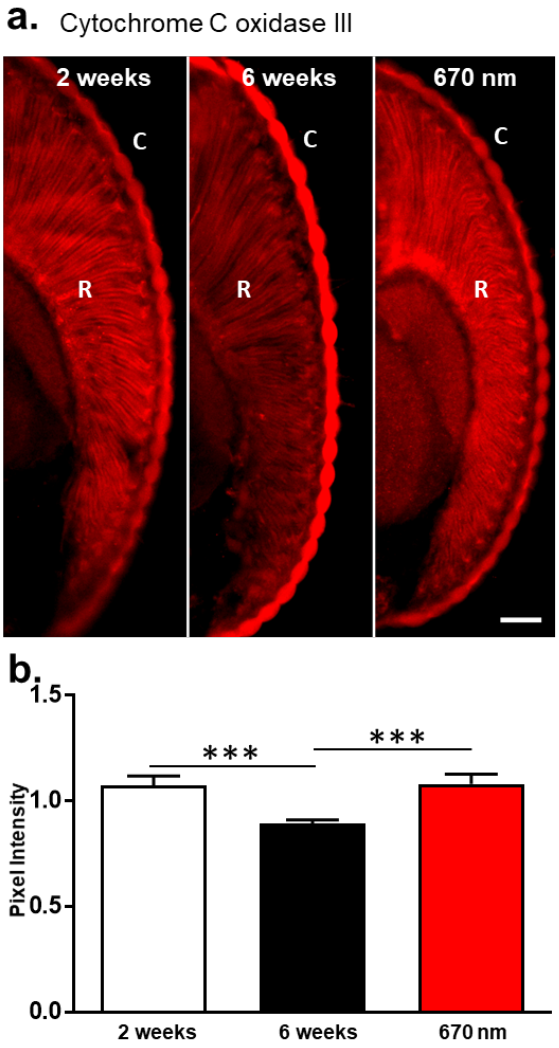

Figure 2.15. Effects of 670 nm exposure on the expression of Cytochrome C oxidase subunit III in the *Drosophila* retina. Transverse eye sections of 2 weeks, 6 weeks and 6 week 670 nm exposed *Drosophila* were stained for cytochrome *c* oxidase subunit III (COXIII). (**A**) Representative images for each group. (**B**) Quantification of COXIII intensity represented graphically, normalised to β-actin, a housekeeping protein not expected to change with 670 nm exposure. 6 week old flies had a significantly lower normalised COXIII levels than 2 week old flies. 670 nm treatment for 1 week increased

relative signal intensity compared to age matched controls, and compared against the 2 week old flies. Results are shown as mean + SEM. Scale bar= 20 μm. Abbreviations R: retina, C: cornea.*p<0.05, ***p < 0.001.

2.3.4.3 Mitochondrial DNA

The relation between 670 nm and mitochondrial DNA is poorly understood. The mitochondrial DNA content varies within different tissues and it decreases with age as discussed in the introduction of this chapter. To our knowledge, no study has focused on mitochondrial DNA content in *Drosophila* when exposed to 670 nm. To assess whether 670 nm affects the mitochondrial DNA content, flies treated for 1 week with 670 nm where analysed for mitochondrial DNA content (Figure 2.16). At 6 weeks of age, *Drosophila* significant drop in relative mitochondrial DNA was observed (normalised to nuclear DNA to take into consideration any loss in cell number). Even though exposure to 670 nm increases the levels of relative mitochondrial DNA, it did not achieve levels found in young flies (2 weeks). Hence, 670 nm light appears to be associated with mitochondrial biogenesis.

The flies in aluminium covered vials had similar mtDNA levels to the age matched 6 week old control group.

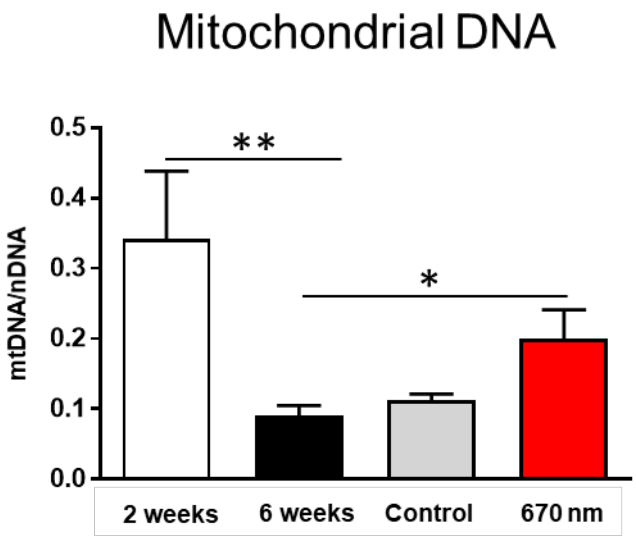

Figure 2.16. Mitochondrial DNA content after 7 day 670 nm exposure. Results are the ratio of mtDNA to nuclear DNA. At 6 weeks there was a significant reduction in mtDNA content compared with young flies. 670 nm exposure significantly increased mtDNA content to similar levels found in 2 week old flies.

2.3.4.4 ROS levels are affected by 670 nm exposure

ROS levels are known to increase with age. As a consequence, we measured ROS levels in fly heads (Figure 2.17). In 6 week old flies total ROS levels significantly increased. However, if the flies received 7 day 670 nm exposure, the ROS levels significantly decreased, achieving similar levels as in the 2 week old group.

Again, the group of flies in blacked out vials had no different ROS levels to 6 week old flies.

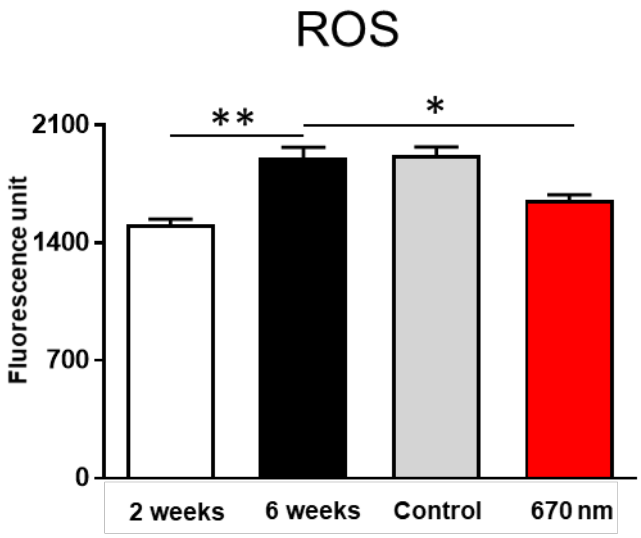

Figure 2.17. 7 days 670 nm exposure and its effects on ROS levels. Results are shown as fluorescence units. At 6 weeks there was a significant increase in ROS, which was significantly reduced with 670 nm treatment.

2.3.4.5 Glycogen, glucose and triglyceride levels in young, old and exposed *Drosophila*

One week 670 nm exposure increases ATP levels due to increased respiration. We asked whether this is translated into increased cellular energy storages, such as triglycerides and glycogen. Here 5 weeks old flies were treated for 1 weeks with 670 nm. After treatment, flies were collected and triglycerides, glycogen and glucose levels determined. The triglycerides, glycogen and glucose levels are shown in Figure 2.18.

One week 670 nm exposure increased glycogen, triglyceride and glucose levels, partially reversing the loss occurred during normal ageing. Glucose and triglyceride levels improved to levels found in 2 week old flies. In the case of glycogen, the 670 nm treatment only partially reversed the loss due to ageing. This observation may indicate

that the energy homeostasis, in terms of energy reserves, is similar to a young fly. In summary, 670 nm exposure during one week increased and partially reserved the effect of normal ageing in triglyceride, glycogen and glucose levels.

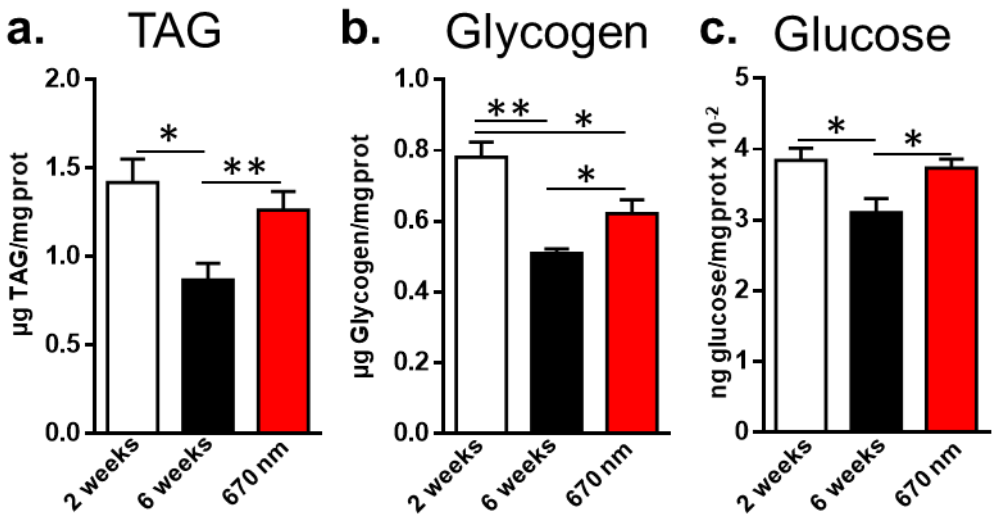

Figure 2.18. Effects of 670 nm on triglycerides, glycogen and glucose. (**A**) Triglycerides were measured and represented as a ratio to protein. At 6 weeks there was a significant reduction triglycerides, but with 670 nm light exposure levels increased to those found in young animals. (**B** and **C**) Glycogen and glucose levels were measured and also represented as a ratio. At 6 weeks there was a significant reduction in glycogen and glucose. 670 nm light exposure improved glycogen and glucose levels significantly. Increased glycogen levels did not reach levels found at 2 weeks. Results are shown as mean + SEM. *$p < 0.05$, **$p < 0.01$.

2.3.4.6 Food starvation and 670 nm exposure

As *Drosophila* exposed to 670 nm had increased levels of glycogen, triglycerides and glucose, we challenged the exposed flies to food starvation (Figure 2.19). Only water was provided. The total and mean lifespan (when 50% of flies are dead) was determined in the different groups. In the 6 week old fly, there was a clear shortening in the total and mean lifespan compared with the 2 weeks old fly. In contrast, when 5 week old flies were exposed one week to 670 nm, this did not translate into a significant change in lifespan. Even though the exposed flies had increased levels of glycogen, glucose and triglycerides, no difference could be observed in resistance to starvation.

This result suggest that even though there is an improvement in mitochondrial function and an increased levels of energy reservoirs, this does not play a major role in the regulation of starvation.

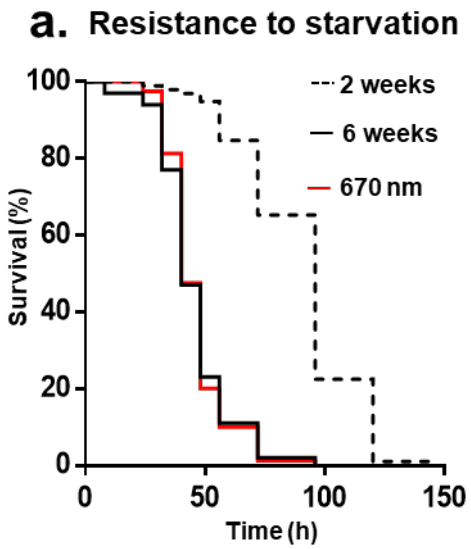

Figure 2.19. Effects of 670 nm on resistance to starvation in *Drosophila*. Resistance to starvation was assessed. Only water was available to the flies. At 6 weeks there was a significant reduction in survival when flies were challenged to food starvation in comparison to two week old flies ($p<0.0001$, log-rank test), where the mean lifespan dropped from 100 h to 50 h. Daily seven day exposure did not increase the survival rate neither the mean lifespan (2 weeks vs 670 nm, $p<0.0001$, log-rank test). N=50 flies in each group; 5 replicates containing 10 flies each.

2.3.4.7 670 nm does not change sensitivity to heat stress but does chilled coma recovery.

To investigate the consequences of improved mitochondrial function and increased energy reserves, the flies were challenged to two types of temperature related stress: heat sensitivity and chilled coma recovery time (Figure 2.20). *Drosophila* showed a steep age-dependent decrease in resistance to heat sensitivity. However, treatment for 1 week with 670 nm did not improve the resistance to heat sensitivity.

In contrast, when chilled coma was induced in flies for 1 h, a delay in the recovery time was observed with age. Old flies treated with 670 nm recovered significantly faster than old untreated flies during the early phase of the recovery period. Moreover, Figure 2.20c, where the recovery time is normalised to young files, shows that 670 nm treated

flies recovered much quicker than untreated old flies. At approximately 4 min, 50% of the old treated flies had recovered, while this happened at about 6-7 min in the case of the old untreated fly group.

This suggests that even though 670 nm improves mitochondrial function, it does not result in a global resistance to high temperature stress, indicating that the mechanisms involved in their regulation are not just regulated by mitochondrial function.

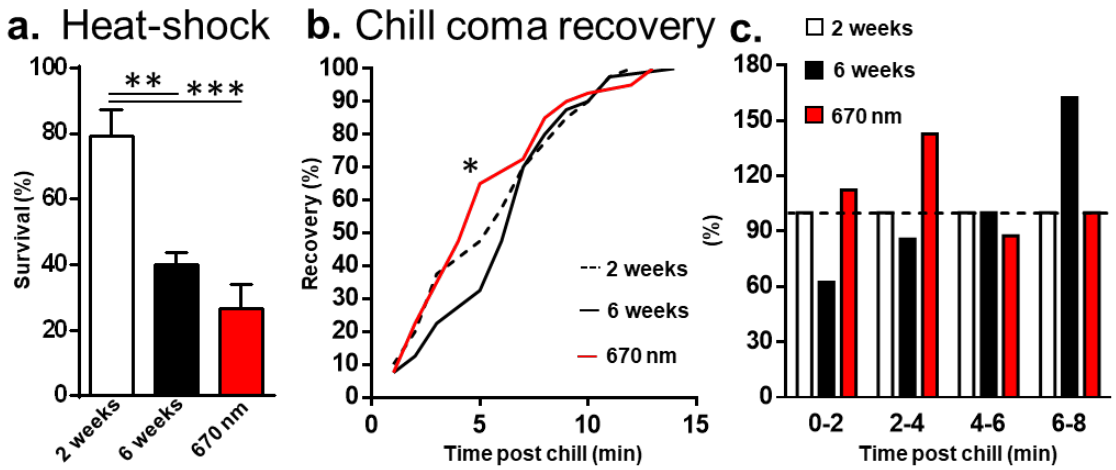

Figure 2.20. Effects of 670 nm on increased stress levels in *Drosophila*. Effects of 670 nm on heat sensitivity (**A**) and chill coma recovery (**B** and **C**). (**A**) Percentage of surviving flies after 24 h heat stress. At 6 weeks there was a significant reduction in survival in comparison to 2 week flies. 670 nm exposure did not change survival rates. (**B**) Chill coma recovery time (CCRT) that required for flies to stand at room temperature after 2h cold stress (0˚C). Cumulative incidence function of CCRT for 2 weeks, 6 weeks and 670 nm treated flies. Differences were apparent from 1-7 min. After 7 min, the curves are identical. Mean CCRT, 2 weeks=5.7 min, 6 weeks=6.3 min and 670 nm=5.3 min. The 670 nm treated group recovered faster compared to the non-treated flies (**C**) CCRT percentage difference in the first 8 min normalised to 2 week animals. 670 nm treated flies recover faster. Results are mean + SEM. *p < 0.05, **p < 0.01, ***p < 0.001.

2.3.4.8 Improvement in locomotor function is associated with 670 nm exposure

Negative geotaxis (or climbing) was tested in flies to assess whether 670 nm can improve locomotor function (Figure 2.21). Changes in the musculature of flies with ageing are very clear, characterised by a progressive loss of skeletal muscle function and muscular mass with age[86]. The motor function assessed by a negative geotaxis

assay revealed that in non-exposed flies the climbing pass rate decreased drastically by an 88% from young adults to 6 week old flies. In contrast, when age matched flies were exposed to 670 nm for one week, the climbing pass rates improved significantly by a 54.7%, which was just 36.2% less than the young adults. Overall, 670 nm flies had a better climbing pass rate ($p<0.01$). Consequently, a 7 day exposure of 670 nm significantly improved the climbing/motor capabilities in the aged fly.

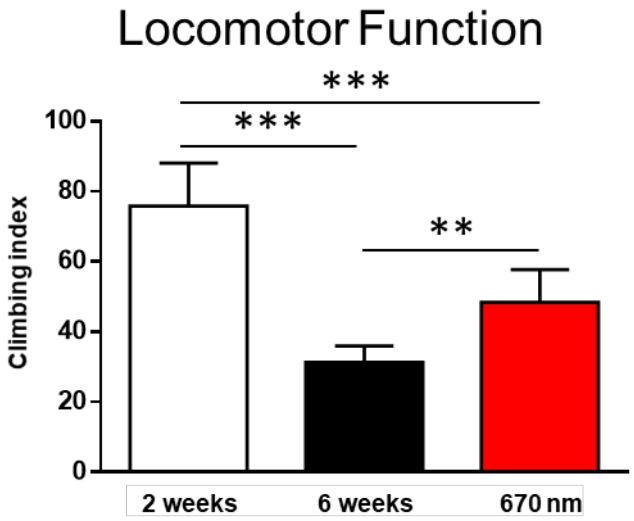

Figure 2.21. The effect of 1 week 670 nm exposure on locomotor function in *Drosophila*. Climbing ability was tested as a mean of locomotor function. At 6 weeks there was a significant reduction in the percentage of flies that climbed above the 8 cm mark. 670 nm significantly improved the capacity of flies to climb; however this improvement did not achieve the percentage found in two week old flies.

2.3.4.9 Changes in cognitive function associated with 670 nm exposure

Short-term memory was tested in flies to assess whether 670 nm exposure could improve cognitive function, as the overall animals health span improved with 670 nm exposure. The results are shown in Figure 2.22. Different studies have shown that *Drosophila* have reduced memory as they age, similarly to other species including humans[5,79]. Flies were trained in an aversive phototactic experiment to stay in the dark chamber while adding quinine to the light chamber. The successfully trained flies were reassessed 6 hours later to the aversive phototactic experiment to test whether they remembered the initially trained task. Only 10% of old trained flies remembered correctly, representing a 72% decrease in comparison to the young adult fly. In contrast,

in the one week 670 nm exposed flies, 39% on the flies remembered the task, similar to the young adult flies.

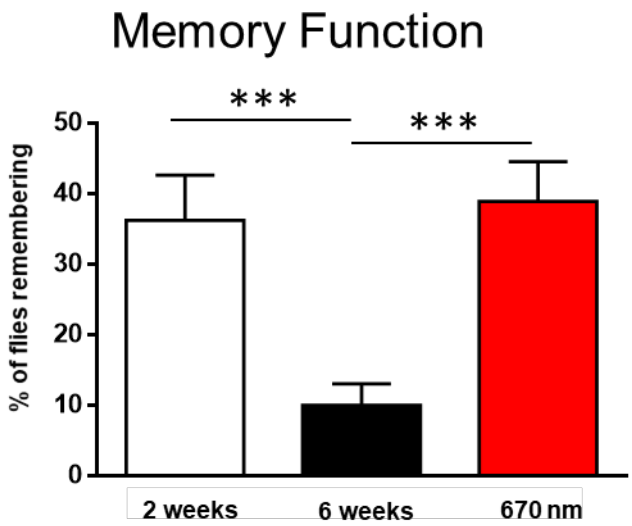

Figure 2.22. Cognitive function after 670 nm treatment. Memory was tested in an aversive phototactic setting. At 6 weeks there was a significant reduction in the percentage of flies not being able to remember an association between light and an aversive stimulus compared to 2 week old flies. 670 nm increased the capacity of flies to remember the association.

2.3.4.10 Consequences of 670 nm exposure for visual function

Flicker ERGs were used to analyse retinal sensitivity to light stimuli in *Drosophila*. The use of the ERG to examine retinal function in the fly is well established[87]. However, little is known how the fly ERG responses change in the fly with age. Flicker ERGs were performed at progressive frequencies in all 3 groups of flies and the amplitude of the responses measured (Figure 2.23). There was a significant reduction in amplitudes between 2 and 6 weeks, but this was improved across the frequency range in 6 week old flies exposed to 670nm light. Figure 2.23a shows responses across the frequency range normalized at baseline (0.5Hz flicker) and Figure 2.23b shows examples of the waveforms obtained from flies in each group.

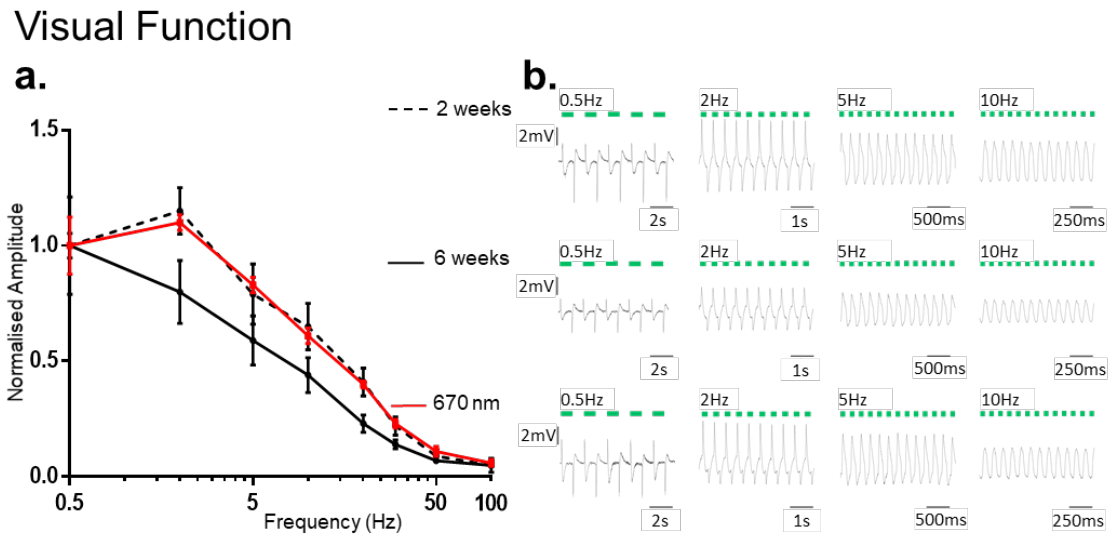

Figure 2.23. Consequences of 670 nm exposure on visual function. (**A**) and (**B**) Flicker electroretinograms were recorded to assess retinal function. (**A**) Amplitudes of the ERG response normalised against the lowest frequency. This clearly shows the overall decline in amplitudes between 2 and 6 weeks. This also reveals the significant improvement in the ERG in 6 week old flies exposed to 670 nm of 1 week. One-tailed ANOVA, (p=0.0166). Mean + SEM. (**B**) Example ERG waveforms from 2 weeks, 6 weeks and 6 weeks exposed to 670 nm flies to flicker stimulus at progressive frequencies. With age, the amplitude of response declined, but this is improved by 670 nm exposure.

2.3.5 Summary of results

A diagram with the summary of results for the 670 nm experiments is shown in **Figure *2.24*. Summary of results for 670 nm experiments.** On the left-hand side, 90 min treatment; right-hand side, 20 min daily for 7 days.

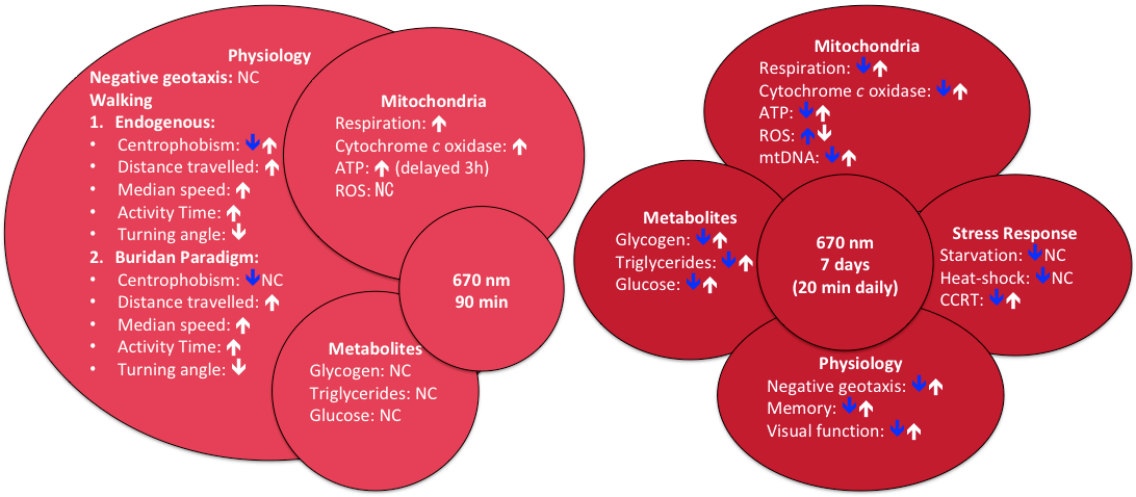

Figure 2.24. Summary of results for 670 nm experiments. On the left-hand side, 90 min treatment; right-hand side, 20 min daily for 7 days. For each treatment, summary for mitochondrial function, metabolites and physiological responses are shown. Additionaly, summary for stress responses are also included in the longer treatment. Arrows depict changes (upwards: positive, downwards: negative). Blue arrows show changes in ageing. White arrows, show changes with treatment. NC: no changes, ROS: reactive oxygen species, ATP: adenosine triphosphate, CCRT: chilled coma recovery time.

2.4 Discussion

One hallmark of biological ageing is a slow decrease in physiological function, known as functional senescence. With increased age, organisms loose locomotor, cognitive and sensory function, and this is particularly relevant in the western world were average lifespan has increased consistently. It has been shown that 670 nm exposure during the whole lifespan of *Drosophila* increases their global ATP levels, cytochrome *c* oxidase protein levels and median lifespan[71,72], i.e. age were 50% of the population is alive. However, the role of short term exposure to 670 nm in different biochemical, behavioural and physiological functions has not been addressed directly.

It is known that mitochondrial function declines with ageing[37]. Many ageing theories have been postulated, as discussed in our first chapter. In all of them, however, mitochondria play an important role. We show that in the fly, ATP levels drop by a 50% between 5 to 6 weeks of age, concomitant with a decrease in the activity of cytochrome *c* oxidase. Similarly, at this age flies show clear signs of functional senescence, in

particular locomotor, sensory and cognitive function. That is why we considered 5-6 weeks a good age to assess the consequences of 670 nm treatment and in particular the implications in biochemical, behavioural and physiological functions. Furthermore, in our laboratory the median lifespan of the fly is 7 to 8 weeks, i.e. when 50% of the initial population is still alive. If older flies were used, the data would be biased towards remaining stronger population.

Several studies have associated increased ROS production with functional senescence[88,89]. Although this needs clarification, as there is evidence for small changes in ROS levels to serve as signalling molecules to regulate biological and physiological processes to allow for adaptation to changes in the nutrient or oxidative nutrient[90]. In ageing however, mitochondrial dysfunction escalates the production of ROS, impairing cellular function and accelerating the ageing process[3]. Consequently mitochondrial function is a key tool to improve or revert functional senescence.

Different chemical compounds and environmental cues are known to modulate mitochondrial function[66,81]. For example, rapamycin, a drug known to improve mitochondrial function has also been shown to increase lifespan, as well as improve or revert signs of functional senescence[91]. Similarly, caloric restriction increases life-span and reduces the rate of ageing in a variety of species (including primates and *Drosophila*) by mechanisms involving mitochondria[92]. Hence, the modulation of mitochondrial function is becoming an increasingly popular therapeutic target, in particular in neurodegenerative diseases where it is thought that increased neuronal degeneration is due to susceptible mitochondrial function. 670 nm is a potential therapy (and economical) as photons will directly interact with the mitochondria and induce improvement in function[46]. 670 nm is hence an effective therapeutic tool to target neurodegenerative processes in ageing, in particular age-related macular degeneration (AMD) or Parkinson's disease[93]. However, the role of 670 nm in modifying the energy homeostasis and function is not well understood.

In this study we show that 7 days irradiation in old flies with 670 nm increases mitochondrial function, via a mechanism directly affecting the electron transport chain. It is known that 670 nm interacts with oxidised CuB molecules in the cytochrome *c* oxidase complex of the electron transport chain (complex IV) while promoting its oxidation and stimulating the electron transport in this highly complex system[44,46]. This

results in an increase of protons pumped into the intermembrane space. Ultimately this leads to an increase in the synthesis of ATP, as the protons induce mechanical force while being tunnelled through the ATP synthase (complex V).

We asked whether we are able to observe an increase in the respiratory rate with a single light dose. In this study, an increase in the production of CO_2 can be observed with a single 90 min 670 nm dose. In *Drosophila*, there is a linear relation between O_2 consumed and CO_2 produced[85]. Consequently, we can say that there is an increase in the rate of oxygen respiration with one 670 nm exposure. Furthermore, this single exposure that provides positive effects on respiration remains apparent over the following 4 days where improved respiration is maintained.

The relatively rapid increase in respiration after the 670 nm exposure is consistent with previous rat experiments where the optical signal from the retina originating from the redox state of COX is monitored *in vivo.* Here the COX redox status changes approximately 5 minutes after the 670 nm exposure and continues to increase over an hour, although the 670 nm light exposure was limited to 10 minutes[94].

An increase in respiration rate should be associated with an increase in the ATP pool in the 670 nm treated flies. Here we observed that there is an increase in ATP, but it is slightly delayed, approximately 3 h after the start of the treatment. However, according to the primary 670 nm mechanism of action, it is expected that with increased respiration an increase of ATP should be found. A reason for this observation could be that at 6 weeks old mitochondrial function is already impaired (the ATP and respiration decrease by a 50% and 40% respectively), so many cellular reactions and mechanism lack an optimal energy supply. In a situation where ATP synthesis is experimentally increased, all these reactions and mechanism will absorb this energy surplus to achieve homeostasis. These results suggest that the excess of ATP produced within the first 3 h is immediately consumed. Furthermore, our technique to quantify ATP has its limitations, as it is not possible to detect dynamic changes in the ATP flux. However, after 3 h the excess in ATP produced is not consumed, so we are able to detect an increase in the ATP pool.

Furthermore, with an increased 670 nm therapeutic window (i.e. 7 days) an increase in ATP levels can be measured already after the last 670 nm dose, concomitant with an

increase in respiration. In this case, with one week, the system has returned to homeostasis and an increase in the global ATP levels are seen.

A further clarification in the context of ATP levels, our measurements are relative. It does not give us the rate of production or consumption. The test allows us to see what the remaining ATP pool is. Ideally, we should use a method that reads the rate of ATP and ATP consumption dynamically.

Furthermore, with one 90 min dose, the locomotor function measured in term of negative geotaxis, does not change compared to untreated flies. However, with a method able to detect small changes in locomotor function, we are able to detect changes in fly walking behaviour. We show that the acute improvement in energy metabolism is associated with a marked impact on aged fly walking behaviour, re-establishing patterns of mobility and exploration that were only found in young animals. In a more detailed analysis we found a discrepancy in our data: the fly behaviour improves right after the acute light exposure and remain better for 7 h after the exposure, at a time when ATP levels have already returned to normal levels.

The impact of the 670 nm light exposure on aged flies was marked and relatively rapid in the open arena, particularly when there was no visual stimulation in the form of balck stripes. This task combines locomotor skills and cognitive ability. Young flies have very stereotypic exploration patterns in such an environment, with a preference to explore the periphery of the platform. Hence young fly behaviours are the same in both conditions. This is presumably because young flies the exploratory component of behaviour is predominant compared to the presence or absence of stripes. However, as they age, the exploratory component reduces allowing the stripe-driven component of behaviour to predominate.

The stereotypic behaviour of young flies breaks down in older animals where they spend more time in the center, associated with reduced movement[84]. Although differences between old controls and old 670 nm treated group are high when there are no visual targets, there is evidence that improvement in centrophobism may have been active after initial exposure as patterns at 1 hour were slightly better than those at 0 hours, immediately after the light was removed. However, such patterns are not better at 3 hours, which is when ATP levels peak. Again, this argues for some form of early signalling from mitochondria that may be independent of their recorded peak production

of ATP. The age effect on this task was reduced when stripes were present indicates that animals are able to respond if stimulated, although differences remain between aged controls and aged treated animals. This shows that linking mitochondrial function with behavioural improvements involves other cellular aspects, and not necessarily just ATP. Even though mitochondrial function is improved with one 90 min 670 nm dose (through increased respiration) this does not necessarily translate directly into improved function. Together, one 670 nm exposure does change mitochondrial function but this is not being translated into functional improvement.

It is accepted that small changes in mitochondrial function are associated with changes in metabolism and signalling, therefore it is not strange to observe drastic changes in some metabolites or improvements in physiological and behavioural responses. Additionally, mitochondria are peculiar structures as they are the only cellular organelles with their own genetic information (mtDNA). MtDNA is essential for mitochondrial function, as it is needed for key components in the electron transport chain and ATP synthesis. It is also involved in mitochondrial biogenesis, cellular metabolism, apoptosis and retrograde mitochondrial-nuclear signalling. As 670 nm alters or modifies directly mitochondrial function, the mtDNA content could be affected.

One week of 670 nm treatment increases flies relative mtDNA content, normalised to nuclear DNA to correct for any changes in cell numbers. Thus partially reverting the loss occurred during ageing. It is known that with ageing there is a decrease in mtDNA levels across different species[35,36,38]. The potential reasons for the increases in relative mtDNA amount include either (1) each mitochondria has an increased number of mtDNA copies or (2) the overall number of mitochondria increases via biogenesis. To our knowledge, no study has focused in this issue. However, this needs further investigation to fully understand the relationship between the 670 nm and mtDNA content in association with mitochondrial biogenesis. As the increase in mtDNA is similar to the levels found in a young fly, an explanation could be that 670 nm induces mitochondrial biogenesis, as with age the number of mitochondria decline. Similarly, calorie restriction, with similar functional consequences as shown here, also induces mitochondrial biogenesis[95].

Exposure of aged flies to 670 nm improves mitochondrial function, associated with increased ATP levels and mtDNA content. As flies have increased energy levels, they could have increased energy reserves, in the form of glycogen and triglycerides. But a single 670 nm light dose does not change the triglycerides, glycogen or glucose levels in the fly. It is very unlikely that a single 670 nm dose would affect in such a great way the energy homeostasis to alter the level of glycogen, glucose and triglycerides. However, if the treatment is extended for 1 week, with a 20 min daily exposure, glycogen, triglyceride and free glucose levels increase significantly. Also, the consequences of ageing affecting the energy system can also be seen here, with a dramatic decrease in triglycerides, glycogen and glucose levels.

An increase in energy reserves in the form of glycogen and triglycerides in one week could indicate a more efficient pattern of energy homeostasis. In an organism, there is little interest in producing excess energy over a long period of time, thus reducing the yield of energy production. To avoid this, the organisms stores the precursors of usable energy (ATP), in this case, triglycerides and glycogen. It could be the case that the excess ATP being produced signals an increase in the biosynthesis of energy reserves. Here, 670 nm successfully increases temporarily ATP levels, associated with a subsequent increase in glycogen and triglyceride levels.

The purpose of energy storages is to consume them when food is limited or the energy required by the organism is greater than the energy obtained from food consumption. In this experiment, the flies were challenged to food starvation and increased stress levels (heat stress and chilled coma). In both cases, the energy stored in the form of triglycerides and glycogen could be used to overcome more successfully these challenges. However, even though treated flies had increased triglyceride and glycogen storages combined with improved mitochondrial function, this did not translate into an increased chance of survival in case of food starvation or heat stress. The resistance to starvation decreases dramatically in the old fly, but 670 nm did not alter it. Similarly, old flies are more sensitive to heat stress. But, 1 week of 670 nm exposure on old flies did significantly improve the resistance to chilled come, associated with a reduced time to acquire a standing position, with times similar to those found in a young fly.

Together, this suggests that even though 670 nm promotes the storage of resources in the form of triglycerides and glycogen it does not affect the survival rate of flies when

they are challenged to food starvation or stress levels. This implies that the regulation of these responses are more complex and do not rely only on mitochondrial function and energy storages.

The target of any therapeutic approach is to improve physiological function and behaviour. Three different physiological and behavioural metrics were studied: climbing (locomotor), middle-term memory (cognitive), and retinal function (sensory). Functional senescence is very clear in all three metrics. The consequences of age decreases by 60% the ability of flies to pass the 8 cm mark in the negative geotaxis test, only a 10% of trained flies remember in comparison to young flies. In the case of retinal function, the magnitude of response to light decreases significantly in the 6 week old fly. Treatment for one week with 670 nm successfully reverses or improves all of these functions. Similarly, long life treatment with 670 nm also increases the capability of flies to improve their locomotor skills.

It is known that triglycerides are important for activities that require high energy levels, like muscular activities for climbing, walking and flying[96]. Thus, it is not surprising that treated flies, characterised by increased triglyceride levels, perform better in this task, compared to untreated flies.

Age-related memory impairment is observed widely with age[79]. Memory impairment during ageing is believed to be a consequence of neuronal dysfunction and increase in neurodegeneration. Previous studies have shown that neurons suffer from high oxidative stress and this correlates with a reduction in temporal memory retention[79]. Neuronal tissue is more vulnerable to oxidative stress than other tissues, due to higher metabolic rate and lower regeneration capacity. Consequently, oxidative stress is considered to be one of the main causal factors involved in the impairment of cognitive function.

Drosophila can be trained successfully and later challenged to remember the learnt task. However, the most common training is the setting performed in this experiment: an aversive photo tactic situation where the fly naturally would go towards the light but the presence of quinine (aversive substance) changes their natural behaviour. Here the flies were trained to remember the task, i.e. the flies do not go towards the light, but decide to remain in the dark chamber. Only the successfully trained flies were tested after 6 hours, assessing their middle-term memory.

In 6 week old flies, the percentage of flies that remembered the task decreased significantly from 36% at 2 weeks to 10% at 6 weeks. If old flies were treated for 1 week with 670, the percentage of flies that remembered increased to 40%, achieving the memory percentage found in 2 week old flies. One week treatment with 670 nm improves biochemical parameters known to decrease with ageing (membrane potential, ATP levels, etc.) and this is indicative of an efficient mitochondrial function. With an efficient mitochondrial function, it is expected that the ROS levels decrease.

There are two possible explanations for this observation: (1) related to memory formation or (2) ageing affects the ability of acquiring information due to a less-attentive state during training or difficulties with sensory perception. Previous studies have shown that old flies retain sufficient attentive state, sensory perception and motor activity to perform the learning task in this experiment[82]. This suggests that reduced ROS levels may be sufficient to improve middle-term memory formation in *Drosophila*, since neurons are the most affected cells by ROS damage. Consequently, the downstream mechanisms of 670 nm must interfere with phases of memory formation via ROS. However, an alternative explanation to this observation is that 670 nm enhances the synaptic machinery induced by training, making a stronger connection that decays more slowly.

Finally, exposure to 670 nm greatly enhanced the response to light stimuli, measured by flicker ERG at multiple intensities. The sensory system is also affected by functional senescence, decreasing the magnitude of response at 6 week of age in comparison to a 2 week old fly. This is consistent with a decrease in RNA transcripts involved in response to light with ageing[8]. One week exposure to 670 nm completely reverts the effect of ageing in this response, achieving the amplitudes found in a young fly, across all intensities. Several explanations could explain our observation. (1) 670 nm increases the membrane potential of mitochondria and improving the synthesis of ATP. In a cell, the majority of chemical energy is used to maintain the membrane potential, through ion pumps (Na^+/K^+ pump most important), and this is particularly important when information needs to be transmitted very fast. As increased ATP levels are available, the cell is able to repolarise quicker (than in a situation where ATP is more limited, like in an old fly). This fast repolarisation allows the cell to become responsive again. Consequently, the signal is transmitted faster through the different cells. (2) Elevated ATP levels could allow faster vesicle trafficking or, (3) elevated transcripts involved in

signal transduction, which decrease with age. Alternatively, and likelier, a combination of these factors.

Taken together, these results suggest that 670 nm exposure for one week in 5 week old *Drosophila* results in improvement of mitochondrial function and energy homeostasis, associated with an increase rate in respiration, higher ATP, glycogen and triglyceride levels, similar to those found in young flies (2 weeks old). This translates into a significant improvement in different physiological mechanisms, including improved locomotor skills, better middle-term memory and enhanced sensory response, in particular to light. However, many questions remain unanswered in the specific molecular mechanisms and networks involved to explain our documented improvements in physiological function and behaviour. Strikingly, no differences were detected when flies were challenged to food starvation or increased stress levels, suggesting that the underlying mechanism regulating these processes are more complex and do not depend only on energy homeostasis, and perhaps, even hardwired in the aged fly.

Furthermore, this study has shown that old flies exposed to 670 nm have increased relative mtDNA levels, with similar levels found in young flies. Together with improved mitochondrial function, this could suggest that changes mitochondrial dynamics are being affected, in particular the mitophagy (mitochondrial specific autophagy) and biogenesis pathways. Autophagy is essential for maintaining long-term cellular homeostasis and is involved in several stress responses[97]. Interestingly, ageing may also be correlated with a decline in autophagy, concomitant with functional senescence[98,99]. Hence, the autophagy pathway could be modified by 670 nm exposure.

Mitochondrial biogenesis is the process of splitting mitochondria into new daughter mitochondria. As the number of mitochondria decline with age, the mitochondrial biogenesis is likely to be affected. Calorie restriction extends life-span and improves physiological and behavioural function in a similar way to the results obtained in this study. The mechanism of calorie restriction is thought to be by improving mitochondrial function and up-regulating mitochondria, i.e. biogenesis. Similarly, 670 nm exposure could induce mitochondrial biogenesis.

2.4.1 Future perspectives

The regulation of mitochondrial dynamics is complex. It is known that *in vitro* mitochondria that show healthy membrane potential are likely to undergo biogenesis. However, no *in vivo* evidence has been found. Similarly, if 670 nm improves the mitochondrial membrane potential, it is likely that mitochondria will undergo biogenesis. This needs to be further investigated.

To assess whether flies treated with 670 nm undergo mitochondrial biogenesis, I would assess:

- qPCR: PGC-1α and TFAM, transcripts known to up-regulate with mitochondrial biogenesis.

It has been reported a link between decreased autophagy activity with ageing, correlated with functional senescence[98,99]. Since 670 nm improves or reverts functional senescence, it may also interact with autophagy. To study autophagy, treated and untreated flies should be tested for:

- Western Blot: LC3-II/LC-3I ratio. The ratio between these components changes with autophagy.

Chapter 3. 9-*cis*-carotene improves mitochondrial function and health-span in *Drosophila melanogaster*.

3.1 Introduction

In the previous Chapter, we successfully improved mitochondrial function with light, with significant associated improvements in metabolism, physiological function and behavioural responses. However, mitochondrial function can be affected with alternative approaches like drugs. However, their commercial value is questionable due to unexpected side effects. Food supplements or additives may also be an approach to deliver products that alter mitochondrial function. Here we investigate how one type of carotenoid improves life and health-span and mitochondrial function in *Drosophila*, that has an established safety profile and is already a component of human diet.

3.1.1 Carotenoids

Carotenoids are a group of pigments that are ubiquitous in nature. They provide pigmentation in animals, plants, and microorganisms, and possess critical roles in biological systems. Carotenoids are characterised by a polyene backbone, consisting of a series of conjugated C=C bonds. This feature makes carotenoids interesting, as such double bonds are able to interact with free radicals and oxygen singlet. Thus, they act as antioxidants.

Alterations in the carotene polyene backbone, modifying the number of conjugated double bonds or the addition of chemical functional groups, alter the reactivity of carotenoids. Consequently, carotenoids can act as light harvesting molecules (in photosynthetic complexes), or they can play protective roles[100].

Carotenoids are not synthetized in humans or other animals, who depend on dietary intake to maintain an adequate supply. Maintaining this supply is important for several reasons, as carotenoids have many biological properties that improve overall health. In fact, epidemiological studies have shown that human diets rich in vegetables and fruits (rich in carotenoids) are associated with reduced incidence of age related diseases[101].

However, in studies were carotenes, particularly all-*trans*-β-carotenes, have been supplemented in normal diet (CARET and ATBC studies[102,103]), results seem to contradict previous epidemiological studies, implying pro-oxidant abilities, highlighting the need to understand better the role of carotenoids in biological systems.

Recent studies with 9-*cis*-β-carotene are more promising, especially in the treatment of retinal diseases, showing beneficial effects in patients and models of retinitis pigmentosa[104,105]. It has been suggested that 9-*cis*-β-carotene can be cleaved *in vivo* forming 9-*cis*-rteinal, replacing the missing native 11-*cis* chromophore in this retinal dystrophy and efficiently bind rhodopsin, forming a light sensitive molecule *in vivo.* However, very little is known about 9-*cis*-β-carotene in other functions, especially its role in acting as an antioxidant, and potentially its impact on mitochondria and ageing.

9-*cis*-β-carotene is characterised by a *cis* double bond between carbon positions 9 and 10, conferring a hinged structure, compared to the all-*trans*-β-carotene. It is known that all-*trans*-β-carotene is able to self-aggregate, which may contribute to the negative effects of carotenoids on dietary supplementation[106]. Perhaps, due to the *cis* configuration, 9-*cis*-β-carotene is less likely to aggregate, and this may contribute to greater potential beneficial aspects.

Nevertheless, the interaction of carotenoids with reactive oxygen species is complex and controversial. In the case of all-*trans*-β-carotene there is evidence for both, anti-oxidant and pro-oxidant properties, while there are reports suggesting a more anti-oxidant protective role in 9-*cis*-β-carotene[107]. Additionally, carotenoids break down, react with other components forming geometric isomers or adducts *in vivo*, whose consequences are little understood. Notably, one of the breakdown products of β-carotene interacts with mitochondria, inhibiting their function[108,109]. Carotenoid cleavage products (CCP), including highly reactive aldehydes and epoxides, are formed during the antioxidative action of carotenoids. *In vitro*, these molecules inhibit oxidative phosphorylation, impairing mitochondrial potential and boosting the release of reactive oxygen species. The researchers also found a decrease in mitochondrial glutathione, essential for ROS scavenging[109].

Little is known regarding whether 9-*cis*-β-carotene has similar properties to all-*trans*-β-carotene, or whether the *cis* form is a potentially beneficial, especially regarding their anti-oxidant function.

Commercially, the green biflagellate halophilic microalga *Dunaliella salina* (DS) has been used as an efficient biological source for β-carotenes. In this algae, more than a 10% of dry weight is β-carotene, as long as the algae is cultivated under certain stress conditions. Two stereoisomers are mainly found in DS: all-*trans* and 9-*cis*-β-carotene[110]. Interestingly, the 9-*cis* to all-*trans* ratio production is directly related to the amount of light given during the division cycle. A high light dose yields higher 9-*cis*-β-carotene production[110].

As ageing is associated with mitochondria dysfunction and an increase in oxidative stress, in this study we investigated the effect of *D. salina* extracts rich in 9-*cis*-β-carotenes on lifespan, mobility and mitochondrial function in *D. melanogaster*, and which components of the extracts are responsible for those observations.

3.1.2 Hypothesis

Here we investigated whether a diet supplemented with *D. salina* extracts rich in 9-*cis*-β-carotenes improved life and health-span and mitochondrial function in *Drosophila*. No work has examined the consequences of a diet rich in 9-*cis*-β-carotene in an aged fly model known to have mitochondrial functional and structural dysfunction. Therefore we tested for the following hypotheses:

- Long-life supplementation in *D. melagnogaster* with *D. salina* extracts rich in 9-*cis*-β-carotenes extends life-span.
- Supplementation with 9-*cis*-β-carotenes improves mitochondrial function which results in an improvement in functional senescence.

3.1.3 Aims

The specific aims of this study are to:

- Investigate the consequences of lifelong *D. saliva* extract supplementation on life-span and mitochondrial parameters (ATP and metabolic rate).
- Assess the effect of short treatment (2 weeks) with *D. saliva* extract on mitochondrial function.
- Explore the consequences on *D. saliva* in aged flies in locomotor function, and to investigate which component of the extract has the biggest impact on this function.

3.2 Methods

3.2.1 Carotenoids extracts

Four carotenoids extracts were prepared in ethanol for fly feeding trials as follows: Synthetic *all-trans* β carotene was obtained from Sigma-Aldrich (UK). An excess amount of the powder was dissolved into ethanol to make a saturated concentration of all-trans β carotene. An extract of lutein was obtained by dissolving a lutein supplement (Lutigold, 6 mg) obtained from Holland & Barrett (UK) in ethanol. A carotenoids extract prepared using supercritical CO_2 was prepared from biomass of *Dunaliella salina* which was cultured in open raceway ponds by Monzon Biotech, Spain, harvested then freeze-dried. The carotenoids extract was obtained after supercritical CO_2 extraction of the biomass, and the extract was dissolved in ethanol for fly feeding. A further carotenoids extract sample containing a very high 9-cis β carotene content was prepared in laboratory incubators by harvesting the biomass from cultures of *D. salina* strain CCAP 19/41 *Dunaliella salina rubeus* PLY_DF-15 maintained according to patent GB1718822.8. Biomass was harvested in batches in 50 ml centrifugation tubes by centrifugation at 3.000 g for 10 min. Cells were ruptured by ultrasonication and vortexed in ethanol to provide a carotenoids extract which was then clarified by centrifugation at 3.000g for 10 min and the supernatant aliquoted into 14 amber glass bottles for fly feeding.

3.2.2 Characterisation of carotenoids extracts

The carotenoids composition of the four carotenoids extracts was analysed using High-performance liquid chromatography with a diode array detection (HPLC-DAD). Each extract in ethanol was filtered through a 0.45 μm syringe filter into amber HPLC vials and then analysed using a YMC30 250 x 4.9 mm I.D S- 5μ HPLC column. The column temperature was set at 25 ºC, and flow rate of motile phase at 1 mL min^{-1} with isocratic elution with 80 % methanol: 20 % methyl tert-butyl ether (MTBE) with a pressure of 88 bar. Absorbance at 450 nm was used to quantify *all-trans* β carotene, *9-cis* β carotene and lutein, and absorbance at 280 nm was used to quantify phytoene. Carotenoids standards of synthetic β carotene, lutein, and phytoene were obtained from Sigma-Aldrich (UK) and the concentrations of *9-cis* and *all-trans* β carotene, lutein, and phytoene in the extracts were estimated using the standard curves.

3.2.3 *D. melanogaster* strain and maintenance conditions

Wild type male and female *Drosophila melanogaster* Dahomey were used in these experiments. Males and females were separately housed in standard fly vials containing a normal cornmeal/sugar/yeast/agar medium food. Standard housing conditions were maintained, 25 °C, 12 h light/dark regime, although flies were positioned in a darker section in the incubator to avoid carotene photo-oxidation.

Experimental flies were produced by breeding: 15-20 male and female pairs were left in each food vial and allowed for oviposition for 24h. When new flies were born and reached the imago development stage, they were separated by sex and transferred to new vials to use in the experiment.

3.2.4 Treatment with *D. salina* extract

Four different concentrations of *D. salina* extract were used in the experiment, based on total β-carotene content (9-*cis*- β-carotene and all-*trans*-β-carotene) dissolved in 100% ethanol: 100 μM, 10 μM, 1 μM and 0.1 μM. Two additional groups were used, one with 100 μM extract (based only on all-*trans*-β-carotene) and one group where normal cornmeal/agar/sucrose/yeast was substituted by a lyophilised *D. salina* in 1% agar compound, on a kcal *like for like* substitution. 100 uL of each concentration was sprayed on top of normal food, for each group. The control group consisted with 100% ethanol only. Food vials were changed three times per week.

3.2.5 *D. melanogaster* lifespan assay

To determine the effects of the *D. salina* extract (rich in carotenoids) on longevity, 140 flies were collected for each experimental group (30 flies per vial). The numbers of dead flies were counted three times per week, and all remaining living flies were transferred to fresh vials. The survival rates were calculated using Kaplan-Meier method and presented as survival curves. The mean, median, and minimum lifespans were determined.

3.2.6 *D.melanogaster* locomotor activity assay

Each experimental variant was examined at 8 weeks, when mobility is significantly affected by ageing, for locomotor activity[111]. Males and females were evaluated separately for each concentration. The measurements were performed using the negative geotaxis assay. Briefly, flies were placed in empty polystyrene vials with an 8 cm mark. The flies were gently tapped to the bottom and number of flies that climbed above the 8

cm mark in 20 s was counted. The test was performed 10 times for each group of 10 flies.

3.2.7 Whole body metabolic rate

Metabolic rate was assessed by measuring CO_2 production in lab-made respirometers following a protocol previously described Yatsenko et al.[76]. In each of the groups there were 5 replicates containing 5 flies. Metabolic rate was measured over 120 min.

3.2.8 Statistics

Data collected was analysed with GraphPad Prism v.6 and statistical analysis was undertaken using two-way Mann Whitney U test unless otherwise stated. A $p<0.05$ value was considered significant and data presented are mean + SEM.

3.3 Results

3.3.1 Carotenoids profile analysis

This work was undertaken by Dr. Yanan Xu and Mr Chiziezi Wosu at Greenwich University. HPLC profiles of the different carotenoids extracts are shown in Figure 3.1 and Table 3.1. All-*trans* β carotene and 9-*cis* β carotene were the most abundant carotenes in the algal extracts, with only small amounts of other carotenoids in the extracts such as lutein, zeaxanthin, α-carotene, and phytoene. The concentrations of major carotenoids in each extract are shown in Table 3.1. The two algal extracts had similar profiles but differ in the composition of the two β carotene isomers. The supercritical CO_2 extract had a 9-*cis*/all-*trans* β carotene ratio of ~1.4, while the high 9-*cis* β carotene extract had a 9-cis/all-*trans* β carotene ratio of ~2.4.

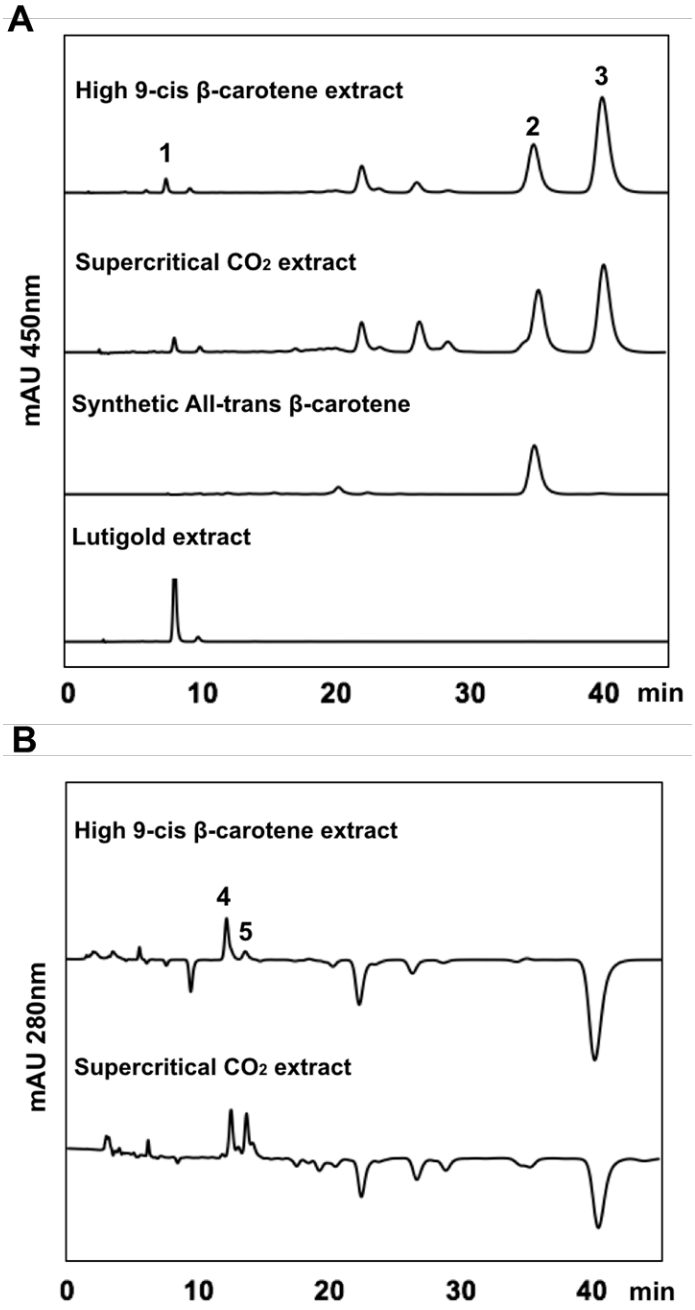

Figure 3.1. HPLC chromatograms of the ethanol extracts of the four carotenoids sources at (A) 450 nm and (B) 280 nm. The major peaks shown are: 1. Lutein; 2. All-*trans* β-carotene; 3. 9-*cis* β-carotene; 4. All-*trans* phytoene; 5. *Cis* phytoene. The supercritical CO_2 and high 9-*cis* extract contain both β-carotene stereoisomers: all-*trans* and 9-*cis.* However, the data shows that the high 9-*cis* extract contains a higher proportion of 9-*cis* compared to all-*trans,* indicating an enrichment of 9-*cis* with our DS cultivation method (patent GB1718822.8). mAU: milli-Absorbance Units.

Sample	*All-trans* β-	*9-cis* β-	Lutein	Phytoene

	carotene $\mu g\ mL^{-1}$	carotene $\mu g\ mL^{-1}$	$\mu g\ mL^{-1}$	$\mu g\ mL^{-1}$
Synthetic all-*trans* β-carotene	33	-	-	-
Lutein	-	-	17	-
Supercritical CO_2 extract	32	45	2	7
High 9-*cis* β-carotene extract	71	168	4	6

Table 3.1. Concentrations of individual carotenoids in the extracts. The concentration for different carotenoids in the different extracts was calculated as shown in the table. The supercritical CO_2 and high 9-*cis* extract contained both β-carotene stereoisomers: all-*trans* and 9-*cis,* but as depicted in Figure 3.1, high 9-*cis* β-carotene extract is enriched with 9-*cis* β-carotene.

3.3.2 *D. melanogaster* life span and locomotor function after DS extract treatment

First we investigated the effects of DS extract on life span when administered at different DS extract (supercritical CO_2 extract) concentration, shown in Figure 3.2 , A and B and Table 3.2. In males (Figure 3.2 A), whereas 0.1, 1, 100 and 100 μM extract had no effect. But significant life span extension occurred at 10 μM, were median life-span increased by 13.5%, but no change in absolute life span. There was an overall increase in life span in the other concentrations, but these were not significant. However, treatment with DS algae, had a significant detrimental effect on life span, were the median life-span decreased by approximately 25.5% compared to controls. The extract rich in carotenoids also increased the life span of females, but on a different scale. In females (Figure 3.2 B) only the 10 μM concentration increased significantly the median lifespan (32.6%), but on average, females had a reduced general median lifespan compared to the male population. Conversely, females fed with DS algae had no significant changes in their life span compared to control flies. These differences in life span extension between sexes could also be observed in other life span extension treatments such as rapamycin[91]. Thus, DS extract increased efficiently median life-span in both sexes in *D. melanogaster*, significantly at a 10 μM concentration.

Treatments that improve life span are often associated with improvements in the locomotor capabilities. At 7 weeks of age locomotor function was assessed by negative

geotaxis. Figure 3.2 C and D shows locomotor function at 8 weeks of age for the different treatment groups. The DS extract did not have an effect on the locomotor function on a dose dependent manner. In the case of males (Figure 3.2 C), only the higher concentrations (10, 100 and 100 μM) had a positive impact on the climbing index. In contrast, only the 10 and 100 μM concentrations resulted in an improvement in females (Figure 3.2 D). In both sexes, 10 μM treatment had an increase in life-span and also an improvement in their locomotor function, suggesting a causal connection between them. The 10 μM concentration was used in subsequent experiments, as it produced the largest increase in median life span and locomotor function.

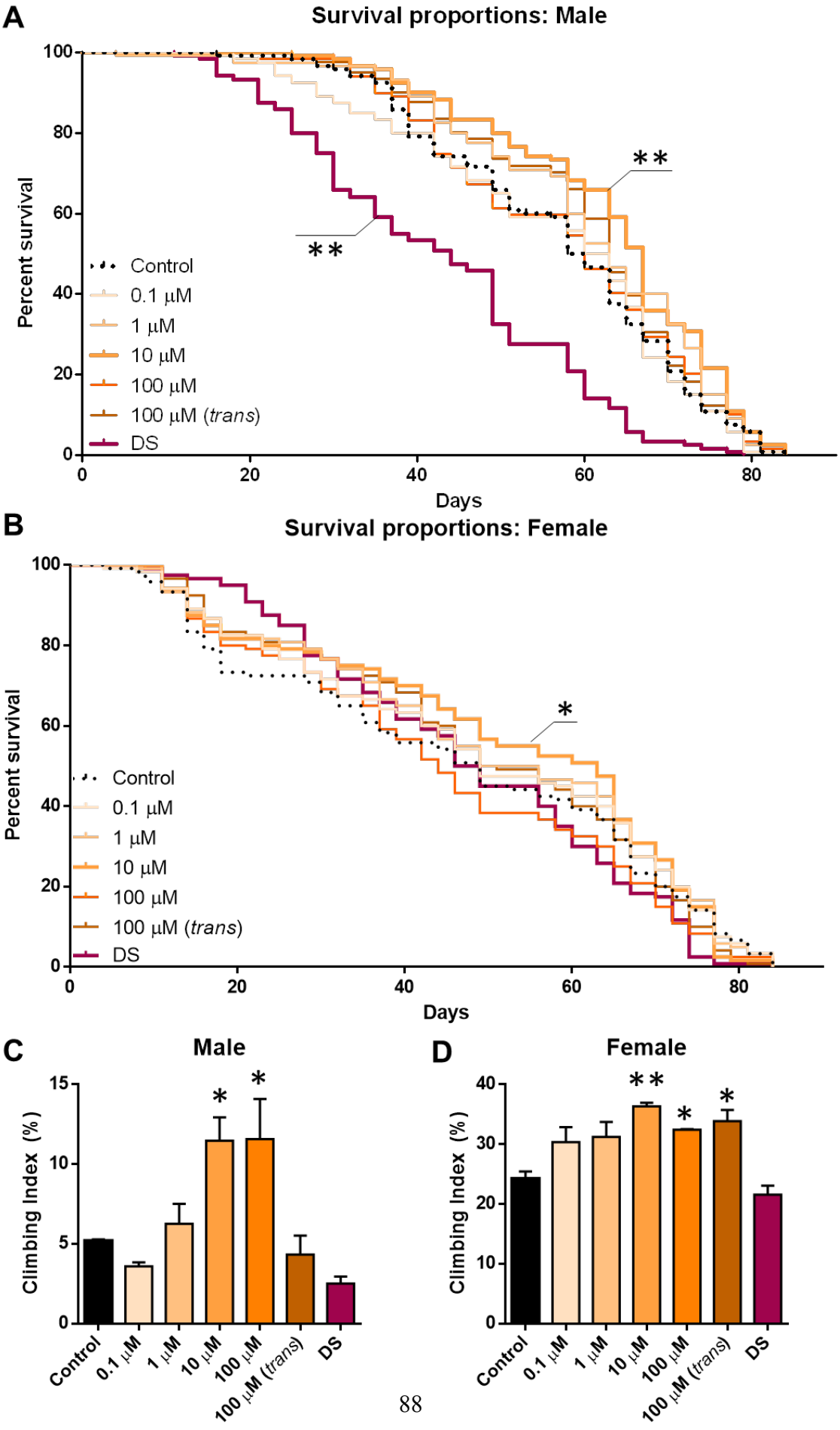
A
Survival proportions: Male
Percent survival
Days
Control
0.1 μM
1 μM
10 μM
100 μM
100 μM (trans)
DS
**
**
B
Survival proportions: Female
Percent survival
Days
Control
0.1 μM
1 μM
10 μM
100 μM
100 μM (trans)
DS
*
C
Male
Climbing Index (%)
Control
0.1 μM
1 μM
10 μM
100 μM
100 μM (trans)
DS
D
Female
Climbing Index (%)
Control
0.1 μM
1 μM
10 μM
100 μM
100 μM (trans)
DS

Figure 3.2. Lifespan (A and B) and locomotor activity (C and D) in flies treated with DS extract. Effect of DS extract on lifespan of *D. melanogaster* males (**A**) and females (**B**) (n=120 flies in each group), Long-rank Mantel Cox test. In **C** and **D**, locomotor activity assessed by negative geotaxis at 7 week old flies treated since birth with DS extract (n=40 flies in each group), one-way ANOVA, multiple comparisons Bonferroni. * p<0.05, ** p<0.01).

Concentration		***Median***	***Mean***	***SEM***	***90%***	***min***	**N**
Males	Control	59	57.11	1.404	77	16	120
	0.1 µM	61.5 (+4.2%)	55.79	1.571	77	16	120
	1 µM	63 (+6.7%)	60.44	1.405	77	4	120
	10 µM	67 (+13.5%)	63.01	1.278	79	25	120
	100 µM	60 (+1.7%)	58.08	1.451	79	18	120
	100 µM *trans*	63 (+6.7%)	60.08	1.285	77	25	120
	DS	44 (-25.4%)	42.51	1.503	65	11	120
Females	Control	49	46.94	2.25	77	4	120
	0.1 µM	49 (±0%)	49.76	2.141	77	4	120
	1 µM	56 (+14.2%)	50.93	2.093	77	11	120
	10 µM	63 (+32.6%)	51.8	2.098	77	11	120
	100 µM	44 (-10.2)	45.12	2.019	74	9	120
	100 µM *trans*	53.5 (+9.2%)	50.38	1.974	77	11	120
	DS	47.5 (-3%)	47.83	1.704	74	9	120

Table 3.2. Lifespan parameters of *D. melanogaster* after DS extract treatment. Median lifespan (age where 50% of the population is dead and 50% is alive) with percentage change (in %), mean lifespan and standard error of the mean (SEM) in days, 90% - age of 90% mortality (days), minimum lifespan, n number of flies in each group. In males, only the 10 µM and DS groups showed significant differences compared to the control group. In females however, only the 10 µM was statistically significant compared to the control group, with a 32.6% improvement in median lifespan.

3.3.3 Effect of DS extract on mitochondrial function

4 week old male flies were treated for two weeks with 10 µM DS extract to assess mitochondrial function (Figure 3.3). Here we studied whole metabolic rate and total ATP levels. Whole metabolic rate was used as a surrogate marker for mitochondrial respiration. Two week treatment increased whole metabolic rate by a 27% (Figure 3.3 A), suggesting an improvement in mitochondrial function.

Similarly, ATP levels at the same age revealed a 26.5% increase after the 2 week DS extract treatment compared with to controls (Figure 3.3 B). The data for whole metabolic rate and total ATP levels suggests that the extract may improve mitochondrial function. This is surprising, however, as it is known that carotenoids breakdown products intervene negatively with mitochondrial function[108].

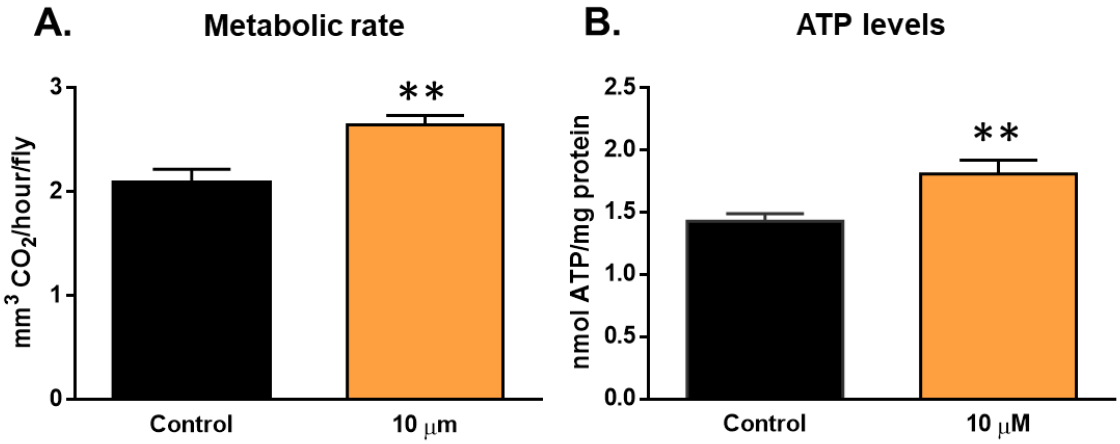

Figure 3.3. 14 day 10 µM DS extract supplementation in aged flies: metabolic rate (A) and ATP levels (B). Treatment with DS carotenoids extract significantly improved mitochondrial function compared to untreated flies, measured by metabolic rate (as a marker of mitochondrial respiration) (**A**) and ATP levels (**B**). 6 replicates containing 5 flies each. Results are mean + SEM. **$p < 0.01$.

3.3.4 DS extract positive effects are mediated by 9-cis-beta-carotene

Our DS extract contains different percentages of different carotenoids, mainly including all-*trans* β-carotene, 9-*cis*-beta carotene or lutein. However, our DS extract is rich in 9-*cis*-beta-carotene, which has been proven to improve health in humans and mice, in contrast to the all-*trans*-β-carotene[104,105]. To investigate which component (or components) of the DS extract was responsible for improvements in life span, locomotor and mitochondrial function, we fed flies with the different carotenoids

independently for two weeks and assessed their locomotor function. However, synthetic routes to produce pure and stable 9CBC have not been established yet. Therefore, a highly enriched with 9CBC solution was produced, with a ratio of 9CBC:ATBC 3:1, used in our experiment. The results are shown in Figure 3.4.

Overall, a two-week intervention treatment did not significantly improve locomotor function of treated flies compared to controls. However, the treatment with 10 µM 9CBC group had a significant improvement on locomotor function increasing it by 36.8%. This suggests that the positive effects of the DS extract seen in previous experiments where due to the 9CBC and not necessarily by other components. A few additional observations were made. First, the 100 µM 9CBC solution did not improve the locomotor function. Surprisingly, neither did the 10 µM DS extract. An explanation for this could be that the treatment window was not long enough for the DS extract to have a positive impact or, as the DS extract is not only rich in 9CBC but also contains large quantities of other carotenoids, the known negative effects of large carotenoids quantities cover the positive results of the 9CBC, which can only be seen at longer treatments as in our previous experiment.

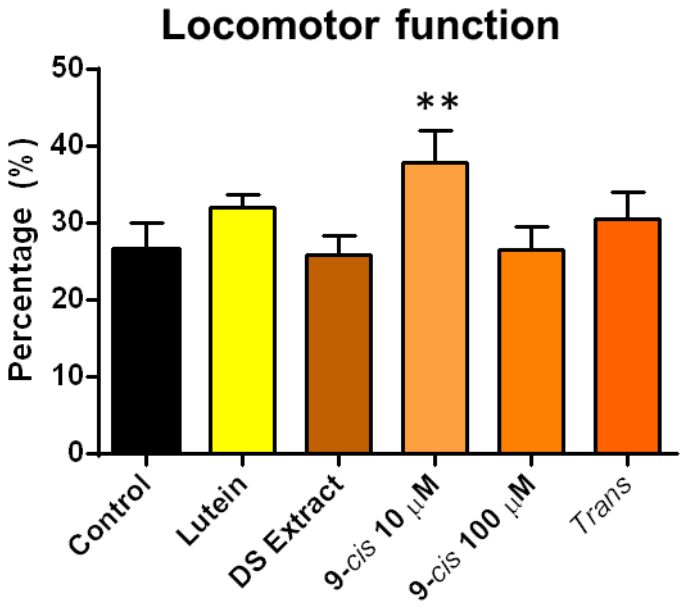

Figure 3.4. 14 day supplementation in aged flies with different carotenoids. Effects on locomotor function assessed by negative geotaxis of different carotenoids supplements. Only the group treated with 9-*cis*-β-carotene 10 µM significantly

improved their climbing index by 36.8%. All other groups had climbing indexes similar to the control group. n=60 flies per group. Results are mean +SEM. **p < 0.01.

3.4 Discussion

We have shown an improvement in mitochondrial function in *D. melanogaster* with an intervention treatment with carotenoids. Importantly, the source of this 9CBC was a natural DS, easily cultivated.

Many studies have shown the geroprotective function of different carotenoids, including lutein, xanthain and β-carotenoids, affecting mitochondrial function and extending their life span and health span[112]. Additionally, it has been suggested that carotenoids modulate the activity of the Insulin/IGF-1 pathway, a pathway that plays a key role in biological ageing[113]. Carotenoids also possess other functions, including anti-inflammatory activities, although more research is needed to fully understand the role of carotenoids in biological systems.

Our data is consistent with data obtained for other carotenoids[112]. Supplementing our DS extract, rich in 9CBC at 10 μM to the food medium increased mean and median life span in *D. melanogaster*. Importantly, the effects were not necessary dose dependent, suggesting that other components of the extract may have opposed or non-related biological activities. The effects on lifespan were different between females and males, indicative of physiological differences between sexes. Notably feeding flies with only DS algae, had drastic consequences on life-span and locomotor activity in males, while life-span and locomotor activity in the same group in females, had no detrimental consequences. An explanation for this observation is that females consume more food during their life than males[112]. Locomotor function improved with extract treatment, and 9CBC is the putative component causative of these effects.

Longevity is associated with mitochondrial function, as it declines with biological ageing[114]. Treating old flies with the carotenoid rich extract reverses mitochondrial function, indicating a link between carotenoid and mitochondrial function. It is known that treatment with carotenoids reduces reactive oxygen species[101]. However, some breakdown components of carotenoids metabolism have been shown to impair mitochondrial function[108,109]. It has to be seen whether the same components are produced with 9CBC, the main carotenoid in our DS extract. An alternative explanation could be that our treatment with the DS extract causes mild stress in the fly, activating

defence mechanism and inducing mitochondrial function protection while boosting reactive oxygen scavenging processes. However more research needs to be undertaken to fully understand the role of 9CBC on mitochondrial function

9-cis-beta-carotene has been shown to be biologically active in rescuing phenotypes in cell lines and animal models with retinal pathologies. Synthetic 9CBC recues M- and S-cone degeneration in eye-cups from a retinitis pigmentosa rodent model[105], while naturally sourced 9CBC from *D. bardawil* algae rescues retinal function in patients with retinitis pigmentosa and defects in their retinoid cycle[104]. The 9CBC enriched algae extract could be a natural and economical route for treatment with patients with retinal dystrophies.

In conclusion, this study presents an economic and natural 9CBC source, with possibilities of scaling up. The obtained extract rich 9CBC is biologically active with geroprotective properties, extending life span, health span and mitochondrial functions in flies treated with the extract.

3.4.1 Future perspectives

We found interesting improved mitochondrial parameters in flies treated with the rich carotenoid algal extract. However, further investigation is required to elucidate the molecular pathways involved, since antioxidant properties of carotenoids are controversial.

To further clarify the role of 9CBC as an antioxidant agent and improving mitochondrial function, different experiments should be performed:

- Supplementing cell culture medium with 9CBC and assess mitochondrial function with SeaHorse, to study mitochondrial function. This data should provide information and guidance whether 9CBC affects mitochondrial function.
- Flies treated with high 9CBC should be analysed for carotenoids and their brake down products with mass-spectrometry, to verify that flies ingest and process carotenoids.
- Determination of ROS levels by DCFH-DA and scavenging mechanisms, such as glutathione peroxidase (Western Blot).

Chapter 4. Circadian rhythms in mitochondrial respiration in *Drosophila melanogaster*

In our studies improving mitochondrial function using 670 nm light in aged flies (Chapter 2), we were unable to replicate the positive impact of 670 nm light exposure when it was delivered in the afternoon. Anecdotal evidence from other 670 nm groups supported this observation. Hence, we examined mitochondrial function after 670 nm exposure in the morning versus afternoon. In Figure 4.1 we show respiration (metabolic rate) in *Drosophila* with different 670 nm exposure time. Treatment with 670 nm for 7 days in the morning (AM) results in a significant increase in respiration, while 670 nm treatment in the afternoon (7 days, PM) has no impact on respiration. When we then treated the PM flies for another 7 days but in the morning (AM+PM), a significant increase in respiration could be observed. Hence, afternoon 670 nm exposure seems not to affect mitochondrial function like in the morning.

These results are an opening for this chapter, where we further investigate circadian rhythms in mitochondrial function.

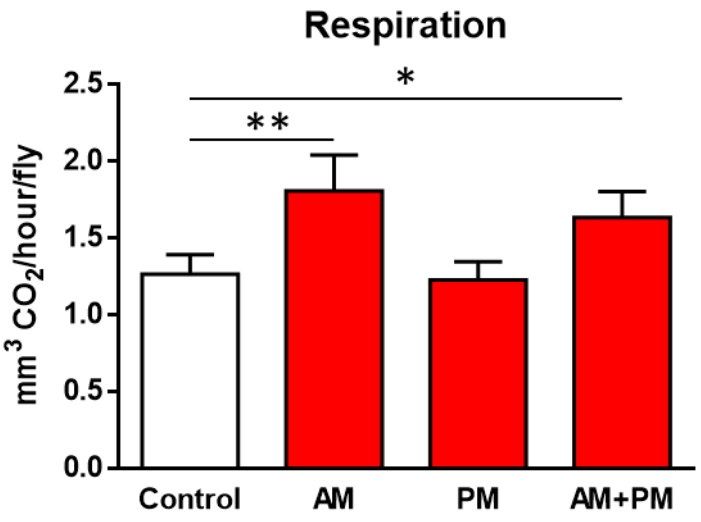

Figure 4.1. Differences in respiration at different times of the day after 670 nm exposure. Flies treated for 1 week in the afternoon (PM, 4 pm) did not have an increased respiration unlike flies exposed in the morning (AM, 10 am), where respiration increased significantly. However, when flies were treated in the first week in

the afternoon, and the following week in the afternoon (AM+PM), significant increase in respiration was observed. 6 replicates containing 5 flies each. One-way Mann Whitney-U test. * $p<0.05$, ** $p<0.01$. Results are shown as mean +SEM.

4.1 Introduction

Mitochondria are the powerhouse of the cells. They supply cellular energy in the form of ATP through nutrient oxidation. However, one big challenge faced by mitochondria is the adaption to changes in energy demand, as ATP cannot be stored. Mitochondria need to sense (via sensors and/or communication) changes in the cellular energy homeostasis so they adjust their function to cellular energy requirements. During periods of high activity, demand for energy is significantly higher compared to resting periods. Mitochondrial function needs to adapt efficiently to these changes in energy demands.

4.1.1 Circadian rhythms

Circadian rhythms are biological events that occur over 24 h, the time it takes the Earth to rotate. All living organisms have adapted to this rhythmic event, developing their own endogenous clock systems, referred as "circadian clock". These molecular clocks allow organisms to predict rhythmic changes in their environment, ultimately increasing their fitness. In *Drosophila*, the molecular clocks control courtship and mating, egg eclosion, determines active and resting periods, temperature preference and feeding times[115–117].

In all organisms, circadian clocks are endogenous. They are able to sustain the rhythmicity even in the absence of any environmental cue. However, various time cues (Zeitgebers), such as light cycles, are able to synchronise these molecular clocks. Normally two types of molecular clocks can be found. A master clock in the brain and molecular clocks in individual cells and tissues, known as peripheral clocks. A complex network between clocks regulates circadian rhythms.

The molecular clocks are generated by a negative transcriptional feedback loop, involving transcription factors that inhibit their own repressors. The repressors are modified (e.g. phosphorylation) during the day and degraded, initiation a new cycle.

The molecular clock in *Drosophila* is shown in Figure 4.2. Here transcription factors *clock* and *cycle* form a heterodimer and promote the expression of *period* and *timeless*.

Period and *timeless* also form a heterodimer and accumulate during the night. This complex then enters the nuclei where it phosphorylates *clock* and *cycle*, rendering them inactive. During the day, *period* and *timeless* are also modified by phosphorylation, identified as a degradation cue. Thus, *clock* and *cycle* are released from *period* and *timeless* repression, starting a new cycle.

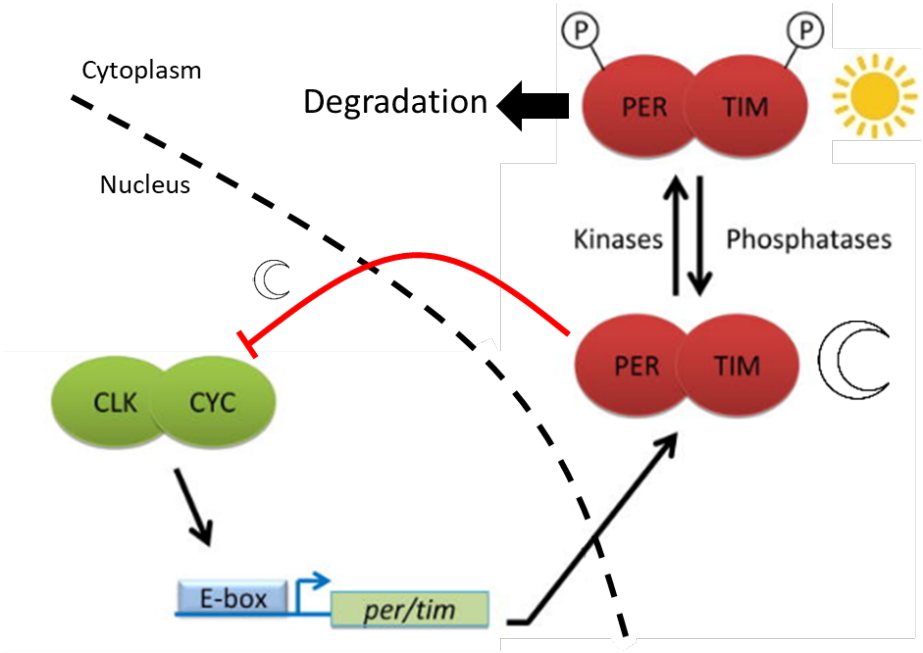

Figure 4.2. The *Drosophila* circadian clock. The transcriptional feedback loop in *Dirosophila* involves *clock* (CLK) and *cycle* (CYC) that promote the expression of the repressors *period* (PER) and *timeless* (TIM). During the night PER and TIM accumulate and inhibit CLK and CYC. During the day, PER and TIM are phosphorylated and degraded, liberating CLK and CYC, initiating a new cycle. Modified from Tataroglu et al[118].

In the adult fly, the central pacemaker in the brain is consequently entrained by daily light-dark cycles[118], synchronising other oscillators in all cells in the body. This synchronisation can be further promoted with other environmental cues, like rhythmic feeding behaviour. Several transcriptomes[119,120], proteomics[121–123] and metabolomics[124] studies have highlighted the role of the circadian control of metabolism, extending the notion towards a control of metabolic route by circadian clocks, as cells need to constantly adapt to changes in their environment.

Resting and activity cycles naturally occur throughout the day, result in pronounced changes in energy demand that needs to be addressed by mitochondrial function, the

main suppliers of cellular energy. However, little is known at the molecular level how mitochondrial function adapt to these changes. Studies have shown how mitochondria from specific tissues (e.g. muscle) change their function[125], but very little is known at the organism scale. To address this question, we examined temporal changes in mitochondrial function from WT *Drosophila melanogaster*, investigating key mitochondrial enzymes involved in OXPHOS and the glycolytic process, global ADP and ATP levels, NAD^+/NADH ratio and whole metabolic rate. As expected, the majority of our markers oscillate during the day, and remarkably many of them accumulate in a diurnal manner in the fly, concomitant with their physiological activity. However, in the dark phase, mitochondria "switch off", while becoming active again before dawn. We propose that the fly organisms anticipate the light phase by boosting mitochondrial function, which reaches its zenith during light phase, thus adapting to the daily changes in energy supply and demand.

4.1.2 Hypothesis and aims

In this study we focus on mitochondrial circadian function in *Drosophila melanogaster*, and how it oscillates during the day. No work has investigated how mitochondrial function is affected by the circadian clocks in a whole organism. We tested the following hypotheses:

- Mitochondrial function changes during the day.
- These changes in mitochondrial function can be matched with changes in fly behaviour.

4.1.3 Aims

The specific aims of this study are to:

- Measure the specific activity of the electron transport chain enzymes in three different time-points.
- Assess whole fly metabolic rate, ATP levels and NAD/NADH ratio at the same time-points.

4.2 Materials and methods

4.2.1 Fly husbandry

Male *Drosophila melanogaster* Dahomey were used throughout this study, maintained under standard lab conditions (12/12 lighting at 25˚C and 70% humidity) and normal cornmeal/sugar/yeast/agar medium food. Newly hatched flies were collected and kept at standard density of 30 male flies in vials (25 x 95 mm) containing 10 mL food medium (changed 3 times per week).

4.2.2 Fly collection

Flies were collected at 6 weeks old (±1 day) at the following times: 0, 8 and 16 h post *Zeit-geber* time (ZT) and snap-frozen in dry-ice.

4.2.3 ATP

For ATP measurements, flies were processed as previously published[74]. Briefly, 5 male flies were homogenised in 100 µl of 6 M guanidine-HCl in extraction buffer (100 mM Tris and 4 mM EDTA, pH 7.8) to inhibit ATPases, followed by freezing in dry ice. The homogenate was then heat treated (95˚C) for 5 min, followed by 3 min centrifugation at maximum speed. The supernatant was collected and diluted (1/50) with extraction buffer. ATP was measured using a commercially available ATP determination kit based on luminescence (Life Technologies, UK). The relative ATP levels were calculated by dividing the luminescence by the total protein concentration (determined by the BCA method). Six replicates containing 5 flies were used for each group.

4.2.4 Metabolic rate

Whole body metabolic rate was assessed by measuring expired CO_2 production in lab-made respirometers following a protocol previously described[76]. The respirometer contains soda lime, which absorbs expelled CO_2 produced by the flies, and thus decreases the pressure in the respirometer. The change in gas volume (decreased pressure) is measured by the displacement of fluid in a glass capillary attached to the sealed respirometer. In each of the groups there were 6 replicates containing 5 flies each. Because metabolic rate is measured over 120 min, the experiment started 1 h before hypothetical collection time, and finished 1 h after.

4.2.5 Mitochondrial enzymes

To examine the daily regulation of mitochondrial function, we measured the enzymatic activities of the complexes in the mitochondrial respiratory chain. Flies were killed at 8

hours intervals, and homogenised. For each time point, 6 biological replicates were analysed.

After collection, flies were homogenised with a pestle in homogenising buffer (0.121 g of Tris, 0.15 g of KCl and 0.038 g of EGTA in 50 mL distilled water, pH 7.4; 0.854 g of sucrose were added 10 ml the buffer on the same day of the experiment). The homogenate was centrifuged at 300 *g* for 5 min at 4˚C, to separate the debris. The supernatant was collected and aliquoted and stored at −80°C for enzyme activity assays. An aliquot was also used to measure protein concentration in each sample, following the commercially available BCA protein assay from ThermoFisher Scientific. This was to standardise the amount of protein added in each enzymatic assay. We assayed the activity from seven biological replicates for each time point post *zg time* (ZT), with the activity of each biological replicate estimated from two technical replicate assays.

4.2.6 Complex I

Complex I (NADH-ubiquinone reductase) of the mitochondrial electron transport chain was measured following a DCIP-couple method adapted from Antoon J.M. Janssen et al[126]. This method is based on the reduction of DCIP by electrons from decylubiquinol, reduced by complex I after NADH oxidation. This avoids nonspecific NADH oxidation (direct method to assay complex I) interfering in the assay. The DCIP method results in a high rotenone sensitivity. The reaction mix contained 25 mM potassium phosphate, 3.5 g/L BSA, 60 µM DCIP, 70 µM decylubiquinone, 1.0 µM antimycine-A, 0.2 mM NADH and 15 µg/mL sample protein. Reduction of DCIP is spectrophotometrically monitored at 600 nm and inhibited with rotenone 1 mM.

4.2.7 Complex II

The catalytic activity of complex II (succinate dehydrogenase) was measured following a protocol previously published[77]. Complex II was monitored by following the reduction of DCPIP at 600 nm, The reaction mixture contained 30 mM NaH2PO4, 100 µM EDTA, 2 mM KCN, 2 µg/mL antimycin A, 2 µg/mL rotenone, 750 µM BSA, 10 mM succinate, 100 µM DCPIP, 100 µM decylubiquinone and 15 µg/mL sample protein, and was inhibited with 400 mM malonate.

4.2.8 Complex III

Complex III (cytochrome c reductase) specific catalytic activity was measured following the increase in reduced cytochrome *c* at 550 nm. The reaction mixture

contained 35 mM NaH2PO4, 2.5 mg/mL BSA, 5 mM MgCl2, 2 mM KCN, 2 µg/mL rotenone, 50 µM cytochrome c, 25 µM decylubiquinol and 15 µg/mL mitochondrial protein, and was inhibited with 5 µg/mL antimycin A. Potassium borohydride was used to reduce decylubiquione.

4.2.9 Complex IV: cytochrome *c* oxidase

The specific activity of complex IV was measured following a protocol previously published[77]. Complex IV activity was measured by determining the rate of oxidation of reduced cytochrome c at 550 nm. The reaction mixture contained 5 mM MgCl2, 2 µg/ml rotenone, 2 µg/ml antimycin A, 1 mM DDM, 45 µM cytochrome c. Each test contained 15 µg of fly homogenate. The reaction was inhibited with 4 mM KCN. Sodium dithionite was used to reduce cytochrome *c*[78].

4.2.10 Glycolysis

The reaction kinetics for glyeraldehyde-3-phosphate dehydrogenase is used as a surrogate marker for glycolysis. The specific activity of the glyceraldehyde-3-phosphate dehydrogenase was measured modifying the procedures described by Krebs[127] and Velick[128]. The activity of this enzyme was measured by determining the increase in the absorption at 340 nm resulting from the reduction of NAD. Briefly, 15 male flies were snap frozen and homogenised in pyrophoshate/arsenate buffer (0.015 M sodium pyrophosphate buffer, pH 8.5 containing 0.03 M sodium arsenate) and total protein content measured with the BCA assay (ThermoFishes Scientific). The reaction mixture contained pyrophosphate/arsenate buffer, supplemented with 0.25 mM NAD, 3 mM DTT. Per sample, 1.5 ug of protein was added to the assay followed by the addition of D-glyceraldehyde-3-phosphate (final concentration of 0.25 mM) to start the reaction.

4.2.11 NAD^+/NADH Ratio

A hydrazine coupled assay was used to measure NAD^+ and NADH as published previously[129]. Fifteen male flies were killed in dry ice and homogenized in 250 µl of homogenization buffer (10 mM nicotinamide, 10 mM Tris-Cl, 0.05% (w/v) Triton X-100, pH 7.4 adjusted using HCl). Then the homogenate was centrifuged at 12000 × g for 1 min at 4 C. The supernatant was treated with equal volume of phenol:chloroform:isoamyl alcohol (25:24:1, v/v), mixed vigorously and centrifuged at 12000 × g for 5 min at 4˚C. The aqueous phase was collected and mix with an equal

volume of chloroform and centrifuged at 12000×g for 5 min at 4 C. The resulting aqueous phase contains pyridine nucleotide and used for the assay.

Because the enzymatic assay does not distinguish between the oxidised and the reduced forms, an additional step is needed. For each sample, two aliquots of 18 µl of the pyridine nucleotide extraction were removed. One of them was mixed with 2 µl of 0.1 M HCl and the other with 2 µl of NaOH so that the final [H+] or [OH-] were 0.01 M. Both aliquots were then heated on a 65°C heat block for 30 min to degrade the reduced or the oxidized pyridine nucleotide respectively. Samples were then immediately placed on ice. Finally, 2 µl of the opposite reagent (NaOH or HCl) wes added to neutralize pH.

The reaction mixture for the NAD/NADH assay contained: 0.1 M BICINE (N,N-bis(2-hydroxyethyl)glycine), 0.6 M ethanol, 50 mM EDTA, 2 mM PES and 0.5 mM MTT, 0.02% hydrazine and 0.2 mg/ml alcohol dehydrogenase (ADH).

For the assay, a NAD^+ standard curve was used (100-50-25-12.5-6.25-3.125-1.57-0 µM). 5 µl of standard or sample were added to each well containing 120 µl of reaction mixture without PES and MTT, which were added to start the reaction together with ADH right before the plate was read at 570 nm. Kinetic curves were taken for the first 5 min to measure reaction velocity. The NAD^+ standard was used to determine the concentration of NAD^+ and NADH in each sample.

4.2.12 RNA extraction and qPCR

This experiment was performed by Dr. Billy Ferrara. Data was analysed by Dr. Billy Ferrara.

RNA was extracted from *Drosophila* heads. About 80-100 heads were used per sample, homogenised in 1 mL of TRIzol Reagend (Ambion, UK) using micro pestles (Sigma). Homogenate was incubated at RT for 5 min. 0.2 mL chloroform was added, shaken vigorously (15 s) and incubated at RT for 3 min. Samples were spun at 12.000 g 15 min at 4 °C. Aqueous phase was collected and RNA was purified using RNeasy mini kit (Qiagen, UK). Genomic DNA was removed using On-Column DNase (Sigma). Purity of eluted RNA was estimated by the OD ratios (A_{260}/A_{280}>2.0) and quantified using the BioDrop spectrophotometer (BioDrop, UK), then stored at -80 °C until needed. 70 ng total RNA from each sample was converted into cDNA using RevertAid First Strand cDNA Synthesis Kit (ThermoScientific) with random hexamer primers as reverse transcription primers.

Three biological samples were analysed in triplicate using gene specific primers, at designated ZT times. Transcription levels were determined using the Step One PCR machine (Applied Biosystems, CA, USA) with the SYBR Green probe (Qiagen). Prepared cDNA was amplified under the following conditions: 1 µL of cDNA, 5 µL of 2X QuantiFast SYBR Green PCR master mix (ThermoFisher Scientific), 1 µL of each forward/reverse primer (10 pmol) and 3 µl of H_2O per 10 µL reaction. The PCR were as follows: initial denaturation 95 °C 5 min, 40 cycles of 95 °C, 30 sec and 58 °C, 1 min. Data was analysed using the ΔΔCt method[130]. Refer to Table 4.1 for primers used.

Target	*Forward sequence (5' to 3')*	*Reverse sequence (5' to 3')*
Gapdh2	CGTTTCTACCGATTTCCT	GTTGTCGTACCAAGAGAT
LrRNA	GTCTAACCTGCCCACTGA	TTCGTCCAACCATTCATTCC
Cox1	TATTAGATGTTGATAACCGAGTAG	TAATCGTCCAGGTGTACC
SdhB	CTGTACGAGTGCATCCTG	GGTCCTTCAACTTGTTCAGA

Table 4.1. Primers for qRT-PCR

4.2.13 Statistics

Data was acquired and analysed with GraphPad Prism v6.0 Analysis of variance was used in cases of multiple comparisons. Differences were considered significant at $p<0.05$ as noted in the figure legends.

4.3 Results

4.3.1 Oscillations in mitochondrial electron transport chain enzymes

Results are shown in Figure 4.3. Complex I (a), II (b) and IV (d) changed their activity significantly at assessed times. Remarkably, in all three cases, activity peaked during the light phase, at Zeit-geber time (ZT) 8h. In all three complexes (I, II and IV), the activity at ZT16, during the dark phase, was significantly lower than in ZO or Z8. The significant fall in activity between Z8 and Z16 was greater in complex II and IV, where the activity dropped by more than 50% in ZT16 compared to ZT8. Interestingly, the activity pattern of complex III (Figure 4.3 c) did not follow a significant oscillatory pattern, even though there was a decline at ZT16 compared to ZT0 and ZT8 this was not significant, neither did the activity peaked at ZT8. However, the overall pattern of activity found in complex III faintly mirrors the pattern found in other respiratory complexes.

Overall, these data suggests that key metabolic enzymes in mitochondrial function, like the complexes in the electron transport chain, increase their function in the light phase, while minimising their activity during the dark phase, during the resting period of the animal. However, the enzymatic activities do not remain constants over the light phase, but are more elevated at ZT8 than ZT0.

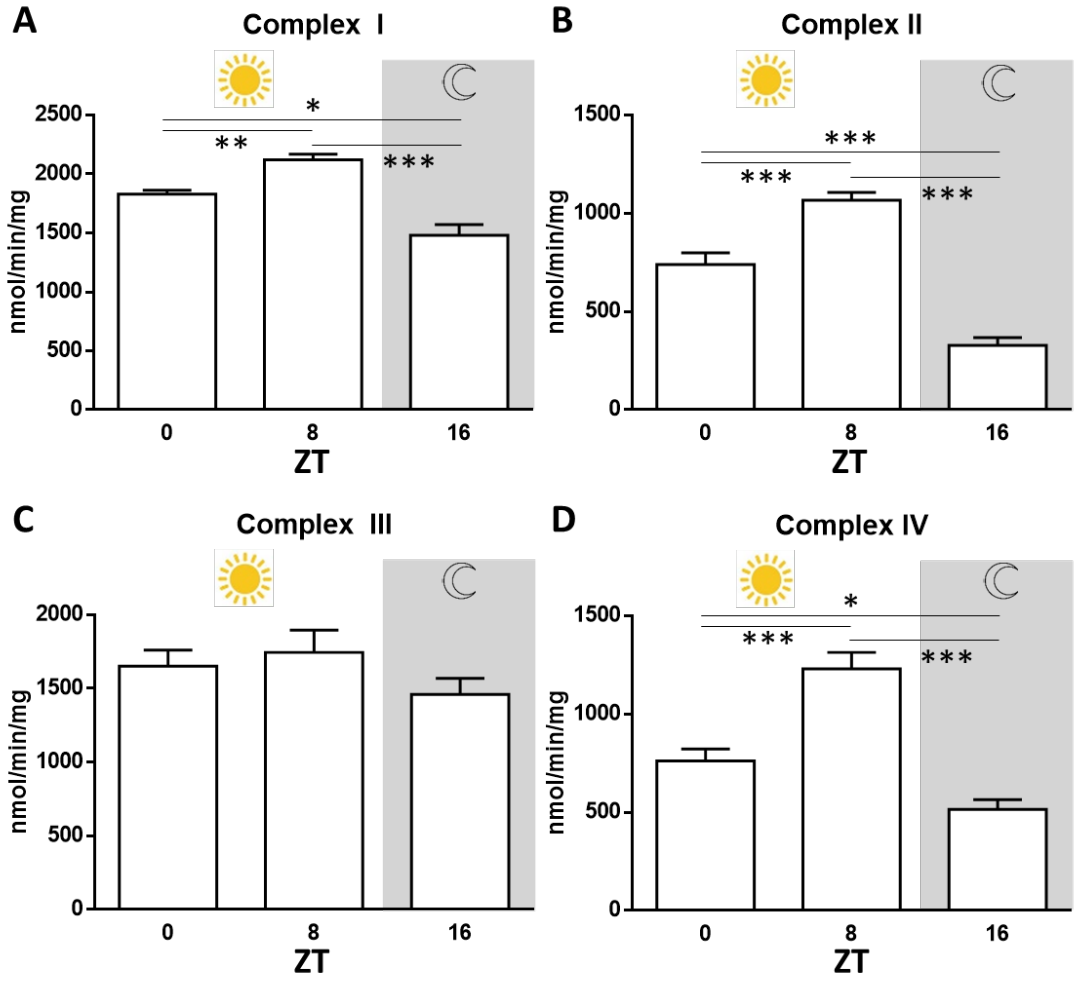

Figure 4.3. Daily oscillation in mitochondrial electron transport chain enzymes. Specific enzymatic activities for electron transport chain enzymes were measured in WT *Drosophila* homogenates collected at indicated times. **A**. Complex I, NADH-ubiquinone reductase, ANOVA $p<0.0001$, **B**. Complex II, succinate dehydrogenase, ANOVA $p<0.0001$, **C**. Copmlex III, cytochrome c reductase, non-significant ANOVA $p=0.2816$, **D**. Complex IV, cytochrome c oxidase, ANOVA $p<0.0001$. Differences between ZT: two way Mann Whitney U-test *$p<0.05$, **$p<0.01$, ***$p<0.001$. Grey shading represents the dark phase. Data are presented as means ± SEMs from 6 biological replicates per time-point.

4.3.2 Circadian changes in complex II and complex IV gene expression

To understand whether changes observed in the activity of electron transport chain enzymes are a consequence of changes in gene expression we investigated the expression of two genes in two key complexes: complex II, as wholly encoded in the nuclear DNA (gene *Sdhb*) and complex IV, encoded in both the mtDNA and nuclear DNA (gene *CoxI*, mtDNA encoded). The obtained expression was normalised to two housekeeping genes: GAPDH2 (nuclear encoded) and LrRNA (mtDNA encoded). The results are shown in Figure 4.4. The expression pattern of our genes did not change during our assessed ZT time points. However, in more detailed analysis, a small decline in the expression of CoxI was observed at ZT16 compared to ZT0 (when normalised to GAPDH2 and LrRNA). Albeit not significant ($p=0.0960$) this mirrored the activity seen in complex IV.

Overall, the data suggests that even though the expression pattern of genes do not changes significantly, the changes in the activity patterns observed in Figure 4.3 could be explained with posttranslational regulation.

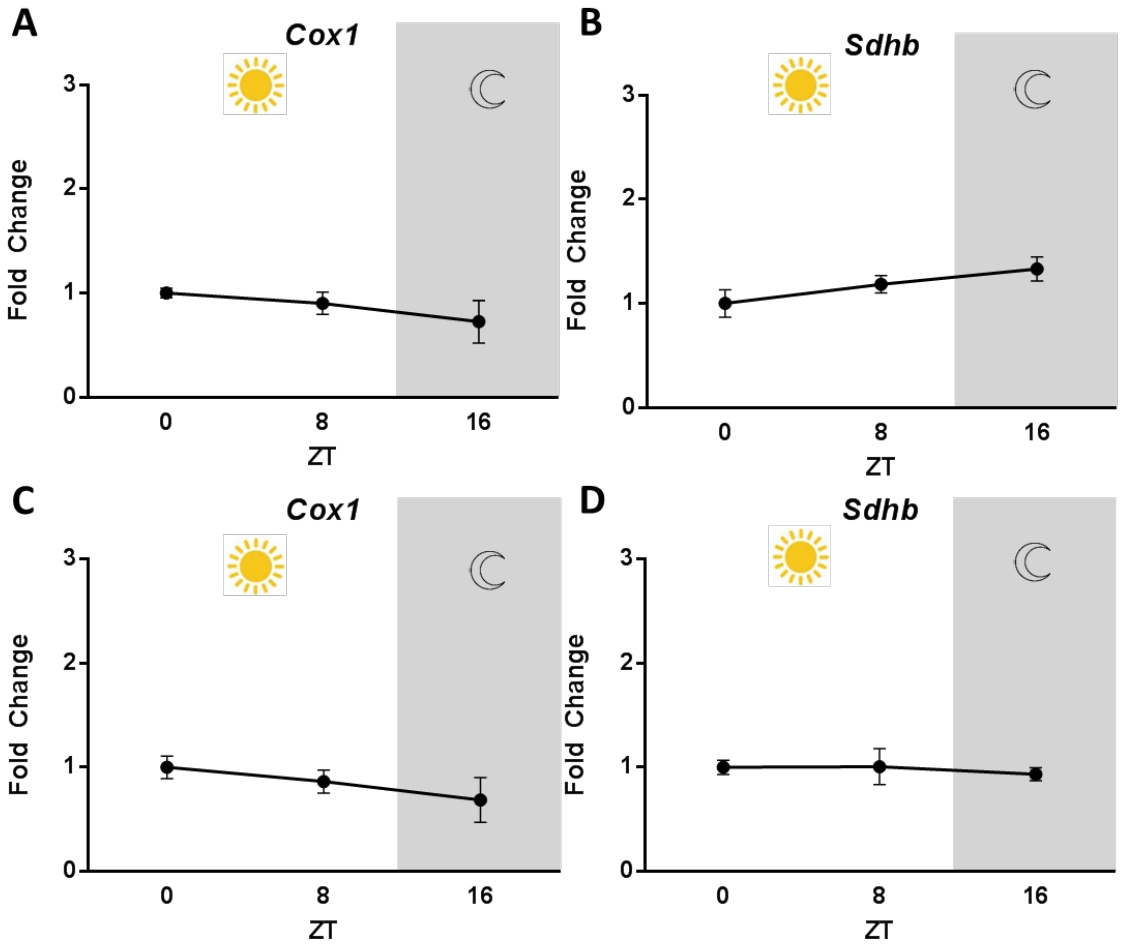

Figure 4.4. Daily changes in *Cox1* and *Sdhb* expression in WT *Drosophila*. *Cox1* and *Sdhb* expression was measured in whole *Drosophila* homogenates at indicated times, and normalised to housekeeping gene glyceraldehyde-3-phosphate dehydrogenase-2 (GAPDH2) (**A** and **B**) and mitochondrial large ribosomal RNA (LrRNA, **C** and **D**). Fold changes were normalised to 0ZT. One-way Anova, *Cox1/Gapdh2* p=0.1640, *Sdhb/Gapdh2* p=0.1548, *Cox1/LrRNA* p=0.0960, *Sdhb/LrRNA* p=00.94755. Data are presented as means ± SEMs from 3 biological replicates (each three technical replicates) per time-point.

4.3.3 Circadian changes in ATP, glycolysis and reducing equivalents

To further understand changes in mitochondrial function and energy metabolism during the day, and link these to overall physiology and behaviour changes in the organisms, we also analysed overall ATP levels, metabolic rate, glycolytic flux and reducing equivalents levels. The same time points were chosen. The results are shown in Figure 4.5. First we looked at whole metabolic rate, as a surrogate marker for whole body respiration, as the expelled CO_2 is measured over a period of time. Figure 4.5 a shows that the amount of expelled CO_2 peaks at ZT8, in concordance with the data in Figure

4.3, where the enzymes in the respiratory chain peaked also at ZT8. Surprisingly, there was no difference between ZT0 and ZT16 in this parameter, suggesting that the differences observed in the activity of complexes in Figure 4.3 between these two time points are indeed due to an overestimation of ZT0 or underestimation in ZT16 in the enzymatic activity. This discrepancy between *in vivo* data (whole body respiration) and *in* vitro (ETC enzymatic activity) could be due to the lack of communication and signalling that is not present in *in vitro* studies.

We subsequently investigated the activity of the main enzyme in the glycolytic pathways, glyceraldehyde-3-phosphate dehydrogenase, as a surrogate marker for glycolysis. The results are shown in Figure 4.5 b. Here we did not observe significant differences in the activity of this enzyme between ZT0 and ZT8. However, the activity increased during the dark phase, at ZT16. This is surprising, as we would expect an increase in the glycolytic flux concomitant with an increase in the respiratory function, as the end product of the glycolytic pathway is the substrate for the Krebs cycle, which provides the energy rich electron to the mitochondrial electron transport chain. This discrepancy in our data would suggest that in ZT8 the oxidative lipid metabolism (beta-oxidation of fatty acids) might be the supplier for energy rich electron to the respiratory chain. Interestingly, the glycolytic activity reached its peak at ZT16, when mitochondrial respiratory function was at its lowest. During the night phase, anabolic routes are boosted, subtracting intermediate metabolites from the Krebs cycle (supplied by the glycolysis pathway) to synthesise amino acids or fatty acids, which would decrease the availability of rich energy electrons to the respiratory chain.

Then we analysed global ATP and ADP levels in the flies, as shown in Figure 4.5 c and d. The ATP levels peak at Z0, but significantly decreased at ZT8 and at ZT16. Again, this is unexpected as the peak in respiratory activity occurs at ZT8, while this is not when ATP peaks. This suggests that the demand for ATP at ZT8 is high, hence an increase in OXPHOS function. But this does not translate into an increase in global ATP levels. However ATP levels dropped at ZT16, in agreement with our OXPHOS data. We also measured ADP levels to check whether the changes in ATP levels were mirrored with changes in ADP. As expected, the overall ADP+ATP pool remained the same, but ATP was converted into ADP.

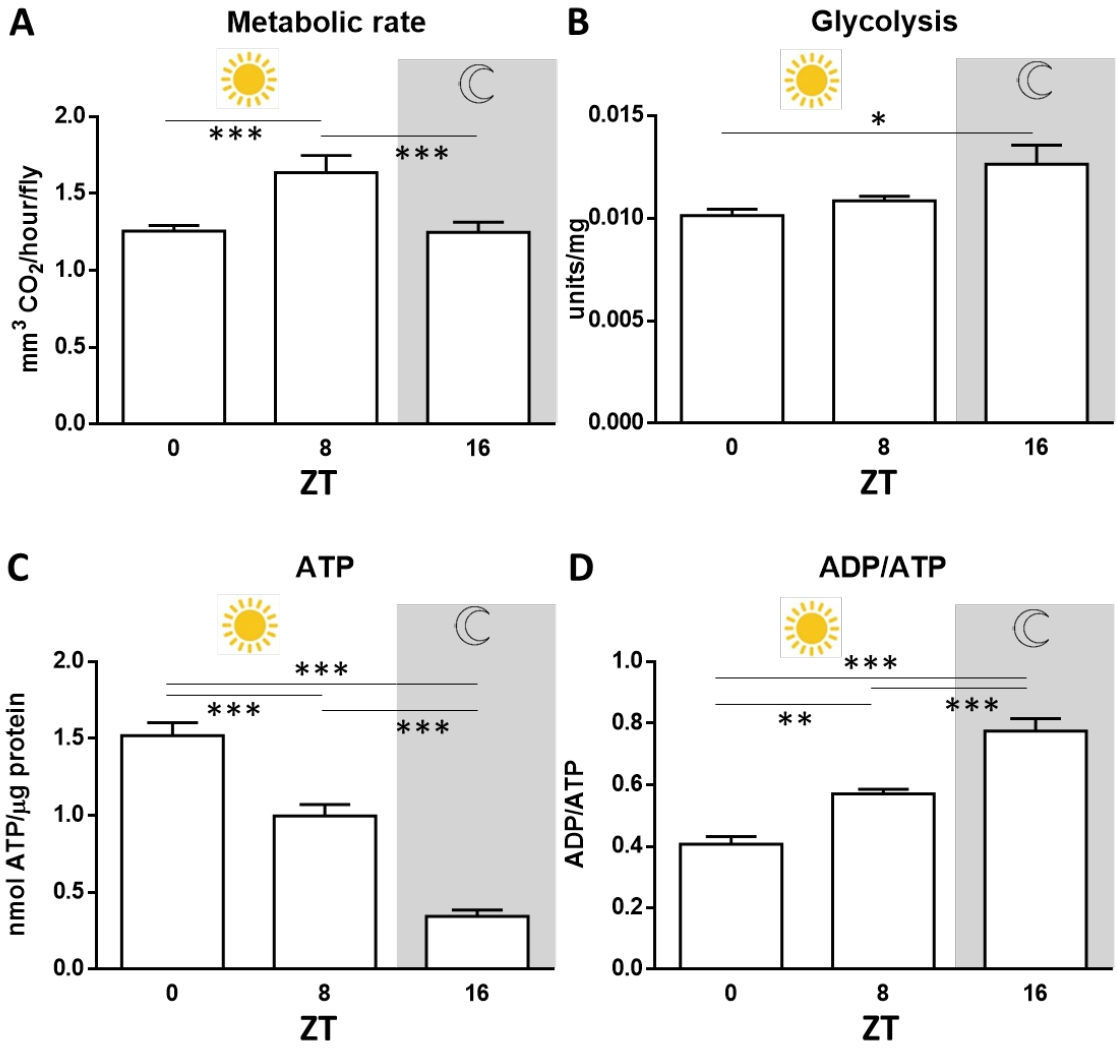

Figure 4.5. Daily changes in metabolic rate, glycolysis and ATP and ADP/ATP ratio in WT *Drosophila*. Whole body metabolic rate was measured in vivo. Whole body ATP, ADP, glycolytic activity were measured in WT *Drosophila* homogenates collected at indicated times. **A**. Whole body metabolic rate in *Drosophila*, ANOVA $p<0.0017$. **B**. Glycolytic activity measured by glyceraldehyde-3-phosphate dehydrogenase enzymatic activity, ANOVA $p=0.0234$. **C**. Whole body ATP levels, ANOVA $p<0.0001$, **D**. ADP/ATP ratio, ANOVA $p<0.0001$. Differences between ZT: two way Mann Whitney U-test *$p<0.05$, **$p<0.01$, ***$p<0.001$. Grey shading represents the dark phase. Data are presented as means ± SEMs from 6 biological replicates per time-point.

To better understand the connection between the glycolysis pathway, Krebs cycle and electron transport chain we investigated the reducing equivalents NAD^+/NADH as shown in Figure 4.6. The NAD^+/NADH ratio peaked at ZT8, similar to the activities of

complexes in the electron transport chain or the metabolic rate, indicative of a rapid consumption of NADH, which is why the ratio is higher compared to the other ZT time points. At ZT16 the ratio dropped significantly to similar levels found in ZT0, with NADH concentration higher than at ZT8, in agreement with glycolysis being very active and fuelling the Krebs cycle, but reduced activity in the electron transport chain, the main consumer of reducing equivalents.

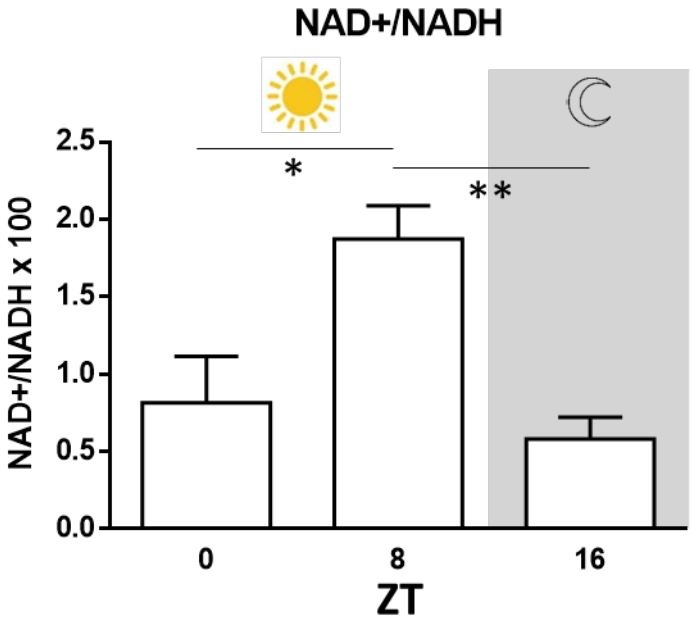

Figure 4.6. Daily oscillations in the NAD$^+$/NADH ratio. Whole body NAD$^+$ and NADH concentrations were measured in *Drosophila* homogenates collected at indicated times. The ratio was then calculated. During the light phase, the ratio peaked at ZT8, indicative of mitochondrial NADH consumption, in agreement with high ETC enzymatic activity and whole body respiration peaking also at ZT8. ANOVA $p<0.0067$. Differences between ZT: two way Mann Whitney U-test *$p<0.05$, **$p<0.01$. Grey shading represents the dark phase. Data are presented as means ± SEMs from 6 biological replicates per time-point.

4.4 Discussion

The circadian clock is strongly associated with mitochondrial function. In this study, we examined the temporal changes in key mitochondrial metabolic parameters, by measuring the activity of the electron transport chain enzymatic complexes, global ATP and ADP levels, glycolytic flux and whole metabolic rate in *Drosophila melanogaster*.

Unexpectedly, we discovered that the majority of electron transport chain enzymes peak ZT8, concomitant with a consumption of NADH. However, ATP levels peak at 0ZT, at the start of the light phase. While glycolytic activity reaches its zenith at ZT16 (dark phase), it coincides with the lowest levels of mitochondrial oxidative phosphorylation activity and global reduced ATP levels. The only plausible explanation is that the fly, during the day predominantly builds up mitochondrial function, peaking at ZT8, producing enough energy for normal active physiological function. However, during darkness, when the fly sleeps, the OXPHOS function is reduced with a simultaneous increase in glycolytic activity and reduced global ATP levels. From our data it seems that the fly anticipates the light phase, with an increase in OXPHOS function and ATP levels. Although it still raises the question how this temporal coordination is achieved at the molecular level.

When we tested the possibility that transcriptional regulation may play a role in this process, we found that the transcripts we analysed did not oscillate in hour time-points. This is in disagreement with previous studies, which found that the majority of the mitochondrial and nuclear transcripts oscillates in a daily manner. They also found that the oscillation in transcripts did not correlate with protein oscillation. It may be that our specific transcripts did not oscillate. However, it is important to clarify that our data was obtained from *Drosophila* housed in 12 h light-dark regimen, while the transcriptome data was acquired from mice (*Mus musculus*) under constant darkness[131]. This difference in experimental design may account for some discrepancy in our observations. Moreover, our data described enzyme activity in the electron transport chain, which does not necessarily correlate with transcriptome or proteome data, as post-translational regulation may play a significant role shaping the circadian mitochondrial function. However, we have not tested for any post-translational regulation in our experiments.

We quantified metabolic rate by measuring the amount of carbon dioxide produced over time at our set time points. As with our enzymatic activity results, the peak activity in these enzymes correlated with the highest amount of carbon dioxide produced. Interestingly, in the case of *Drosophila* the amount of carbon dioxide produced is equimolar to the amount of oxygen consumed, being a *bona fide* method to study mitochondrial oxygen consumption *in vivo*. However, the lowest point in ETC complexes activity did not correlate with the lowest level in metabolic rate. This is

indicative of, as pointed out previously, the problem of *in vitro* vs *in vivo* experiments. *In vitro* experiments do not allow the study of complex regulations of the cell, tissue or organism.

Previously, oscillation in NAD^+ and NADH has received much attention. Analysing the oscillation in the NAD^+/NADH ratio would help understanding the redox homeostasis. In cells, the amount of NADH is always lower than the oxidised counterpart, suggesting that energy-rich electrons in the NADH are rapidly consumed. In this study, we examined the redox oscillations over a day by measuring the NAD^+/NADH ratio in *Drosophila*. We show that the peak in NAD^+ correlated with the peak in ETC enzymes and metabolic rates. Importantly, previous data on mRNA levels for nicotinamide phosphoribosyltransferase, involved in the biosynthesis of NAD^+, shows an oscillatory pattern similar to the NAD^+/NADH pattern found in our data, where the mRNA levels started peaking at about ZT8[132]. Furthermore, the highest level of NADH and lowest of NAD^+ correlated not only with the dark phase (lowest ETC activity), but also with the highest level of glycolytic flux, suggesting that many Krebs cycle intermediates are used for other anabolic reactions. Hence, the NAD^+/NADH is an excellent parameter to link our glycolysis and mitochondrial function data.

Our data also links with *Drosophila* circadian behavioural data. Locomotor activity peaks before dawn and in late afternoon, anticipating both the light and night phase, similar to our data on respiration (metabolic rate) and ETC enzymatic activity. Associated with locomotor function, are other behavioural responses that display a similar circadian pattern, like mating and courtship[116], temperature preference[115] or food intake[133]. However, we still need to demonstrate that our data is true circadian data orchestrated by the main molecular clocks, by doing similar set of experiments but in constant darkness.

It is still important to clarify that we do not know how circadian mitochondrial function is regulated on a molecular level. We show no oscillation in transcript levels, but the activities of the enzymes in the electron transport chain oscillated during the day, which influences oscillations in key metabolites (ATP, ADP or NADH, NAD^+).

4.4.1 Future perspectives

We found interesting aspects of circadian mitochondrial function in *Drosophila*. The problems remains as to how this is regulated at the molecular level, specifically how the circadian clock is able to regulate mitochondrial function.

However we still need to investigate whether the results shown here are controlled by the molecular clock, or are in fact, behaviour related. For that purpose, flies need to be maintained under constant darkness and experiments replicated. Only this way we will know whether the data shown here is controlled by the circadian clock.

No oscillations were found in our analysed transcripts, but proteins are subject to a whole set of posttranslational regulation, which would explain our results. To investigate the presence of posttrasnaltaional regulation western blot would be performed, targeting phosphorylated and non-phosphorylated forms:

- Complex I: subunit NDUFB10 (phosphorylation decreases activity) or NDUSF4 (phosphorylation increases activity).
- Complex III, phosphorylation of subunits I and II decreases the activity of this complex.
- Complex IV, phosphorylation of CIV-I and CIV-IV increases its activity.

Chapter 5. S-cones and blue vision: correlating structure and function in aged primates

Some of the data shown in this section has been published in Scientific Reports:

Weinrich, T. W., Powner, M. B., Lynch, A., Jonnal, R. S., Werner, J. S., & Jeffery, G. (2017). No evidence for loss of short-wavelength sensitive cone photoreceptors in normal ageing of the primate retina. *Scientific reports*, 7, 46346.

5.1 Introduction

Primates are regarded as vision-oriented mammals. Old world primates, including humans, possess trichromatic vision (unique within mammals) characterised by three retinal photopigments tuned to peak wavelengths of ~430 nm (blue), ~535 nm (green) and ~562 nm (red)[134]. As primates age, physiological function in the retinae declines. This may relate to photoreceptors having the highest energy demand in the body[135]. Therefore, ageing is associated with a disruption in energy metabolism due to mitochondrial dysfunction.

5.1.1 Structure of the retina

The vertebrate retina consists of an outer monolayer of cells, the retinal pigment epithelium (RPE), and an inner neural retina, a complex network or highly organised neurons. The outer layer of the neural retina contains the light-sensitive photoreceptos, rods a cones. Photoreceptors possess the highest mitochondrial density, containing 75% of the mitochondria in the retina. The inner retinal layers and ganglion cell layers process the light signal generated by photoreceptors and transmit them to the brain visual cortex via the optic nerve.

In primates, the central retina has a 5 – 6 mm diameter “macula”, which contains the fovea at the centre, specialised for high acuity vision. The fovea is characterised by only containing cone photoreceptor cells and being the region of highest cell density mediating high visual acuity.

There is a close inter-relationship between photoreceptors, RPE and the adjacent vascular bed "choroid", which nourishes the outer retina. Hence, dysfunction in any of these components may cause secondary dysfunction in the others. However, if photoreceptors are affected, as in ageing or disease, this leads to cellular dysfunction and potentially cell death, resulting in visual loss.

5.1.1.1 Photoreceptors

The majority of vertebrates have a duplex retina, consisting of two different types of photoreceptor cells:

- Rods: highly sensitive to light (respond to a single photon), responsible for scotopic vision (dim light) and do not discern colour. Rods saturation levels (when all chromophores in a photoreceptor have been transformed from 11-*cis*-retinal to 11-*trans*-retinal) are low (3 orders of magnitude), at the level were cones start to respond. The rods light response is slow, with a significant delayed recovery after the termination of the light stimulus.
- Cones: less sensitive to light, responsible for vision at higher light levels (light vision), high acuity vision and colour vision. Very high light saturation level (9 orders of magnitude). Cones responds to light stimulus without significant delay.

In old world primates, including humans, high acuity is achieved by densely packed cone in the fovea. In humans, cone density in the fovea is around 100,000–200,000 cells/mm^2 [136]. Thus, changes in cones due to aging should have an impact on the quality of vision.

5.1.2 Cone photoreceptors

Cone photoreceptors are highly specialised neurons responsible for catching light and initiate vision, by transforming light into a biochemical signal. They are able to sample light at different wavelength by spectrally distinct cone types defined by their opsin class. Opsin is the light sensitive molecule present in all photoreceptor cells and is divided according to peak sensitivities in: (1) Short wavelength sensitive opsin (SWS1) or S/blue opsin with λ_{max} at around 410–430 nm and (2) mid to long wavelength sensitive opsin (M/LWS) or L/M or red–green opsins, with λ_{max} at around 530–560 nm[137]. Hence, cones are responsible for colour sensation. Humans almost completely rely on cone function, as they manipulate their environmental light and are rarely truly dark-adapted.

Structurally, cones are defined by four discrete regions (Figure 5.1):

- Outer segment: contains the phototransduction machinery.
- Inner segment: contains protein synthesis machinery (myeloid) and mitochondria (ellipsoid). Cones contain the highest density of mitochondria, compared to any other cell.
- Nuclei: RNA transcription
- Synaptic terminal: downstream signal transmission to bipolar cells.

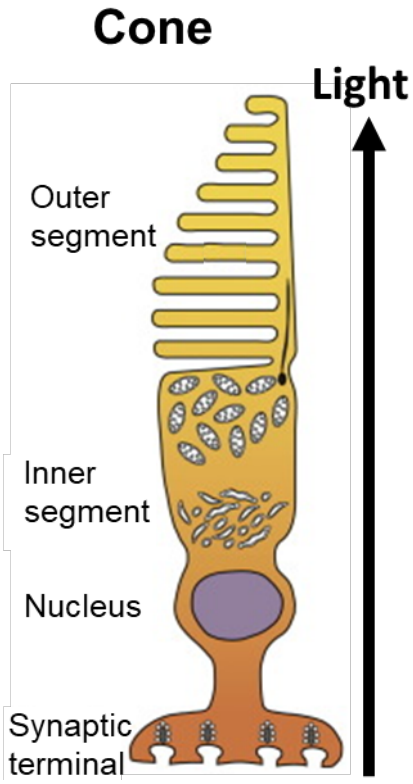

Figure 5.1. Structure of a cone photoreceptor cell. The outer segment contains the machinery to capture light and initiate phototransduction. Mitochondria and protein synthesis machinery are located in the inner segment. The synaptic terminal transmits the information to bipolar cells. Arrow indicated direction of light. Image adapted from Warrant et al[138].

Not all cones age in the same way, and S-cones have some unique properties that differentiate them from their counterpart M/L-cones. Evolutionary, S-cones are more ancient than their M/L-cones counterparts, as it is thought that the S-opsin evolved from an ancestral rod pigment more than 500 million years ago[139]. S-opsin shares 43% of the amino acids sequence with L-cones, and 44% with M-cones. M- and L-cones share 99%

of their amino acids sequence[139]. Cones represent approximately 15-20% of total human retinal photoreceptors. Within the cone population, S-cones represent a 5-15% of the total cone population. Although S-cones are scare, they are regularly distributed across the retina forming a mosaic[140]. In humans, an area of 100–200 μm diameter at the centre of the fovea lacks S-cones[136]. However, in some old-world primates, such as *Macaca fascicularis* (used in this study), S-cones are present in the fovea, although at reduced density[141].

Morphologically and physiologically S-cones are also different to M/L-cones: S-cones have longer inner segments but smaller pedicles[142,143], and they saturate faster compared to their M/L counterparts[144].

With ageing, especially blue colour perception is specifically affected, suggesting that S-cones are more vulnerable to the effects of the ageing process than other cone types. Moreover, in pathological conditions, S-cone pathways are preferentially affected, such as in retinitis pigmentosa, glaucoma and diabetes[145–147]. Strikingly, at high altitude, S-cone function starts to attenuate[148]. Thus, S-cones function is vulnerable in ageing and disease, particularly diabetes.

Cone photoreceptors are packed with mitochondria and possess the largest metabolic demand in the body. Hence it is not surprising that the cone function decreases with age due to the role of mitochondria in ageing. However, very little is known about the aged related cone photoreceptors loss in the aged retina.

5.1.2.1 The ageing retina

With ageing, visual function declines in terms of: colour perception[149], visual acuity[150], dark adaptation[151] and photopic and scotopic sensitivity[152]. Many of these physiological changes have been correlated with age associated structural changes. The most significant change is the loss of neuronal cells. Primates lose about 30% of their rod photoreceptors as they age[153]. Retinal ganglion cells and rod bipolar cells also see reduced populations due to ageing[154,155].

The loss in rod photoreceptors could explain some of the physiological changes observed, but not all, particularly those related to colour vision and acuity. However, little is known about changes in cone populations in the retina during ageing. Therefore, here we explore whether some of the physiological changes observed in the ageing vision system can be explained due to changes in cone populations, particularly those

related to S-cones that appear to suffer markedly in ageing. Thus, we do not know if there is S-cone loss with age of what may account for their decline.

There is evidence that cones do not suffer from the same degree of loss as found in rods[153]. However, this comes from total cone counts where changes in the smaller S-cone population would probably not be detected.

5.1.3 Cellular stress

Cells responds to stress, like oxidative stress due to mitochondrial dysfunction, in a variety of ways: from pathways that promote cell survival to pathways that will elicit programmed cell death (apoptosis) to eliminate damaged cells. Initially, the cells response to stressful stimuli is balanced towards the activation of defend mechanisms against the stress in order to recover. If stress is persistent, the cell may activate programmed cell death pathways. Generally, these responses are highly conserved throughout evolution, as the cell's survival depends on the successful activation of the appropriate response towards intracellular o environmental stress stimuli. For example, heat shock proteins and antioxidant defence mechanisms against oxidative stress can be found in higher organisms, like mammals, and in lower organisms, such as protozoa.

There are many different types of cell stress, and depending on the amplitude, different mechanisms and pro-survival strategies are mounted. If unsuccessful, cell death programs are activated to eliminate the damaged cells.

For the purpose of this chapter, we will focus on mitochondrial oxidative stress and their role in age related changes in the primate S-cone population.

5.1.3.1 The heat shock response

The heat shock response was described historically as the biochemical defence of cells to mild heat stress[156]. Nowadays we know that many other stress stimuli are able to activate the heat shock response, including oxidative stress and heavy metals[157]. The main consequence of stresses at molecular level is protein damage. Consequently the damaged proteins accumulate and aggregate in an unfolded status, rendering them dysfunctional. To counteract this, cells increase the expression of chaperon proteins that assist in folding misfolded proteins, alleviating protein aggregation. This confers protection, status known as thermotolerance, where anti-apoptotic pathways are activated and cells become more resistant to different toxic and stress stimuli, including higher temperatures or greater oxidative stress[158,159].

Heat-shock proteins (Hsp) are the chaperon protein expressed that help alleviate stress. They are a group of evolutionary conserved proteins grouped into subfamilies with molecular weights of approximately 110, 90, 70, 60, 40, and 15–30 kDa with different expression patterns. For example, Hsp90 are constitutively expressed and act as molecular chaperones, preventing premature folding of nascent polypeptides[160]. Others, like the Hsp60 group of Hsp, are mainly located in the mitochondria, where they assist in protein folding inside the micohondria[161].

5.1.4 The role of mitochondria in S-cones

Cones are packed with mitochondria that provide energy in the form of ATP for their function. Mitochondria have an absorption spectrum in the 400-450 nm range, which clashes with the peak sensitivity of S-opsin around 430 nm. Before photons are absorbed by outer segments, light needs to cross the whole retina, including the mitochondria rich inner segments of photoreceptors. Our laboratory's most recent publication (submitted) has demonstrated that S-cones actually have fewer mitochondria to avoid filtering shorter wavelengths and rely heavily on glycolysis as a source for ATP. This manuscript can be found in the Appendix.

5.2 Hypothesis and aims

In this study we investigated whether the differential decline in blue colour vision with age can be partially attributed to a loss in the S-cone population and/or cellular stress. To date, no work has examined in detail the S-cone population with age and whether S-cones are affected by cellular stress.

Therefore we test the hypothesis that:

- Due to the high metabolic rate in cone photoreceptors, the retina suffers from cone photoreceptor cone loss with ageing.
- Since S-cone physiology is particularly affected by ageing compared to the M/L population, proportionally there is a bigger loss in the S-cone populations compared to the M/L-cone population.
- S-cones suffer from a greater cellular stress than their M/L-cone population.

We studied the cone populations in the retina of an old-world primate (*Macaca fascicularis*) comparing aged *vs.* young subjects. Additionally, we will assess whether the aging process affects the distribution of the S-cone photoreceptor mosaic in the

retina. Finally, we will study different cellular stress markers to test whether S-cone are specifically affected by cellular stress. This will help us to understand whether changes in the physiological behaviour of cones are correlated with structural changes and cellular stress.

5.3 Materials and methods

5.3.1 Retinal Tissue

Ocular tissues were acquired from *Macaca fasciularis* from an established colony managed by *Public Health England* under U.K. Home Office regulation. Eyes were retrieved at death following sedation with ketamine and overdose of intravenous sodium pentobarbital. The primary purpose was different from the aims of this study. Eyes (N=16, 8 young at 6 years and 8 old at 17 years) were removed. Macroscopic and microscopic examination confirmed that all retinae used were normal.

5.3.2 Histology

To assess natural ageing in our model, we stained young and old sections to see whether we are able to identify ageing features in the retina. *Macaca fascicularis* eyes were fixed in 2% PFA and 2% glutaraldehyde in PBS for 2 – 3 days at 4˚C. The eyes were then washed in PBS for 10 min, followed by dissection, removing the cornea, ciliary body and lens and keeping the retina. 1 cm wide retinal strips, from the optic nerve head towards the temporal periphery, containing the fovea, were cut and selected for plastic embedding. Prior to dehydration, retinal stripes were incubated in 1% osmium tetroxide in PBS for 2 h.The tissues were dehydrated in increasing concentrations of ethanol, from 50% to 100%. After dehydration, the samples were prepared for plastic embedding following the manufacturers protocol (Technovit 7100). Briefly, after dehydration samples were placed in a pre-infiltration solution for 2 h, followed by incubation in infiltration solution for 24-72 h at 4˚C. After the infiltration solutions, samples are ready to be embedded in the polymerisation solution in plastic moulds. The samples were then left to harden for about 1 week. 5 µm section were cut with a glass knife using an ultramicrotome. The sections were then dried onto glass slides. The retinal sections were counterstained with 1% toluidine blue in PBS to visualise morphology.

5.3.3 ATP measurement

ATP extracts were performed using 6M guanidine hydrochloride to each frozen neural retinal samples (N=5 per region and group) and were homogenized using a sonicator.

The homogenates were briefly frozen on dry ice and then denatured at 95˚C for 5 mins. Then they were centrifuged at max speed for 10 mins at 4˚C and the supernatants were transferred into a new centrifuge tube. The samples were diluted 50-fold with deionized water and 10 μL of this diluted extract was used for this analysis. ATP concentration in all extracts was measured by using an ATP determination kit (ThermoFisher scientific, UK) and normalised to protein concentration, measured by the BCA method.

5.3.4 Whole-mount immunofluorescence

Retina was labelled for S-opsin and M/L-opsin to study the distribution of S-cones and M/L-cones across the temporal meridian. Macaca fascicularis eyes (N=3 eyes for each group) and placed in 4% paraformaldehyde for approximately 24 h. They were then washed in phosphate buffer. The anterior eye was removed and the retina dissected free as a whole mount. The temporal retina running from the optic nerve head to the periphery in a strip approximately 1cm wide was dissected (Figure 5.2). This was permeabilised in 3% Triton X-100 in PBS containing 5% normal donkey serum (NDS) (Jackson Labs USA) followed by primary antibody incubation with S-opsin (1/1000) (goat polyclonal, SC-14363, Santa Cruz Biotecnhology, Inc., USA) and M/L-opsin (1/600) (rabbit polyclonal, AB5405, EMD Millipore, Temecula, California, USA) in PBS 1% NDS at room temperature (RT). Retinal strips were washed in phosphate buffered saline before incubation with secondary fluorescent labelled antibodies (1/2000) for 2h (donkey anti-rabbit Alexa Fluor 568 (A10042) and donkey anti-goat Alexa Fluor 488 (A11055), Invitrogen). Strips were washed with PBS and tris buffered saline (TBS) and then mounted in Vectashield (Antifade Mounting Media, H1000, Vectashield), coverslipped and sealed.

The temporal retina segments were viewed at X20 under epifluorescence. Images were captured at 1280 x 1024 pixels using a Digital Eclipse DXM 1200 camera (Nikon, Japan). These formed a continuous corridor from the fovea towards the temporal periphery over about 15mm. Images were stitched together. The tissue outlines were traced on a systematic random grid placed over the photographed elements. Counts of labelled cones were undertaken in a frame of 200 x 200 μm in the upper right corner of each square. 597 sites were included in the sampling area across the retinae with an average of 99±6.4 (SEM) counting sites per retina. Sites were counted only where cones were arranged in a matrix-like pattern and the image was clear and undamaged. The

density of S-cones and M/L cones cells was determined at each sampled site, as the number of cells divided by the area counted at that site.

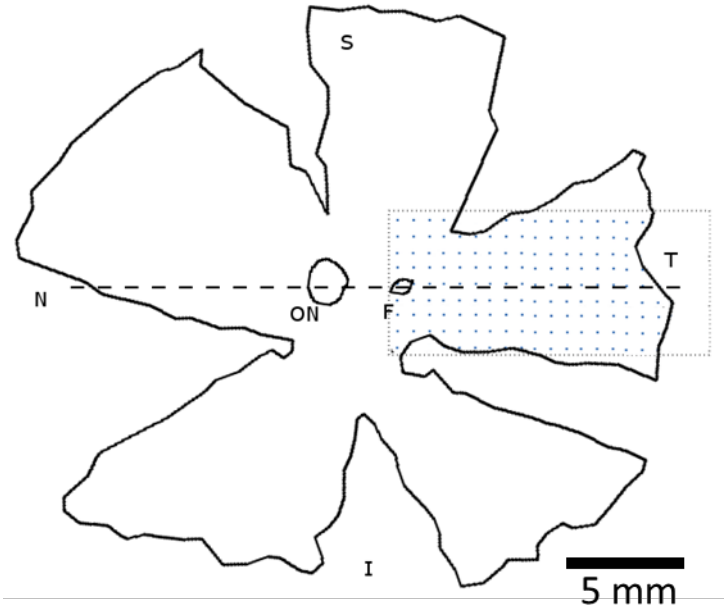

Figure 5.2. **Schematic representation of a retinal flat mount.** Diagram showing the strategy used for a continuous sampling from the fovea towards the temporal periphery. N: nasal, S: superior, I: inferior, T: temporal, F: fovea, ON: optic nerve.

5.3.5 Spatial Analysis

S-cones were automatically identified in the anti-S-opsin stained images (the green channel in the RGB images shown in Figure 5.5) as follows. First, the fundamental spatial frequency of the S-cones was determined from the spatial power spectrum (2D FFT). Next, using this frequency a custom band pass filter was used to smooth the image, followed by thresholding the image above the noise floor. The resulting image contained easily identifiable structures corresponding to the S-cones, the centres of mass of which were taken to be the S-cone coordinates.

S-cone coordinates were used to generate Voronoi diagrams using the Qhull37 and Fortune's38 algorithms, implemented in Python, where each resulting Voronoi domain consists of those points in the image closer to the domain's S-cone anchor than any other S-cone. Each domain consists of a polygon, and domain areas were computed using the shoelace formula (or surveyor's formula). Variance among the domain areas was computed for all images (Voronoi domain area regularity index, or VDARI), which is an indication of the uniformity of the S-cones' spatial distribution.

5.3.6 Immnofluorescence and immunohistochemistry

To investigate damage by oxidative stress and stress response, retinal sections were labelled for different markers. Details of antibodies used can be found in Table 5.1.

Macaca fascicularis eyes and placed in 4% paraformaldehyde for approximately 24h (N=5 eyes for each group). They were then washed in phosphate buffer. The anterior eye was removed and the retina dissected in strips. The retinal strips were then cryoprotected in 30% sucrose (in PBS) solution, followed by embedding in OCT. Retinas were sectioned on a cryostat at a thickness of 10 μm, collected on slide, left to dry for 6 h and stored at -80 °C until used.

For immunofluorescence, cryostat cut sections were thawed for 60 min before use. Sections were briefly rinsed in PBS, following a 1 h blocking step with 5% normal donkey serum in 0.5% Triton X-100 un PBS to block unspecific antibody binding. After the blocking, the diluted primary antibody was applied and incubated for 24 h at 4˚C followed by a 1 h incubation at RT (diluted in PBS containing 2% NDS, Triton X-100 0.5%). The slides were washed 3 times with PBS + Triton-X 100 0.5% for 5 min each time. The fluorochrome conjugated secondary antibody was added and incubated for 1.5 hours at room temperature. The slides were washed 3 times in PBS containing Triton X-100 0.5%, followed by a single wash in PBS only. The coverslips were added and mounted in Vectashield Hardset (Vector Laboratories, Burlingame, CA, USA). Slides were left to dry at room temperature for 2 h and sealed with nail varnish. Slides were stored at 4˚C.

For immunohistochemistry, two different methods were used.

1. Label for S-opsin: horseradish peroxidase – 3,3'-Diaminobenzidine (DAB)

Sections were thawed as above, followed by one wash in tris-buffered-saline (TBS). Sections were then blocked for 1 h with 5% normal donkey serum in 0.5% Triton X-100 un TBS to block unspecific antibody binding. After the blocking, the diluted primary antibody was applied and incubated for 24 h at 4˚C followed by a 1 h incubation at RT (diluted in TBS containing 2% NDS, Triton X-100 0.5%). The slides were washed 3 times with washing buffer (TBS + Triton-X 100 0.5%) for 5 min each time. To quench peroxidase activity in the tissues, sections were incubated with 0.3% H_2O_2 in TBS for 30 min. The slides were washed 3 times with washing buffer for 5 min each time. The secondary antibody, conjugated to horseradish peroxidase (HRP) was added and

incubated for 1.5 h at RT. The substrate DAB was prepared by mixing equal quantities of reagent A and reagent B. Sections were incubated for 1-5 min, or until desired stain intensity develops, followed by 3 washes in TBS. Sections were either caballed with pTau or stained with Sudan Black B.

2. Label for p-Tau: alkaline phosphatase

After S-cone labelling with HRP-DAB method, the same section were labelled for p-Tau with an alkaline phosphatase immunohistochemistry method, using a commercially available kit (VECTASTAIN ABC, Vector Laboratories). S-opsin labelled sections were blocked with 1.5% normal horse serum (in 0.3% Triton X-100/TBS) for 1h at RT. Slides were rinsed in TBS once followed by ON incubation with the diluted primary antibody in 1.5% normal horse serum (in 0.3% Triton X-100/TBS). The following day, slides were incubated with secondary biotinylated antibody (supplied in the kit) diluted in 1.5% normal horse serum in 0.3% Triton X-100/TBS for 1 h. Slides were washed thrice in TBS, followed by alkaline phosphatase reagent treatment, supplied with the kit, by mixing A:B in 1:100 dilution. Slides were washed again three times. Finally, the supplied alkaline phosphatase substrate solution was applied and incubated between 20-25 min, or until desired intensity develops. Slides were washed four times with TBS, prior to mounting with glycerol, cover slipped and sealed.

Antigen	**Structure**	**Host**	**Dilution**	**Source**	**Catalogue number**
Primay antibodies					
8-Oxo-2'-deoxyguanosine (8-oxo-dG)	Damaged DNA	Mouse monoclona	1/100	Abcam	AB62623
Acrolein	Acrolein-conjugated proteins	Rabbit	1/500	Abcam	AB37110
Hsp90	Chaperone Hsp90	Mouse monoclona	1/50	Abcam	AB13492
Hsp60	Chaperone Hsp60	Rabbit	1/50	Abcam	AB46798
P-Tau	Hyperphosphorylated Tau	Mouse monoclona	1/200	ThermoFisher Scientific	MN1020
S-opsin	S-cones	Goat	1/1000	Santa Cruz Biotechnology	SC-14363

Secondary antibodies					
Alexa Fluor 568	Anti-rabbit	Donkey	1/2000	Invitrogen	A11004
Alexa Fluor 568	Anti-mouse	Donkey	1/2000	Invitrogen	A10042
Alexa Fluor 488	Anti-goat	Donkey	1/2000	Invitrogen	A11055
HRP-conjugated	Anti-goat	Rabbit	1/1000	Daki	P0449

Table 5.1. Primary and secondary antibodies used in this study.

5.3.7 Sudan Black B stain

To check for different lipid staining pattern in the age groups, Sudan Black B stain was used. Sudan Black B is a lipophilic stain. Frozen sections are left to dry, labelled with S-opsin and then stained with Sudan Black B solution (1% solution 70/30 ethanol/dH_2O), for 2 h. Slides were rinsed twice in dH_2O before mounting in glycerol and cover slipped. Slides were left to dry at room temperature for 2 h and sealed with nail varnish. Slides were stored at 4˚C.

5.3.8 Image acquisition and analysis

Flat-mount: the temporal retina segments were viewed at X20 under epifluorescence. Images were captured at 1280 x 1024 pixels using a Digital Eclipse DXM 1200 camera (Nikon, Japan). These formed a continuous corridor from the fovea towards the temporal periphery over about 15 mm. Images were stitched together. The tissue outlines were traced on a systematic random grid placed over the photographed elements. Counts of labelled cones were undertaken in a frame of 200 x 200 μm in the upper right corner of each square. 597 sites were included in the sampling area across the retinae with an average of 99±6.4 (SEM) counting sites per retina. Sites were counted only where cones were arranged in a matrix-like pattern and the image was clear and undamaged. The density of S-cones and M/L cones cells was determined at each sampled site, as the number of cells divided by the area counted at that site.

Immunofluorescence and immunohistochemistry: epi-fluorescence and bright field images were taken in JPEG format at X40 using an epi-fluorescence bright-field microscope (Olympus BX50F4, Japan).

Measurement of 8-oxo-dG, acrolein, Hsp90, Hsp60: average pixel depth was measured in FIJI/ImageJ 1.48v (NIH, USA) using the lasso tool to draw a line around the photoreceptor layer.

5.3.9 Statistical analysis

A Mann-Whitney U test was used to compare the two groups unless otherwise indicated. Data was analysed using Graph pad Prism, version 5.0 (Graphpad, San Diego, CA).

5.4 Results

5.4.1 Qualitative histological assessment: young *vs* old

Eyes were obtained from young and old *Macaca fascicularis,* an old world primate, with retinae highly similar to those in humans: cone photoreceptors (S-, M-, and L-cones) and a well-developed central region containing the fovea. However, unlike humans, S-cones are present in the fovea of *Macaca fascicularis* retinae[141]. In terms of photoreceptor function, photoreceptor psychophysics are very similar between this old world primates and humans[162,163].

For the purpose of this study, animals were grouped into young (6 years) and old (17 years). At 6 years, the eyes are fully developed. The 17 years old macaques have clear signs of physical ageing, with deposition of lipofuscin.

First we analysed whether the consequences of ageing could also be seen in a simple histological observation. The retinal tissue was processed for plastic embedding followed by cutting 5 μM sections. After left to dry, the retinal sections where stained with toluidine blue. A representative image of the staining for each group is shown in Figure 5.3.

Here we observed that retinae suffer from qualitative morphological changes due to ageing, including vacuoles (as cells die), and inner nuclear layer thinning. Additionally, the photoreceptor outer segments were linear in young subjects, while they acquired a more tortuous morphology in the aged animals. The two anatomical parts of the cone photoreceptors were clearly identified in young animals (ellipsoid and myeloid), while these became diffuse in older animals.

This qualitative histological retinal assessment leads us to believe that ageing is being manifested in the retinal structure and morphology.

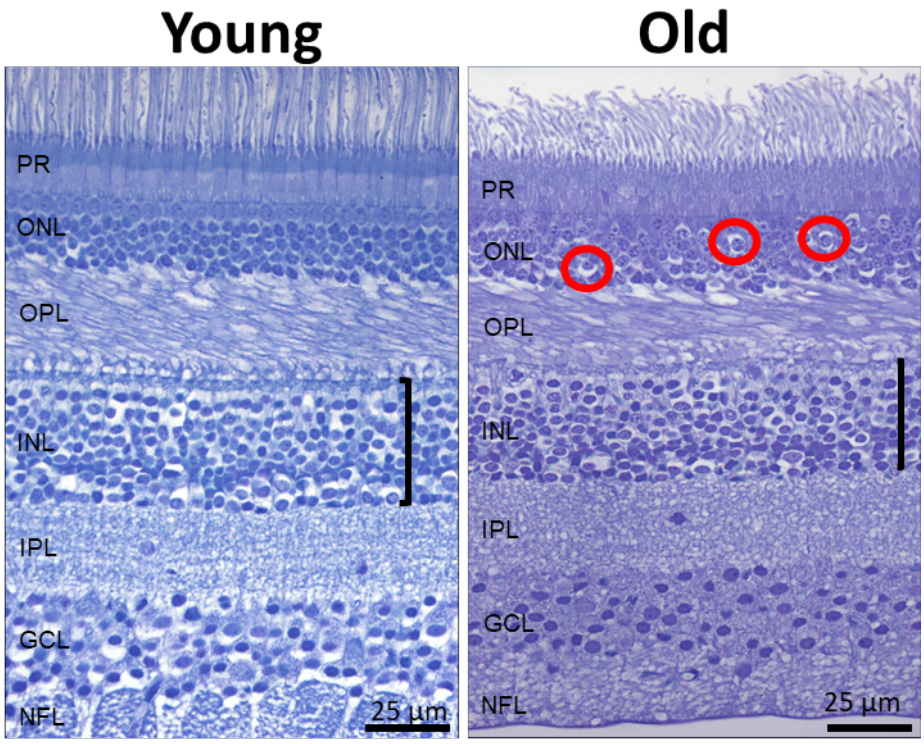

Figure 5.3. **Histological qualitative assessment.** Representative images of histology in young and old *M. fascicularis*. Retinae suffered from qualitative morphological changes with ageing, including vacuoles (red open circles), and inner nuclear layer (INL) thinning. (OS: outer segment, IS: inner segment, ONL: outer nuclear layer, OPL: outer plexiform layer, INL: inner nuclear layer, IPC: inner plexiform layer, GCL: ganglion cell layer).

5.4.2 Ageing is associated with a significant decrease in ATP levels

We measured ATP levels in the retina to investigate whether it declines in this neural tissue, as a consequence of dysregulation of energy homeostasis known to be hallmark of ageing[164]. Figure 5.4 shows the ATP level in young and old primates both in periphery and macular regions of the retina. Interestingly, global ATP levels were higher in the periphery compared to the macular region, indicating a greater consumption to production ratio in the macula compared to the periphery. In both cases, ATP levels decreased significantly with ageing. In the macular, the ATP levels decreased by a 57% while in the periphery the declined was 64%. These data suggests significant mitochondrial decline in the retina with age. Furthermore, as the data is normalised for protein, they are independent of any cell loss, especially rod photoreceptor loss.

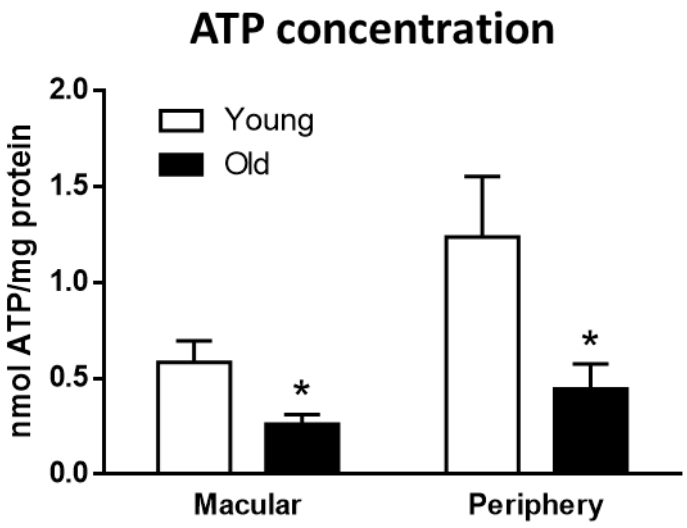

Figure 5.4. Ageing is associated with a significant decline in ATP levels. ATP levels measured in peripheral and macular regions in retina from *Macaca fasciularis* show a significant decline with ageing. In the periphery, ATP levels dropped by 63% in old compared to young animals. In the macular region, the drop in ATP levels was a 55%. N=5 in each group. Two-way Mann Whitney U-test. * $p<0.05$.

5.4.3 Cone distribution across the temporal meridian

To investigate whether aging would affect the numbers of cones in the retina, flat mounted retina were uniformly stained with two antibodies, one for the combined M/L-cone opsin and one for the S-cone opsin. The distribution of labelled cones conformed to previous similar studies, revealing a significant decreasing gradient between the central macular region and the peripheral retina, as can be seen in Figure 5.5. The retinae were systemically mapped from the central towards the temporal periphery at approximately 100 locations per retina (0.0016 mm^2 each).

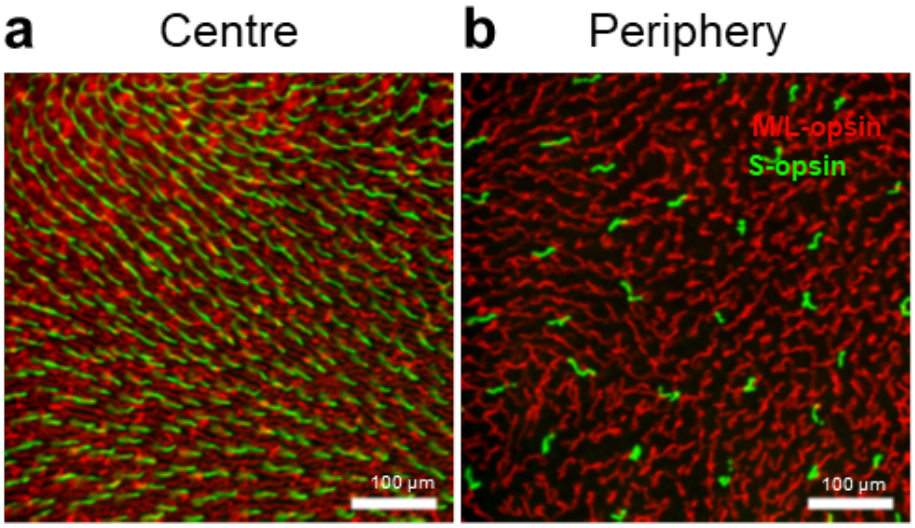

Figure 5.5. The spatial distribution of cones stained for M/L-opsin (red) and S-opsin (green) from a young animal. (**A**) Was taken in the temporal parafovea (1.3 mm eccentricity). (**B**) Was taken in the temporal periphery (10 mm eccentricity). There was a clear gradient in cone density across this axis, but no obvious differences in cone density between young and old animals.

Figure 5.6 shows eccentricity-dependent variation in cone density, grouped by age and cone spectral class. Figure 5.6 a and b are M/L-cone cell densities in both age groups, while c and d are the S-cone densities over the same region. Counts for M/L-cone cells did not extend into the central fovea because cell density here was too high for accurate counting.

At any given retinal eccentricity, variation in M/L-cone density appear greater among the young animals than in the older ones, although this was less than the variability reported for the total cone population in humans[136]. However, in the young animals variability was higher, largely due to data from one individual. Overall aggregate dependence of M/L-cone density on eccentricity was similar in the two age groups (Figure 5.6 a and b). Plots for S-cone densities in young and old primates over the same regions were again very similar with the steepest decline in density occurring over the 4 mm closest to the fovea (Figure 5.6 c and d). Figure 5.6 e and f show cone densities for both young and old animals, grouped by cone spectral class. Overall, these data is indicative of no evidence for a difference in S-cone cell population numbers between the two age groups.

To deepen the analysis we calculated half-life, the eccentricity at which cone density reaches half its maximum. Within each spectral class, data from young and old animals were fitted separately with the function $D(E) = D0e^{-\lambda E}$, using nonlinear least-squares regression. $D(E)$ is the cone density at eccentricity E, $D0$ is the maximum density, and λ is the decay constant. Permutations of λ such as time constant ($\tau = 1/\lambda$) and half-life ($E1/2 = (\ln 2)/\lambda$) describes the rate of decay.

For M/L-cones, there was a small difference in half-life between young and old animals, with E1/2=5.1 mm and E1/2= 4.0 mm, respectively. This small difference could be attributed to differences in peripheral densities. For S-cones, however, there was no difference between both age groups: E1/2= 1.5 mm for the young animals, and E1/2=1.48 mm for the old group, indicating that in both young and old animals the S-cone cell density fell to half its peak value at 1.5 mm.

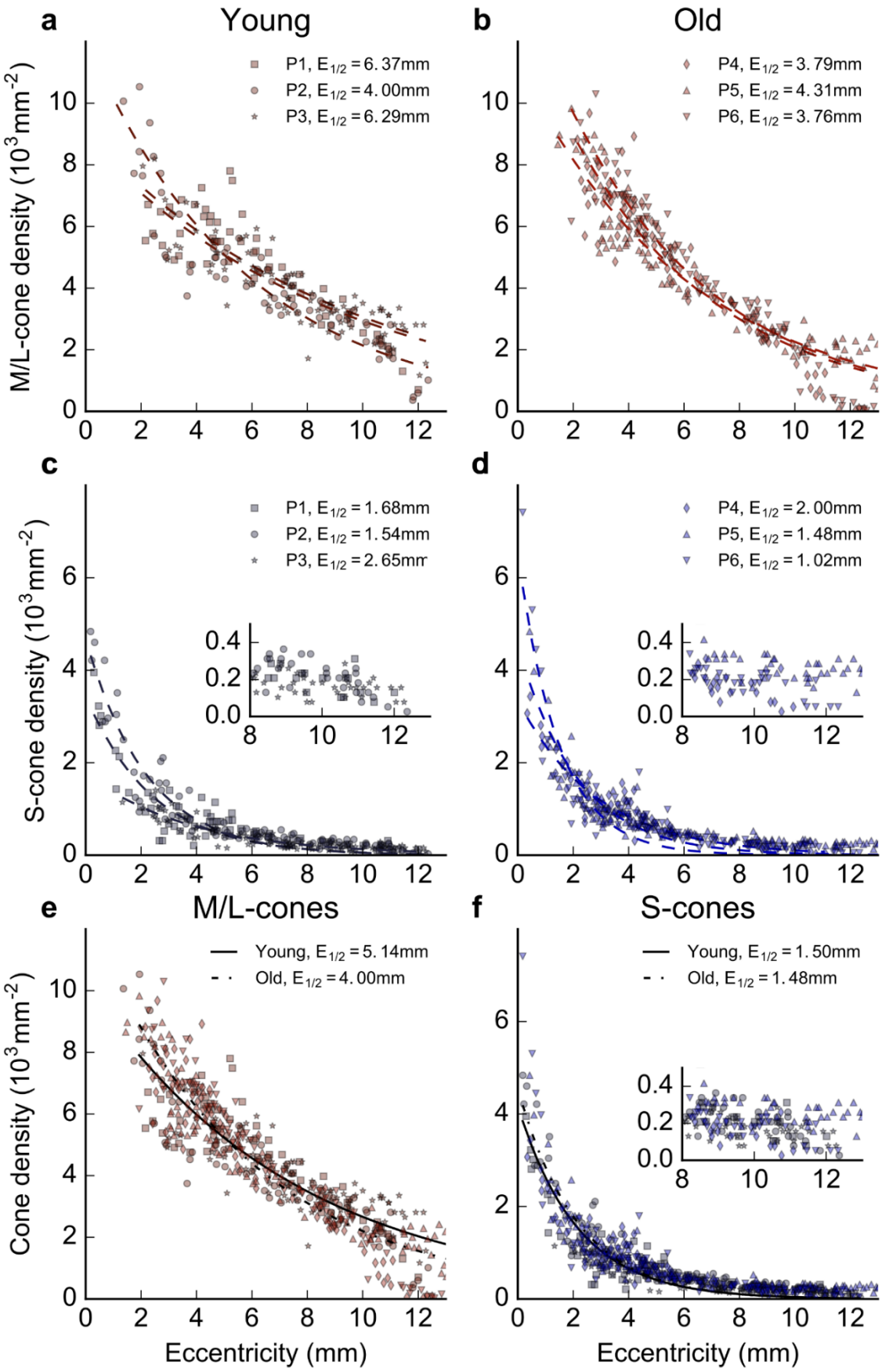
a
Young
P1, E1/2 = 6.37mm
P2, E1/2 = 4.00mm
P3, E1/2 = 6.29mm
M/L-cone density (10^3 mm^-2)
b
Old
P4, E1/2 = 3.79mm
P5, E1/2 = 4.31mm
P6, E1/2 = 3.76mm
c
P1, E1/2 = 1.68mm
P2, E1/2 = 1.54mm
P3, E1/2 = 2.65mm
S-cone density (10^3 mm^-2)
d
P4, E1/2 = 2.00mm
P5, E1/2 = 1.48mm
P6, E1/2 = 1.02mm
e
M/L-cones
Young, E1/2 = 5.14mm
Old, E1/2 = 4.00mm
Cone density (10^3 mm^-2)
Eccentricity (mm)
f
S-cones
Young, E1/2 = 1.50mm
Old, E1/2 = 1.48mm
Eccentricity (mm)

Figure 5.6. Cone density and eccentricity in young and old animals. Densities of M/L- and S-cones in young and old macaques extending from the central retina to 13 mm temporal periphery. (**a**) M-/L-cone densities in 3 young (6 years old) animals. (**b**) Corresponding data for 3 old macaques (17 years old). Data was not provided for the central most location as cell density was too great for reliable counting. (**c**) Counts of S-cones over exactly the same region in 3 young animals. (**d**) Counts of S-cones over the same region in 3 old primates. In each case patterns were very similar for the two age groups. (**e**) and (**f** Density of the two age groups were overlaid, for L-/M-cones and S-cones, respectively. (**e**) Densities for M-/L-cones in young and old primates with regression lines for the two populations. Data sets for the two ages matched closely except in the far periphery. (**f**) Densities for S-cones in young and old primates with regression lines for the two populations. Again these matched closely. Taken together the data in the 6 graphs show that there is no difference between young and old primates in terms of cone densities. Because of the low S-cone density in the periphery, their densities have been represented twice at different scales in the regions beyond 7 mm eccentric. The first is on the same scale as other counts (Figure 5.6 a and b) and the second is on an expanded Y axis to provide a clearer picture of their distribution.

To estimate the aggregate density of each cone class in each animal, numerical integration over the exponential decay models was computed. This step allows for a fair simple comparison of cone density between young and old animals, even in the presence of minor variations in the rate of exponential decay with eccentricity. The resulting values are shown in Table 5.2. Two one-way ANOVAs were performed: first between the old and young aggregate S-cone densities, and second between the old and young aggregate M/L-cone densities. In neither case was a significant difference in density detected ($p = 0.88$ and $p = 0.71$, respectively).

	S-densities (cones/mm^2)		***M/L-densities (cones/mm^2)***	
	Young	**Old**	**Young**	**Old**
	371	478	4553	4,217
	431	392	4162	4,160
	378	283	4387	4,530
Mean	**393**	**384**	**4368**	**4,302**

Table 5.2. Mean cone densities grouped by age and cone spectral class. Exponential decay curve models were plotted for each animal. Cone densities at 10 mm eccentricity were calculated by interpolation from the exponential, as a simple comparison between animals.

The S-cone distribution in the macaque retina is highly regular (non-random). This is known as a mosaic. In the hypothetical case of loss of S-cones with age, this would result in increased disarray associated with a change in the mosaic, due to increases in the separation of S-cones. To test the hypothesis that while S-cone function may be diminished by age, the cells are not lost in significant numbers, Voronoi domain analysis was used to quantify disarray in the S-cone mosaics. The Voronoi diagrams partitioned the image into regions, based upon proximity of the nearest S-cone. Variance among the areas or effective radii of these regions is an indication of mosaic disarray. The Voronoi domain area regularity index for the young was 3.761 while in the old group was 3.986, at 1.07 mm and 1.17 mm eccentricity, respectively. In summary, the data reveals that there was no difference in these measures of disarray

between the two age groups, irrespective of retinal location, confirming that no appreciable S-cone loss occurred with ageing (Figure 5.7).

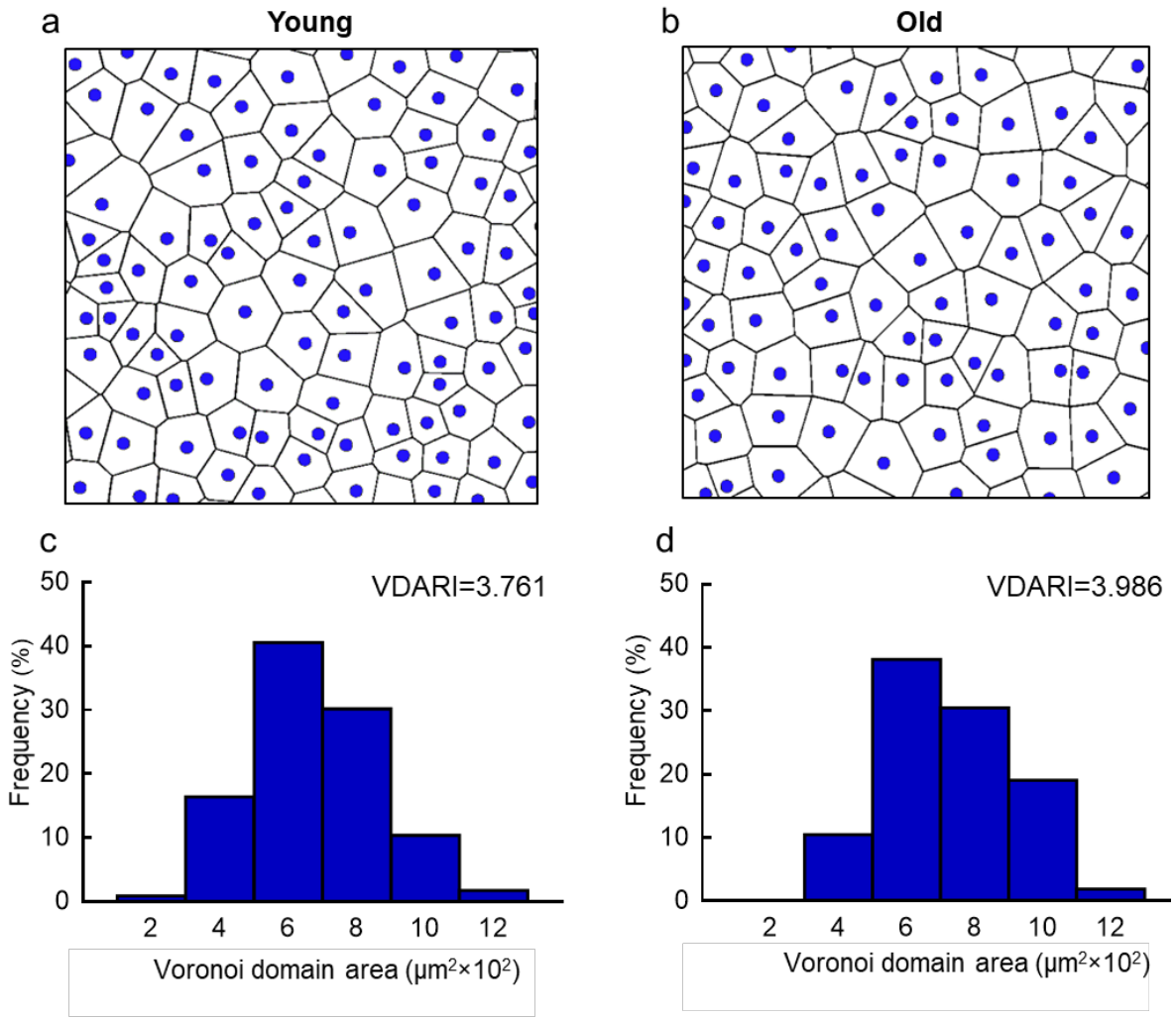

Figure 5.7. Voronoi domain analysis provides both diagrams and metrics of mosaic regularity. (**a**) and (**b**). Voronoi diagrams of S-cones in 200 × 200 μm regions of young (**a**) and old (**b**) retinae, at 1.07 mm and 1.17 mm eccentricity respectively. For each S-cone, a polygonal domain was created by identifying pixels that are closer to it than any other S-cone. The two diagrams are qualitatively similar. (**c**) and (**d**). Frequency distributions of Voronoi domain area for the diagrams shown in a and b, respectively. The distributions were similar, echoed by the small difference between the Voronoi domain area regularity indices (VDARI), which is the area mean divided by the area standard deviation, for each sample. Together, these data show that S-cone regularity was not impacted by age, which implies no age-related loss in S-cones since such loss would result in a loss of regularity.

In spite of declining cone function[145], this study demonstrares that there is no evidence for cone cell loss in the aging retina in this old-world primate. This is particularly unexpected for functions mediated by S-cones in ageing and disease, where age-related cell loss might have been expected[146,165,166].

However, it could be argued that because our analysis was confined to the temporal meridian we may have missed aged related cone loss in other areas. However, there is no evidence for specific regional S-cone loss and no evidence for it when examining the retinae used in this study.

5.4.4 Ageing is associated with increased oxidative stress in photoreceptor cells

As we found no evidence of a loss in the S-cone population in the old world primate, consistent with previous human data[153], we aimed to investigate whether oxidative stress related to mitochondrial dysfunction differentially affects the S-cone population. To achieve this, we performed an immunohistochemistry experiment on primate retinal sections with a panel of stress markers: Hsp60, Hsp90, acrolein, 8-Oxo-2'-deoxyguanosine (8-oxo-dG) and hyperphosphorylated-Tau, co-stained with S-opsin. As photoreceptor outer segments are rich in lipids synthetised in the mitochondria (e.g. phosphatidylethanolamine is the most abundant phospholipid), we also stained with a lipid stain Sudan Black B to investigate whether there was a change in the staining pattern between the young and old group, to identify changes in the lipid metabolism as a consequence of mitochondrial dysfunction. Below, we describe the typical labelling patterns, from the outer retina for each of these markers. In all cases, the S-cone population were positively stained for S-opsin (Figure 5.8, Figure 5.9 and Figure 5.10).

Photoreceptors contain about 75% of the retinal mitochondria, consistent with the highest COX activity and oxygen consumption in the retina[167]. Ageing is associated with an increase in oxidative stress due to mitochondrial dysfunction, and a decline in ATP levels as shown in Figure 5.4. We analysed markers of oxidative stress damage in proteins (acrolein) and in DNA (8-oxo-dG), shown in Figure 5.8. The intensity of 8-oxo-dG labelling increased significantly in the outer retina with ageing (Figure 5.8 b), in accordance with previous ageing studies. However, a more detailed analysis in the photoreceptor inner segments revealed strong label intensity in the myeloid region of the photoreceptor, particularly cone photoreceptor (Figure 5.8 a). This region corresponds to the region where mitochondria are localised in the inner segment[168].

Thus, our results suggest damage in mitochondrial DNA in the aged population, hence the strong 8-oxo-dG staining in the older group. However, there was no obvious difference between cone populations, but our data show decreased label intensity in the rods population, indicative of reduced DNA damage in this photoreceptor population. This is not surprising, since cone photoreceptors have 10 times more mitochondria than rods[168,169], suggesting a greater vulnerability to oxidative stress in the cone population.

Acrolein is one toxic byproduct of cellular lipid peroxidation caused by oxidative stress[170]. Acrolein reacts with cysteine, histidine, and lysine residues of proteins, forming adducts and disrupting their function[171,172]. These modified proteins accumulate in cells altering protein homeostasis. Thus, labelling for protein-conjugated acrolein is a method to study oxidative stress related damage in proteins. Our data, in Figure 5.8 c and d, shows that the intensity of acrolein label was high in the aged group compared to the young animals (Figure 5.8 d). This is in agreement with previous studies where acrolein conjugated proteins accumulate during ageing[173]. On a more detailed analysis, our data shows a distinct distal region in cone inner segments where the label is absent (Figure 5.8 c, arrow). When we co-labelled with S-opsin, the data revealed that only the S-cone population had the absent signal in this region. There was also a strong label in the outer segments across all rod and cone populations and rod inner segments.

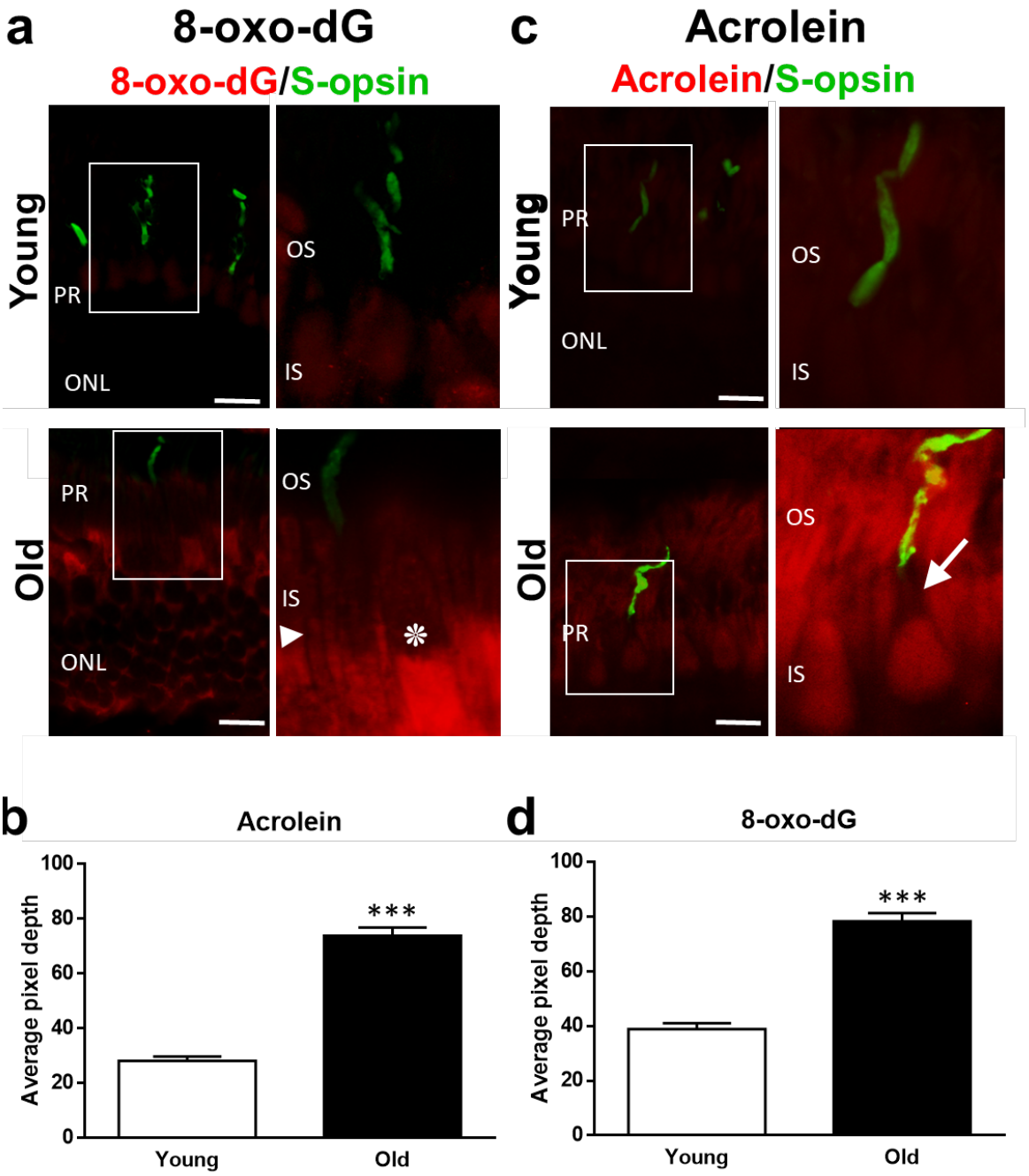

Figure 5.8. Molecular markers of oxidative stress damage: protein conjugated acrolein (acrolein) and 8-oxoo-2'-deoxyguanosine (8-oxo-dG). (**A**) and (**C**), fluorescence microscopy image of outer retina labelled for S-opsin and 8-oxo-dG (**A**) or acrolein (**C**) in young and old animals. (**B**) and (**D**) average pixel intensity obtained from analysed images in the outer retina labelled with (**B**) 8-oxo-dG or (**D**) acrolein. (**A**) Retina stained for 8-oxo-dG, a DNA damage marker. Note however, the intense signal in the cone photoreceptor inner segments (*) compared to rods (arrowhead). (**B**) Retina stained for acrolein, a marker for damaged protein due to oxidative stress. Outer

segments and inner segments were heavily stained in the aged animals, but the S-cones were characterised by a region absent of signal (arrow). Significant increases in pixel depth in ageing in the outer retina in both 8-oxo-dG (**B**) and acrolein (**D**). Scale bar equal 10 μm. Data shown as mean + SEM. N=5 in each group. PR: photoreceptor, OS: outer segment, IS: inner segment, ONL: outer nuclear layer. ***p<0.001.

The heat-shock defence mechanism is activated by oxidative stress. Ageing is associated with a disruption in protein homeostasis due to oxidative stress, correlated with a change in the expression of heat-shock proteins (Hsp) chaperones, responsible for maintaining protein homeostasis within cells. We targeted Hsp60 as a mitochondrial chaperone, and Hsp90, a cytoplasmic chaperone. The results are shown in Figure 5.9. The intensity of the Hsp60 signal increased in the aged animals compared to the young ones (Figure 5.9 b), consistent with previous reports in human ageing[174]. However, the Hsp60 labelling was mainly confined to the cone and rod outer segments (Figure 5.9 a). The data is in disagreement with the notion that Hsp60 is a mitochondrial chaperone, involved in the import and adequate folding of proteins within the mitochondrial compartment. There are reports, however, that suggest a cytoplasmic and extracellular Hsp60 involved in cell survival and other roles[175,176]. Our data showed, however, a very strong labelling in the outer segments, with membrane structures that could resemble a mitochondria, suggesting that Hsp60 may play a role in maintaining proteostasis in the cone and rod outer segments. Double labelling with S-opsin, revealed no differences in the staining pattern between S- and M/L-cone population, neither with the rod population.

Figure 5.9 c shows moderate Hsp90 labelling in the cone cytoplasm. The intensity of the label did increase with ageing (Figure 5.9 d), as has been shown previously in primates and other organisms. Hsp90 is a cytoplasmic chaperone with many functions, with a key role in assisting protein maturation and folding in order to maintain protein homeostasis[177,178]. Interestingly, cone photoreceptors were strongly labelled for this marker, while rod photoreceptors show reduced label intensity. Again, cone and rod outer segments were strongly labelled for Hsp90, similarly to Hsp60, suggesting their roles in maintaining protein homeostasis in this photoreceptor compartment. There were no differences between S- and M/L-cone photoreceptors.

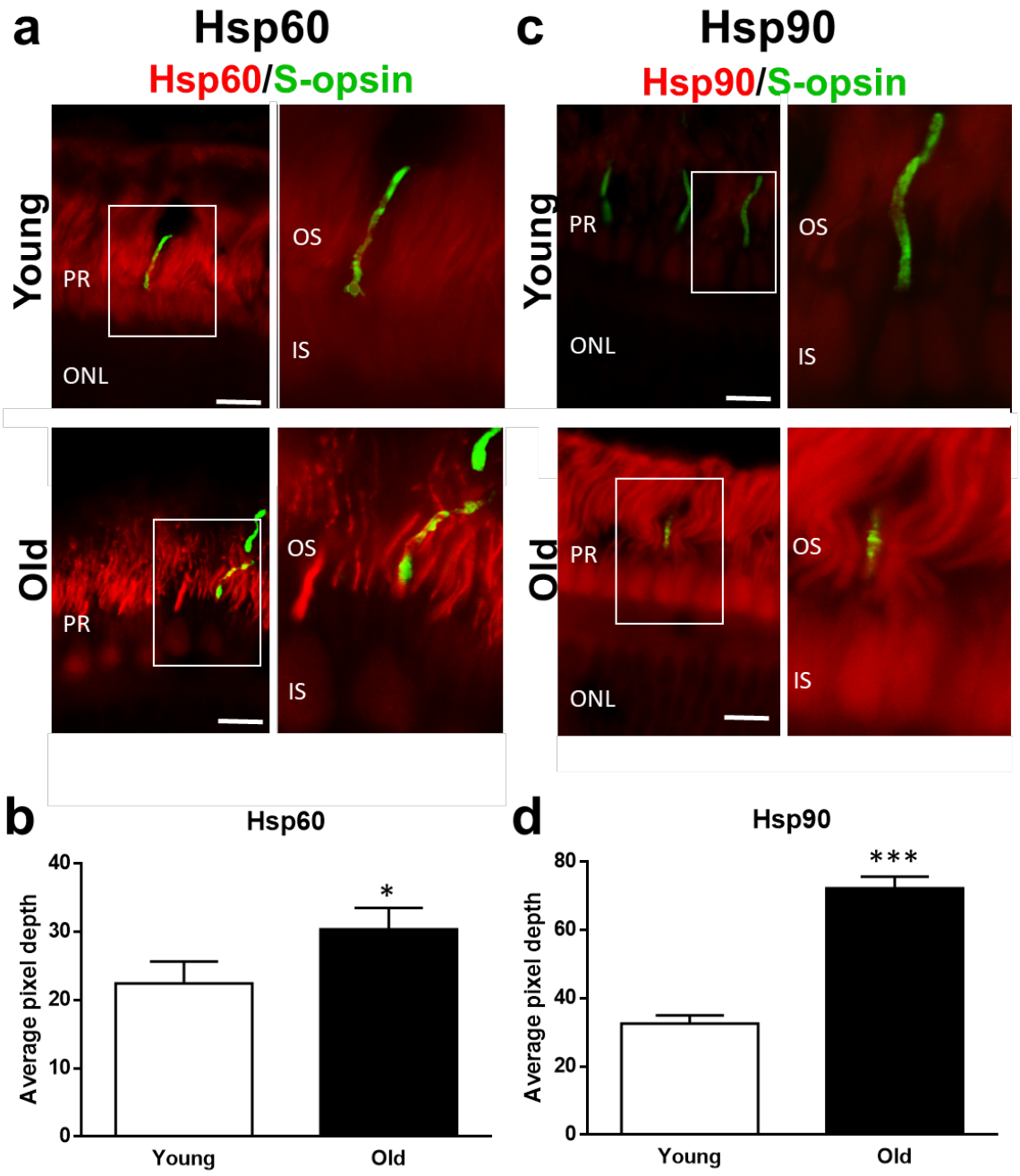

Figure 5.9. Molecular markers cellular stress response: heat-shock proteins. (**A**) and (**C**), fluorescence microscopy image of outer retina labelled for S-opsin and Hsp60 (**A**) or Hsp90 (**C**) in young and old animals. (**B**) and (**D**) average pixel intensity obtained from analysed images in the outer retina labelled with (**B**) Hsp60 or (**D**) Hsp90. (**A**) Retina stained for Hsp60, a mitochondrial Hsp. Note however, the intense signal in the photoreceptor outer segments. (**B**) Retina stained for Hsp90, a cytoplasmic Hsp. Outer segments were heavily stained but also other cone regions. Significant increase in the pixel depth in ageing in the outer retina in both Hsp60 (**B**) and Hsp90 (**D**). Scale bar equal 10 µm. Data shown as mean + SEM. N=5 in each group.PR:

photoreceptor, OS: outer segment, IS: inner segment, ONL: outer nuclear layer. *p<0.05, ***p<0.001.

For a cell to function properly good communication between different cellular compartments is needed. This is especially true for photoreceptors, due to their peculiar anatomy. Proteins synthetised in inner segments need to be transported towards the outer segments of photoreceptors. In addition, rod and cone outer segments suffer from shedding. In this process, the retinal pigmented epithelium digests the tips of the cone and rod outer segments, essential to recycle the photoacceptor 11-*cis* retinal, needed for phototransduction, the process of transforming electromagnetic energy into an action potential. Microtubules are the main platform for intracellular transport, but are also involved in maintaining the structure and shape of the cell. Thus, microtubules are essential for transporting material from the inner segments towards the outer segments. Here the protein tau plays an important role. Tau is a major microtubule-associated protein in neurons, responsible for promoting microtubule assembly and stabilisation. Like many cellular proteins, the function of tau is regulated by phosphorylation[179]. It has also been shown that increased phosphorylation of tau destabilizes tau-microtubule interactions, leading to microtubule instability and transport interruption along microtubules. Figure 5.10 a shows photoreceptors labelled with hyperphosphorylated tau. The intensity of the label increased with age, consistent with previous reports in mice and human brain cells[180]. The label was restricted to the photoreceptor inner segments, with no apparent label in the outer segments. Like the acrolein label, the staining was heterogeneous between the S- and M/L- cone population. A more detailed observation in S-cones, positively labelled for S-opsin, revealed a region where the hyperphosphorylated tau label was absent (open circle). This seems to be the same region as in the case of the acrolein marker, in the distal region of the inner segment, juxtaposed to the connective cilium. These data suggests that in the case of S-cones, this region is particularly well preserved from cellular anomalies like oxidative stress damage or tau hyperphosphorylation.

Finally, we investigated whether changes in the lipid pattern could be observed between young and old subjects, as outer segments are constantly shedded by the overlaying RPE. This results in a constant synthesis and transport of lipid material towards the outer segment. A change in the lipid pattern would suggest a change in the lipid metabolism, since the lipid turnover in photoreceptor cells is very high. Figure 5.10 b

shows the lipid staining pattern with Sudan Black B in young and old animals. The label was particularly strong in the myeloid inner segment regions and in the cone and outer segments. However, no difference in the staining pattern were observed comparing both groups. These data leads us to believe that the membrane lipid metabolism does not change significantly during the ageing process.

Taken together, the data suggest that oxidative stress damage and its response combined with tau hyperphosphorylation may have a role in cone photoreceptor dysfunction: avoiding the apoptosis pathway, but not fully functional. Interestingly, S-cones are characterised by a "virgin" region absent from tau hyperphosphorylation and acrolein label. Perhaps, the S-cone ROS scavenging machinery is very active in this region.

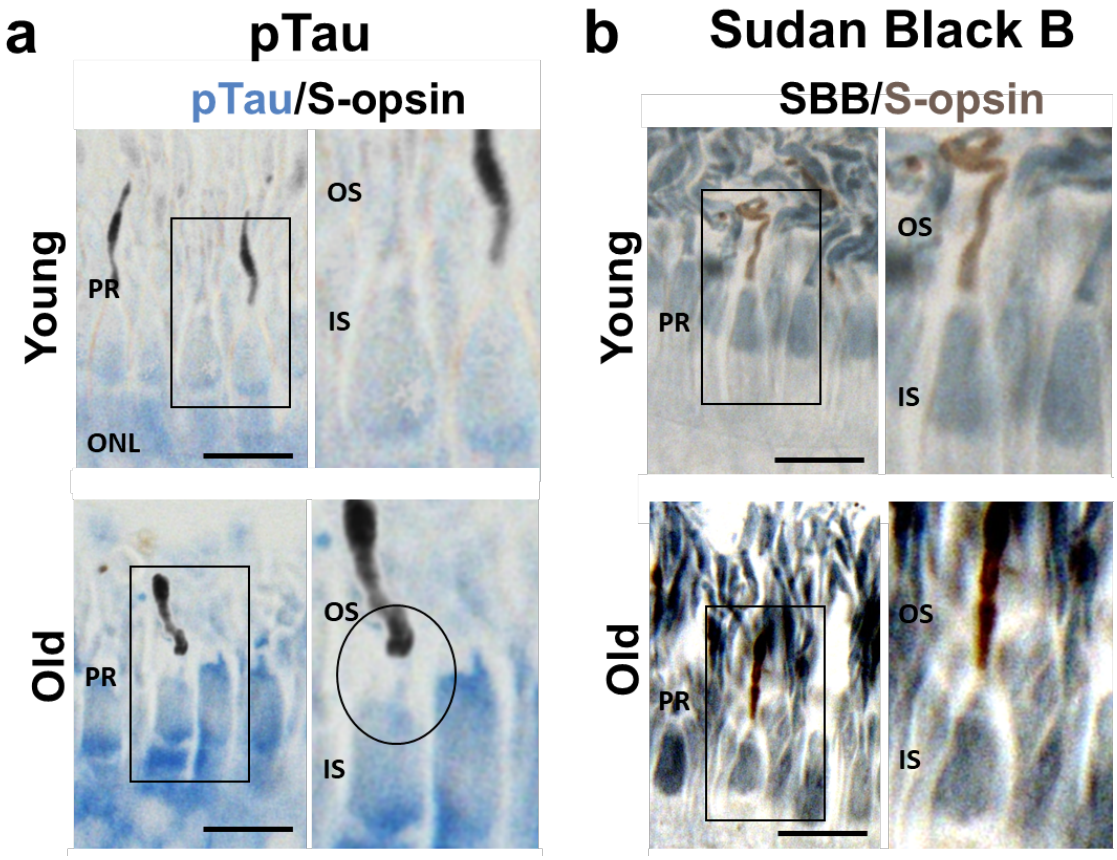

Figure 5.10. Hyperphosphorylated tau (pTau) and lipids in the outer retina. (**A**) and (**B**), microscopy image of outer retina labelled for S-opsin and pTau (**A**) or stained with Sudan Black B, a marker for lipids (**B**) in young and old animals.(**A**) Retina stained S-opsin and pTau, indicative of microtubule destabilisation. Note increased signal intensity with ageing. Strikingly, the distal region of the S-cone inner segment did not have an increased labelling (open circle) (**B**) Outer retina label for S-opsin and stained with Sudan Black B. No changes in staining pattern were be observed within the

age groups. Scale bar equal 10 μm. PR: photoreceptor, OS: outer segment, IS: inner segment.

5.5 Discussion

In this study we examined young and old primate retinae labelled to differentiate cone photoreceptor populations. We show no age-related cone loss in either cone type and S-cones are as regularly distributed in old as young primates. Furthermore, when we labelled for different cellular and mitochondrial oxidative stress markers in young and old retinae, as expected, label intensity was higher in the old group. However, we could not find differences in these markers between cone types, except for acrolein and hyperphosphorylated tau, where an apical region in the S-cone inner segment was absent of signal, suggesting that S-cones metabolism is less dependent on mitochondria.

Human retinal anatomical data for the ageing cone population is controversial, with inconsistent evidence for both the preservation and age-related loss[153,181]. Moreover, in rodent the cone populations suffer in the first year of life (biased towards the M/L-cone population). This early cone loss preceded rod loss within the rodent population[182]. However, there are fundamental anatomical and functional differences between the rodent and primate retina. Furthermore, there are differences in the relative numbers and distribution between the rodent and primate retina that may undermine the value of a direct comparison[182]. Based on this study, it might be argued that we lack evidence for a decline in S-cone mediated vision in non-human primates, but we have specifically sourced old world primates to ensure that our model is as close to the human as possible, and as such, likely to reflect the age related changes found in humans that is free of environmental influence such as diet, smoking or lifestyle. In spite of this, it is possible that there are differences in retinal ageing between humans and primates that our data have failed to reveal. An additional qualification is that we need to stress that our animal numbers in each of the two groups are relatively low and as such not amenable to statistical analysis. Lack of difference is not evidence for equality. Consequently, these results on cone populations should be regarded with caution.

In primates, no previous attempt has been made to count the separate S- and M/L-cone populations over age. As S-cones form only about 10% of the total cone population in

these animals[183], significant changes could occur in their number that would easily be missed in counts of the overall cone population. Further, in the case of human retinae, tissues inevitably come from a heterogeneous population in which there has been differential exposure to environmental factors that may modulate cell survival, such as diet and smoking.

In contrast, our primate data are derived from animals that were not exposed to such factors. Poor diet and smoking are risk factor for age-related disease, such as age-related macular degeneration (AMD), which is the largest cause of visual loss in humans over 60 years of age in the western society. But studies of photoreceptor loss in AMD may be relevant to our findings, as with the spread of degeneration cones appear to remain while rods are lost, consistent with the notion that these cells are relatively robust in both ageing and disease[184,185].

From our results, there is no evidence that these physiological changes observed in the S-cone population are correlated with a loss in S-cone cell numbers. During ageing, it seems that the cells are still present but they do not work as well as a young cell. One explanation could be that the observed functional senescence is correlated with mitochondrial dysfunction associated with increased cellular and oxidative stress with reduced cellular functionality. We have tested the hypothesis that the cone population is affected by cellular and oxidative stress, that could explain their cellular dysfunction, and ultimately, functional senescence. In this study we labelled retina photoreceptor for a panel of cellular and oxidative stress markers, specifically Hsp60, Hsp90, 8-oxo-dG and acrolein. Overall, the intensity of the signal for each marker increased in the aged group. This is in agreement with the mitochondrial theory of ageing, where with age there is an increased oxidative stress[15].

The data reveals some interesting observation regarding Hsp60. The Hsp60 chaperone is a well-known mitochondrial protein, assisting in the import and adequate folding of mitochondrial proteins. However, our results show that this cellular stress marker accumulated in the photoreceptor outer segments, but to our knowledge, there are no mitochondria in the outer segments. Therefore, Hsp60 must have a role in the maintenance of protein homeostasis in the photoreceptor outer segments, perhaps due to the morphological similarity between the outer segments discs and mitochondrial membranes. Similarly, the Hsp90 chaperon also strongly accumulated in the

photoreceptor outer segments, again suggesting the importance of protein homeostasis in this region of the cell. Furthermore, it is important to address the role of the RPE in the shedding of outer segments. On a diurnal basis, the RPE phagocytes small packets of membranous discs from the distal end of outer segments, to eliminate toxic photo-oxidative products as well as aid photopigment 11-*cis*-retinal recycling. However, the photoreceptor needs to maintain a constant outer segment length, by assembling new membranous discs at the proximal end of the outer segment, elongating the outer segment by a few μm every day. This requires a constant delivery and proper folding of proteins in the outer segment: chaperones are needed for this, so it is not surprising to see a high expression of them in this region of the cell. Moreover, our Hsp90 data revealed strong label in the remaining cellular body and processes, indicating abundance of this chaperone. Interestingly, in a rat model of retinitis pigmentosa, characterised by an early dysfunction and progressive loss of photoreceptor cells, inhibition of Hsp90 leads to an improvement in visual function and delayed photoreceptor degeneration[186].

Strikingly, since Hsp90 is involved in the folding of several oncogene proteins, Hsp90 has emerged as an important target for anticancer therapy[187]. In a clinical trial for solid tumours a different inhibit for Hsp90 was used (AUY922), a significant proportion of the patients developed visual impairment, which was reversed once treatment stopped[188]. This clearly suggests, that Hsp90 is an essential chaperone needed for correct visual function. Thus, it is not surprising that with ageing the expression of chaperones increases in the outer segment, probably to preserve function.

We also studied two markers for oxidative stress damage: protein conjugated acrolein and 8-oxo-dG, a markers for DNA damage. As expected, the intensity of these two markers increased with age, although their labelling patterns were different. While the acrolein label was absent in the young animals, the signal strongly increased in both cones and rods. Our results revealed a similar pattern in the case for 8-oxo-dG marker, with increased staining in the older animals. In this case, however, the cone population was preferentially labelled for this marker. This is not surprising as cone photoreceptors have at least 10 times more mitochondria than rod cells, suggesting a greater impact of oxidative stress damage in them. Without data for antioxidant pathways in cone photoreceptors, it is difficult to differentiate between increased production of reactive oxygen species or reduced efficiency of antioxidant metabolic routes. However, as

mitochondrial dysfunction is a feature of ageing, it is likely that the amount of associated oxidative damage should increase.

Our data revealed an interesting feature of S-cones regarding acrolein labelling. A distal region in the inner segment from S-cones is absent from acrolein, a region we term "virgin". There is no direct explanation for this observation and further investigation is needed to understand this anatomical location, as other markers, like hyperphophorylated tau, were also absent here in the S-cones. Perhaps it acts a central cargo-hub for trafficking material towards the outer segments, which need to be renewed on a daily basis. This would imply that materials are constantly transported away to the outer segment from this distal region. This would make sense, especially since tau is needed for adequate microtubule polymerisation, which would not happen with hyperphosphorylated tau. This result, however, leads as to a very interesting question. Why does this "virgin" region exist only in S-cones and not M/L-cones? This needs further investigation to understand the role of this region in S-cones.

There are, however, other putative explanations for the decline in S-cone function with ageing in humans, like age-related brunescence of the lens, which selectively attenuates short wavelength light. But this cannot explain all of the age-related changes in S-cone sensitivity[145]. There is a slowing of the S-cone pathway with age even after compensating for changes in the lens[166].

In both humans and old world primates, colour vision is substantially the same[162,163]. S-cone function is known to be selectively lost in specific metabolic conditions, which may highlight potential mechanisms of dysfunction. In each case where S-cone function declines there is a significant association with restricted metabolism, which is important in the retina as photoreceptors have the greatest energy demands in the body[189]. Hence, reduced S-cone function is found in diabetes[146], where cellular access to glucose is compromised due to insulin resistance (type II) or inexistent (type I). Likewise, when oxygen is reduced S-cone function declines[148]. Oxygen is critical for ATP production in mitochondria, which are densely packed in photoreceptor inner segments[168]. Other pathologies where there is evidence of selective functional decline of S-cones include retinal detachment[190] and macular degeneration[191–193], and these also have a direct link with oxygen. In retinal detachment, the outer retina is separated from its choroidal blood supply and

becomes hypoxic. In macular degeneration there is deposition of extracellular material under the RPE that restricts the passage of oxygen and metabolites to photoreceptors.

These pathologies may cast light on age-related changes that selectively impact on S-cones, however this need further investigation as the majority of markers we used were not differentially expressed in different cone populations. With normal ageing, Bruch's membrane, which sits between the choroidal blood supply and the RPE thickens due to the accumulation of extra-cellular deposits, and consequently the outer retina becomes increasingly hypoxic[194,195]. If S-cones lack adaptive flexibility to respond to this they will suffer functional decline, although this appears to not result in cell death. If such cells do not die, there may be an opportunity to restore function in this functionally vulnerable but anatomically robust cell type.

5.5.1 Future perspectives

We found no evidence for loss in cone cell population as a consequence of ageing. This is true for the M/L-cone and S-cone population. However, it is known that the physiological function of S-cones is impaired in aged individuals.

Nowadays, there is good evidence to detect single S-cones in the living human retina with advanced imaging technology. This should be combined with *in vivo* cone function (e.g. 40 hz flicker ERG) to test the validity of our results and animal model.

From our results, we found that physiological changes observed in the S-cone population were not correlated with a loss in S-cone cell numbers. Since the cells are still present but do not work as well as a young cell, we tested whether the underlying reasons are related to mitochondrial oxidative stress and their responses. Furthermore, investigating the role of other stress responses, particularly the endoplasmic reticulum unfolded-protein response would give further information regarding the protein homeostasis and lipid metabolism in the photoreceptors, particularly labelling retinal sections with the following markers: PERK, ATF6, and IRE1.

Chapter 6. Mitochondrial function in the retina *in vivo*

In our previous chapters we show how mitochondrial function is affected by ageing and how we can modulate mitochondrial function to achieve improvements in physiological function. In addition, it has been reported that many neurodegenerative diseases have aspects of mitochondrial dysfunction. Again, modulating mitochondrial function in this environment, we are able to improve disease progression and prognosis. However, mitochondrial dysfunction encompasses many different aspects as there are different types. Therefore, we need methods to screen whether the therapy used to target mitochondrial function is successful. Perhaps the most suitable screening method is to study mitochondrial function *in vivo.*

Previous studies have used brain cortex to successfully investigate mitochondrial function *in vivo*[196]. However, this approach is very invasive and not translatable to the human being. In contrast, the retina as part of the CNS, is accessible non-invasively being an excellent to investigate mitochondrial function *in vivo.*

6.1 Introduction

Efficient mitochondrial function is essential for retinal physiology and vision. Many diseases, including retinal diseases, are associated with mitochondrial dysfunction[197,198]. Other neurological pathologies, such as multiple sclerosis[199] or Parkinson's disease[200], have also been associated with mitochondrial dysfunction.

The involvement of mitochondria in both health and disease emphasises the role for a deeper understanding of this organelle in physiological and pathological situations. However, assessment of mitochondrial function is mostly restricted to *in vitro* assays (outside physiological setting), removing all other aspects of the surrounding environment. Notwithstanding, the surrounding environment is critical for physiological and pathological processes. Consequently, there is still a need for dynamic *in vivo* assessments of mitochondrial function, maintaining as close as possible to reality, physiological and pathological conditions.

6.1.1 The retina: accessible mitochondria

The retina is a thin, transparent and highly sensitive to light tissue that lines the back of the eye in the inside. It is a highly organised structure with different cell types grouped into different complex layers, fed by a vascular bed[201].

The distribution of mitochondria in the retina is relatively compartmentalised. Mitochondria are commonly found in the inner and outer plexiform layers, the ganglion cell layer and the inner segment of photoreceptors, which contain the highest mitochondrial density. Given the limited nature of the retinal vasculature, necessary for clear optics[201], and highly organised mitochondrial distribution, the retina constitutes a heterogeneous and organised tissue, in terms of oxygen delivery and consumption. Parts of the retina, including the inner segments of photoreceptors (characterised by high metabolism), are located in avascular regions. However, they are the first in line to receive the provisions from the choriocapillaris, the vascular bed. Although this vascular bed is well oxygenated, it lacks an adequate response to changes in the local metabolic need, especially photoreceptors, which may prevent adequate vascular responses during changes in metabolic demand[201]. Combining a highly metabolic active tissue[135], and a vascular supply that does not react fast to changes in local demands[201], results in a highly spatial heterogeneity in tissue oxygenation[202]. This makes the retina an ideal model on which to study the relationship between inflammation, oxygenation and mitochondrial function *in vivo*.

Interestingly, the retina is an accessible tissue from the exterior, thanks to the transparent properties of cornea, lens and vitreous, the overlying tissues of the retina. Using light, we are able to study the role of mitochondrial function *in vivo* in health and disease in the retina.

6.1.2 Flavoprotein autofluorescence: a non-invasive measure of mitochondrial function

Historically, mitochondrial function has been exclusively assessed *in vitro*. More recently, techniques based on the use of light have been used to study mitochondrial function *in vivo*. Particularly, confocal or two-photon microscopy linked with membrane potential-sensitive dyes, like tetramethylrhodamine methyl ester (TMRM). However, we can also rely on autofluorescent markers present in cells, including oxidised flavoproteins and reduced nicotinamide adenine dinucleotide (phosphate)

(NAD(P)H)[203]. Other techniques employed are based on the reflectance properties of some mitochondrial macromolecules, such as cytochrome *c* oxidase[204].

Oxidised flavoproteins exhibit different fluorescent properties which differ significantly from their reduced counterparts[203]. This property allows for the investigation of mitochondrial membrane potential that combined with the temporal and spatial resolution provided by imaging techniques provides an excellent tool to assess mitochondrial function dynamically.

Mitochondria contain the majority of flavoproteins of a cell[205]. In the mitochondria, flavin adenine dinucleotide (FAD) and flavin mononucletodie (FMN) form the pool of mitochondrial flavoproteins. However, one aspect of flavoproteins is that they form complexes with enzymes and proteins, quenching their fluorescent properties[206,207]. In spite of this, primarily the flavins from electron transport flavoproteins (transferring electrons from β-oxidation of fatty acids to ubiquinone) and α-lipoamide dehydrogenase (with a role in the conversion of pyruvate to acetyl-CoA and the Krebs cycle), seem to contribute significantly to the observed autofluorescence associated with changes in the redox state of mitochondria (Figure 6.1)[206,208].

In the retina, it should be clarified that β-oxidation of fatty acids is limited as fat is not a major energy source in this environment. Therefore, the flavoprotein signal observed in the retina is likely to be dominated by α-lipoamide dehydrogenase, together with a significant proportion of unspecific green autofluorescence, which is not sensitive to changes in mitochondrial membrane potential or associated with changes in the local oxygen environment.

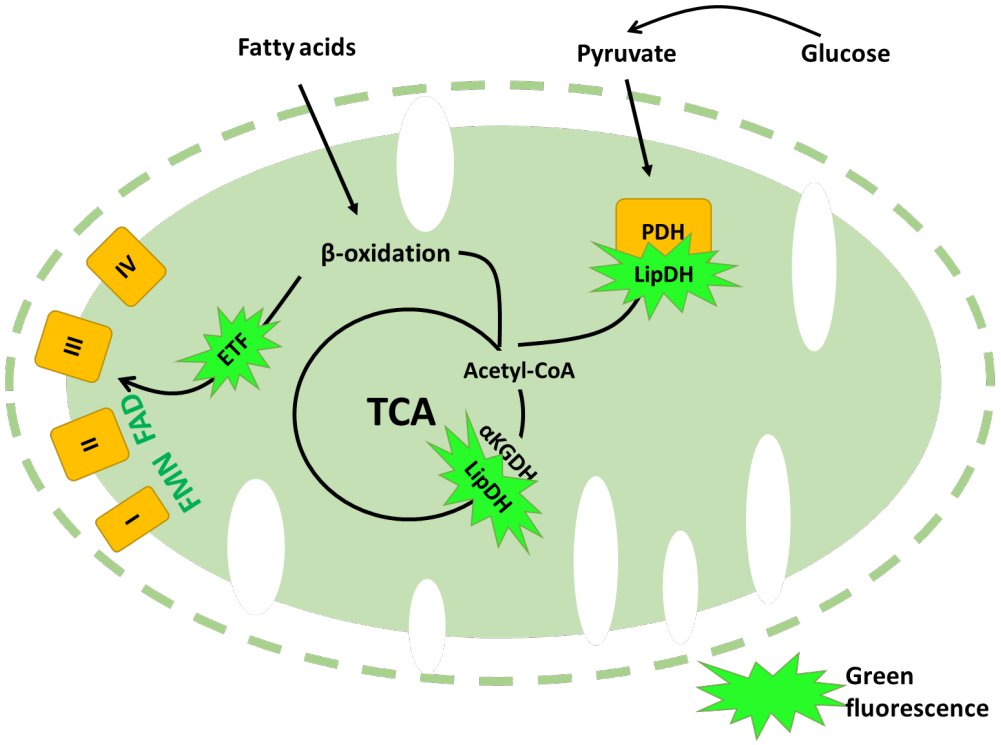

Figure 6.1. Mitochondrial flavoproteins. This diagram shows the main source of flavoprotein autofluorescence in the mitochondria. Abbreviations: FMN, flavin mononucleotide; FAD, flavin dinucleotide; ETF, electron transfer flavoproteins; LipDH, lipoamide dehydrogenase; αKGDH, alpha ketoglutarate dehydrogenase; PDH, pyruvate dehydrogenase complex; TCA, tricarboxylic acid cycle, I, II, III and IV, electron transport chain complexes.

6.1.3 Oxygen in the CNS

Oxygen is crucial and necessary for correct mitochondrial respiratory function. In the mitochondrial electron transport chain, electrons are transferred to successively higher affinity electron acceptors (Complex I/II to III and IV), where finally O_2 accepts the electrons from the last complex, cytochrome *c* oxidase. Hence, in situations of hypoxia, the lack of O_2 availability is capable of blocking the flow of electrons, resulting in the accumulation of reduced components across the electron transport chain. This process of reduction, when there is limited O_2 supply, can be visualised using flavoprotein fluorescence in the mouse brain cortex (Figure 6.2).

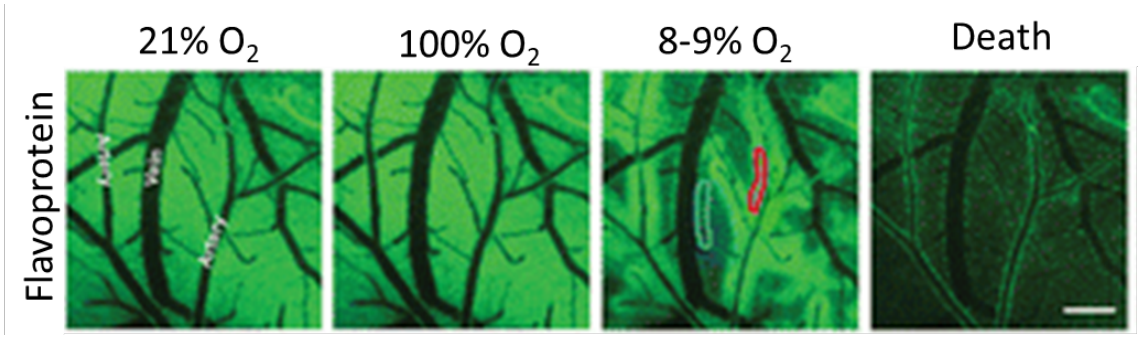

Figure 6.2. Flavoprotein imaging in the mouse brain cortex. Changes in flavoprotein fluorescence (green) associated with changes in inspired oxygen concentration. During room air (21% O_2) or 100% inspired oxygen conditions, mitochondria show relatively high flavoprotein fluorescence. When the inspired oxygen is reduced to 10%, regions around vein (green area) show fainted flavoprotein signal, while regions around arteries (red area) still display relatively high flavoprotein fluorescence. Whoever, once the animal is dead, all flavoprotein fluorescence disappears. Scale bar = 200 μm.

6.1.3.1 Supply and oxygen in the vascularised retina

For retinal function, the maintenance of a good oxygen supply is critical. In the retina, oxygen is delivered via two routes: (1) the choroidal vascular bed (choriocapillaris), immediately under the retina at the back of the eye, and (2) the retinal vasculature, whose vessels lie within the inner retina and are derived from the optic nerve head.

The retina has the highest oxygen consumption per gram of tissue in the body, higher than the oxygen consumption of the brain[168]. This, combined with the sparse retinal vasculature, contributes to the vulnerability of the retina to vascular diseases. One peculiarity of oxygen is that it cannot be stored in tissues. Thus an adequate and constant supply is essential to guarantee retinal function. Therefore, a lack of an adequate oxygen supply in the retina is associated with blindness. In summary, oxygen is a key metabolite essential for normal retinal function.

6.2 Hypothesis

- The endogenous autofluorescence of flavoproteins can be used to assess mitochondrial redox state *in vivo* in the retinas of anaesthetised mice.
- Local inflammation affects the redox state of mitochondrial function, which should affect the endogenous autofluorescence of flavoproteins.

6.3 Aims and objectives

First we will try and develop a protocol to assess mitochondrial redox potential in relation to the retinal vasculature (arteries *vs*. veins) in real time in the mouse retina during normoxia, hypoxia and hyperoxia. To achieve this, we will use the endogenous autofluorescence of flavoproteins as a surrogate marker for mitochondrial redox state imaged using confocal microscopy.

Once the protocol is established, we will aim to determine the effects of changes in inspired oxygenation concentration on flavoproteins fluorescence in the retina. This will be achieved by manipulating the oxygen proportion in inspired air supply.

Additionally, we will assess whether mitochondrial redox state is affected by inflammation, through changes in the flavoproteins autofluorescence signal. This would then allow us to test whether mitochondria in an inflamed environment are more vulnerable to changes in the local oxygenation, assessed via changes in the oxygen concentration in the inspired air.

6.4 Materials and methods

C57bl/6 mice (~23 g) were housed in a 12 hour light/dark cycle with food and water *ad libitum*. All experiments were performed in accordance with current legislation (UK Home Office Animals (Scientific Procedures) Act (1986)).

6.4.1 Animal preparation for retinal imaging.

In the majority of experiments, animals were anaesthetised with ~2% isoflurane in room air. In certain experiments, the air used during anaesthesia had an altered oxygen concentration by either 15% or 40-45%. Pupils were dilated with 1% Tropicamide and maintained hydrated with Viscotears. Mice were then placed on a custom made stage, with a homeothermic heating mat to maintain their body temperature at 37-38˚C, measured with a rectal temperature probe. The mouse body was slightly placed on its side, while the head was adjusted so the eye was facing up. The cornea was cleaned with sterile saline, while hairs that could interfere with the imaging procedure were removed.

Once the eye was clear from hair and any remaining debris, the cornea was protected with Viscotears. A circular 10 mm transparent glass coverslip was used. The coverslip was stabilized and sealed using petroleum jelly (Vaseline, Unilever, UK). Following

pre-imaging preparations, the mice were moved to a custom-made stage for confocal microscopy, and the inspired oxygen concentration was varied, as indicated, by changing the mixture of oxygen delivered to the animal via a nose cone. This was achieved by supplementing room air with either oxygen or nitrogen. The advantage of this retinal imaging protocol is non-invasive, allowing a fast and reproducible animal preparation, minimising variability between mice. Finally, this protocol also allows both eyes to be imaged.

6.4.2 Disease model: experimental autoimmune uveitis (EAU)

To assess the effect of inflammation on mitochondrial function, we induced anautoimmune disease. We chose experimental autoimmune uveitis as it induces local inflammation in the retina. Ten male C57Bl/6 mice were injected subcutaneously, dorsally near the beginning of the tail, with 200 µl of complete Freund's adjuvant (CFA) (Sigma-Aldrich) containing 1mg/ml heat-killed and dried *Mycobacterium tuberculosis*, 30 µg recombinant Interphotoreceptor retinoid-binding protein peptide 161–180 (IRBP) (Severn Biotech, UK). Additionally *Bordetella pertussis* toxin (15 µg) was injected intraperitoneally (Sigma-Aldrich), to boost the immune response.

Two weeks after immunisation, clinical signs were assessed bilaterally. The eye fundus was inspected under a binocular microscope and graded on a scale from 0 (no disease) to 4 (severe disease) following the criteria described in Table 6.1. Mice were monitored weekly for clinical signs until the grade was suitable for retinal imaging.

Grade	*Criteria*
0	No change
0.5 (trace)	Few (1–2) very small, peripheral focal lesions; minimal vasculitis/ Vitritis.
1	Mild vasculitis; <5 small focal lesions; 1 linear lesion
2	Multiple (>5) chorioretinal lesions and/or infiltrations; severe vasculitis (large size, thick wall, infiltrations); few linear lesions (<5)
3	Pattern of linear lesions; large confluent lesions; subretinal neovascularization; retinal hemorrhages; papilledema
4	Large retinal detachment; retinal atrophy

Table 6.1 Clinical Scoring of EAU in the mouse retina. Each assessed retina is given a grade according to clinical manifestations based on Caspi et al[209].

6.4.3 Image acquisition and processing.

The retinal endogenous flavoprotein signal (excitation: 488nm, emission: 505-570nm) were imaged with a LSM laser-scanning confocal microscope (Zeiss, Germany), using time lapse recordings with an in-plane resolution of 512 by 512 pixels and maximum pinhole aperture. Higher resolution images were also recorded at 1024 x 1024 pixels.

Images were processed using Fiji/ImageJ Version 1.48v (NIH, USA). Time-lapse sequences were aligned using the 'Stackreg'-Plugin. Areas of interest were selected using the free hand selection tool. To assess the flavoprotein fluorescence absolute pixel intensity was measured from regions around arteries and veins. The values were normalised to the average signal in the first 5 min of imaging which was plotted in the graphs (FAD signal). The change in relative periarterial and perivenular fluorescence intensity was compared during different inspired levels of oxygen concentration. For some experiments (section 6.5.3. 6.5.3 Flavoprotein signal is responsive to prolonged changes in oxygen concentration), the absolute intensity was used, selecting three different regions between vessels (average was used).

6.5 Results

6.5.1 The naïve retina

During room air inspired imaging, a green autofluorescent signal was present uniformly across the retina, except where obscured by vasculature, which is highlighted in negative contrast (Figure 6.3, left). The intensity of the green autofluorescent signal decreased once the animals died (Figure 6.3, right). This change in autofluorescene could be attributed to a decrease in the mitochondrial redox state.

Veins and arteries were distinguished morphologically, where arteries were typically smaller in diameter (and lumen) compared to veins. Additionally, once the animal was dead, the arteries were observed due to intrinsic autofluorescence of the arterial wall (Figure 6.3, right, A).

Finally, increased green autofluorescence was observed around the optic nerve head, the intensity of which was maintained after the animals death. This signal could originate from lipofuscin, which fluoresces strongly in the same wavelengths as flavoproteins[210,211].

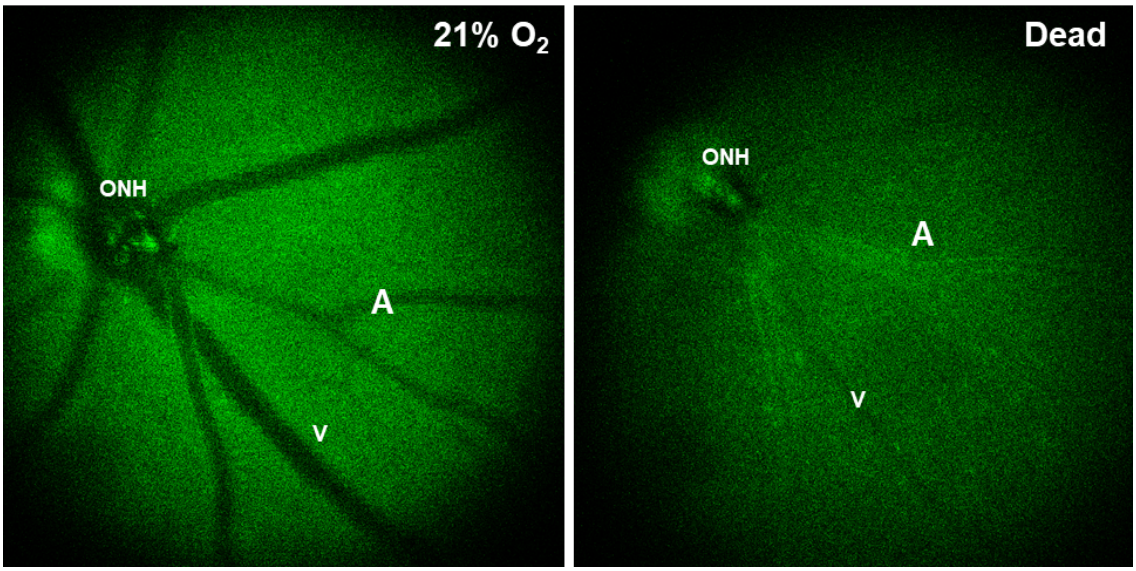

Figure 6.3. Retinal green autofluorescence. Left: living rodent *in vivo* retina. Right, dead rodent retina *in vivo*. Arteries and veins can be distinguished morphologically by the size of the vessels: veins had a bigger diameter compared to arteries. The intensity of the green autofluorescent signal was homogenously distributed in the living eye (left, inspiring 21% O_2). Once the animal died, the intensity of the signal decreases (right, dead) revealing green intrinsic autofluorescence of the arterial wall. A: artery, V: vein, ONH: optic nerve head.

6.5.2 Modulation of inspired oxygen concentration changes the intensity of the green autofluorescent signal

Increasing the inspired oxygen concentration from 21% to 100% had no effect on the intensity of the green signal. However, reducing the inspired oxygen concentration to 11-10% resulted in a change in flavoprotein fluorescence (Figure 6.4.a, 11%),). This change was characterised by decreased signal intensity, which preferentially affected areas around veins and regions far from arteries. As a consequence, regions surrounding arteries were characterised by preserved flavoprotein autofluorescence signal. This pattern typically appeared at around 11-10% inspired oxygen percentage. In contrast, smaller decreases in inspired oxygen (e.g. 18%, 15%) had no effect on the intensity of the green flavoprotein signal (Figure 6.4.a, 15%). The relative change in the intensity of green autofluorescence was monitored for the whole duration of the experiment. In Figure 6.4.b we show the profiles of green fluorescent signal in regions around arteries and veins, as the inspired oxygen was altered (Figure 6.4.c). This intensity profile suggests a sharp threshold at which retinal mitochondrial function is affected by

changes in inspired oxygen. Here, the hypoxia was introduced gradually, with smaller changes in inspired oxygen concentration every 3-4 minutes: 21% - 100% - 21% - 15% - 11% and 100% or 21%. The shown profile indicates that changes in flavoprotein occur drastically around 11-10%% inspired oxygen, especially in perivenular regions.

Moreover, the reduction in the intensity of flavoprotein autofluorescence observed under hypoxic conditions was reversible if the animals were returned to room air and allowed to recover. Interestingly, some animals showed an increased flavoprotein fluorescent intensity signal following recovery to 21-100% after a period of hypoxia.

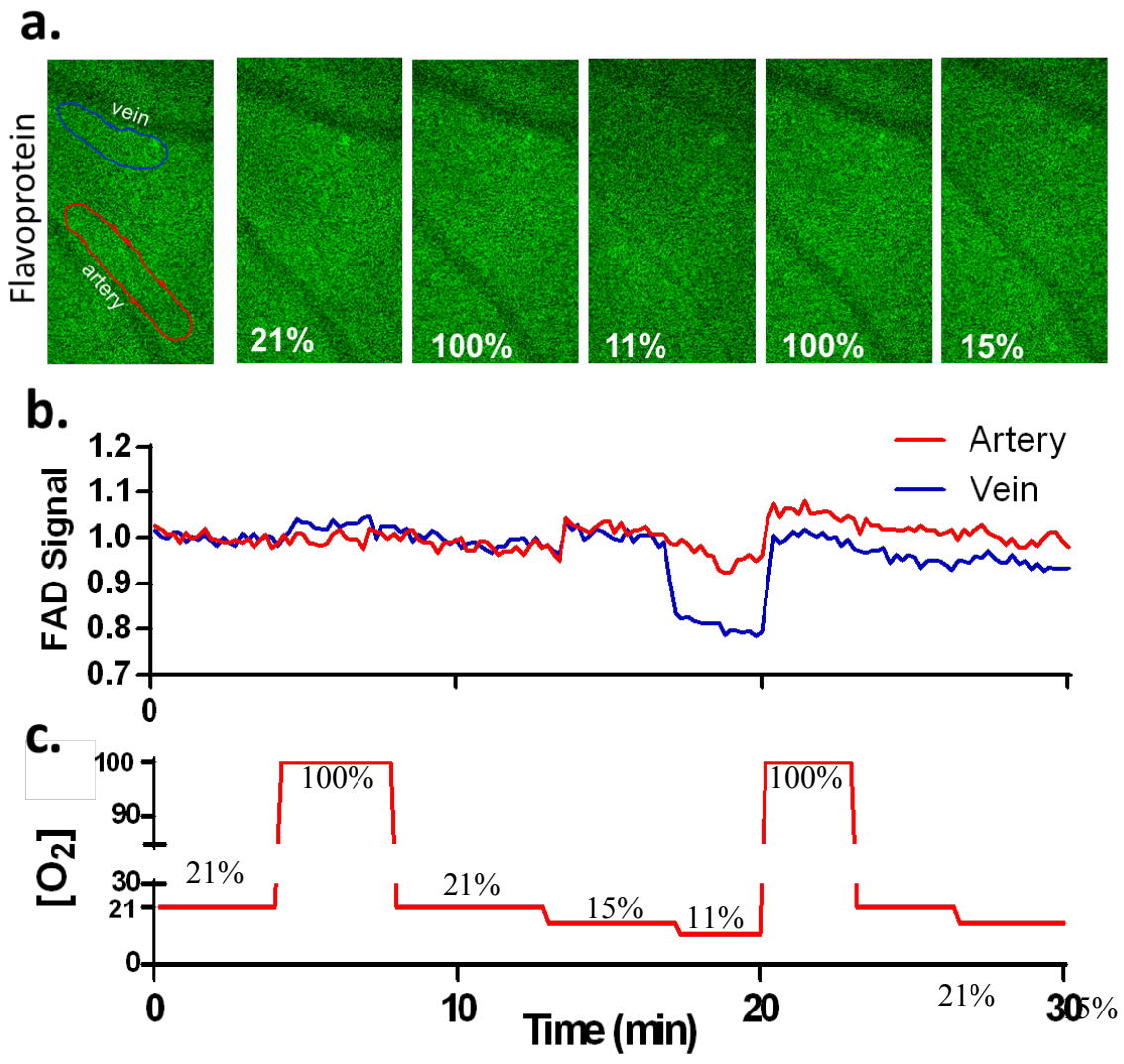

Figure 6.4. Flavoprotein autofluorescence during normoxia, hyperoxia and hypoxia. (**A**) Representative images of changes in retinal flavoprotein fluorescence in response to changes in inspired oxygen concentration. An increase in inspired oxygen above 21% did not change the intensity of flavoprotein fluorescence. However, a

decrease in inspired oxygen concentration at 11-10% reduced the intensity of flavoprotein signal, with preserved signal around arteries. (**B**) Profile plot showing the change in normalised flavoprotein fluorescence in areas around veins and arteries, while the inspired oxygen concentration was modulated (**C**).

6.5.3 Flavoprotein signal is responsive to prolonged changes in oxygen concentration

To understand further the relationship between oxygen and flavoprotein fluorescence, we designed an experiment where we conditioned animals at different oxygen concentrations. The reason for this experiment was to test whether prolonged times with reduced oxygen delivery, mirroring the environment during inflammation, neurodegenerative disease or ageing, translated into changes in flavoprotein signal. Here we simulated this hypothetical situation, conditioning animals at reduced and higher oxygen concentration, and flavoprotein signal analysed.

Specifically, we conditioned a cohort of animals for 20 min to different oxygen concentrations: 15%, RA and 30-45%. This conditioning was started prior to anaesthesia induction and imaging. The absolute flavoprotein intensity profile for these animals is shown in Figure 6.5. This graph shows that animals conditioned at a higher oxygen concentration (30-45%) had a brighter absolute signal compared to animals conditions in normoxia. Conversely, when the oxygen concentration was set at 15%, a reduction in the absolute intensity of the signal was observed, compared to animals in the 21% oxygen group.

This indicated a positive correlation between the oxygen concentration provided to the animal and the intensity of the flavoprotein signal acquired from the retina. Hence, retinal mitochondria are highly responsive to the environmental oxygen conditions.

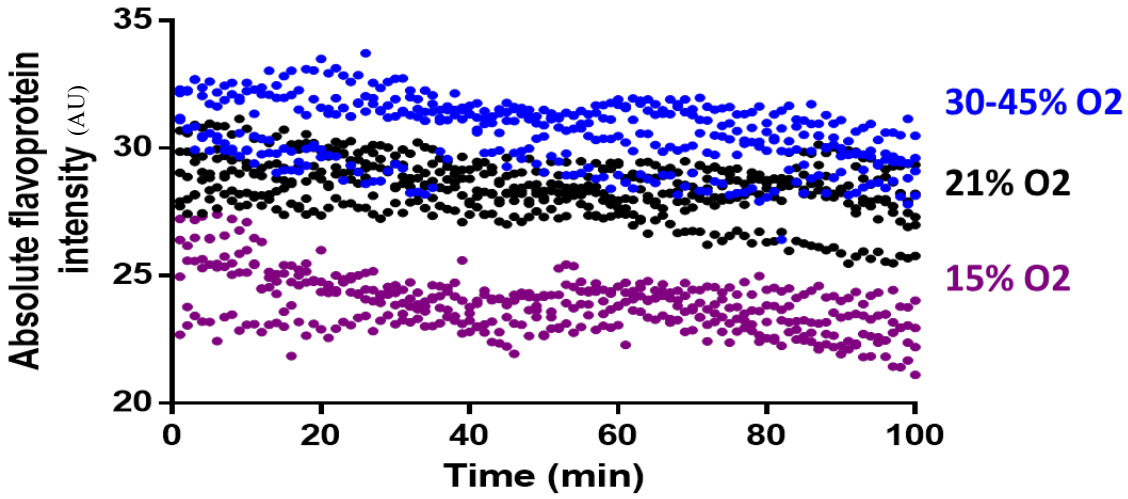

Figure 6.5. Absolute retinal flavoprotein autofluorescence. Plot profiles of the whole cohort of animals that were conditioned at different inspired oxygen concentration (30-45%, 21% and 15% oxygen). Animals that had 30-45% inspired oxygen concentration had on average higher flavoprotein autofluorescence intensity compared to room air conditioned animals. Similarly, animals at 15% oxygen, had reduced flavoproteins autofluorescence levels. Total N=13, 4 in each group except 30-45% which had 5 animals.

6.5.4 Flavoprotein autofluorescence cannot be distinguished from inflammatory associated autofluorescence

In the previous sections, we demonstrated that flavoprotein autofluorescence is highly sensitive to changes in the inspired oxygen concentration. We chose an animal model with local retinal inflammation, specifically experimental autoimmune uveitis (EAU) to further deepen our understanding of retinal mitochondrial function *in vivo* during inflammation. Such a model was used in contrast to models with systemic inflammation (e.g. EAE) to minimise side effects on physiological parameters, like blood flow or cardiac output, variables that would interfere directly on mitochondrial function.

A cohort of 10 animals were immunised following the appropriate protocol, and disease progression was monitored on a weekly basis. With the exception of two animals, all animals developed disease with variations in their clinical grade. However, no retina reached grade 3 or 4, being 4 the most severe clinical phenotype.

Our target was to select animals (retinae) with a clinical grade between 1 and 2, as we predicted that at higher grades the retinal structure would be damaged resulting in severe mitochondrial dysfunction. Therefore, grades 1 and 2 were chosen as optimum,

as the inflammatory process would impair mitochondrial function but not alter retinal morphology. This would allow us to challenge the animals with alterations in their inspired oxygen concentration, and study how this affects flavoprotein signal in the inflamed retina.

When imaged, all mice exposed to room air showed a relatively even green fluorescent background signal covering the retina, except in regions where blood vessels could be observed. In inflamed retina however, very bright green autofluorescent spots distributed through the retina contaminated the flavoprotein signal (Figure 6.6a). The amount of very bright green autofluorescent spots were positively correlated with disease progression, where lower clinical grades had a reduced number of spots compared to higher clinical grades. Consequently, the flavoprotein signal could not be distinguished from autofluorescent signal originating from inflammatory related processes.

An increase in inspired oxygen to 100% had no influence on the flavoprotein signal on animals in the diseased animals, similar to data obtained in naïve. Similarly, decreases to 15% in inspired oxygen concentration did not alter the flavoprotein signal. Only when the inspired oxygen concentration was lowered to 12-11% changes in the green signal could be observed in all animals, in agreement with our previous data. The green signal recovers with normoxia after a situation of hypoxia at 11-10% inspired oxygen concentration. All animals survived the challenge to lower inspired oxygen concentration.

As in our previous data, the analysis also suggests the presence of a brighter area around arteries when the animals are challenged with low inspired oxygen concentration, which was not present in areas surrounding veins.

The overall green autofluorescent profile (putative flavoprotein signal) was not different between naïve and inflamed retina, as can be obeserved in Figure 6.6 compared to naïve retinae in Figure 6.4.

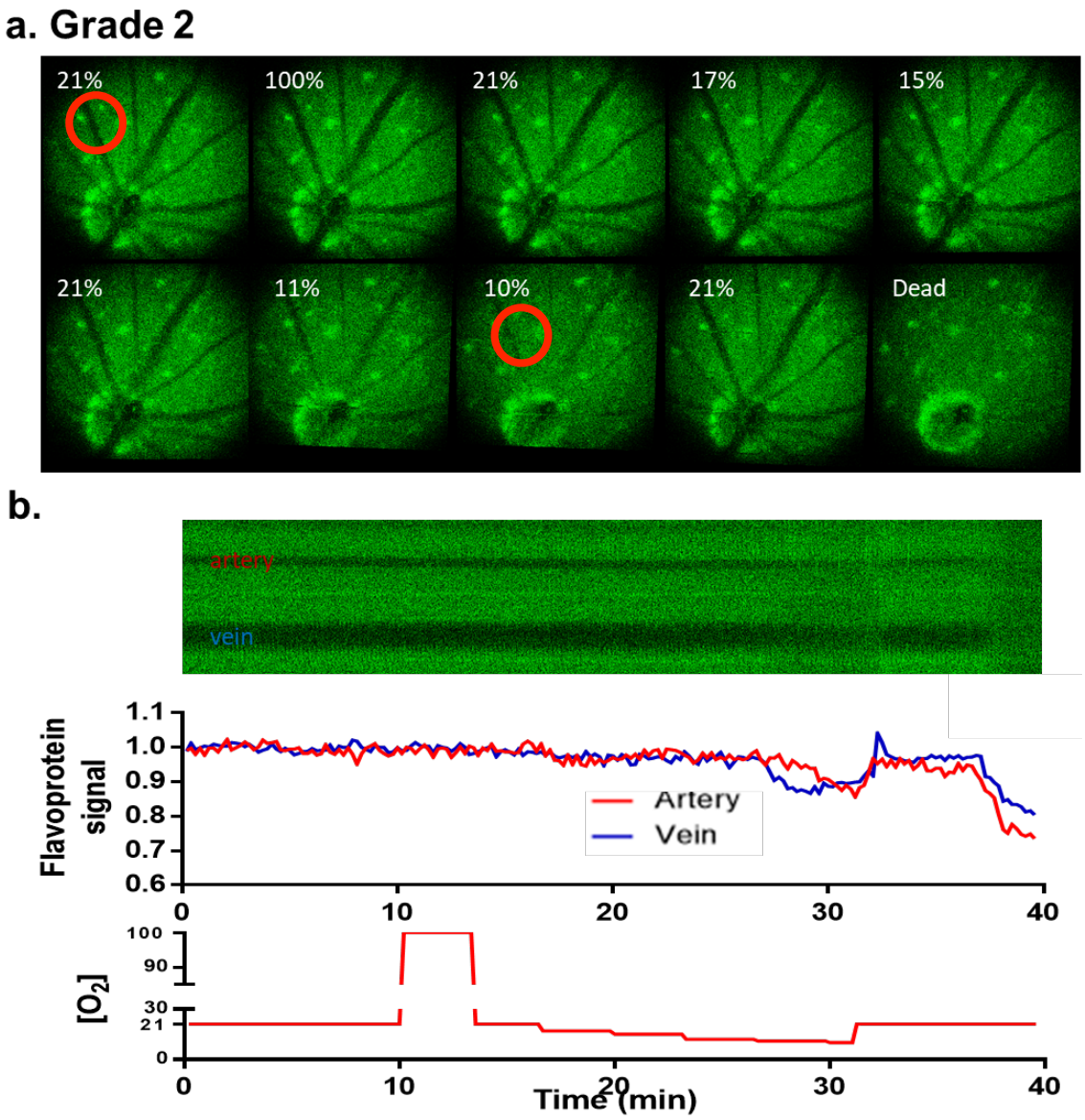

Figure 6.6. Flavoprotein autofluorescence in an EAU animal with clinical grade 2. Representative example of a retina imaged for flavoprotein autofluorescence with clinical grade 2. (**A**) Representative images of changes in flavoprotein autofluorescence at each inspired oxygen concentration. Highlighted in red circles, bright autofluorescent spots unrelated to flavoprotein fluorescence (**B**) Profile plot showing the change in flavoprotein fluorescence during the gradual change in inspired oxygen concentration in a representative tissue section (including a region around arteries and veins). The corresponding flavoprotein signal and inspired oxygen graphs are represented under the profile plot.

6.6 Discussion

We have shown that it is possible to use flavoprotein autofluorescence, imaged using standard confocal microscopy, in the retina of anaesthetised mice, as a measure of mitochondrial function. Further, using this method we have shown that retinal mitochondrial function is selectively impaired at low concentrations of inspired oxygen. This affects selective areas surrounding veins and tissues further away from arteries. Additionally, the intensity of flavoprotein signal was positively correlated with conditioning at different oxygen concentrations.

When animals where challenged with local retinal inflammation, although the signal was contaminated with autofluorescence derived from inflammatory related processes, the pattern of mitochondrial function seen in naïve retinae was unaltered.

6.6.1 Flavoprotein signal reflects changes in mitochondrial function

Using flavoprotein autofluorescence as a marker of mitochondrial function is well established[203,205,212–214]. However, the application of flavoprotein autofluorescence *in vivo* using microscopy to assess mitochondrial function in the CNS has been limited to the cerebellar[203] and brain cortex[214]. Furthermore, studying flavoprotein autofluorescence in the brain and cerebellar cortex represents an invasive procedure. Interestingly, the transparent tissues in the eye (cornea, lens and vitreous) should make the retina accessible to microscopy, allowing us to study flavoprotein autofluorescence in the retina *in vivo* non-invasively. To our knowledge, flavoprotein autofluorescence has not been previously used to evaluate retinal mitochondrial function in response to changes in inspired oxygen with the high spatial and temporal resolutions of confocal microscopy shown here.

Here we imaged the retina non-invasively *in vivo,* acquiring a non-specific green autofluorescent signal. Even though we cannot be certain that the majority of this signal is attributed to mitochondrial flavoproteins, we obtain a profile for retinal green signal as we modulate inspired oxygen concentration similar to profiles for green signal acquired in the cortex in a similar experimental setup[214]. This leads us to believe that the majority of the acquired signal can be attributed to mitochondrial flavoproteins. Additionally, once the animal dies, the observed drop in green signal would represent a mitochondrial *shut-down*, indicating that this green signal derives from mitochondrial

flavoproteins. However, even after the animals death a low-intensity green background is still present.

It is believed that lipofuscin, a toxic by-product formed of complex bisretinoids and fluorophores due to incompletely degraded photoreceptor outer segments in the retinal pigmented epithelium (RPE) cytosol[215,216], possesses a wide excitation spectrum ranging from 300 to 600 nm and an emission spectrum from 480 to 800 nm[217]. The spectrum of lipofuscin overlaps with the emission spectrum of flavoproteins, excitation around 488 nm and emission 505 to 570 nm. This suggests that the green autofluorescent background signal we observe in the retina after the animals death in the retina, when it is believed mitochondrial function has stopped, can be attributed to lipofuscin autofluorescence.

6.6.2 Flavoprotein signal is highly sensitive to oxygen changes

Under normoxic conditions (21% inspired oxygen), we found that the retinal oxygen supply was sufficient to maintain optimum mitochondrial function uniformly. Increasing acutely inspired oxygen concentration had no effect on flavoprotein autofluorescence, indicating that oxygen availability was not a rate limiting factor during normoxia. This is in agreement with similar reports where an uniform signal was observed in brain cortex, that did not increase with an acute increase in inspired oxygen concentration[196,218]. In contrast, when the animals were imaged after being in an oxygen enriched atmosphere (45-50%) for about 20 min, we observed an increase in absolute flavoprotein signal intensity, compared to animals inspiring room air (21% oxygen). The reason for this could be that an increase in flavoprotein signal due to an oxygen enriched atmosphere can only be observed after prolonged time in this condition. An alternative explanation is that oxygen enriched atmosphere was started before anaesthesia induction (5 min), and maintained for 15 min after, suggesting that perhaps the anaesthesia may intervene in this process.

In our experiments, reductions of inspired oxygen concentration to 15% had no effect on the flavoprotein signal, indicating that shorter periods of inspired oxygen concentration of 15% in healthy, anaesthetised animals is sufficient to sustain an efficient pool of oxidised mitochondria throughout the retina. A further decrease in the concentration of inspired oxygen to 11-10%, however, resulted in a characteristic change in the flavoprotein signal. This change was characterised by a reduction of the

flavoprotein signal in avascular regions and areas close to veins, while maintaining flavoprotein autofluorescence in areas closer to arteries. This observation is in agreement with previous observations in the brain cortex, however to achieve similar changes in the brain cortex a lower inspired oxygen concentration (5-8%) was required [214,219].

As in the case of a prolonged oxygen enriched atmosphere, a prolonged period (20 min) in a reduced oxygen atmosphere (15%) decreased the absolute flavoprotein signal. This is in contrast to acute small oxygen reductions, where no differences could be observed compared to normoxia. As explained above, the reason for this discrepancy could be that to visualise changes in flavoprotein signal with small changes in inspired oxygen concentrations, a longer period of time is required. Alternatively, the effects of the anaesthesia may interfere, as here the reduced oxygen atmosphere was provided prior to the induction of anaesthesia.

Altogether, these results suggest that flavoprotein signal is highly sensitive to changes in local oxygenation. Also, the threshold for retinal mitochondria dysfunction is at 11-10% inspired oxygen concentration according to our flavoprotein autofluorescence data, despite a gradual decrease in inspired oxygen concentration from normoxia. Furthermore, the results show that oxygen delivered via retinal arteries is physiologically relevant maintaining mitochondrial function during periods of hypoxia, and this could be of relevance to tissue function in pathological conditions where the blood flow would be impaired

It should be stressed, that after an acute period of hypoxia the retinal flavoprotein signal was reversible if normal room air or oxygen enriched air was delivered. Additionally, a subset of animals showed an increase in flavoprotein signal after recovery from hypoxia. There is no simple explanation for this observation. Perhaps, the difference in flavoprotein signal intensity between recovery and normoxia before hypoxia was induced, is indicative of the mitochondrial reserve respiratory capacity. However, we have no evidence to support this, as this observation did not occur in all animals and properly designed experiments for this hypothesis should executed.

6.6.3 EAU phenotype “contaminates” flavoprotein signal

Many reports suggest a direct relationship between mitochondrial function and inflammation. It is known that inflammation impairs mitochondrial function[220]. While

the opposite is also true, here we focus on the role of inflammation on mitochondrial function *in vivo*. Therefore, here we investigated how local retinal inflammation affects mitochondrial function *in vivo,* assessing flavoprotein autofluorescence. We chose a model for retinal inflammation, as opposed to a model of systemic inflammation. The reason is that in systemic inflammation many physiological parameters are affected (e.g. cardiac output) that would bias the results, and would not be correlated with the inflammatory process.

We chose experimental autoimmune uveitis (a model that resembles human uveitis), characterised by retinal inflammation, specifically on photoreceptors, the retinal cells with the highest metabolic demand. In this model, blood borne activated macrophages infiltrate the retina and produce an array on inflammatory cytokines and chemokines. This exacerbates the process with the recruitment of additional macrophages and T lymphocytes and other inflammatory cells to the retinal tissue[221,222]. However, the accumulation of inflammatory cells is associated with an increase in reactive oxygen species production that contributes and enhances the production of lipofuscin[223].

As pointed out in the results section, the excitation and emission spectrum of lipofuscin overlaps with the excitation and emission spectrum of flavoproteins. Effectively, the green signal derived from excess lipofuscin contaminates the flavoprotein derived signal. In fact, in diseased retinae it is obvious that green bright spots are spread throughout the whole retina, in numbers positively correlated with disease severity. Interestingly, other smaller bright spots appear to be moving (data not shown), and could be associated with moving macrophages. This is in agreement with other reports, where macrophages and other inflammatory cells are highly autofluorescent in the same spectrum range like flavoproteins[224]. This makes the analysis of diseased retinae more complicated than initially expected.

Wherever possible, the analysis of diseased retina was carried forward, focusing on regions not contaminated by bright spots. However, the relative flavoprotein autofluorescence profiles were no different to naïve retinae. These data suggests that the animals are as tolerant as naïve animals to low inspired oxygen levels, the drop in flavoprotein signal occurred at the same threshold as naïve animals (around 10-11% inspired oxygen concentration) and the inflammatory process had no apparent effect on the flavoprotein signal profile compared to naïve animals. This is in disagreement with

the majority of published literature, where it is accepted that inflammation has an important detrimental effect on mitochondrial function[57]. However, we have failed to observe this mitochondrial dysfunction *in vivo* in a rodent model of experimental autoimmune uveitis, with clear clinical signs of inflammation. The reason for this failure is unknown. Perhaps, we have systematically underestimated the fluorescent properties of lipofuscin especially in a pathological condition that is known to generate an excess of lipofuscin[217]. This lipofuscin underestimation may explain why we were not able to observe mitochondrial dysfunction during the inflammatory process.

6.6.4 Limitation

Being able to investigate mitochondrial function *in vivo* has many advantages compared to doing it *in vitro*. With current techniques, the retina is the only CNS tissue accessible from the exterior, thanks to the transparent properties of the cornea, lens and vitreous. However, the most obvious limitation is that investigating mitochondrial function with light (confocal microscopy) in a tissue that is highly sensitive to light is not ideal. Photoreceptors are specialised neurons highly sensitive to light that are able to transform electromagnetic energy (light) into electric energy (action potentials), that translates into a cascade of downstream synaptic communications from retinal cells to the visual cortex, that ultimately results in an image projection. In the presence of light, these cells are constantly hyper- and hypo-polarising, which requires a vast energy demand. By using light to investigate mitochondrial function we are indeed, interfering and altering the cellular function. In addition with the previous statement, the effects of anaesthesia (i.e. isoflurane) on mitochondrial function is unknown.

An additional qualification is that we have to be cautious regarding the "green autofluorescence" interpretation. The pattern in intensity observed of the green signal changing as the inspired oxygen concentration is modulated, overlaps strongly with the spectral of flavoproteins *in vitro*[225]. However, we cannot disclose the presence of other molecules with similar and overlapping excitation and emission spectra, whose intensity is strongly associated with mitochondrial function. To strengthen the interpretation of the results, an additional autofluorescent marker associated with mitochondrial function should be used. A good candidate could be the measurement of autofluorescence form nicotinamide adenine dinucleotide, also associated to mitochondrial metabolism[226]. The autofluorescent pattern of nicotinamide adenine dinucleotide would complement flavoprotein autofluorescence, as it would bright when mitochondria are reduced

(during hypoxia). Therefore, a combination of two autofluorescent mitochondrial markers would be a better approach to understand and deepen the knowledge of mitochondrial function *in vivo,* under physiological and pathological conditions.

6.6.5 Future perspectives

We aimed to study mitochondrial function *in vivo* based on flavoprotein imaging. But this may not be the most suitable approach. Perhaps, using a different approach based on the redox state of cytochrome *c* oxidase is more suitable, and has proven to be sensitive to small changes in the surrounding oxygen environment. Furthermore, our animal model with local inflammation in the retina should not interfere with the cytochrome *c* oxidase signal, providing us with a better understanding of mitochondrial function during inflammation.

Once the appropriate model and screening method is established, target mitochondria as a therapy. The screening method should allow us to see how *in vivo* mitochondrial function is changing with therapy. On one had this allows us a better understanding of mitochondrial function during inflammation; on the other hand, it should give us information whether the mitochondrial targeted therapy is successful.

On a specific level, I would attempt the following experiments:

- Complement our naïve and inflamed retinal flavoprotein data with retinal NAD(H) autofluorescence data *in vivo.* The advantage is that reduced $NADH^{+}$ has a clear emission peak at 340 nm, and would fluoresce when flavoprotein signal is absent. This would strengthen flavoprotein as a surrogate marker for mitochondrial function and allow analysis during inflammation.
- Treat EAU animals with 670 nm therapy and assess its consequences on mitochondrial function *in vivo* with flavoprotein and $NADH^{+}$ fluorescent, to investigate treatment efficacy and predict disease progression.

Chapter 7. Discussion and conclusion

Only once, about 1–1.5 billion years ago, an event occurred shaping future life on earth. An α-proteobacteria (ancestor of mitochondria) and an archaeal host chose to live together, giving rise to the eukaryotic cell. Throughout evolution, mitochondria in eukaryotic cells have been key components to give rise to complex multicellular organisms, as we know them today. Otherwise, *why aren't there human bacteria?* The relationship between mitochondria and cellular components has developed into a complex one. Mitochondria, known as the cells powerhouse, are not only important in producing and providing vast amounts of ATP through oxidative phosphorylation. They are also involved in infinite cellular functions, and importantly, their structural and functional health is key for cellular survival. When mitochondria become dysfunctional, the eukaryotic cell dies.

The data presented in this thesis provides evidence that ageing is associated with mitochondrial dysfunction, and in turn, enhancements in mitochondrial function in aged organisms result in improvements in physiological function. Additionally, we show data that it is possible to assess mitochondrial function *in vivo* in the retina.

Developing the idea that ageing is associated with mitochondrial dysfunction[13,15] and that this can lead to functional senescence, we report an investigation where we treat aged *Drosophila* with 670 nm light to improve mitochondrial function and consequences assessed via a range of health parameters. We chose aged *Drosophila* flies as a model, as it is a simple tool to investigate the effects of ageing, and consequently, assess any therapies aiming to modify the ageing process. Indeed, aged flies suffer from mitochondrial dysfunction and this can be reverted with 670 nm light therapy, as we have demonstrated functional improvements in a range of physiological and behavioural parameters. Interestingly, our data not only shows an improvement of mitochondrial function, but also indicated an increase in mitochondrial content, measured by mtDNA quantification. This suggests that improvements in mitochondrial function can translate in mitochondrial biogenesis. This is in agreement with reports that proposes the mitochondrial membrane potential as a quality control metric for healthy mitochondria: rising potentials are indicative of biogenesis processes, while declining potentials indicate mitochondrial degradation via mitophagy[227]. Even though we did not assess mitochondrial membrane potential in our experiments, previous studies reported

these findings in cells treated with 670 nm[228]. Taken together, the increased ATP production and respiration shown in our data are likely caused by improvements in mitochondrial membrane potentials.

Despite mitochondria being compartmentalised in double membranes inside the cells cytosol, they are not isolated from other cellular components. A continuous communication network is present between mitochondria and other cellular components (including nuclei), key for efficient cellular and mitochondrial function. In fact, cellular and environmental cues are able to modulate mitochondrial function and translate this into changes in cellular function, such as 670 nm exposure in our experiments. Hence, our data suggests that mitochondria communicate with other cellular components and structures, providing them information about mitochondrial homeostasis. Otherwise, it is not possible to explain changes in physiological function and behavioural responses with only changes in mitochondrial function.

Our data indicates that 670 nm is absorbed by cytochrome *c* oxidase, boosting the transfer of electrons in the ETC. This results in improvements in mitochondrial membrane potentials, ATP levels and other mitochondrial parameters. We speculate that this is then communicated to the nuclei, where the improvement in energy homeostasis translates into the activation of gene transcription that will shape cellular function mirroring juvenile flies. However, we failed to reveal molecular mechanisms that help to understand this communication between mitochondria and other cellular components.

One of the most novel aspects of this research is the finding that functional improvements after treatment occur very fast, with the first evidence being immediately after 670 nm exposure. Strikingly, these events occur before improvements in mitochondrial parameters can be detected, particularly ATP production. This is likely due to discrepancies in our methodology, as our methods to analyse mitochondrial parameters (such as ATP) are static and do not detect dynamic changes in the ATP pool. However, functional improvements observed right after exposure are subtle and can only be detected with very sensitive fly tracking techniques as shown in this work. When treatment is extended over one week, robust changes in functional metrics are detected. Together, the consequences of 670 nm treatment has immediate implications in animal behaviour, but to detect robust changes a prolonged dose over different days is needed. This has implications when the treatment is translated into humans. While

Drosophila flies are easily irradiated followed by assessment of several physiological and behavioural functions, in humans this is not possible. To translate this into humans, it should be targeted at tissue or organs affected by biological ageing or pathological conditions with implications of mitochondrial dysfunction.

In spite of this, many aspects of the 670 nm mechanism of action remain to be elucidated, particularly those related to routes of communication between mitochondria and other cellular components, providing a molecular link between mitochondrial function and physiological and behavioural responses. We provide evidence for this association, however we lack any molecular links, albeit that they may be related to energy availability. This implies that mitochondrial functional phenotype not only determines energy metabolism, but they are also implicated as an important drivers of the capacity to regulate and perform cognitively complex tasks and behaviours. In fact, it has been shown that there is a link between mitochondrial structure and function and the ability for a bird to perform complex behaviours, suggesting mechanistic links between mitochondrial function and neurogenesis, energy homeostasis and key pathways involved in this ability[229].

We know what happens with one dose of 670 nm and also with a longer period of 7 days exposure. We also know what happens when the treatment is life-long[71]. However, we do not know what happens if the treatment is interventional and persists over a long period of time. Perhaps a longer treatment window would show a different phenotypic paradigm, and if treatment is stopped, severe consequences may arise particularly in pathological environments environments. This is particularly relevant in subjects with certain pathological conditions, as in the case of rapamycin the consequences of a chronic therapy is deleterious in an animal model of fragile X syndrome[230]. This needs to be assessed case by case to support the safety and efficacy of 670 nm therapy when translated into humans.

Furthermore, we have to emphasise one important qualification to some data presented in this thesis, especially relevant for light therapy. Our animal models are housed in standard laboratory environments, with no natural light. It could be argued that if animals are housed under natural light conditions, the phenotypic outcomes of the 670 nm therapy may be different, or perhaps, inexistent, as natural light already provides a 670 nm dose. This needs to be assessed, as particularly the human population is more or

less exposed to natural light. If 670 nm therapy is translated into human population, these need to be taken into consideration.

Our data also reveal some interesting aspects regarding circadian regulation of mitochondrial function. Interestingly, our 670 nm therapy did only show effective results when light was irradiated at certain times of the day, specifically during mornings. This has one very important consequence if therapies are translated in to the clinic: mitochondrial targeted therapes must take consideration of circadian mitochondrial function. It could be that a promising mitochondrial targeted therapy could have beneficial results *in vivo*, but because it was delivered at the wrong time of day, it has no positive impact. Thus, testing mitochondrial targeted therapies at different times of day is primordial before it is translated effectively to patients with diseases associated with mitochondrial dysfunction.

After light therapy, we propose to investigate other approaches to target mitochondrial function, as light might not be the appropriate approach. We chose to investigate the role of 9-*cis*-β-carotene, with its potential role as an antioxidant. Albeit this investigation was not as extensive as the 670 nm therapy, our data suggests that *Drosophila* fed with an algae extract rich in this carotene hve improved mitochondrial function. Strikingly, carotenes are food supplements in today's diet. If all-*trans*-β-carotene are substituted by 9-*cis*-β-carotene which claims better antioxidant therapies, the impact on human health is unquestionable.

Additionally, we have evidence that despite declining physiological function, cellular structure may still be present in aged tissue. This is particularly relevant to mitochondrial rich photoreceptor cone cells in the ageing primate retina, that suffer significant decline in physiological function with ageing. In our model, aged old world primate, we show that cone photoreceptor cell numbers do not decline with ageing compared to young individuals, despite declining cone physiological function. Moreover, we report that some of these changes may be explained due to cellular oxidative stress, associated with declining mitochondrial function. Interestingly, targeting therapies to mitochondrial function in the retina, we may be able to restore or recover physiological function, as the cells are present but not working efficiently. Here a 670 nm therapy would play an important role, especially as the retina is an accessible tissue to 670 nm light. In an aged animal model of AMD, 670 nm therapy improves

retinal physiology, particularly those functions related to cone function[231]. This has exciting clinical implications in human health and disease. With an increased aged society, associated with age related diseases with impact on the retina and mitochondria, such as AMD[232], treatment with 670 nm would ameliorate signs and symptons. If the mechanisms of action of 670 nm is further investigated and deciphered, combined with an appropriate therapy timing, 670 nm therapy may be an exciting, affordable and available tool that would decreased the burden of today's national health system.

Finally, we have also shown that it is possible to measure mitochondrial function *in vivo* in the retina*,* with adequate spatial and temporal resolutions. We report an investigation of a retinal model of inflammation (EAU) assessing their reliability, level of inflammation and applicability to confocal flavoprotein imaging. However, this model is problematic, as the inflammatory process in the retina interferes directly with the flavoprotein reading, limiting the spatial and temporal assessment of mitochondrial function *in vivo* when mitochondria are challenged to acute periods of hypoxia. There are two main reasons why we focused on the assessment of flavoproteins as a surrogate marker for mitochondrial function. First, the retina, part of the central nervous system, is the tissue with the highest metabolic rate in the body. This makes it an excellent candidate to assess mitochondrial function, especially in mitochondrial diseases or inflammation. In a situation of mitochondrial targeted therapy, assessing mitochondrial function *in vivo* would allow for personalised and continuous assessment of treatment efficacy. Secondly, the retina is the only CNS tissue that can be accessed non-invasively, providing significant clinical potential. Today, confocal scanning laser ophthalmoscopes are used regularly in the clinic[233,234]. It might be possible to assess mitochondrial function *in vivo* in the retina (via flavoprotein imaging), by introducing acute phases of insults (e.g. hypoxia) investigating how mitochondrial adapt to changes in their oxygen environment in pathological conditions (e.g. AMD), providing a metrix for retinal mitochondrial health in human subjects.

However, we should emphasize that investigating mitochondrial function *in vivo* via flavoprotein imaging may not be the most suitable approach. Near-Infrared Spectroscopy (NIRS) could be an alternative approach. This technic measures non-invasively *in vivo* changes in mitochondrial function, and this can be applied to the retina[94]. This approach provides an excellent temporal read out, but lacks spatial resolution. In spite of this, NIRS is being already used in different clinical settings, such

as in infant brains with diagnostic implications[235]. Even though NIRS lacks spatial resolution, it could readily be applied in human retina, providing *in vivo* mitochondrial function. Nevertheless, an approach providing spatial and temporal resolution should be developed further, as spatial resolution complements temporal resolution. Here flavoprotein (and NADH) imaging would be an excellent complement to NIRS spectroscopy.

7.1 Conclusion

Overall, this thesis aimed to explore mitochondrial function in ageing, how it can be recovered or restored to improve physiological function, and a tool to investigate mitochondrial function *in vivo* in the retina. This was achieved using a combination of three different models: the fruit fly, primate and mouse. As mitochondria are highly conserved across species, it allowed us to use different models in our experiments, depending on our needs.

We believe the data shown provides a solid perspective of the role of mitochondrial function in ageing, linking mitochondria targeted therapy with outcomes in physiological and behavioural functions. We also approach mitochondrial function *in vivo* and its implication in inflammation. Given the considerable and increasing burden of the ageing human population in pathological conditions where mitochondrial function is affected, these data have exciting translational appeal to human mitochondrial targeted therapies.

Publications associated with this thesis

Weinrich, T. W., Coyne, A., Salt, T. E., Hogg, C., & Jeffery, G. (2017). **Improving mitochondrial function significantly reduces metabolic, visual, motor and cognitive decline in aged *Drosophila melanogaster***. *Neurobiology of aging*, 60, 34-43.

Weinrich, T. W., Powner, M. B., Lynch, A., Jonnal, R. S., Werner, J. S., & Jeffery, G. (2017). **No evidence for loss of short-wavelength sensitive cone photoreceptors in normal ageing of the primate retina**. *Scientific reports*, 7, 46346.

Weinrich, T. W., Hogg, C., & Jeffery, G. (2018). **The temporal sequence of improved mitochondrial function on the dynamics of respiration, mobility and cognition in aged *Drosophila*.** *Neurobiology of aging,* 70, 140-147.

Sections of this thesis were supplemented in part with material from the published manuscripts

Appendix

SCIENTIFIC REPORTS

OPEN

No evidence for loss of short-wavelength sensitive cone photoreceptors in normal ageing of the primate retina

Received: 25 October 2016
Accepted: 14 March 2017
Published: 12 April 2017

Tobias W. Weinrich[1], Michael B. Powner[2], Aisling Lynch[1], Ravi S. Jonnal[3], John S. Werner[3] & Glen Jeffery[1]

In old world primates including humans, cone photoreceptors are classified according to their maximal sensitivity at either short (S, blue), middle (M, green) or long (L, red) wavelengths. Colour discrimination studies show that the S-cone pathway is selectively affected by age and disease, and psychophysical models implicate their loss. Photoreceptors have high metabolic demand and are susceptible to age or disease-related losses in oxygen and nutrient supply. Hence 30% of rods are lost over life. While comparable losses are not seen in cones, S-cones comprise less than 10% of the cone population, so significant loss would be undetected in total counts. Here we examine young and aged primate retinae stained to distinguish S from M/L-cones. We show there is no age-related cone loss in either cone type and that S-cones are as regularly distributed in old as young primates. We propose that S-cone metabolism is less flexible than in their M/L counterparts, making them more susceptible to deficits in normal cellular function. Hypoxia is a feature of the ageing retina as extracellular debris accumulates between photoreceptors and their blood supply which likely impacts S-cone function. However, that these cells remain in the ageing retina suggests the potential for functional restoration.

With ageing and disease there is cell loss and reduced function. Age-related changes are partly linked to metabolic rate with a high metabolic rate associated with a faster pace of ageing[1]. The CNS has a very high metabolic rate[2], and within this the retina has the greatest stress due to the energy demands of photoreceptors[3]. Consequently, there is significant age related photoreceptor loss. Within the rod population there is around a 30% loss with normal ageing in human and rodent[4,5]. In humans and old world primates cone photoreceptors are classified according to their maximal sensitivity at either short (S, blue), middle (M, green) or long (L, red) wavelengths. There are key differences between M/L cones and S-cones. S-cones constitute less than 10% of the total cone population whereas the other two types account each for around 45%. S-cones have distinct anatomical and physiological properties compared to M/L cones[6,7]. Also, colour discrimination studies show that the S-cone pathway is selectively affected by age and disease[8–11]. The ageing effect was thought to relate to brunescence of the lens as this would selectively absorb shorter wavelengths[8]. However, there are also significant changes in S-cone timing with age that are not related to lens brunescence[12]. Psychophysical models implicate differential S-cone loss with age, which would represent the most parsimonious explanation for reductions in their function. However, because they only form such a small percentage of the total population, counts of total cone numbers are unlikely to reveal any significant changes in their S-cone population.

Here we examine old world primate retinae from young and old animals stained to reveal S- and M/L-cone populations to determine patterns of age-related cell loss.

Results

Retinae were acquired from young and old Mauritian *Macaca fascicularis* from a long established breeding colony. These old world primates have retinae highly similar to those in humans[13], with a well-developed central

[1]Institute of Ophthalmology; University College London, London, EC1V 9EL, United Kingdom. [2]Division of Optometry and Visual Sciences; City, University of London, London, EC1V 0HB, United Kingdom. [3]Department of Ophthalmology and Vision Science; University of California, Davis, Sacramento, CA 95817, United States of America. Correspondence and requests for materials should be addressed to G.J. (email g.jeffery@ucl.ac.uk)

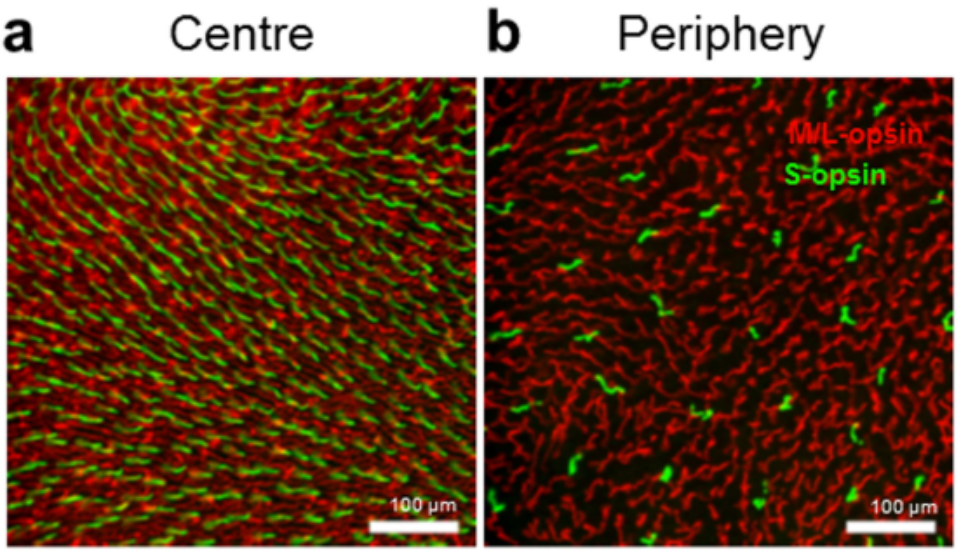

Figure 1. An example of changes in cone density across the temporal retina. The spatial distribution of cones stained for M/L-opsin (red) and S-opsin (green) from a young animal. (**a**) Was taken in the temporal parafovea (1.3 mm eccentricity). (**b**) Was taken in the temporal periphery (10 mm eccentricity). There was a clear gradient in cone density across this axis, but no obvious differences in cone density between young and old animals.

region that includes a fovea and trichromatic vision[14,15]. Further, photoreceptor function measured psychophysically is also very similar between humans and this species of old world primate[16,17]. Animals were grouped into young (6 years) and old (17 years). At 6 years eye size is fully mature. At 17 years animals appear physically old and have clear signs of retinal ageing including extra-cellular deposition of lipofuscin[18,19]. Primates in the source colony rarely lived beyond 20 years. Macroscopic and microscopic examination confirmed that all retinae used were normal.

Flat mounted retinae were uniformly stained with two antibodies, one for S-cone opsin and the other for the combined M/L-cone opsin. The distribution of labelled cones conformed to previous studies with a significant gradient between the central macular and the peripheral retina[15,20] as shown in Figs 1 and 2. Retinae were systematically mapped from the central macula out toward the temporal periphery at approximately 100 locations per retina in a region 0.1 mm^2 in each of 6 retinae, 3 from each age group.

Figure 2 shows eccentricity-dependent variation in cone density, grouped by age and cone spectral class. Figure 2a and b are M/L-cone densities from the two age groups, and Fig. 2c and d are S-cone densities in each group over the same region. Counts for M/L cones do not extend into the central macula because cell density here was too great for accurate counting. At any given retinal eccentricity, the variance in M/L-cone density appears greater among young animals than old, although this was less than the variability reported for the total cone population in humans[21]. Further, in the young animals the variability was largely due to data from one individual. However, overall aggregate dependence of M/L-cone density on eccentricity is similar in the two age groups (Fig. 2a and b). Plots for S-cone densities in young and old primates over the same regions are again very similar with the steepest decline in density occurring over the 4 mm closest to the fovea (Fig. 2c and d). There is no evidence for a difference in S-cone cell numbers between the two age groups.

Figure 2e and f show cone densities for both young and old animals, grouped by cone spectral class. Within each spectral class, data from young and old animals were fitted separately with the function $D(E) = D_0 e^{-\lambda E}$, using nonlinear least-squares regression. $D(E)$ is the cone density at eccentricity E, D_0 is the maximum density, and λ is the decay constant. Permutations of λ such as time constant ($\tau = 1/\lambda$) and half-life ($E_{1/2} = (ln\ 2)/\lambda$) describes the rate of decay. The half-life represents the eccentricity at which cone density reaches half its maximum. For M/L-cones, there was a small difference in half-life between young and old animals, with $E_{1/2} = 5.1\ mm$ and $E_{1/2} = 4.0\ mm$, respectively, which appears to be largely due to differences in peripheral densities (Fig. 2e). For S-cones, however, there was no difference; in both young and old animals the S-cone density fell to half its peak value at 1.5 mm (Fig. 2f).

To estimate the aggregate density of each cone class in each animal, numerical integration over the exponential decay models was computed. This step permitted fair comparison of cone density between young and old animals, even in the presence of minor variations in the rate of exponential decay with eccentricity. The resulting values are shown in Table 1. Two one-way ANOVAs were performed: first between the old and young aggregate S-cone densities, and second between the old and young aggregate M/L-cone densities. In neither case was a significant difference in density detected ($p = 0.88$ and $p = 0.71$, respectively).

Because the S-cone distribution in the macaque retina is highly regular (nonrandom), loss of S-cones would result in increased disarray. In order to test the hypothesis that while S-cone function may be diminished by age,

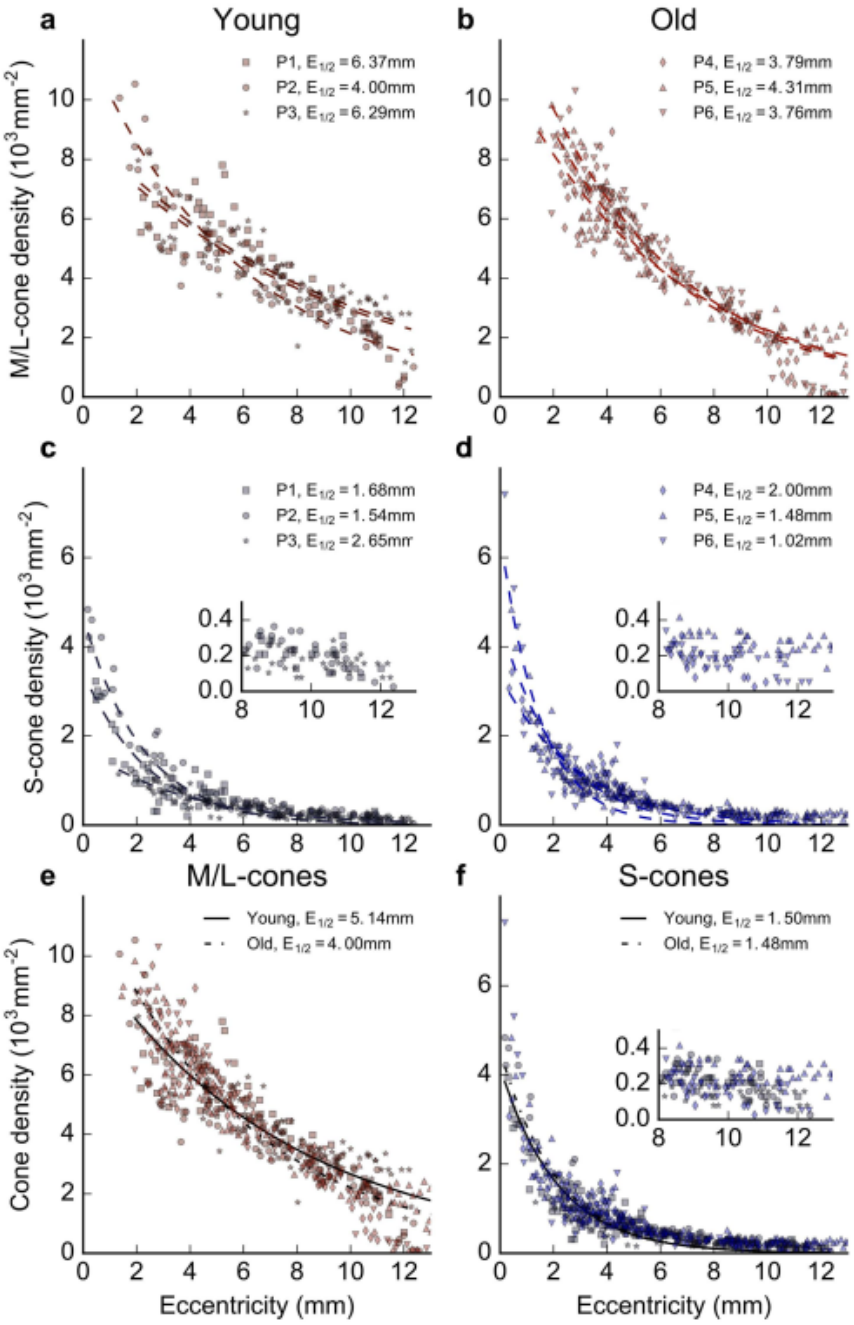

Figure 2. Cone density and eccentricity in young and old animals. Densities of M/L- and S-cones in young and old macaques extending from the central retina to 13 mm temporal periphery. (**a**) The densities of M-/L-cones in 3 young (6 years old) animals. (**b**) Corresponding data for 3 old (17 years old) macaques. Data are not provided for the central most location as cell density was too great for reliable counting. (**c**) Counts of S-cones over exactly the same region in 3 young animals. (**d**) Counts of S-cones over the same region in 3 old primates. In each case patterns are very similar for the two age groups. (**e**) and (**f**) Density of the two age groups are overlaid, for L-/M-cones and S-cones, respectively. (**e**) Densities for M-/L-cones in young and old primates with regression lines for the two populations. Data sets for the two ages match closely except in the far periphery. (**f**) Densities for S-cones in young and old primates with regression lines for the two populations. Again these match closely. Taken together the data in the 6 graphs show that there is no difference between young and old primates in terms of cone densities. Because of the low S- cone density in the periphery, their densities have been represented twice at different scales in the regions beyond 7 mm eccentric. The first is on the same scale as other counts (Fig. 2a and b) and the second is on an expanded Y axis to provide a clearer picture of their distribution.

	S-densities (cones/mm²)		M/L-densities (cones/mm²)	
	Young	Old	Young	Old
	371	478	4553	4,217
	431	392	4162	4,160
	378	283	4387	4,530
Mean	**393**	**384**	**4368**	**4,302**

Table 1. Mean cone densities grouped by age and cone spectral class. Cone densities derived from exponential models by interpolating cone density over the central 20 mm.

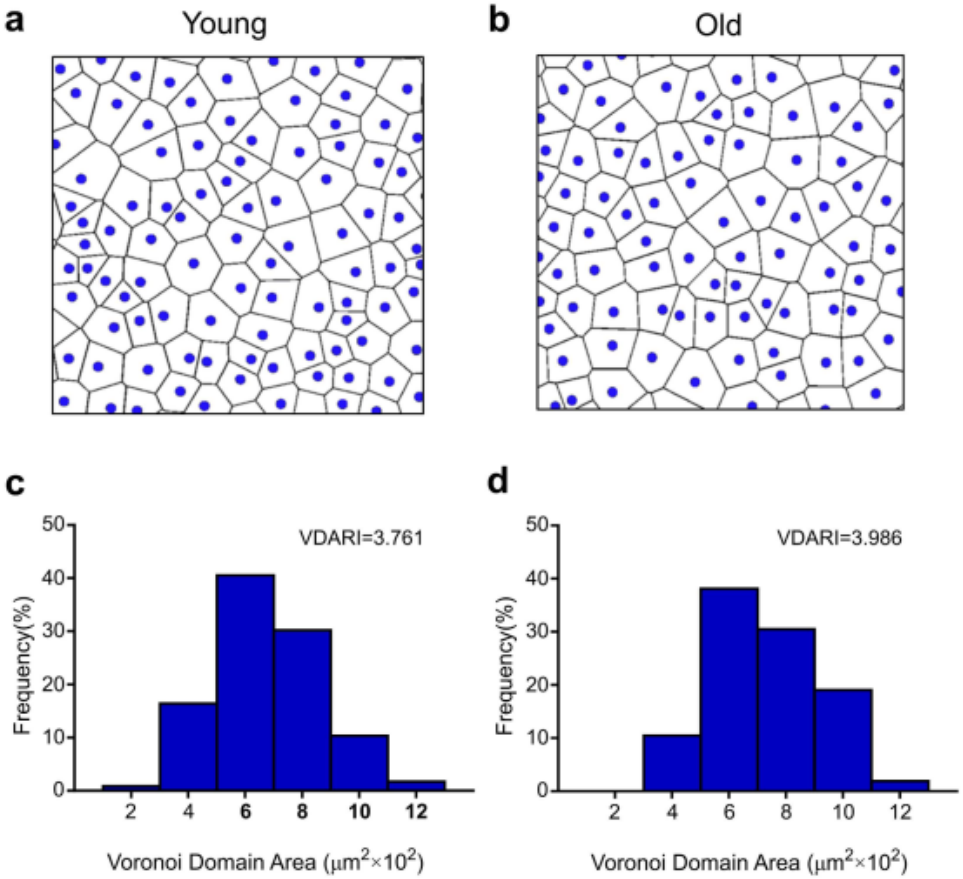

Figure 3. Voronoi domain analysis provides both diagrams and metrics of mosaic regularity. (**a**) and (**b**). Voronoi diagrams of S-cones in 200 × 200 μm regions of young (**a**) and old (**b**) retinae, at 1.07 mm and 1.17 mm eccentricity respectively. For each S-cone, a polygonal domain was created by identifying pixels that are closer to it than any other S-cone. The two diagrams are qualitatively similar. (**c**) and (**d**). Frequency distributions of Voronoi domain area, for the diagrams shown in A and B, respectively. The distributions are similar, echoed by the small difference between the Voronoi domain area regularity indices (VDARI), which is the area mean divided by the area standard deviation, for each sample. Together, these data show that S-cone regularity is not impacted by age, which implies no age-related loss in S-cones since such loss would result in a loss of regularity.

the cells are not lost in significant numbers, Voronoi domain analysis[22] was used to quantify disarray in the S-cone mosaics. The Voronoi diagrams partitioned the image into regions, based upon proximity of the nearest S-cone. Variance among the areas or effective radii of these regions is an indication of mosaic disarray. There was no difference in these measures of disarray between the two age groups, irrespective of retinal location, confirming that no appreciable S-cone loss occurred with ageing (Fig. 3).

In spite of declining cone function[8], these old world primates have no significant age-related reduction in cone numbers. This is particularly unexpected for functions mediated by S-cones in ageing and disease, where age-related cell loss might have been expected[9,23,24]. It could be argued that because our analysis was confined to

the horizontal meridian we may have missed aged related cone loss in other areas. However, we know of no evidence for specific regional loss and saw no evidence for it when examining the retinae used in this study.

Discussion

Human anatomical data for the ageing cone population is mixed with seemingly inconsistent evidence for both preservation and age-related loss[4,25]. Complicating matters further, is a recent study in mice that showed significant cone loss in the first year of life that was relatively biased towards loss of the M/L-cone population. This early cone loss preceded loss within the rod population[26]. However, there are fundamental differences in the cone populations and their relative distribution between mouse and primate that may undermine the value of a direct comparison[26]. In light of this, it may be argued that we lack evidence for a decline in S-cone mediated vision in non-human primates, but we have specifically sourced old world primates to ensure that our model is as close to the human as possible, and as such, likely to reflect the age related changes found in humans. In spite of this, it is possible that there are differences in retinal ageing between humans and primates that our data have failed to reveal. A further qualification is that we need to stress that our animal numbers in each of the two groups are relatively low and as such not amenable to statistical analysis. Lack of difference is not evidence for equality. Consequently, our results should be regarded with caution.

In primates no previous attempt has been made to count the separate S- and M/L-cone populations over age. As S-cones form only about 10% of the total cone population in these animals[27], significant changes could occur in their number that would easily be missed in counts of the overall cone population. Further, in the case of human retinae, tissues inevitably come from a heterogeneous population in which there has been differential exposure to environmental factors that may modulate cell survival, such as poor diet and smoking. In contrast, our primate data are derived from animals that were not exposed to such factors. Poor diet and smoking are risk factors in age-related macular degeneration (AMD), which is the largest cause of visual loss in humans over 60 years of age in the western world. But studies of photoreceptor loss in AMD may be relevant to our findings, as with the spread of degeneration cones appear to remain while rods are lost, consistent with the notion that these cells are relatively robust in both ageing and disease[28,29].

S-cone function declines with age in humans and while age-related brunescence of the lens selectively attenuates short-wavelength light, it does not explain all of the age-related changes in S-cone sensitivity[30]. There is a slowing of the S-cone pathway with age even after compensating for changes in the lens[24]. In both humans and old world primates, colour vision is substantially the same[16,17]. S-cone function is known to be selectively lost in specific metabolic conditions, which may highlight potential mechanisms of dysfunction. In each case where S-cone function declines there is a significant association with restricted metabolism, which is important in the retina as photoreceptors have the greatest energy demands in the body[31]. Hence, reduced S-cone function is found in diabetes[9], where access to glucose is compromised. Likewise, when oxygen is reduced S-cone function declines[32]. Oxygen is critical for ATP production in mitochondria, which are densely packed in photoreceptor inner segments[33]. Other pathologies where there is evidence of selective functional decline of S-cones include retinal detachment[34] and macular degeneration[35–37], and these also have a direct link with oxygen. In retinal detachment, the outer retina is separated from its choroidal blood supply and becomes hypoxic. In macular degeneration there is deposition of extracellular material under the retinal pigment epithelium (RPE) that restricts the passage of oxygen and metabolites to photoreceptors.

These pathologies may cast light on age-related changes that selectively impact on S-cones. With normal ageing, Bruch's membrane, which sits between the choroidal blood supply and the RPE thickens due to the accumulation of extra-cellular deposits, and consequently the outer retina becomes increasingly hypoxic[38,39]. If S-cones lack adaptive flexibility to respond to this they will suffer functional decline, although this appears to not result in cell death. The fact that in ageing such cells do not die implies that there may be an opportunity of restoring aged functional decline in this functionally vulnerable but anatomically robust cell type.

Methods

Retinal tissue. Ocular tissues were acquired from *Macaca fasciularis* from an established colony under U.K. Home Office regulation. Eyes were retrieved at death following sedation with ketamine and overdose of intravenous sodium pentobarbital. The primary purpose of animal usage was different from the aims of this study and eyes were only retrieved after death. Eyes (N = 6, 3 young at 6 years and 3 old at 17 years) were removed and placed in 4% paraformaldehyde for approximately 24 h. They were then washed in phosphate buffer. The anterior eye was removed and the retina dissected free as a whole mount. The temporal retina running from the optic nerve head to the periphery in a strip approximately 1 cm wide was dissected. This was permeabilised in 3% Triton X-100 in PBS containing 5% normal donkey serum (NDS) (Jackson Labs, USA) followed by primary antibody incubation with S-opsin (1/1,000) (goat polyclonal, SC-14363, Santa Cruz Biotecnhology, Inc., USA) and M/L-opsin (1/600) (rabbit polyclonal, AB5405, EMD Millipore, Temecula, California, USA) in PBS 1% NDS at room temperature (RT). Retinal strips were washed in phosphate buffered saline before incubation with secondary fluorescent labelled antibodies (1/2,000) for 2 h (donkey anti-rabbit Alexa Fluor 568 (A10042) and donkey anti-goat Alexa Fluor 488 (A11055), Invitrogen, Belgium). Strips were washed with PBS and Tris-buffered saline (TBS) and then mounted in Vectashield (Antifade Mounting Media, H1000, Vectashield, Burlingame, California, USA), coverslipped and sealed.

The temporal retina segments were viewed at X20 under epifluorescence. Images were captured at 1,280 × 1,024 pixels using a Digital Eclipse DXM 1200 camera (Nikon, Japan). These formed a continuous corridor from the fovea towards the temporal periphery over about 15 mm. Images were stitched together. The tissue outlines were traced on a systematic random grid placed over the photographed elements. Counts of labeled cones were undertaken in a frame of 200 × 200 μm in the upper right corner of each square. 597 sites were included in the sampling area across the retinae with an average of 99 ± 6.4 (SEM) counting sites per retina. Sites

were counted only where cones were arranged in a matrix-like pattern and the image was clear and undamaged. The density of S-cones and M/L cones cells was determined at each sampled site, as the number of cells divided by the area counted at that site.

All general chemicals were acquired from Sigma Aldrich (Dorset, United Kingdom).

Spatial analysis. S-cones were automatically identified in the anti-S-opsin stained images (the green channel in the RGB images shown in Fig. 1) as follows. First, the fundamental spatial frequency of the S-cones was determined from the spatial power spectrum (2D FFT). Next, using this frequency a custom bandpass filter was used to smooth the image, followed by thresholding the image above the noise floor. The resulting image contained easily identifiable blobs corresponding to the S-cones, the centers of mass of which were taken to be the S-cone coordinates.

S-cone coordinates were used to generate Voronoi diagrams using the Qhull[40] and Fortune's[41] algorithms, implemented in Python, where each resulting Voronoi domain consists of those points in the image closer to the domain's S-cone anchor than any other S-cone. Each domain consists of a polygon, and domain areas were computed using the shoelace formula (or surveyor's formula). Variance among the domain areas was computed for all images (Voronoi domain area regularity index, or VDARI) which is an indication of the uniformity of the S-cones' spatial distribution.

References

1. Speakman, J. R. Body size, energy metabolism and lifespan. *J. Exp. Biol.* **208,** 1717–30 (2005).
2. Wang, Z. *et al.* Specific metabolic rates of major organs and tissues across adulthood: Evaluation by mechanistic model of resting energy expenditure. *Am. J. Clin. Nutr.* **92,** 1369–1377 (2010).
3. Linsenmeier, R. A. & Padnick-Silver, L. Metabolic dependence of photoreceptors on the choroid in the normal and detached retina. *Investig. Ophthalmol. Vis. Sci.* **41,** 3117–3123 (2000).
4. Curcio, C. A., Millican, C. L., Allen, K. A. & Kalina, R. E. Aging of the human photoreceptor mosaic: Evidence for selective vulnerability of rods in central retina. *Investig. Ophthalmol. Vis. Sci.* **34,** 3278–3296 (1993).
5. Cunea, A. & Jeffery, G. The ageing photoreceptor. *Vis. Neurosci.* **24,** 151–5 (2007).
6. Stromeyer, C. F., Kronauer, R. E. & Madsen, J. C. Response saturation of short-wavelength cone pathways controlled by color-opponent mechanisms. *Vision Res.* **19,** 1025–1040 (1979).
7. Ahnelt, P. K., Kolb, H. & Pflug, R. Identification of a subtype of cone photoreceptor, likely to be blue sensitive, in the human retina. *J. Comp. Neurol.* **255,** 18–34 (1987).
8. Werner, J. S. The Verriest Lecture : Short-wave-sensitive cone pathways across the life span. *J. Opt. Soc. Am. A* **33,** A104–22 (2016).
9. Greenstein, V. C., Hood, D. C., Ritch, R., Steinberger, D. & Carr, R. E. S. (blue) cone pathway vulnerability in retinitis pigmentosa, diabetes and glaucoma. *Investig. Ophthalmol. Vis. Sci.* **30,** 1732–1737 (1989).
10. Birch, J. *et al. Congenital and Acquired Color Vision Defects*. (Grune & Stratton, 1979).
11. Köllner H. *Die Störungen des Farbensinnes: ihre klinische Bedeutung und ihre Diagnose*. (S. Karger, 1912).
12. Schefrin, B. E., Shinomori, K. & Werner, J. S. Contributions of neural pathways to age-related losses in chromatic discrimination. *J. Opt. Soc. Am. A* **12,** 1233–1241 (1995).
13. Kremers, J. *The Primate Visual System: A Comparative Approach*. (John Wiley & Sons, Ltd, 2005).
14. Nunn, B. J., Schnapf, J. L. & Baylor, D. A. Spectral sensitivity of single cones in the retina of Macaca fascicularis. *Nature* **309,** 264–266 (1984).
15. Martin, P. R. & Grünert, U. Analysis of the short wavelength-sensitive ('blue') cone mosaic in the primate retina: Comparison of New World and Old World monkeys. *J. Comp. Neurol.* **406,** 1–14 (1999).
16. De Valois, R. L., Morgan, H. C., Polson, M. C., Mead, W. R. & Hull, E. M. Psychophysical studies of monkey vision-I. Macaque luminosity and color vision tests. *Vision Res.* **14,** 53–67 (1974).
17. De Valois, R. L., Morgan, H. & Snodderly, D. M. Psychophysical studies of monkey Vision-III. Spatial luminance contrast sensitivity tests of macaque and human observers. *Vision Res.* **14,** 75–81 (1974).
18. Julien, S. & Schraermeyer, U. Lipofuscin can be eliminated from the retinal pigment epithelium of monkeys. *Neurobiol. Aging* **33,** 2390–2397 (2012).
19. Pallitto, P. *et al.* A2E and lipofuscin distributions in macaque retinal pigment epithelium are similar to human. *Photochem. Photobiol. Sci.* **14,** 1888–1895 (2015).
20. Calkins, D. J. Seeing with S cones. *Progress in Retinal and Eye Research* **20,** 255–287 (2001).
21. Curcio, C. A., Sloan, K. R., Kalina, R. E. & Hendrickson, A. E. Human Photoreceptor Topography. *J. Comp. Neurol.* **523,** 497–523 (1990).
22. Reese, B. E. & Keeley, P. W. Design principles and developmental mechanisms underlying retinal mosaics. *Biol. Rev.* **90,** 854–876 (2014).
23. Zlatkova, M. B., Coulter, E. & Anderson, R. S. Short-wavelength acuity: Blue-yellow and achromatic resolution loss with age. *Vision Res.* **43,** 109–115 (2003).
24. Shinomori, K. & Werner, J. S. Aging of human short-wave cone pathways. *Proc. Natl. Acad. Sci. Unites States Am.* **109,** 13422–13427 (2012).
25. Panda-Jonas, S., Jonas, J. B. & Jakobczyk-Zmija, M. Retinal photoreceptor density decreases with age. *Ophthalmology* **102,** 1853–9 (1995).
26. Cunea, A., Powner, M. B. & Jeffery, G. Death by color: Differential cone loss in the aging mouse retina. *Neurobiol. Aging* **35,** 2584–2591 (2014).
27. Wikler, K. C., Williams, R. W. & Rakic, P. Photoreceptor mosaic: Number and distribution of rods and cones in the rhesus monkey retina. *J. Comp. Neurol.* **297,** 499–508 (1990).
28. Curcio, C. A., Medeiros, N. E. & Millican, C. L. Photoreceptor loss in age-related macular degeneration. *Investig. Ophthalmol. Vis. Sci.* **37,** 1236–1249 (1996).
29. Curcio, C. A. Photoreceptor topography in ageing and age-related maculopathy. *Eye (Lond).* **15,** 376–383 (2001).
30. Verriest, G. Further studies on acquired deficiency of color discrimination. *J. Opt. Soc. Am.* **53,** 185–195 (1963).
31. Winkler, B. S. Glycolytic and oxidative metabolism in relation to retinal function. *J. Gen. Physiol.* **77,** 667–92 (1981).
32. Schatz, A. *et al.* Attenuation of S-cone function at high altitude assessed by electroretinography. *Vision Res.* **97,** 59–64 (2014).
33. Hoang, Q. V., Linsenmeier, R. a., Chung, C. K. & Curcio, C. a. Photoreceptor inner segments in monkey and human retina: mitochondrial density, optics, and regional variation. *Vis. Neurosci.* **19,** 395–407 (2002).
34. Nork, T. M., Millecchia, L. L., Strickland, B. D., Linberg, J. V. & Chao, G. M. Selective loss of blue cones and rods in human retinal detachment. *Arch Ophthalmol* **113,** 1066–1073 (1995).
35. Beirne, R. O. *et al.* Severity staging by early features of age-related maculopathy exhibits weak relationships with functional deficits on SWS grating acuity. *Investig. Ophthalmol. Vis. Sci.* **47,** 4624–4631 (2006).

36. Frennesson, C., Nilsson, U. L. & Nilsson, S. E. G. Colour contrast sensitivity in patients with soft drusen, and early stage of ARM. *Doc. Ophthalmol.* **90,** 377–386 (1995).
37. Remky, A. & Elsner, A. E. Blue on yellow perimetry with scanning laser ophthalmoscopy in patients with age related macular disease. *Br. J. Ophthalmol.* **89,** 464–9 (2005).
38. Arjamaa, O., Nikinmaa, M., Salminen, A. & Kaarniranta, K. Regulatory role of HIF-1alpha in the pathogenesis of age-related macular degeneration (AMD). *Ageing Research Reviews* **8,** 349–358 (2009).
39. Kurihara, T. Development and pathological changes of neurovascular unit regulated by hypoxia response in the retina. *Prog. Brain Res.* **225,** 201–211 (2016).
40. Barber, C. B., Dobkin, D. P. & Huhdanpaa, H. The quickhull algorithm for convex hulls. *ACM Trans. Math. Softw.* **22,** 469–483 (1996).
41. Fortune, S. A sweepline algorithm for Voronoi diagrams. *Algorithmica* **2,** 153–174 (1987).

Acknowledgements

We thank Jaimie Hoh Kam, Sandie Holmes and Peter Levick for their technical assistance. This work was supported by grants NIH AG04058, EY026068, EY024239 and BBSRC BB/N000250/1. We thank PHE for provision of valuable/essential tissues.

Author Contributions

G.J. and J.S.W. conceived and designed the experiment; T.W.W., M.B.P., A.L. and G.J. performed the experiments; T.W.W., R.S.J. analysed the data. T.W.W., R.S.J., J.S.W. and G.J. wrote the main manuscript. All authors revised the manuscript.

Additional Information

Competing Interests: The authors declare no competing financial interests.

How to cite this article: Weinrich, T. W. *et al.* No evidence for loss of short-wavelength sensitive cone photoreceptors in normal ageing of the primate retina. *Sci. Rep.* **7**, 46346; doi: 10.1038/srep46346 (2017).

Publisher's note: Springer Nature remains neutral with regard to jurisdictional claims in published maps and institutional affiliations.

Mitochondrial absorption of short wavelength light drives primate blue retinal cones into glycolysis and old age

Jaimie Hoh Kam[1], Tobias W. Weinrich[1], Harpreet Sangha[1], Michael B. Powner[2], Robert Fosbury[1, 3] and Glen Jeffery[1]

[1]University College London, Institute of Ophthalmology, [2]City, University of London, Centre for Applied Vision Research and [3]European Southern Observatory, Munich, Germany.

Correspondence to
Glen Jeffery
Institute of Ophthalmology
University College London
11-43 Bath St
London EC1V 9EL, UK
Phone +44 2076086837
Email g.jeffery@ucl.ac.uk

Abstract

Photoreceptors have high energy demands and densely packed mitochondria through which light passes before phototransduction. Old world primates including humans have 3 cone photoreceptor types mediating colour vision with short (S blue), medium (M green) and long (L red) wavelength sensitivities. But S-cones are enigmatic. They comprise <10% of the total cone population and are not present in the human fovea, their responses saturate early and they are susceptible in ageing and disease, especially diabetes. Here we show that primate S-cones actually have few mitochondria and are fueled by glycolysis, not mitochondrial respiration. Glycolysis has a limited ability to sustain activity, explaining early S-cone saturation.

Mitochondria act as optical filters showing reduced light transmission at 400-450nm where S-cones are most sensitive (420nm). This absorbance is likely to arise in a mitochondrial porphyrin that absorbs strongly in the Soret band. Hence, reducing mitochondria will improve S-cone sensitivity but result in increased glycolysis as an alternative energy source, increasing diabetic vulnerability due to restricted glucose access. Further, glycolysis carries a price resulting in premature functional decline as seen in aged S-cones. Soret band absorption will also impact on mitochondrial rich M and L cones by reducing sensitivity at the lower end of their spectral sensitivity range resulting in increased differentiation from S-cone responses.

There is little of biological advantage in human/primate environments that is blue, and much in the eye that filters shorter wavelengths. Further, our S-cones are few and relatively frail. They are scarce in most mammals and some have lost them completely. Their value, particularly to a progressively ageing population may be limited.

48 **Introduction**

49 Photoreceptors have the greatest energy demand in the body, mediated by densely packed
50 mitochondria in their inner segments (IS) (Nakajima *et al.*). Trichromatic vision in old world primates
51 is achieved via signaling from three cone types with different spectral sensitivities: to blue (420nm),
52 green (530nm) and red (560nm) light (Knowles *et al.*, 1977); (Mollon, 1982). However, relatively rare
53 S-cones exhibit morphologically distinct IS (Curcio *et al.*, 1991). Also, their psychophysical responses
54 saturate early, similar to rod photoreceptors rather than other cones (Mollon & Polden, 1977).
55 Although their number does not decline with age (Weinrich *et al.*, 2017), they are functionally
56 vulnerable (Greenstein *et al.*, 1989). We ask if these unique characteristics result from fundamental
57 metabolic differences. Metabolic activity is driven by ATP generated either via mitochondrial
58 respiration or glycolysis. The separate pathways can be identified by either pyruvate dehydrogenase to
59 mark mitochondrial oxidative phosphorylation or lactate dehydrogenase marking glycolysis (Fig.1A).
60 The mitochondrial route of production is more efficient while glycolysis provides rapid ATP delivery,
61 but only briefly. However, glycolysis can be toxic (Xing *et al.*, 2013). We use these markers to
62 determine which are employed by primate S-cones and if this differs from other cone types and why
63 this should be.
64

65 **Materials and methods**

66 Ocular tissues were acquired from *Macaca fasciularis* from an established colony under U.K. Home
67 Office regulation and maintained by Public Health England. Eyes were retrieved at death following
68 termination after sedation with ketamine and overdose of intravenous sodium pentobarbital. The
69 primary purpose of animal usage was different from the aims of this study and eyes were only
70 retrieved after death. The eyes were removed rapidly were fixed in 4% paraformaldehyde in 0.1M
71 phosphate buffered saline (PBS) for several days and then transferred to phosphate buffer saline
72 containing 0.025% sodium azide. Samples were taken from 5 young animals between 4-5 years and 5
73 old primates 14-15 years. Primates in this colony rarely lived beyond 18 years.
74
75 To determine if patterns of S-cone labeling in primates were conserved in other mammalian retinae
76 mice were also used in this study. Four month old C57 BL/6 were housed in standard conditions.
77 These were sacrificed (N=4) by cervical dislocation and eye orientation marked by a small burn mark
78 made to the dorsal aspect of the eye using a hot 18-gauge needle. The eyes were enucleated and fixed
79 in 4% paraformaldehyde in PBS for 1 hour and cryoprotected in 30% sucrose overnight and embedded
80 in OCT. 10 μm sections were cut and thaw-mounted onto charged slides. Slides were immunostained
81 with a rabbit polyclonal anti-pyruvate dehydrogenase E2 from Abcam (ab66511, 1:200) and a goat
82 polyclonal anti-OPN1SW (N-20) from Santa Cruz biotechnology, UK (sc-14363, 1:1000).
83
84 **Immunohistochemistry.** Primate eyes were fixed in 4% paraformaldehyde in PBS. After a few days,
85 eyes were washed in PBS, dissected and the anterior tissues removed. A horizontal strip containing the
86 retina, RPE and choroid was removed running from the temporal periphery, through the macular and
87 fovea into the nasal retina. These were cryoprotected in 30% sucrose and then embedded in OCT
88 (Optimal Cutting Temperature Tissue-Tek compound, Leica). Frozen sections were cut at 10 μm and

89 immunostained with markers of mitochondrial metabolism with primary antibodies: Rabbit
90 monoclonal anti-Lactate Dehydrogenase from Abcam, UK (ab134187, 1:200); Mouse monoclonal
91 anti-Pyruvate Dehydogenase E1β subunit from Abcam, UK (ab110331, 1:200); a rabbit polyclonal
92 anti-pyruvate dehydrogenase E2 from Novus biologicals (NBP2-34065), a goat polyclonal anti
93 OPN1SW (N-20 from Santa Cruz Biotechnology, UK) (sc-14363, 1:1000). A rabbit polyclonal voltage
94 dependent anion channel 1 marker from Novartis Biologicals (NBP1-45921). Secondary antibodies in
95 the double labelling experiment were fluorescent conjugate Alexa Fluor 568 (1:2000, Invitrogen, UK)
96 or 488 (1:2000, Invitrogen, UK). The nuclei were counterstained with a nuclear marker 4', 6-diamino-
97 2-phenylindole (DAPI) (Sigma-Aldrich, UK). Slides were mounted in Vectashield (Vector
98 Laboratories, UK) and coverslipped. Sections were viewed and images captured using an Epi-
99 fluorescence and bright-field microscope (Olympus BX50F4, Olympus, UK) and a Nikon DXM1200
100 (Nikon, UK) digital camera.
101
102 **Resin embedded histology.** 5 eyes from young and 5 eyes from old primates were dissected and a
103 horizontal strip of the neural retina was removed running from the periphery through the centre was
104 used as flatmount and processed for immunohistochemistry. After several PBS washes, the retinal
105 tissues were blocked and permeabilised with 5% Normal Donkey serum in 3% (v/v) Triton X-100 in
106 PBS for 2h. Samples were incubated overnight in a goat polyclonal antibody to OPN1SW (N-20 from
107 Santa Cruz Biotechnology, UK) (sc-14363, 1:1000) made in 1% Normal Donkey Serum in 3% Triton
108 X-100 in 0.1M PBS. After primary antibody incubation, samples were washed repeatedly in PBS and
109 incubated in a biotinylated anti goat secondary antibody for 2 hours at room temperature. After the
110 secondary antibody incubation, the flatmounts were washed several times and incubated in a ready to
111 use horseradish peroxidase Streptavidin solution (VECTOR Laboratories, UK) for 30 minutes,
112 followed by a peroxidase substrate solution, 3,3-diaminobenzidine (DAB) for 5 minutes. The

flatmounts were afterwards processed for resin embedded plastic and were therefore fixed with 2% paraformaldehyde and 2% glutaldehyde in PBS for 24h, followed by repeated PBS washing and then were post fixed in 1% OsO4 in 0.1M PBS for 2h. They were then thoroughly washed in distilled water and dehydrated through a graded series of ethanol. Then infiltrated, polymerised and embedded in Technovit 7100 historesin (Taab Laboratories equipment, UK). Resin sections were cut at 2.5µm, histologically stained with Sudan Black B and mounted in Depex and coverslipped.

Statistical analysis. For comparison between the two groups, a Mann-Whitney U test was used. Data were analysed using GraphPad Prism version 5.0 for windows (GraphPad, San Diego, USA).

Mitochondrial absorption modeling. Measurements of the optical absorbance of a suspension of mitochondria taken from guinea pig livers were extracted from the transmittance data shown in Fig. 3 of Nakajima et al.(Nakajima *et al.*, 1993) After measuring their 'Reduction' and 'Oxidation' transmission curves, central absorbance values and bandwidths (FWHM) were derived for the selective absorption curves centred at 418nm by interpolating a continuum across the band from both their reduced and oxidised measurements. This results in central absorbance values for the band alone of 0.061 and 0.055 respectively, yielding an average of 0.06 with an estimated error of ~0.01. This calculation assumes the difference between the reduced and oxidized Nakajuma et al.(Nakajima *et al.*, 1993) transmission curves is entirely due to the continuous extinction and not to the Soret band absorption.

This average value was then scaled for the ratios of transmission pathlength and of the mitochondrial volume density values from the Nakajuma et al.(Nakajima *et al.*, 1993) experiment and a schematic cone inner segment model consisting of a cylinder of diameter d µm and length l µm.

137 To produce Figure 4, we assumed d = 5 and l = 15 and that the IS of M/L-cones have a mitochondrial
138 filling factor of unity for the M/L cones and 0.35 for the S cone. The transmission curves are than
139 calculated using a Lorentzian absorbance profile having a FWHM of 45nm.
140
141
142

143 **Results**

144 Retinae from the old world primate *Macaca fascicularis* were immunostained for pyruvate or lactate
145 dehydrogenase (PDH/LDH) and S-opsin. Pyruvate dehydrogenase complex has three enzymes E1, E2
146 and E3 converting pyruvate into acetyl-CoA. PDHE1β is the rate limiting factor for the pyruvate
147 dehydrogenase complex as it catalyses the reaction of PDHE2. Cones were distinguished
148 morphologically by their clear cone shaped IS. Cones were positive for both PDHE1β and PDHE2
149 with labelling confined to the mitochondrial containing IS. Staining for the two PDHE markers was
150 very similar in cones across the retina. However, S-cones were consistently negative for both labels
151 (Fig. 1B and C). All cones, irrespective of type, were LDH positive present throughout inner and outer
152 segments (Fig. 1D). Hence, S-cones do not appear to employ mitochondria for ATP production but
153 rely on glycolysis.
154
155 Mitochondria were revealed by staining with osmium and Sudan Black. Mitochondrial density was
156 consistently lower in S-cones than other cone types. Fig. 2A shows an S-cone (arrow head) and
157 adjacent, two non-S-cones. Also in S-cones, mitochondria never extended to the tip of the IS as found
158 in other photoreceptors.
159
160 Sections were also stained for S-opsin and a voltage dependent anion channel marker (VDAC) present
161 in outer mitochondrial membranes. VDAC mediates ATP and pyruvate transport across mitochondrial
162 membranes and is linked with metabolic activity and regulates Ca^{2+} transport across the membrane
163 (Dubey *et al.*, 2016). Fig. 2B shows VDAC label in red and the S-opsin in green. VDAC profiles are
164 confined to outer IS regions reflecting patterns seen in Fig. 1B. However, in S-cones there is markedly
165 reduced label. The area occupied by VDAC labelled profiles was measured in S-opsin cones and
166 others. In S-opsin cells this was significantly lower ($P<0.01$), being reduced by approximately 65%

across the population (Fig. 2C). Reduced VDAC labelling in S-cones is consistent with the absence of pyruvate dehydrogenase in these cells (Fig.1B and C). VDAC channels are also associated with the anti-apoptotic proteins Bcl2 and BclxL. These proteins maintain an open conformation of the channel. In doing so, they promote cell survival (Gottlob *et al.*, 2001). It is assumed that increased VDAC expression promotes cell death, while reduced expression is associated with cell survival (Dubey *et al.*, 2016). The reduced VDAC levels are consistent with S-cones survival with age in primates (Weinrich *et al.*, 2017). Hence, S-opsin cones have relatively few mitochondria and do not express pyruvate dehydrogenase, which is a key marker of mitochondrial respiration.

If primate S-cones are fueled by glycolysis, is this a conserved feature of vertebrate photoreceptor function? Hence, we label both mouse and frog retinae for S-opsin and pyruvate or lactate dehydrogenase. Mice have only two cone types, S and combined M/L. They separate these with most S-cones located in the ventral retina, and most M/L-cones in the dorsal retina (Bowmaker, 2008). In mouse, staining for pyruvate dehydrogenase was much greater in dorsal than ventral retina, consistent with the S-cone population being less reliant on mitochondrial function. Staining for lactate dehydrogenase was similar across the retina (Fig. 3A & B). Sections from frog (*Xenopus Laevis*) S-opsin cells were distributed throughout the retina. However, S-cones were mixed with some positive for pyruvate dehydrogenase and others negative (Fig. 3C). Again, staining for lactate dehydrogenase was relatively uniform. Hence, fueling of S-cone function may be different between mammals and amphibians.

As glycolytically fueled activity cannot be sustained, data from primates apparently explains why human S-cone psychophysical responses saturate early (Mollon & Polden, 1977). These data also

190 explain selective S-cone functional decline in diabetes (Greenstein *et al.*, 1989), because here cells
191 have restricted access to glucose on which glycolysis depends.
192
193 Glycolytic reliance is toxic due to production of methylglyoxal, termed “the dark side of glycolysis”.
194 Methylglyoxal mediates glycation of proteins forming advanced glycation end products (AGEs) that
195 increase endoplasmic reticulum stress driving neuronal degeneration and/or reduced function (Xing *et*
196 *al.*, 2013). Such processes may underpin the selective early decline in aged human S-cone function. As
197 primate S-cones are not lost with age (Weinrich *et al.*, 2017), their functional decline is likely due to
198 their distinct metabolism.
199
200 A driver for S-cone glycolysis is likely related to the reduced mitochondrial content in their IS. It had
201 previously been noted by Curcio et al. (Curcio *et al.*, 1991) that human S-cone IS were
202 morphologically different from those of M- and L-cones. Given the very high packing density of
203 mitochondria in M- and L-cones it is not surprising that reducing mitochondrial content by >60%
204 influences their morphology. However, in spite of this, Curcio et al. (Curcio *et al.*, 1991) do not
205 comment on the absence of mitochondria in the electron microscopic image of the S-cone IS compared
206 with that of the M/L cone they present (their Fig. 3).
207
208
209

Discussion

Why should S-cones have reduced mitochondrial density and employ glycolysis as their energy source? An explanation is suggested by the reverse orientation of photoreceptors in the vertebrate retina which demands that incoming light has to traverse the mitochondrion-rich IS before detection. Mitochondria have a marked drop in spectral transmittance at approximately 400–450nm that spans the peak S-cone sensitivity at 420nm (Bowmaker *et al.*, 1991; Nakajima *et al.*, 1993). Bowmaker et al. (Bowmaker *et al.*, 1991) noted the presence of a photostable pigment in the cones of the tree shrew, *Tupaia glis,* which might be associated with a porphyrin Soret band (Brunet *et al.*, 2012). They show an absorbance spectrum with a peak at 418nm from a cone IS transverse spectral measurement yielding an absolute peak absorbance of 0.02. They also suggest that this could be associated with cytochrome c, part of the final stage of the electron transport chain in mitochondrial ATP production. This identification is supported by the extensive work on light-mitochondrion interactions by Karu and collaborators (Karu, 1999).

Nakajima et al. (Nakajima *et al.*, 1993) measured the spectral absorbance of a known column density of suspended mitochondria extracted from guinea pig livers. Their transmission spectra showed a generally increasing extinction, extending into the blue, on which was superposed an absorption band with a width (FWHM) of about 45nm and centred at 418nm. This shows a close spectral similarity to the pigment measured by Bowmaker et al. (Bowmaker *et al.*, 1993).

By isolating this band from the associated continuum extinction, we have scaled the Nakajima et al. (Nakajima *et al.*, 1993) absorbance result to the IS dimensions and mitochondrial content of primate cones. Note that the strength of the continuum extinction depends strongly on the redox state of the mitochondria while the band absorption remains constant. The result is expressed in Fig. 4, which shows the resulting effect on the transmission of light in a longitudinal direction through the S- and the

M/L- cones. We represent the IS as a cylinder with a diameter of 5µm and a length of 15µm, maximally filled with mitochondria representing the M/L-cones and a reduced population (by 65%) for the S-cones. Whilst only an estimate of the magnitude of the potential filtering effect: a loss of 35% in blue sensitivity for a full mitochondrial population and only 15% for the reduced population does provide a quantitatively feasible explanation for the special behavior of the S-cones.

If mitochondria spectrally filter it should be possible to identify psychophysical irregularities in spectral sensitivity curves of M- and L-cones in the region of the Soret band because of the high density of mitochondria in these cells. Both M- and L-cone sensitivity curves are asymmetric and have reduced sensitivity between 420–450nm that may be due to porphyrin filtering (Stockman & Sharpe, 1998). This would enhance discrimination between M/L- and S-cone sensitivities.

There is a wider evolutionary context to mitochondrial optical filtering in cone IS. In birds, reptiles and amphibians and some fish, the cone IS contains large oil droplets with different chromatic properties that act as lenses channeling and spectrally filtering light before absorption by outer segment opsins (Walls, 1942; Vorobyev, 2003; Kram *et al.*, 2010; Stavenga & Wilts, 2014; Wilby & Roberts, 2017). Mitochondria in front of the droplet may act to focus light onto the droplet surface (Wilby & Roberts, 2017). Droplets are absent in mammals with the exception of some marsupials where they are uncoloured (Walls, 1942). Our data indicate that the inner segment remains a region of optical filtering across many species and its presence in the light path provides one advantage in the transition from a compound eye to the inverted retina found in vertebrates. The price paid for reducing mitochondria is increased reliance on glycolysis with its inherent problems from an increased pace of ageing (Xing *et al.*, 2013). However, throughout the vast majority of human evolution, lifespan was probably <40 years, which is an age prior to significant human S cone decline (Werner, 2016). Hence, adoption of

glycolysis would have carried little cost. Only with recent expansion in Western lifespan do its damaging consequences become apparent.

Primate S-cones remain enigmatic. Our data explain some of their unique characteristics but not their evolution. Mammalian cones are different from those in birds, fish and amphibians and have been subject to different evolutionary drivers. The evolution of short wavelength vision in fish and amphibians was driven by the aquatic light environment where shorter wavelengths provide greater visual penetrance (Bowmaker, 2008). But a rational for short wavelength sensitivity is harder to discern in mammals where there is little of significance in the environment that is blue. It is possible that, because of this, primates are losing their S-cones, which may explain their relatively low number here and in other mammals (Calkins, 2001; Bowmaker, 2008). A reason for this absence may be because chromatic aberration at shorter wavelengths will increase central retinal blur that may be important in human vision due to our attention to detail, particularly at short distances.

S-cones are labile compared to M- or L-cones that again mark them out as distinct. All cetaceans have lost their S-cones (Peichl *et al.*, 2001). While there is a rare human condition termed enhanced S-cone syndrome (Haider *et al.*, 2000) where S-cone function is elevated and S-cone number may be >10 times greater than normal (Ripamonti *et al.*, 2014). During development, S-cones are the first to express opsin and many cells that subsequently express L- or M-opsin transiently express S-opsin (Cornish *et al.*, 2004). These features along with those described here mark S-cones out as distinct as and potentially more plastic than other photoreceptors.

279 **Author contributions.** JHK, TWW and GJ conceived of the experiment. Experiments were performed
280 by, JHK, TWW, MBP, HS and RF. Data analysis was undertaken by JHK, TWW, HS, and RF. All
281 authors wrote and revised the manuscript.
282
283 **Acknowledgments.** The research was funded by the BBSRC (BB/N000250/1). We thank Public
284 Health England for the supply of tissue used in this study and S. Holmes for her technical assistance.
285
286 **Author information.** Reprints and permissions, information is available at www.nature.com/reprints.
287 All authors declare that they have no competing interest. Correspondence and requests for materials
288 should be addressed to g.jeffery@ucl.ac.uk
289
290
291
292
293

294 **References**

295 BOWMAKER, J.K. (2008). Evolution of vertebrate visual pigments. *Vision Res* **48,** 2022-2041.
296
297 BOWMAKER, J.K., ASTELL, S., HUNT, D.M. & MOLLON, J.D. (1991). Photosensitive and photostable
298 pigments in the retinae of Old World monkeys. *J Exp Biol* **156,** 1-19.
299
300 BOWMAKER, J.K., KOVACH, J.K., WHITMORE, A.V. & LOEW, E.R. (1993). Visual pigments and oil
301 droplets in genetically manipulated and carotenoid deprived quail: a microspectrophotometric
302 study. *Vision Res* **33,** 571-578.
303
304 BRUNET, C., ANTOINE, R., LEMOINE, J. & DUGOURD, P. (2012). Soret Band of the Gas-Phase Ferri-
305 Cytochrome c. *J Phys Chem Lett* **3,** 698-702.
306
307 CALKINS, D.J. (2001). Seeing with S cones. *Prog Retin Eye Res* **20,** 255-287.
308
309 CORNISH, E.E., XIAO, M., YANG, Z., PROVIS, J.M. & HENDRICKSON, A.E. (2004). The role of opsin
310 expression and apoptosis in determination of cone types in human retina. *Exp Eye Res* **78,**
311 1143-1154.
312
313 CURCIO, C.A., ALLEN, K.A., SLOAN, K.R., LEREA, C.L., HURLEY, J.B., KLOCK, I.B. & MILAM, A.H.
314 (1991). Distribution and morphology of human cone photoreceptors stained with anti-blue
315 opsin. *J Comp Neurol* **312,** 610-624.
316
317 DARTNALL, H.J., BOWMAKER, J.K. & MOLLON, J.D. (1983). Human visual pigments:
318 microspectrophotometric results from the eyes of seven persons. *Proc R Soc Lond B Biol Sci*
319 **220,** 115-130.
320
321 DUBEY, A.K., GODBOLE, A. & MATHEW, M.K. (2016). Regulation of VDAC trafficking modulates cell
322 death. *Cell Death Discov* **2,** 16085.
323
324 GOTTLOB, K., MAJEWSKI, N., KENNEDY, S., KANDEL, E., ROBEY, R.B. & HAY, N. (2001). Inhibition of
325 early apoptotic events by Akt/PKB is dependent on the first committed step of glycolysis and
326 mitochondrial hexokinase. *Genes Dev* **15,** 1406-1418.
327
328 GREENSTEIN, V.C., HOOD, D.C., RITCH, R., STEINBERGER, D. & CARR, R.E. (1989). S (blue) cone
329 pathway vulnerability in retinitis pigmentosa, diabetes and glaucoma. *Invest Ophthalmol Vis*
330 *Sci* **30,** 1732-1737.
331
332 HAIDER, N.B., JACOBSON, S.G., CIDECIYAN, A.V., SWIDERSKI, R., STREB, L.M., SEARBY, C., BECK, G.,
333 HOCKEY, R., HANNA, D.B., GORMAN, S., DUHL, D., CARMI, R., BENNETT, J., WELEBER, R.G.,
334 FISHMAN, G.A., WRIGHT, A.F., STONE, E.M. & SHEFFIELD, V.C. (2000). Mutation of a nuclear
335 receptor gene, NR2E3, causes enhanced S cone syndrome, a disorder of retinal cell fate. *Nat*
336 *Genet* **24,** 127-131.
337
338 KARU, T. (1999). Primary and secondary mechanisms of action of visible to near-IR radiation on cells.
339 *J Photochem Photobiol B* **49,** 1-17.

340

KNOWLES, A., DAVSON, H. & DARTNALL, H.J.A. (1977). *The Photobiology of Vision*: Academic Press.

KRAM, Y.A., MANTEY, S. & CORBO, J.C. (2010). Avian cone photoreceptors tile the retina as five independent, self-organizing mosaics. *PLoS One* **5,** e8992.

MOLLON, J.D. (1982). Color vision. *Annu Rev Psychol* **33,** 41-85.

MOLLON, J.D. & POLDEN, P.G. (1977). Saturation of a retinal cone mechanism. *Nature* **265,** 243-246.

NAKAJIMA, Y., IWAKABE, H., AKAZAWA, C., NAWA, H., SHIGEMOTO, R., MIZUNO, N. & NAKANISHI, S. (1993). Molecular characterization of a novel retinal metabotropic glutamate receptor mGluR6 with a high agonist selectivity for L-2-amino-4-phosphonobutyrate. *J Biol Chem* **268,** 11868-11873.

PEICHL, L., BEHRMANN, G. & KROGER, R.H. (2001). For whales and seals the ocean is not blue: a visual pigment loss in marine mammals. *Eur J Neurosci* **13,** 1520-1528.

RIPAMONTI, C., ABOSHIHA, J., HENNING, G.B., SERGOUNIOTIS, P.I., MICHAELIDES, M., MOORE, A.T., WEBSTER, A.R. & STOCKMAN, A. (2014). Vision in observers with enhanced S-cone syndrome: an excess of s-cones but connected mainly to conventional s-cone pathways. *Invest Ophthalmol Vis Sci* **55,** 963-976.

STAVENGA, D.G. & WILTS, B.D. (2014). Oil droplets of bird eyes: microlenses acting as spectral filters. *Philos Trans R Soc Lond B Biol Sci* **369,** 20130041.

STOCKMAN, A. & SHARPE, L.T. (1998). Human cone spectral sensitivities: a progress report. *Vision Res* **38,** 3193-3206.

VOROBYEV, M. (2003). Coloured oil droplets enhance colour discrimination. *Proc Biol Sci* **270,** 1255-1261.

WALLS, G.L. (1942). *The vertebrate eye and its adaptive radiation*. New York: Hafner Publishing Company

WEINRICH, T.W., POWNER, M.B., LYNCH, A., JONNAL, R.S., WERNER, J.S. & JEFFERY, G. (2017). No evidence for loss of short-wavelength sensitive cone photoreceptors in normal ageing of the primate retina. *Sci Rep* **7,** 46346.

WERNER, J.S. (2016). The Verriest Lecture: Short-wave-sensitive cone pathways across the life span. *J Opt Soc Am A Opt Image Sci Vis* **33,** A104-122.

WILBY, D. & ROBERTS, N.W. (2017). Optical influence of oil droplets on cone photoreceptor sensitivity. *J Exp Biol* **220,** 1997-2004.

XING, Y., ZHANG, X., SONG, X., LV, Z., HOU, L. & LI, F. (2013). Injury of cortical neurons is caused by the advanced glycation end products-mediated pathway. *Neural Regen Res* **8,** 909-915.

389 **Figures**

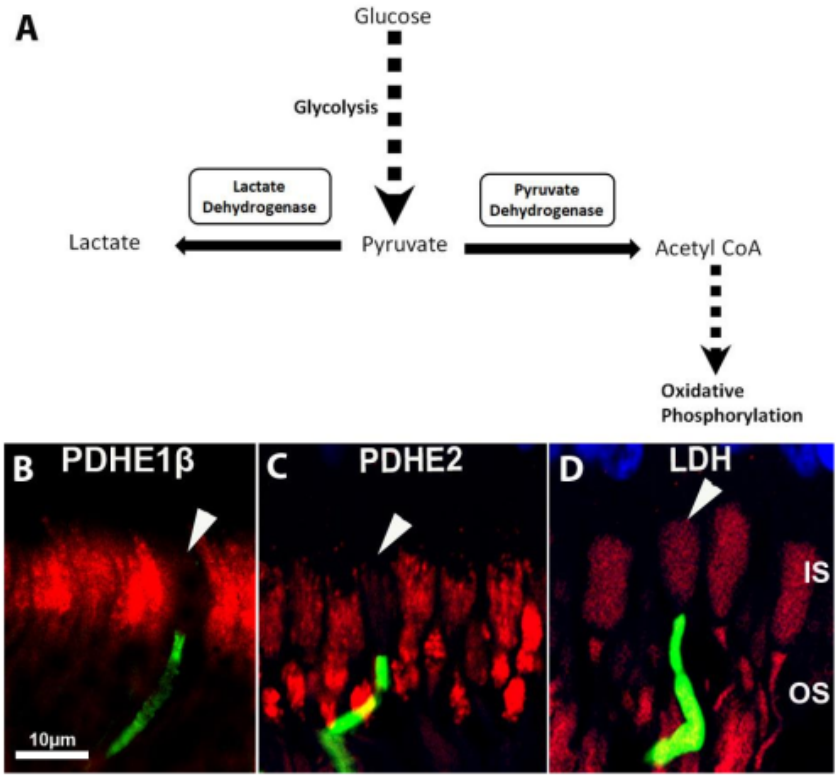

390
391

392 **Figure 1**. **A**. Schematic representation of pathways for ATP production via either pyruvate
393 dehydrogenase leading to mitochondrial oxidative phosphorylation or via lactate dehydrogenase as part
394 of glycolysis. **B-D**. We use pyruvate dehydrogenase (PDH) and lactate dehydrogenase (LDH) markers
395 to define these pathways labelling central primate retina. Labelling for PDH is subdivided into
396 PDHE1β (B) and PDHE2 (C). PDHE1β is the rate limiting factor for the pyruvate dehydrogenase
397 complex as it catalyses the reaction of PDHE2. PDH is in red in B and C. S-cones are labeled in green
398 and marked with a white arrow head. PDH label is confined to mitochondrial containing inner
399 segments (IS). However, the S-cones are negative for both PDH forms. D is stained for LDH. Here
400 label is present in inner (IS) and outer segments (OS). All photoreceptors, including S-cones are LDH
401 positive. Blue staining to the top is the outer nuclear layer.

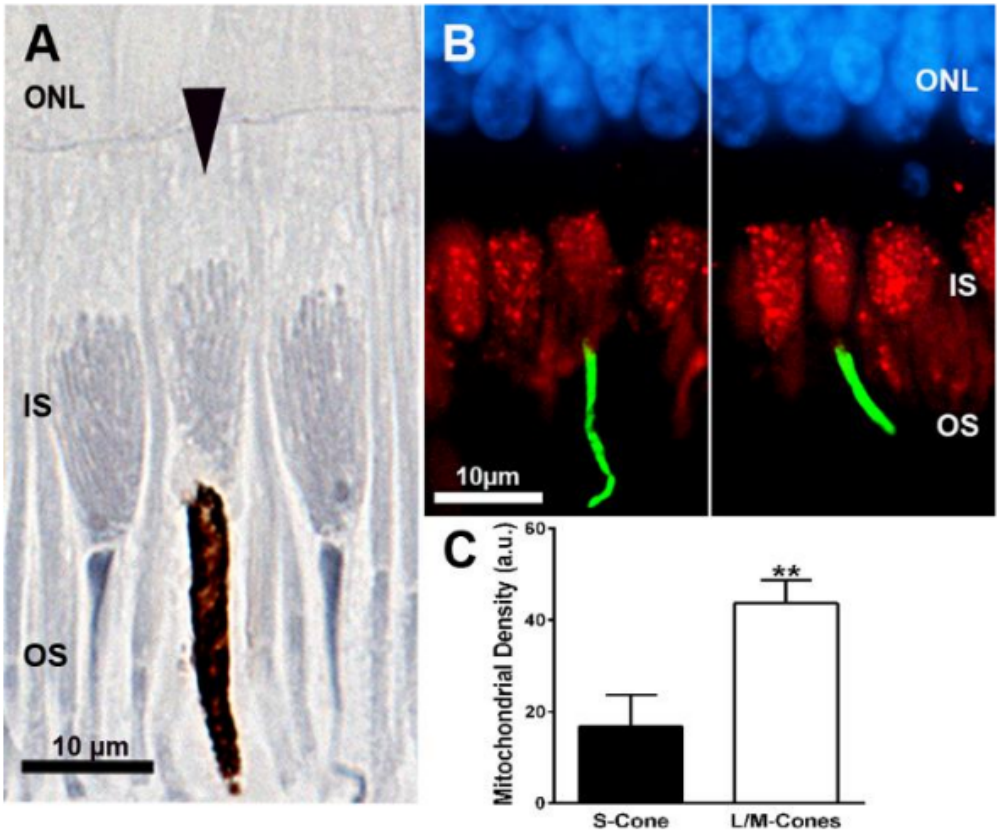

Figure 2. Cone inner segments (IS) where mitochondria have been labelled with two separate methods along with S-opsin. A. Sections stained with osmium and Sudan Black. Here mitochondria are seen as elongated structures within the IS oriented towards the OS. The central cone marked with an arrow head has an S-opsin positive OS. In this cell mitochondrial density is relatively low and mitochondria do not extend fully to the OS. B. Two images from the central retina stained with a voltage dependent anion channel (VDAC) present in mitochondria (red) and S-opsin (green). Photoreceptor nuclei in the outer nuclear layer (ONL) are stained in blue. C. The area of VDAC label in the cones has been measured in S-opsin positive and S-opsin negative cells. There is >60% significant reduction in the area occupied by VDAC label in S-cones compared to other cone types.

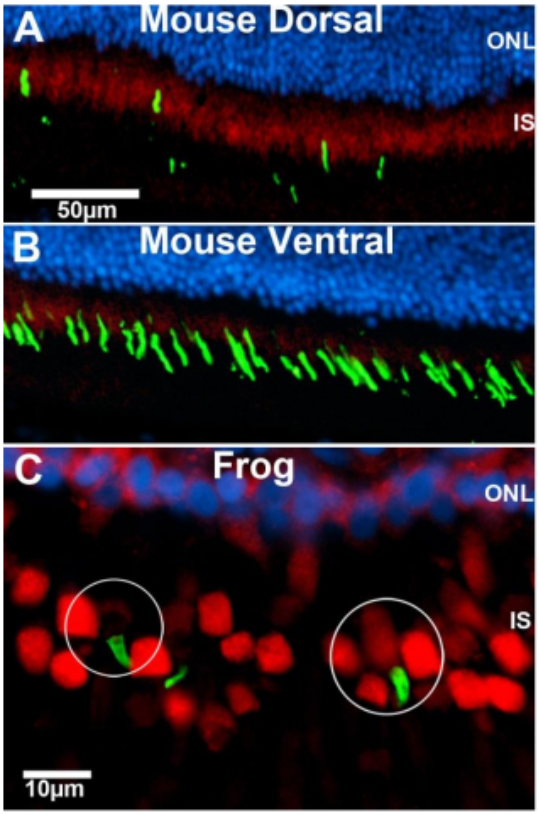

Figure 3. Staining for pyruvate dehydrogenase (red) and S-opsin (green) in mouse (upper panels) and frog (lower panel). In rodents S-cones are largely confined ventrally. In this region of the retina there was much less pyruvate dehydrogenase than in dorsal regions consistent with the notion that these cones may not be using mitochondrial respiration similar to primates. However, in frogs S-cones were identified that were both positive and negative for pyruvate dehydrogenase. An example of each is circled.

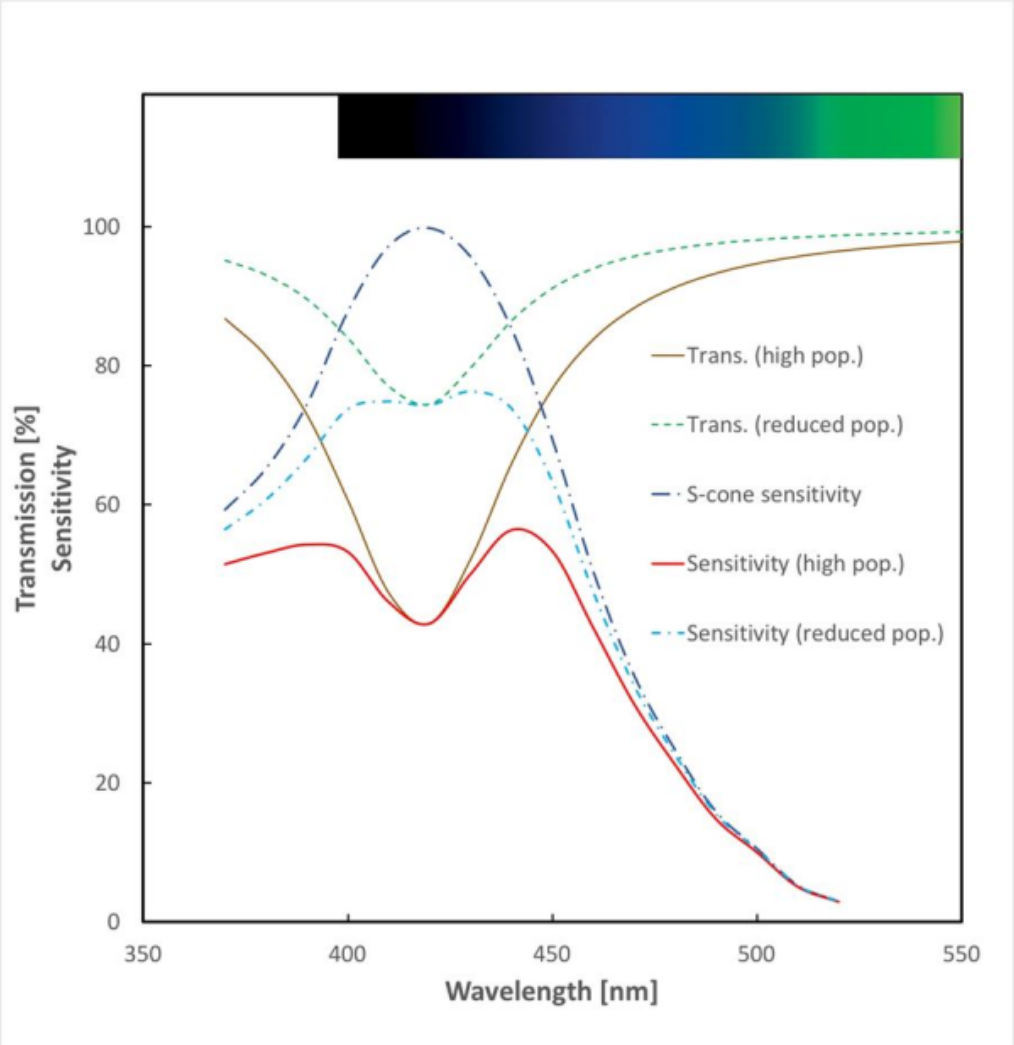

Figure 4 Schematic representation of the effect on S-cone response to Soret band absorption by the population of mitochondria in the inner segment of the cell. This is based on our scaling of the mitochondrial absorbance measured by Nakajima et al.[8] and our own estimates of mitochondrial numbers in primate S- and M/L-cones. The solid lines (brown and red) show the response as it would be if the S-cones had the same high complement of mitochondria seen in the M- and L-cones. The dashed lines (green and blue) show the higher response resulting from the reduced mitochondrial number seen in the S-cone cells. Integrals (between 370 and 470nm) of the absorbed Dartnall et al. (Dartnall *et al.*, 1983) S-cone sensitivity curve with these two populations show a sensitivity loss of

35% with the high M/L cone population which is reduced to 15% loss with the reduced S-cone numbers.

References

1. Guarente, L. & Kenyon, C. Genetic pathways that regulate ageing in model organisms. *Nature* **408,** 255–262 (2000).
2. Kenyon, C. J. The genetics of ageing. *Nature* **464,** 504–512 (2010).
3. López-Otín, C., Blasco, M. A., Partridge, L., Serrano, M. & Kroemer, G. The Hallmarks of Aging. *Cell* **153,** 1194–1217 (2013).
4. Gargano, J., Martin, I., Bhandari, P. & Grotewiel, M. Rapid iterative negative geotaxis (RING): a new method for assessing age-related locomotor decline in. *Exp. Gerontol.* **40,** 386–395 (2005).
5. Grotewiel, M. S., Martin, I., Bhandari, P. & Cook-Wiens, E. Functional senescence in Drosophila melanogaster. *Ageing Research Reviews* **4,** 372–397 (2005).
6. Iliadi, K. G., Knight, D. & Boulianne, G. L. Healthy Aging – Insights from Drosophila. *Front. Physiol.* **3,** (2012).
7. Tamura, T. *et al.* Aging Specifically Impairs amnesiac-Dependent Memory in Drosophila. *Neuron* **40,** 1003–1011 (2003).
8. Landis, G., Shen, J. & Tower, J. Gene expression changes in response to aging compared to heat stress, oxidative stress and ionizing radiation in Drosophila melanogaster. *Aging (Albany. NY).* **4,** 768–789 (2012).
9. Weismann, A. *Über die Dauer des Lebens*. (Fischer, 1882).
10. Rubner, M. *Das Problem der Lebensdauer und seine Beziehungen zu wachstum und ernährung*. (Oldenbourg, 1908).
11. Bjorksten, J. The crosslinkage theory of aging. *J. Am. Geriatr. Soc.* **16,** 408–27 (1968).
12. Gerschman, R., Gilbert, D. L., Nye, S. W., Dwyer, P. & Fenn, W. O. Oxygen poisoning and x-irradiation: a mechanism in common. *Science* **119,** 623–6 (1954).
13. Harman, D. Aging: A Theory Based on Free Radical and Radiation Chemistry. *J. Gerontol.* **11,** 298–300 (1956).
14. Gensler, H. L. & Bernstein, H. DNA damage as the primary cause of aging. *Q. Rev. Biol.* **56,** 279–303 (1981).
15. Harman, D. The aging process. *Proc. Natl. Acad. Sci. U. S. A.* **78,** 7124–7128 (1981).
16. Afanas'ev, I. Signaling and Damaging Functions of Free Radicals in Aging-Free Radical Theory, Hormesis, and TOR. *Aging Dis.* **1,** 75–88 (2010).
17. Gladyshev, V. N. The free radical theory of aging is dead. Long live the damage theory! *Antioxid. Redox Signal.* **20,** 727–31 (2014).

18. Tait, S. W. G. & Green, D. R. Mitochondria and cell signalling. *J. Cell Sci.* **125,** 807–815 (2012).

19. Blake, R. & Trounce, I. A. Mitochondrial dysfunction and complications associated with diabetes. *Biochim. Biophys. Acta - Gen. Subj.* **1840,** 1404–1412 (2014).

20. Reddy, P. H. Abnormal tau, mitochondrial dysfunction, impaired axonal transport of mitochondria, and synaptic deprivation in Alzheimer's disease. *Brain Res.* **1415,** 136–148 (2011).

21. Cho, D.-H., Nakamura, T. & Lipton, S. A. Mitochondrial dynamics in cell death and neurodegeneration. *Cell. Mol. Life Sci.* **67,** 3435–3447 (2010).

22. Bayrhuber, M. *et al.* Structure of the human voltage-dependent anion channel. *Proc. Natl. Acad. Sci.* **105,** 15370–15375 (2008).

23. Palade, G. E. The fine structure of mitochondria. *Anat. Rec.* **114,** 427–51 (1952).

24. Ugalde, C. *et al.* Human mitochondrial complex I assembles through the combination of evolutionary conserved modules: a framework to interpret complex I deficiencies. *Hum. Mol. Genet.* **13,** 2461–2472 (2004).

25. Loschen, G., Flohé, L. & Chance, B. Respiratory chain linked H(2)O(2) production in pigeon heart mitochondria. *FEBS Lett.* **18,** 261–264 (1971).

26. Brand, M. D. The sites and topology of mitochondrial superoxide production. *Exp. Gerontol.* **45,** 466–472 (2010).

27. Kussmaul, L. & Hirst, J. The mechanism of superoxide production by NADH:ubiquinone oxidoreductase (complex I) from bovine heart mitochondria. *Proc. Natl. Acad. Sci.* **103,** 7607–7612 (2006).

28. Murphy, M. P. How mitochondria produce reactive oxygen species. *Biochem. J.* **417,** 1–13 (2009).

29. Sies, H. Strategies of antioxidant defense. *Eur. J. Biochem.* **215,** 213–9 (1993).

30. Ghafourifar, P. & Cadenas, E. Mitochondrial nitric oxide synthase. *Trends Pharmacol. Sci.* **26,** 190–195 (2005).

31. St-Pierre, J. *et al.* Suppression of Reactive Oxygen Species and Neurodegeneration by the PGC-1 Transcriptional Coactivators. *Cell* **127,** 397–408 (2006).

32. Sena, L. A. & Chandel, N. S. Physiological Roles of Mitochondrial Reactive Oxygen Species. *Mol. Cell* **48,** 158–167 (2012).

33. Anderson, S. *et al.* Sequence and organization of the human mitochondrial genome. *Nature* **290,** 457–465 (1981).

34. Gustafsson, C. M., Falkenberg, M. & Larsson, N.-G. Maintenance and Expression of Mammalian Mitochondrial DNA. *Annu. Rev. Biochem.* **85,** 133–160 (2016).

35. Salvioli, S. *et al.* The impact of mitochondrial DNA on human lifespan: A view from studies on centenarians. *Biotechnol. J.* **3,** 740–749 (2008).

36. Santoro, A. *et al.* Mitochondrial DNA involvement in human longevity. *Biochim. Biophys. Acta - Bioenerg.* **1757,** 1388–1399 (2006).

37. Bratic, A. & Larsson, N. G. The role of mitochondria in aging. *Journal of Clinical Investigation* **123,** 951–957 (2013).

38. Hartmann, N. *et al.* Mitochondrial DNA copy number and function decrease with age in the short-lived fish Nothobranchius furzeri. *Aging Cell* **10,** 824–831 (2011).

39. Zabihi Diba, L., Mohaddes Ardebili, S. M., Gharesouran, J. & Houshmand, M. Age-related decrease in mtDNA content as a consequence of mtDNA 4977 bp deletion. *Mitochondrial DNA. Part A, DNA mapping, Seq. Anal.* **27,** 3008–12 (2016).

40. Tatarková, Z. *et al.* Effects of aging on activities of mitochondrial electron transport chain complexes and oxidative damage in rat heart. *Physiol. Res.* **60,** 281–9 (2011).

41. Petrosillo, G., De Benedictis, V., Ruggiero, F. M. & Paradies, G. Decline in cytochrome c oxidase activity in rat-brain mitochondria with aging. Role of peroxidized cardiolipin and beneficial effect of melatonin. *J. Bioenerg. Biomembr.* **45,** 431–40 (2013).

42. Müller-Höcker, J., Schneiderbanger, K., Stefani, F. H. & Kadenbach, B. Progressive loss of cytochrome c oxidase in the human extraocular muscles in ageing--a cytochemical-immunohistochemical study. *Mutat. Res.* **275,** 115–24 (1992).

43. Ren, J.-C., Rebrin, I., Klichko, V., Orr, W. C. & Sohal, R. S. Cytochrome c oxidase loses catalytic activity and structural integrity during the aging process in Drosophila melanogaster. *Biochem. Biophys. Res. Commun.* **401,** 64–8 (2010).

44. Karu, T. Primary and secondary mechanisms of action of visible to near-IR radiation on cells. *Journal of Photochemistry and Photobiology B: Biology* **49,** 1–17 (1999).

45. Karu, T. I., Pyatibrat, L. V., Kolyakov, S. F. & Afanasyeva, N. I. Absorption measurements of a cell monolayer relevant to phototherapy: Reduction of cytochrome c oxidase under near IR radiation. *J. Photochem. Photobiol. B Biol.* **81,** 98–106 (2005).

46. Karu, T. I. Cellular and Molecular Mechanisms of Photobiomodulation (Low-Power Laser Therapy). *IEEE J. Sel. Top. Quantum Electron.* **20,** 143–148 (2014).

47. Turrens, J. F. Mitochondrial formation of reactive oxygen species. *J. Physiol.* **552,** 335–344 (2003).

48. Lucas, S.-M., Rothwell, N. J. & Gibson, R. M. The role of inflammation in CNS injury and disease. *Br. J. Pharmacol.* **147,** S232–S240 (2009).

49. Tufekci, K. U., Meuwissen, R., Genc, S. & Genc, K. Inflammation in Parkinson's disease. *Adv. Protein Chem. Struct. Biol.* **88,** 69–132 (2012).

50. Pérez-Cerdá, F., Sánchez-Gómez, M. V. & Matute, C. The link of inflammation and neurodegeneration in progressive multiple sclerosis. *Mult. Scler.*

Demyelinating Disord. **1,** 9 (2016).

51. Heppner, F. L., Ransohoff, R. M. & Becher, B. Immune attack: the role of inflammation in Alzheimer disease. *Nat. Rev. Neurosci.* **16,** 358–72 (2015).

52. Perez, V. L. & Caspi, R. R. Immune mechanisms in inflammatory and degenerative eye disease. *Trends Immunol.* **36,** 354–363 (2015).

53. Ventura, M. T., Casciaro, M., Gangemi, S. & Buquicchio, R. Immunosenescence in aging: between immune cells depletion and cytokines up-regulation. *Clin. Mol. Allergy* **15,** 21 (2017).

54. Dunston, C. R. & Griffiths, H. R. The effect of ageing on macrophage Toll-like receptor-mediated responses in the fight against pathogens. *Clin. Exp. Immunol.* **161,** 407–416 (2010).

55. Franceschi, C. & Campisi, J. Chronic Inflammation (Inflammaging) and Its Potential Contribution to Age-Associated Diseases. *Journals Gerontol. Ser. A Biol. Sci. Med. Sci.* **69,** S4–S9 (2014).

56. Picca, A. *et al.* Fueling Inflamm-Aging through Mitochondrial Dysfunction: Mechanisms and Molecular Targets. *Int. J. Mol. Sci.* **18,** 933 (2017).

57. van Horssen, J., van Schaik, P. & Witte, M. Inflammation and mitochondrial dysfunction: A vicious circle in neurodegenerative disorders? *Neurosci. Lett.* (2017). doi:10.1016/j.neulet.2017.06.050

58. López-Armada, M. J. *et al.* Mitochondrial activity is modulated by TNFα and IL-1β in normal human chondrocyte cells. *Osteoarthr. Cartil.* **14,** 1011–1022 (2006).

59. Pacher, P., Beckman, J. S. & Liaudet, L. Nitric Oxide and Peroxynitrite in Health and Disease. *Physiol. Rev.* **87,** 315–424 (2007).

60. Schwarze, S. R., Weindruch, R. & Aiken, J. M. Oxidative stress and aging reduce COX I RNA and cytochrome oxidase activity in Drosophila. *Free Radic. Biol. Med.* **25,** 740–747 (1998).

61. Brandt, T. *et al.* Changes of mitochondrial ultrastructure and function during ageing in mice and Drosophila. *Elife* **6,** (2017).

62. Passarino, G., De Rango, F. & Montesanto, A. Human longevity: Genetics or Lifestyle? It takes two to tango. *Immun. Ageing* **13,** 12 (2016).

63. Villa-Cuesta, E., Holmbeck, M. A. & Rand, D. M. Rapamycin increases mitochondrial efficiency by mtDNA-dependent reprogramming of mitochondrial metabolism in Drosophila. *J Cell Sci* **127,** 2282–2290 (2014).

64. van Heemst, D. Insulin, IGF-1 and longevity. *Aging Dis.* **1,** 147–57 (2010).

65. Tosato, M., Zamboni, V., Ferrini, A. & Cesari, M. The aging process and potential interventions to extend life expectancy. *Clinical interventions in aging* (2007). doi:10.1007/s10522-008-9191-1

66. Rojas, J. C. & Gonzalez-Lima, F. Low-level light therapy of the eye and brain. *Eye Brain* **3,** 49–67 (2011).

67. Chung, H. *et al.* The Nuts and Bolts of Low-level Laser (Light) Therapy. *Ann. Biomed. Eng.* **40,** 516–533 (2012).

68. Desmet, K. D. *et al.* Clinical and Experimental Applications of NIR-LED Photobiomodulation. *Photomed. Laser Surg.* **24,** 121–128 (2006).

69. Karu, T. I. Mitochondrial Signaling in Mammalian Cells Activated by Red and Near-IR Radiation. *Photochem. Photobiol.* **84,** 1091–1099 (2008).

70. Belevich, I. *et al.* Initiation of the proton pump of cytochrome c oxidase. *Proc. Natl. Acad. Sci.* **107,** 18469–18474 (2010).

71. Begum, R. *et al.* Near-infrared light increases ATP , extends lifespan and improves mobility in aged Drosophila melanogaster. *Biol. Lett.* **11,** 25–28 (2015).

72. Begum, R., Powner, M. B., Hudson, N., Hogg, C. & Jeffery, G. Treatment with 670 nm Light Up Regulates Cytochrome C Oxidase Expression and Reduces Inflammation in an Age-Related Macular Degeneration Model. *PLoS One* **8,** e57828 (2013).

73. Tennessen, J. M., Barry, W. E., Cox, J. & Thummel, C. S. Methods for studying metabolism in Drosophila. *Methods* **68,** 105–115 (2014).

74. Costa, a C., Loh, S. H. Y. & Martins, L. M. Drosophila Trap1 protects against mitochondrial dysfunction in a PINK1/parkin model of Parkinson's disease. *Cell Death Dis.* **4,** e467 (2013).

75. Andersen, J. L. *et al.* How to assess Drosophila cold tolerance: chill coma temperature and lower lethal temperature are the best predictors of cold distribution limits. *Funct. Ecol.* **29,** 55–65 (2015).

76. Yatsenko, A. S., Marrone, A. K., Kucherenko, M. M. & Shcherbata, H. R. Measurement of metabolic rate in Drosophila using respirometry. *J. Vis. Exp.* e51681 (2014). doi:10.3791/51681

77. Meiklejohn, C. D. *et al.* An Incompatibility between a Mitochondrial tRNA and Its Nuclear-Encoded tRNA Synthetase Compromises Development and Fitness in Drosophila. *PLoS Genet.* **9,** e1003238 (2013).

78. Spinazzi, M., Casarin, A., Pertegato, V., Salviati, L. & Angelini, C. Assessment of mitochondrial respiratory chain enzymatic activities on tissues and cultured cells. *Nat. Protoc.* **7,** 1235–1246 (2012).

79. Haddadi, M. *et al.* Brain aging, memory impairment and oxidative stress: A study in Drosophila melanogaster. *Behav. Brain Res.* **259,** 60–69 (2014).

80. Helfrich-Förster, C. Immunohistochemistry in Drosophila: sections and whole mounts. *Methods Mol. Biol.* **362,** 533–47 (2007).

81. Villa-Cuesta, E., Holmbeck, M. a & Rand, D. M. Rapamycin increases mitochondrial efficiency by mtDNA-dependent reprogramming of mitochondrial metabolism in Drosophila. *J. Cell Sci.* **127,** 2282–90 (2014).

82. Ali, Y. O., Escala, W., Ruan, K. & Zhai, R. G. Assaying locomotor, learning, and memory deficits in Drosophila models of neurodegeneration. *J. Vis. Exp.* 1–5 (2011). doi:10.3791/2504

83. Colomb, J., Reiter, L., Blaszkiewicz, J., Wessnitzer, J. & Brembs, B. Open Source Tracking and Analysis of Adult Drosophila Locomotion in Buridan's Paradigm with and without Visual Targets. *PLoS One* **7,** e42247 (2012).

84. Valente, D., Golani, I. & Mitra, P. P. Analysis of the Trajectory of Drosophila melanogaster in a Circular Open Field Arena. *PLoS One* **2,** e1083 (2007).

85. Van Voorhies, W. a, Melvin, R. G., Ballard, J. W. O. & Williams, J. B. Validation of manometric microrespirometers for measuring oxygen consumption in small arthropods. *J. Insect Physiol.* **54,** 1132–7 (2008).

86. Demontis, F., Piccirillo, R., Goldberg, A. L. & Perrimon, N. Mechanisms of skeletal muscle aging: insights from Drosophila and mammalian models. *Dis Model Mech* **6,** 1339–1352 (2013).

87. Dolph, P., Nair, A. & Raghu, P. Electroretinogram recordings of Drosophila. *Cold Spring Harb. Protoc.* **6,** (2011).

88. Correia-Melo, C. & Passos, J. F. Mitochondria: Are they causal players in cellular senescence? *Biochim. Biophys. Acta - Bioenerg.* **1847,** 1373–1379 (2015).

89. Davalli, P., Mitic, T., Caporali, A., Lauriola, A. & D'Arca, D. ROS, Cell Senescence, and Novel Molecular Mechanisms in Aging and Age-Related Diseases. *Oxid. Med. Cell. Longev.* **2016,** 1–18 (2016).

90. Finkel, T. Signal transduction by reactive oxygen species. *J. Cell Biol.* **194,** 7–15 (2011).

91. Bjedov, I. *et al.* Mechanisms of Life Span Extension by Rapamycin in the Fruit Fly Drosophila melanogaster. *Cell Metab.* **11,** 35–46 (2010).

92. Lanza, I. R. *et al.* Chronic Caloric Restriction Preserves Mitochondrial Function in Senescence without Increasing Mitochondrial Biogenesis. *Cell Metab.* **16,** 777–788 (2012).

93. Reinhart, F. *et al.* Near-infrared light (670 nm) reduces MPTP-induced parkinsonism within a broad therapeutic time window. *Exp. Brain Res.* **234,** 1787–1794 (2016).

94. Kaynezhad, P., Tachtsidis, I. & Jeffery, G. Optical monitoring of retinal respiration in real time: 670 nm light increases the redox state of mitochondria. *Exp. Eye Res.* **152,** 88–93 (2016).

95. Lopez-Lluch, G. *et al.* Calorie restriction induces mitochondrial biogenesis and bioenergetic efficiency. *Proc. Natl. Acad. Sci.* **103,** 1768–1773 (2006).

96. Liu, Z. & Huang, X. Lipid metabolism in Drosophila: development and disease. *Acta Biochim. Biophys. Sin. (Shanghai).* **45,** 44–50 (2013).

97. Murrow, L. & Debnath, J. Autophagy as a Stress-Response and Quality-Control Mechanism: Implications for Cell Injury and Human Disease. *Annu. Rev. Pathol. Mech. Dis.* **8,** 105–137 (2013).

98. Rubinsztein, D. C., Mariño, G. & Kroemer, G. Autophagy and Aging. *Cell* **146,** 682–695 (2011).

99. Gewirtz, D. A. Autophagy and senescence. *Autophagy* **9,** 808–812 (2013).

100. Phillip, D. *et al.* The Binding of Xanthophylls to the Bulk Light-harvesting Complex of Photosystem II of Higher Plants. *J. Biol. Chem.* **277,** 25160–25169 (2002).

101. Ziegler, R. G. Vegetables, fruits, and carotenoids and the risk of cancer. *Am. J. Clin. Nutr.* **53,** 251S–259S (1991).

102. Omenn, G. S. *et al.* Risk factors for lung cancer and for intervention effects in CARET, the Beta-Carotene and Retinol Efficacy Trial. *J. Natl. Cancer Inst.* **88,** 1550–9 (1996).

103. Alpha-Tocopherol, B. C. C. P. S. G. The effect of vitamin E and beta carotene on the incidence of lung cancer and other cancers in male smokers. *N. Engl. J. Med.* **330,** 1029–35 (1994).

104. Rotenstreich, Y. *et al.* Treatment With 9- cis β-Carotene–Rich Powder in Patients With Retinitis Pigmentosa. *JAMA Ophthalmol.* **131,** 985 (2013).

105. Sher, I. *et al.* Synthetic 9-cis-beta-carotene inhibits photoreceptor degeneration in cultures of eye cups from rpe65rd12 mouse model of retinoid cycle defect. *Sci. Rep.* **8,** 6130 (2018).

106. Lu, L., Wu, J., Wei, L. & Wu, F. Temperature dependence of aggregated structure of β-carotene by absorption spectral experiment and simulation. *Spectrochim. Acta Part A Mol. Biomol. Spectrosc.* **169,** 116–121 (2016).

107. Jimenez, C. & Pick, U. Differential Reactivity of [beta]-Carotene Isomers from Dunaliella bardawil Toward Oxygen Radicals. *Plant Physiol.* **101,** 385–390 (1993).

108. Siems, W. *et al.* β-Carotene breakdown products may impair mitochondrial functions — potential side effects of high-dose β-carotene supplementation. *J. Nutr. Biochem.* **16,** 385–397 (2005).

109. SIEMS, W. *et al.* β-Carotene cleavage products induce oxidative stress in vitro by impairing mitochondrial respiration. *FASEB J.* **16,** 1289–1291 (2002).

110. Ben-Amotz, A., Katz, A. & Avron, M. Accumulation of beta-carotene in halotolerant algae: Purification and characterization of beta-carotene-rich globules fromDunaliella bardawil (Chlorophyceae). *J. Phycol.* **18,** 529–537 (1982).

111. Jones, M. A. & Grotewiel, M. Drosophila as a model for age-related impairment in locomotor and other behaviors. *Exp. Gerontol.* **46,** 320–325 (2011).

112. Lashmanova, E. *et al.* Fucoxanthin increases lifespan of Drosophila melanogaster and Caenorhabditis elegans. *Pharmacol. Res.* **100,** 228–241 (2015).

113. Yazaki, K., Yoshikoshi, C., Oshiro, S. & Yanase, S. Supplemental Cellular Protection by a Carotenoid Extends Lifespan via Ins/IGF-1 Signaling in Caenorhabditis elegans. *Oxid. Med. Cell. Longev.* **2011,** 1–9 (2011).

114. Bratic, I. & Trifunovic, A. Mitochondrial energy metabolism and ageing. *Biochim. Biophys. Acta - Bioenerg.* **1797,** 961–967 (2010).

115. Kaneko, H. *et al.* Circadian Rhythm of Temperature Preference and Its Neural Control in Drosophila. *Curr. Biol.* **22,** 1851–1857 (2012).

116. Sakai, T. & Ishida, N. Circadian rhythms of female mating activity governed by clock genes in Drosophila. *Proc. Natl. Acad. Sci.* **98,** 9221–9225 (2001).

117. Zhang, Y. & Emery, P. in *Insect Molecular Biology and Biochemistry* 513–551 (Elsevier, 2012). doi:10.1016/B978-0-12-384747-8.10015-7

118. Tataroglu, O. & Emery, P. Studying circadian rhythms in Drosophila melanogaster. *Methods* **68,** 140–150 (2014).

119. Zhang, R., Lahens, N. F., Ballance, H. I., Hughes, M. E. & Hogenesch, J. B. A circadian gene expression atlas in mammals: Implications for biology and medicine. *Proc. Natl. Acad. Sci.* **111,** 16219–16224 (2014).

120. McCarthy, J. J. *et al.* Identification of the circadian transcriptome in adult mouse skeletal muscle. *Physiol. Genomics* **31,** 86–95 (2007).

121. Robles, M. S., Cox, J. & Mann, M. In-Vivo Quantitative Proteomics Reveals a Key Contribution of Post-Transcriptional Mechanisms to the Circadian Regulation of Liver Metabolism. *PLoS Genet.* **10,** e1004047 (2014).

122. Ma, D., Li, S., Molusky, M. M. & Lin, J. D. Circadian autophagy rhythm: a link between clock and metabolism? *Trends Endocrinol. Metab.* **23,** 319–325 (2012).

123. Neufeld-Cohen, A. *et al.* Circadian control of oscillations in mitochondrial rate-limiting enzymes and nutrient utilization by PERIOD proteins. *Proc. Natl. Acad. Sci.* **113,** E1673–E1682 (2016).

124. Dallmann, R., Viola, A. U., Tarokh, L., Cajochen, C. & Brown, S. A. The human circadian metabolome. *Proc. Natl. Acad. Sci.* **109,** 2625–2629 (2012).

125. de Goede, P., Wefers, J., Brombacher, E. C., Schrauwen, P. & Kalsbeek, A. Circadian rhythms in mitochondrial respiration. *J. Mol. Endocrinol.* **60,** R115–R130 (2018).

126. Janssen, A. J. M. *et al.* Spectrophotometric Assay for Complex I of the Respiratory Chain in Tissue Samples and Cultured Fibroblasts. *Clin. Chem.* **53,** 729–734 (2007).

127. Krebs, H. A. & Hems, R. Phosphate-transfer reactions of adenosine and inosine nucleotides. *Biochem. J.* **61,** 435–41 (1955).

128. Velick, S. F. [60] Glyceraldehyde-3-phosphate dehydrogenase from muscle. *Methods Enzymol.* **1,** 401–406 (1955).

129. Zhu, C. T. & Rand, D. M. A Hydrazine Coupled Cycling Assay Validates the Decrease in Redox Ratio under Starvation in Drosophila. *PLoS One* **7,** (2012).

130. Livak, K. J. & Schmittgen, T. D. Analysis of Relative Gene Expression Data Using Real-Time Quantitative PCR and the 2−ΔΔCT Method. *Methods* **25,** 402–408 (2001).

131. Hughes, M. E. *et al.* Harmonics of Circadian Gene Transcription in Mammals. *PLoS Genet.* **5,** e1000442 (2009).

132. Ramsey, K. M. *et al.* Circadian Clock Feedback Cycle Through NAMPT-Mediated NAD+ Biosynthesis. *Science (80-.).* **324,** 651–654 (2009).

133. Barber, A. F., Erion, R., Holmes, T. C. & Sehgal, A. Circadian and feeding cues integrate to drive rhythms of physiology in Drosophila insulin-producing cells. *Genes Dev.* **30,** 2596–2606 (2016).

134. Jacobs, G. H. & Deegan, J. F. Uniformity of colour vision in Old World monkeys. *Proc. R. Soc. B Biol. Sci.* **266,** 2023–2028 (1999).

135. Linsenmeier, R. A. & Padnick-Silver, L. Metabolic dependence of photoreceptors on the choroid in the normal and detached retina. *Investig. Ophthalmol. Vis. Sci.* **41,** 3117–3123 (2000).

136. Curcio, C. A., Sloan, K. R., Kalina, R. E. & Hendrickson, A. E. Human Photoreceptor Topography. *J. Comp. Neurol.* **523,** 497–523 (1990).

137. Kawamura, S. *et al.* in *Post-Genome Biology of Primates* 93–120 (1999).

138. Warrant, E. J. Photoreceptor Evolution: Ancient 'Cones' Turn Out to Be Rods. *Curr. Biol.* **25,** R148–R151 (2015).

139. Mollon, J. D. The Uses and Origins of Primate Colour Vision. *J. exp. Biol* **146,** 21–38 (1989).

140. Marc, R. E. & Sperling, H. G. Chromatic organization of primate cones. *Science* **196,** 454–6 (1977).

141. Martin, P. R. & Grünert, U. Analysis of the short wavelength-sensitive ('blue') cone mosaic in the primate retina: Comparison of New World and Old World monkeys. *J. Comp. Neurol.* **406,** 1–14 (1999).

142. Ahnelt, P. K., Kolb, H. & Pflug, R. Identification of a subtype of cone photoreceptor, likely to be blue sensitive, in the human retina. *J. Comp. Neurol.* **255,** 18–34 (1987).

143. Ahnelt, P., Keri, C. & Kolb, H. Identification of pedicles of putative blue-sensitive cones in the human retina. *J. Comp. Neurol.* **293,** 39–53 (1990).

144. Stromeyer, C. F., Kronauer, R. E. & Madsen, J. C. Response saturation of short-wavelength cone pathways controlled by color-opponent mechanisms. *Vision Res.* **19,** 1025–1040 (1979).

145. Werner, J. S. The Verriest Lecture : Short-wave-sensitive cone pathways across the life span. *J. Opt. Soc. Am. A* **33,** A104-22 (2016).

146. Greenstein, V. C., Hood, D. C., Ritch, R., Steinberger, D. & Carr, R. E. S (blue) cone pathway vulnerability in retinitis pigmentosa, diabetes and glaucoma. *Investig. Ophthalmol. Vis. Sci.* **30,** 1732–1737 (1989).

147. Birch, J. *et al. Congenital and Acquired Color Vision Defects*. (Grune & Stratton, 1979).

148. Schatz, A. *et al.* Attenuation of S-cone function at high altitude assessed by electroretinography. *Vision Res.* **97,** 59–64 (2014).

149. Ohta, Y. & Kato, H. Color perception changes with age: test results by P-N

anomaloscope. *Mod. Probl. Ophthalmol.* **17,** 345–2 (1976).

150. Weale, R. A. Senile changes in visual acuity. *Trans Ophthamol Soc UK* **95,** 36–8 (1975).

151. McFarland, R. A., Domey, R. G., Warren, A. B. & Ward, D. C. Dark Adaptation as a Function of Age: I. A Statistical Analysis. *J. Gerontol.* **15,** 149–154 (1960).

152. Jackson, G. R. & Owsley, C. Scotopic sensitivity during adulthood. *Vision Res.* **40,** 2467–73 (2000).

153. Curcio, C. A., Millican, C. L., Allen, K. A. & Kalina, R. E. Aging of the human photoreceptor mosaic: Evidence for selective vulnerability of rods in central retina. *Investig. Ophthalmol. Vis. Sci.* **34,** 3278–3296 (1993).

154. Gao, H. & Hollyfield, J. G. Aging of the human retina. Differential loss of neurons and retinal pigment epithelial cells. *Invest. Ophthalmol. Vis. Sci.* **33,** 1–17 (1992).

155. Aggarwal, P., Nag, T. C. & Wadhwa, S. Age-related decrease in rod bipolar cell density of the human retina: an immunohistochemical study. *J Biosci.* **32,** 293–8 (2007).

156. Lindquist, S. The Heat-Shock Response. *Annu. Rev. Biochem.* **55,** 1151–1191 (1986).

157. Kalmar, B. & Greensmith, L. Induction of heat shock proteins for protection against oxidative stress. *Adv. Drug Deliv. Rev.* **61,** 310–318 (2009).

158. Samali, A. & Cotter, T. G. Heat Shock Proteins Increase Resistance to Apoptosis. *Exp. Cell Res.* **223,** 163–170 (1996).

159. Samali, A., Holmberg, C. I., Sistonen, L. & Orrenius, S. Thermotolerance and cell death are distinct cellular responses to stress: Dependence on heat shock proteins. *FEBS Lett.* **461,** 306–10 (1999).

160. Lindquist, S. & Craig, E. A. The Heat-Shock Proteins. *Annu. Rev. Genet.* **22,** 631–677 (1988).

161. Cheng, M. Y. *et al.* Mitochondrial heat-shock protein hsp60 is essential for assembly of proteins imported into yeast mitochondria. *Nature.* **337,** 620–5 (1989).

162. De Valois, R. L., Morgan, H. & Snodderly, D. M. Psychophysical studies of monkey Vision-III. Spatial luminance contrast sensitivity tests of macaque and human observers. *Vision Res.* **14,** 75–81 (1974).

163. De Valois, R. L., Morgan, H. C., Polson, M. C., Mead, W. R. & Hull, E. M. Psychophysical studies of monkey vision-I. Macaque luminosity and color vision tests. *Vision Res.* **14,** 53–67 (1974).

164. Houtkooper, R. H. *et al.* The metabolic footprint of aging in mice. *Sci. Rep.* **1,** 134 (2011).

165. Zlatkova, M. B., Coulter, E. & Anderson, R. S. Short-wavelength acuity: Blue-yellow and achromatic resolution loss with age. *Vision Res.* **43,** 109–115 (2003).

166. Shinomori, K. & Werner, J. S. Aging of human short-wave cone pathways. *Proc. Natl. Acad. Sci. Unites States Am.* **109,** 13422–13427 (2012).

167. Johnson, J. E. *et al.* Spatiotemporal regulation of ATP and Ca2+ dynamics in vertebrate rod and cone ribbon synapses. *Mol. Vis.* **13,** 887–919 (2007).

168. Hoang, Q. V, Linsenmeier, R. a, Chung, C. K. & Curcio, C. a. Photoreceptor inner segments in monkey and human retina: mitochondrial density, optics, and regional variation. *Vis. Neurosci.* **19,** 395–407 (2002).

169. Perkins, G. a, Ellisman, M. H. & Fox, D. a. Three-dimensional analysis of mouse rod and cone mitochondrial cristae architecture: bioenergetic and functional implications. *Mol. Vis.* **9,** 60–73 (2003).

170. Uchida, K. Current Status of Acrolein as a Lipid Peroxidation Product. *Trends Cardiovasc. Med.* **9,** 109–113 (1999).

171. Furuhata, A., Nakamura, M., Osawa, T. & Uchida, K. Thiolation of Protein-bound Carcinogenic Aldehyde. *J. Biol. Chem.* **277,** 27919–27926 (2002).

172. Biswal, S., Acquaah-Mensah, G., Datta, K., Wu, X. & Kehrer, J. P. Inhibition of cell proliferation and AP-1 activity by acrolein in human A549 lung adenocarcinoma cells due to thiol imbalance and covalent modifications. *Chem. Res. Toxicol.* **15,** 180–6 (2002).

173. Stadtman, E. Protein oxidation and aging. *Science (80-.).* **257,** 1220–1224 (1992).

174. Cappello, F. *et al.* Hsp60 and human aging: Les liaisons dangereuses. *Front. Biosci. (Landmark Ed.* **18,** 626–37 (2013).

175. Chun, J. N. *et al.* Cytosolic Hsp60 Is Involved in the NF-κB-Dependent Survival of Cancer Cells via IKK Regulation. *PLoS One* **5,** e9422 (2010).

176. Cappello, F., Conway de Macario, E., Marasà, L., Zummo, G. & Macario, A. J. L. Hsp60 expression, new locations, functions, and perspectives for cancer diagnosis and therapy. *Cancer Biol. Ther.* **7,** 801–809 (2008).

177. Buchner, J. & Li, J. Structure, Function and Regulation of the Hsp90 Machinery. *Biomed. J.* **36,** 106 (2013).

178. Taipale, M., Jarosz, D. F. & Lindquist, S. HSP90 at the hub of protein homeostasis: emerging mechanistic insights. *Nat. Rev. Mol. Cell Biol.* **11,** 515–528 (2010).

179. BILLINGSLEY, M. L. & KINCAID, R. L. Regulated phosphorylation and dephosphorylation of tau protein: effects on microtubule interaction, intracellular trafficking and neurodegeneration. *Biochem. J.* **323,** 577–591 (1997).

180. Wharton, S. B. *et al.* Epidemiological pathology of Tau in the ageing brain: application of staging for neuropil threads (BrainNet Europe protocol) to the MRC cognitive function and ageing brain study. *Acta Neuropathol. Commun.* **4,** 11 (2016).

181. Panda-Jonas, S., Jonas, J. B. & Jakobczyk-Zmija, M. Retinal photoreceptor density decreases with age. *Ophthalmology* **102,** 1853–9 (1995).

182. Cunea, A., Powner, M. B. & Jeffery, G. Death by color: Differential cone loss in the aging mouse retina. *Neurobiol. Aging* **35,** 2584–2591 (2014).

183. Wikler, K. C., Williams, R. W. & Rakic, P. Photoreceptor mosaic: Number and distribution of rods and cones in the rhesus monkey retina. *J. Comp. Neurol.* **297,** 499–508 (1990).

184. Curcio, C. A., Medeiros, N. E. & Millican, C. L. Photoreceptor loss in age-related macular degeneration. *Investig. Ophthalmol. Vis. Sci.* **37,** 1236–1249 (1996).

185. Curcio, C. A. Photoreceptor topography in ageing and age-related maculopathy. *Eye (Lond).* **15,** 376–383 (2001).

186. Aguilà, M. *et al.* Hsp90 inhibition protects against inherited retinal degeneration. *Hum. Mol. Genet.* **23,** 2164–2175 (2014).

187. Pearl, L. H., Prodromou, C. & Workman, P. The Hsp90 molecular chaperone: an open and shut case for treatment. *Biochem. J.* **410,** 439–453 (2008).

188. Sessa, C. *et al.* First-in-Human Phase I Dose-Escalation Study of the HSP90 Inhibitor AUY922 in Patients with Advanced Solid Tumors. *Clin. Cancer Res.* **19,** 3671–3680 (2013).

189. Winkler, B. S. Glycolytic and oxidative metabolism in relation to retinal function. *J. Gen. Physiol.* **77,** 667–92 (1981).

190. Nork, T. M., Millecchia, L. L., Strickland, B. D., Linberg, J. V & Chao, G. M. Selective loss of blue cones and rods in human retinal detachment. *Arch Ophthalmol* **113,** 1066–1073 (1995).

191. Frennesson, C., Nilsson, U. L. & Nilsson, S. E. G. Colour contrast sensitivity in patients with soft drusen, and early stage of ARM. *Doc. Ophthalmol.* **90,** 377–386 (1995).

192. Beirne, R. O. *et al.* Severity staging by early features of age-related maculopathy exhibits weak relationships with functional deficits on SWS grating acuity. *Investig. Ophthalmol. Vis. Sci.* **47,** 4624–4631 (2006).

193. Remky, a & Elsner, a E. Blue on yellow perimetry with scanning laser ophthalmoscopy in patients with age related macular disease. *Br. J. Ophthalmol.* **89,** 464–9 (2005).

194. Arjamaa, O., Nikinmaa, M., Salminen, A. & Kaarniranta, K. Regulatory role of HIF-1alpha in the pathogenesis of age-related macular degeneration (AMD). *Ageing Research Reviews* **8,** 349–358 (2009).

195. Kurihara, T. Development and pathological changes of neurovascular unit regulated by hypoxia response in the retina. *Prog. Brain Res.* **225,** 201–211 (2016).

196. Chisholm, K. I. *et al.* In vivo imaging of flavoprotein fluorescence during hypoxia reveals the importance of direct arterial oxygen supply to cerebral cortex tissue. in *Advances in Experimental Medicine and Biology.* **876,** 233–239 (2016).

197. Barot, M., Gokulgandhi, M. R. & Mitra, A. K. Mitochondrial dysfunction in

retinal diseases. *Curr Eye Res.* **36,** 1069–77 (2011).

198. Lefevere, E. *et al.* Mitochondrial dysfunction underlying outer retinal diseases. *Mitochondrion.* **36,** 66–76 (2017).

199. Witte, M. E., Mahad, D. J., Lassmann, H. & van Horssen, J. Mitochondrial dysfunction contributes to neurodegeneration in multiple sclerosis. *Trends Mol. Med.* **20,** 179–187 (2014).

200. Korlipara, L. V. P. & Schapira, A. H. V. in *Mitochondrial Function and Dysfunction*. **53,** 283–314 (2002).

201. Yu, D.-Y. & Cringle, S. J. Oxygen distribution in the mouse retina. *Invest. Ophthalmol. Vis. Sci.* **47,** 1109–12 (2006).

202. Oxygen Distribution and Consumption within the Retina in Vascularised and Avascular Retinas and in Animal Models of Retinal Disease.

203. Reinert, K. C., Gao, W., Chen, G. & Ebner, T. J. Flavoprotein autofluorescence imaging in the cerebellar cortex in vivo. in *Journal of Neuroscience Research* **85,** 3221–3232 (2007).

204. Bale, G., Elwell, C. E. & Tachtsidis, I. From Jobsis to the present day: a review of clinical near- infrared spectroscopy measurements of cerebral cytochrome-c-oxidase. *J. Biomed. Opt.* **21,** 091307 (2016).

205. Huang S., H. A. & Webb. Two-Photon Fluorescence Spectroscopy and Microscopy of NAD(P)H and Flavoprotein. *Biophys. J.* (2002).

206. Kunz, W. S. & Kunz, W. Contribution of different enzymes to flavoprotein fluorescence of isolated rat liver mitochondria. *Biochim. Biophys. Acta - Gen. Subj.* **841,** 237–246 (1985).

207. Ragan, C. I. & Garland, P. B. The Intra-Mitochondrial Localization of Flavoproteins Previously Assigned to the Respiratory Chain. *Eur. J. Biochem.* **10,** 399–410 (1969).

208. Kunz, W. S. & Gellerich, F. N. Quantification of the Content of Fluorescent Flavoproteins in Mitochondria from Liver, Kidney Cortex, Skeletal Muscle, and Brain. *Biochem. Med. Metab. Biol.* **841,** 237–246 (1993).

209. Caspi, R. R. Understanding autoimmunity in the eye: from animal models to novel therapies. *Discov. Med.* **17,** 155–62 (2014).

210. Bindewald, A., Jorzik, J. J., Loesch, A., Schutt, F. & Holz, F. G. Visualization of retinal pigment epithelial cells in vivo using digital high-resolution confocal scanning laser ophthalmoscopy. *Am.J Ophthalmol* (2004).

211. Wabbels, B. *et al.* Fundus autofluorescence in children and teenagers with hereditary retinal diseases. *Graefe's Arch. Clin. Exp. Ophthalmol.* **244,** 36–45 (2006).

212. Chance, B., Schoener, B., Oshino, R., Itshak, F. & Nakase, Y. Oxidation-reduction ratio studies of mitochondria in freeze-trapped samples. NADH and flavoprotein fluorescence signals. *J. Biol. Chem.* (1979).

213. Scholz, R., Thurman, R. G., John, R. & Chance, Britton, Bucher, T. Flavin and

Pyridine Nucleotide Oxidation-Reduction Changes in Perfused Rat Liver. *J. BIOLOQICAL Chem.* (1969).

214. Chisholm, K. I. *et al.* In vivo imaging of flavoprotein fluorescence during hypoxia reveals the importance of direct arterial oxygen supply to cerebral cortex tissue. in *Advances in Experimental Medicine and Biology* **876,** 233–239 (Springer New York LLC, 2016).

215. Delori, F. C. *et al.* In vivo fluorescence of the ocular fundus exhibits retinal pigment epithelium lipofuscin characteristics. *Investig. Ophthalmol. Vis. Sci.* (1995).

216. Weiter, J. J., Delori, F. C., Wing, G. L. & Fitch, K. A. Retinal pigment epithelial lipofuscin and melanin and choroidal melanin in human eyes. *Investig. Ophthalmol. Vis. Sci.* (1986).

217. Durrani, K. & Foster, C. S. Fundus autofluorescence imaging in posterior uveitis. *Seminars in Ophthalmology.* **27,** 228–235 (2012).

218. Erecińska, M. & Silver, I. A. Tissue oxygen tension and brain sensitivity to hypoxia. in *Respiration Physiology.* **128,** 263–76 (2001).

219. Kasischke, K. A. *et al.* Two-photon NADH imaging exposes boundaries of oxygen diffusion in cortical vascular supply regions. *J. Cereb. Blood Flow Metab.* **31**, 68–81 (2011).

220. Wilkins, H. M. & H. Swerdlow, R. Relationships Between Mitochondria and Neuroinflammation: Implications for Alzheimer's Disease. *Curr. Top. Med. Chem.* **16**, 849–57 (2016).

221. Forrester, J. V., Huitinga, I., Lumsden, L. & Dijkstra, C. D. Marrow-derived activated macrophages are required during the effector phase of experimental autoimmune uveoretinitis in rats. *Curr. Eye Res.* **17,** 426–37 (1998).

222. Jiang, H. R., Lumsden, L. & Forrester, J. V. Macrophages and dendritic cells in IRBP-induced experimental autoimmune uveoretinitis in B10RIII mice. *Investig. Ophthalmol. Vis. Sci.* (1999).

223. Okada, A. A. *et al.* Angiography of experimental autoimmune uveoretinitis with ultrastructural correlation. *Graefe's Arch. Clin. Exp. Ophthalmol.* (1998). doi:10.1007/s004170050172

224. Aubin, J. E. Autofluorescence of viable cultured mammalian cells. *J. Histochem. Cytochem*. **27,** 36–43 (1979).

225. Kunz, W. S. Spectral properties of fluorescent flavoproteins of isolated rat liver mitochondria. *FEBS Lett.* (1986).

226. Eng, J., Lynch, R. M. & Balaban, R. S. Nicotinamide adenine dinucleotide fluorescence spectroscopy and imaging of isolated cardiac myocytes. *Biophys. J.* **55,** 621–30 (1989).

227. Ni, H.-M., Williams, J. A. & Ding, W.-X. Mitochondrial dynamics and mitochondrial quality control. *Redox Biol.* **4,** 6–13 (2015).

228. Kokkinopoulos, I., Colman, A., Hogg, C., Heckenlively, J. & Jeffery, G. Age-

related retinal inflammation is reduced by 670 nm light via increased mitochondrial membrane potential. *Neurobiol. Aging* **34,** 602–609 (2013).

229. Koch, R. E. & Hill, G. E. Behavioural mating displays depend on mitochondrial function: a potential mechanism for linking behaviour to individual condition. *Biol. Rev*. **93,** 1387–1398 (2018).

230. Saré, R. M. *et al.* Negative Effects of Chronic Rapamycin Treatment on Behavior in a Mouse Model of Fragile X Syndrome. *Front. Mol. Neurosci.* **10,** (2018).

231. Sivapathasuntharam, C., Sivaprasad, S., Hogg, C. & Jeffery, G. Aging retinal function is improved by near infrared light (670 nm) that is associated with corrected mitochondrial decline. *Neurobiol. Aging* **52,** 66–70 (2017).

232. Riazi-Esfahani, M., Kuppermann, B. & Kenney, Mc. The role of mitochondria in AMD: Current knowledge and future applications. *J. Ophthalmic Vis. Res.* **12,** 424 (2017).

233. Wollstein, G., Garway-Heath, D. F. & Hitchings, R. A. Identification of early glaucoma cases with the scanning laser ophthalmoscope11The authors have no proprietary interest in the development or marketing of this or a competing instrument. *Ophthalmology* **105,** 1557–1563 (1998).

234. Helb, H.-M. *et al.* Clinical evaluation of simultaneous confocal scanning laser ophthalmoscopy imaging combined with high-resolution, spectral-domain optical coherence tomography. *Acta Ophthalmol.* **88,** 842–849 (2010).

235. Siddiqui, M. F. *et al.* Non-invasive measurement of a metabolic marker of infant brain function. *Sci. Rep.* **7,** 1330 (2017).